UC San Diego

UC San Diego Electronic Theses and Dissertations

Title

Small but mighty rhomboid pseudoprotease Dfm1 mediates a novel role in regulating lipid homeostasis and proteotoxic stress

Permalink

https://escholarship.org/uc/item/5mc2x25v

Author

Aguayo, Analine

Publication Date

2024

Peer reviewed|Thesis/dissertation

eScholarship.org Powered by the California Digital Library
University of California

UNIVERSITY OF CALIFORNIA SAN DIEGO

Small but mighty rhomboid pseudoprotease Dfm1 mediates a novel role in regulating lipid homeostasis and proteotoxic stress

A dissertation submitted in partial satisfaction of the
requirements for the degree Doctor of Philosophy

in

Biology

by

Analine Aguayo

Committee in charge:

Professor Sonya E. Neal, Chair
Professor Randolph Y. Hampton
Professor Maho Niwa Rosen
Professor Samara Reck-Peterson

2024

Copyright
Analine Aguayo, 2024
All rights reserved.

The Dissertation of Analine Aguayo is approved, and it is acceptable in quality and form for publication on microfilm and electronically.

University of California San Diego

2024

DEDICATION

Dedico esta obra a mis padres, Adán Aguayo y Ana Line Aguayo. Hace más de treinta y cinco años que se mudaron a este país extranjero para darnos una vida mejor a mis hermanes y a mí. Con sangre, sudor, y lágrimas, nos han apoyado toda nuestra vida, y por eso, les agradecemos. Los quiero mucho y no habría logrado lo que he alcanzado sin su cariño, lecciones, y fuerza. Gracias.

Un fuerte abrazo, especialmente para mi mamá, quien, durante este año en el que he escrito esta disertación, ella ha luchado día tras día para rehabilitarse. Juntas, hemos logrado mucho, y espero que continuemos luchando juntas.

And to my siblings, Juan, Oswaldo, and Juliana: Thank you for growing with me and continuing to grow together. We Aguayo Robles are a resilient bunch, and I do not see that changing anytime soon. Each of you inspires me uniquely; I hope I can continue to inspire you, too. I love you all.

TABLE OF CONTENTS

DISSERTATION APPROVAL PAGE iii
DEDICATION iv
TABLE OF CONTENTS v
TABLE OF FIGURES viii
ACKNOWLEDGEMENTS x
VITA xviii
ABSTRACT OF THE DISSERTATION xix
Chapter 1: Introduction 1
1.1 Protein homeostasis is essential for cell survival 2
1.1.1 Proteostasis network (PN) works through protein synthesis, maintenance, and degradation 4
1.1.2 Combating proteotoxic stress via proteostasis network degradation pathways 6
1.2 Degradation routes of the cell 7
1.2.1 Ubiquitin processing marks substrates for degradation 8
1.3 Proteasomal degradation and associated pathways 13
1.3.1 Inner nuclear membrane-associated degradation (INMAD) 14
1.3.2 San-1-dependant degradation 17
1.3.3 Endoplasmic reticulum associated degradation (ERAD) 19
1.3.4 Endosome and Golgi-associated degradation (EGAD) 22
1.3.5 Golgi apparatus-related degradation (GARD) 25
1.4 Vacuolar degradation 26
1.4.1 Autophagy 28
1.4.2 Dsc complex: VPS and AP3 29
1.4.3 Golgi membrane-associated degradation (GOMED) 33
1.5 Lipids in the proteostasis network 34
1.5.1 Lipid assemblies 35
1.5.2 Lipid droplets and deposition sites for protein aggregates 36
1.5.3 Lipid dysregulation activates the UPR 37
1.5.4 Sphingolipid biosynthesis and the PN 38
1.5.5 Degradation of sphingolipid biosynthetic enzymes is complex and understudied 39
1.6 Conclusion and Perspectives 40
1.7 Acknowledgements 41
1.8 References 42

Chapter 2: Yeast Derlin Dfm1 Employs a Chaperone-Like Function to Resolve Misfolded Membrane Protein Stress 62
2.1. Introduction 63
2.2. Results 67
2.2.1. Absence of Dfm1 and expression of integral misfolded membrane proteins causes growth stress 67
2.2.2. Disease-associated membrane proteins cause growth stress 70
2.2.3. Dfm1 has a dual role in ER protein stress and ERAD retrotranslocation 71
2.2.4. Human derlins relieve growth stress 73
2.2.5. Dfm1 solubilizes misfolded membrane protein aggregates independent of Cdc48 recruitment 74
2.2.6. Misfolded membrane proteins do not activate the unfolded protein response 78
2.2.7. Accumulation of misfolded membrane proteins up-regulates proteasome components 80
2.2.8. The transcription factor Rpn4 is involved in misfolded membrane protein stress 82
2.2.9. Misfolded membrane protein stress in *dfm1*Δ cells leads to proteasome impairment 84
2.2.10. Misfolded membrane protein stress does not cause proteasome sequestration 86
2.2.11. Growth defect in *dfm1*Δ cells is ubiquitination dependent 86
2.2.12. Ubiquitin homeostasis is disrupted with misfolded membrane protein accumulation 89
2.2.13. Deubiquitinases prevent or resolve misfolded membrane protein stress 90
2.2.14. Absence of deubiquitinases and RPN4 in combination with DFM1 do not exacerbate toxicity 91
2.2.15. Misfolded protein aggregation toxicity requires protein ubiquitination 92
2.2.16. Increased expression of Dfm1 relieves misfolded membrane protein stress in *rpn4*Δ and *ubp6*Δ cells 92
2.3. Discussion 93
2.4. Materials and Methods 101
2.5. Acknowledgements 112
2.6. References 113
Chapter 3: An ERAD-independent role for rhomboid pseudoprotease Dfm1 in mediating sphingolipid homeostasis 169
3.1. Introduction 170
3.2. Results 175
3.2.1. Derlin Dfm1 interacts with members of the sphingolipid biosynthetic pathway 175

3.2.2. DFM1 genetically interacts with TSC3 177
3.2.3. *dfm1*Δ*tsc3*Δ cells have increased steady-state levels of ceramides and complex sphingolipids 178
3.2.4. DFM1 genetically interacts with ORM1 179
3.2.5. Orm2 is targeted by Dfm1 for degradation 181
3.2.6. Derlin Dfm1's Cdc48 recruitment function is not required for Orm2 degradation 181
3.2.7. Orm2 degradation is dependent on EGAD, but not ERAD or INMAD 184
3.2.8. Dfm1 does not function at the post-ubiquitination step of Orm2 degradation pathway 186
3.2.9. Dfm1 does not directly function in EGAD 186
3.2.10. Dfm1 is required for Orm2 export from the ER to the Golgi 187
3.2.11. Loss of Dfm1 does not affect COPII-mediated trafficking 189
3.2.12. Dfm1 interacts with Ypk1-dependent phosphorylated Orm2 190
3.3. Discussion 192
3.4. Methods 197
3.5. Acknowledgements 207
3.6. References 208
Chapter 4: Scs7 is degraded via the ubiquitin proteasome system 241
4.1. Introduction 242
4.2. Results 248
4.2.1. Surveying candidate sphingolipid biosynthesis enzymes and regulators targeted by ubiquitin proteasome system (UPS) 248
4.2.2. Scs7 degradation is stabilized in *cdc48-1*, *hrd2-1*, *tul1*Δ, and *asi1*Δ strains 249
4.2.3. Scs7 localizes in the ER in *cdc48-2*, *hrd2-1*, *tul1*Δ, and *asi1*Δ cells 253
4.3. Discussion 255
4.4. Materials and Methods 258
4.5. Acknowledgements 261
4.6. References 262
Chapter 5: Conclusions and Closing Remarks 279
5.1 Conclusions and Closing Remarks 280

TABLE OF FIGURES

Figure 1.2.1. Two terminal degradation paths of ubiquitinated misfolded proteins 58

Figure 1.3.1. Overview of proteasomal degradation pathways in proteostasis network.....59

Figure 1.4.1. Overview of autophagy-lysosomal/vacuolar degradation pathways in proteostasis network.....60

Figure 2.2.1. Integral membrane protein overexpression causes a growth defect in *dfm1*Δ cells in an ERAD independent manner.....121

Figure 2.2.2. Dfm1 retrotranslocation defective mutants show differing abilities to restore growth.....123

Figure 2.2.3. Dfm1 reduces misfolded membrane protein toxicity through a chaperone-like activity.....125

Figure 2.2.4. Dfm1 specifically influences solubility of misfolded membrane proteins.....127

Figure 2.2.5. Misfolded membrane protein stress in *dfm1*Δ cells does not activate the UPR 129

Figure 2.2.6. Misfolded membrane protein toxicity results in proteasome impairment.....131

Figure 2.2.7. Ubiquitin stress contributes to misfolded membrane protein toxicity.....133

Figure 2.2.8. Model for misfolded membrane protein-induced toxicity.....135

Supplemental Figure 2.2.1. Hmg2-GFP microscopy puncta are unaffected by Dfm1.....136

Supplemental Figure 2.2.2. Transcriptional changes in membrane protein-stressed *dfm1*Δ cells 138

Supplemental Figure 2.2.3. Misfolded membrane protein stress in *dfm1*Δ cells does not affect Hac1 splicing 140

Supplemental Figure 2.2.4. *Rpn4*Δ toxicity is Specific to misfolded membrane proteins.....141

Supplemental Figure 2.2.5. *Ubp6*Δ toxicity is Specific to misfolded membrane proteins.....142

Supplemental Figure 2.2.6. Not all deubiquitinates mediate misfolded membrane toxicity and toxicity is specific to misfolded membrane proteins.....143

Supplemental Figure 2.2.7. Genetic interactions between Dfm1, Rpn4, and Ubp6 in resolving misfolded membrane protein toxicity.....144

Supplemental Table 2.4.1. Plasmid List.....146

Supplemental Table 2.4.2. Yeast Strains Used in this Study.....150

Figure 3.2.1. BioID proximity-based labeling to identify interaction partners of Dfm1.....213

Figure 3.2.2. Dfm1 colocalizes and binds to SPOTS complex proteins.....215

Figure 3.2.3. Dfm1 genetically interacts with Tsc3.....216

Figure 3.2.4. Dfm1 genetically interacts with Orm1.....218

Figure 3.2.5. Dfm1 targets Orm2 for degradation.....220

Figure 3.2.6. Orm2 degradation requires EGAD, but not ERAD or INMAD pathway.....222

Figure 3.2.7. dfm1Δ accumulates phosphorylated Orm2 exclusively in the ER 224
Figure 3.2.8. Dfm1 binds to phosphorylated Orm2.....226
Supplemental Figure 3.2.1. Dfm1 does not genetically interact with Lcb1, Lcb2, and Sac1 228
Supplemental Figure 3.2.2. Orm2 is degraded in WT strains.....230
Supplemental Figure 3.2.3. Dfm1 does not interact with EGAD components 232
Supplemental Figure 3.2.4. Orm2-3A accumulates exclusively in the ER 233
Supplemental Table 3.4.1. Plasmids Used in this Study 234
Supplemental Table 3.4.2. Yeast Strains Used in this Study 235
Supplemental Table 3.4.3. Key Resources Table 240
Figure 4.1.1. Maturation of sphingolipids from the ER to the Golgi 268
Figure 4.1.2. Investigating the sphingolipid pathway in yeast requires and enzyme-centric approach.....269
Figure 4.2.1. Approach to investigate candidate Dfm1-regulated sphingolipid biosynthesis enzymes 270
Figure 4.2.2. Scs7 degradation is stabilized in *cdc48-1*, *hrd2-1*, *tul1*Δ, and *asi1*Δ strains ...271
Figure 4.2.3. Scs7 localizes in the ER in *cdc48-2*, *hrd2-1*, *tul1*Δ, and *asi1*Δ cells.....273
Supplemental Table 4.4.1. Plasmids Used in this Study 275
Supplemental Table 4.4.2. Yeast Strains Used in this Study 276
Supplemental Table 4.4.3. Key Resources Table 278

ACKNOWLEDGEMENTS

I would like to thank my advisor, Dr. Sonya Elina Neal. You are such a kind, comforting, and strong woman – a definite role model of mine. You have taught me what it is to be a woman of color in academia, one who continues on despite the barriers and negative attitudes of others – one who carries her values with her into the classroom while teaching, to the bench while doing science, to the table at faculty meetings, and to the lunchroom when eating with students and colleagues. Your humanity and empathy are a few of the many qualities that make you such a great leader and mentor. I cannot count the number of times that I have felt seen, heard, comforted, motivated, and inspired by you. Thank you. I cannot repay you enough, but I will try to by treating my future students and mentees the way I have seen you treat us all so kindly and authentically.

I would also like to thank current and former Neal lab members, the ones that have helped me through graduate school. I would especially like to thank Dr. Rachel Kandel Green and Jasmine Jung. Rachel, you have honestly helped me the entire way through graduate school. You were my peer mentor from day one, helped me in lab daily, and even after you graduated. You even gifted me my graduation regalia that I will treasure dearly. It is a true prize for me as it shows just how much you have helped me from day zero all the way to the end. Jasmine, you were a constant positive force for me in the lab and I enjoyed learning with you. I am so glad that I was able to laugh, cry, be silly, and even Pvolve with you during graduate school. I always felt seen and comfortable expressing myself around you, thank you. Still, I have no doubts that you will rule the world one day.

A special thank you to my cohort-mates. Especially, Christina Liem, Emily Armbruster, and Chloe Welch. Christina, you are a real contemporary of mine, and you were always there to support me when I did not feel I belonged in graduate school. Your support went as far as our “If You Dropout, I Dropout Pact,” that in recent times, has transformed to an “If I Graduate, You Graduate Pact.” See you soon, Doctor! Emily, you are one of the wisest and most compassionate people I know. I much enjoyed our walks and teatime, and you always understood me. The amount of knowledge of science and the world astounds me and you inspire me dearly. I cannot wait to call you Doctor, too! Chloe, you are a real and down-to-earth scientist and human being. Thank you for hanging out with me, running errands, and just existing with me in such a safe space you created for us. Your aptitude for science and mentorship is incredible, and I know that your past, current, and future mentees see you as a gem, as I do, too. I know I will be calling you Doctor soon, too!

I would also like to share a special thank you to the family at the Raza Resource Centro, Dr. Omar Padilla, Cristian Fuentes Hernandez, and Dr. Gerardo “G” Arellano. I found a haven at the RRC where I could exist in all my identities, especially my Latina one. Omar, you cheered for me from the beginning and even pushed me to embrace my candidacy title when I advanced. You were one of the first people to call me Doctora, and I thank you for that. Whenever I doubted myself, you reassured me that I would make big moves no matter what. Cristian, thank you for being you. I was able to karaoke with you during our down time and be dramatic like the señoras from telenovelas. G, thank you for all the opportunities you gave me. You always hyped me up to your colleagues and spoke about me in such big language, that I started to believe I was “big potatoes.” I always felt respected when you would acknowledge us all as “scholars,” which is why I have adopted the word, too, thank

you. Another thanks to Dra. Marisol Cuong and Dra. Jessica Aguilar. You are both powerful, inspirational Latinas, and if it were not for you, I would have never found the RRC as home. Thank you so much.

Thank you to my committee members, Dr. Randy Hampton, Dr. Maho Niwa, and Dr. Samara Reck-Peterson. I appreciate all the input into my project, and you have all done so much to strengthen the direction of this work. I also would like to thank you for the flexibility and empathy that you have shown me this last year as I worked to finish my training despite personal circumstances. Had you all not been so willing to work with me, I do not believe that this dissertation would have happened. Thank you. I would also like to thank our collaborators listed within each chapter of this dissertation.

A special shoutout to Dr. Emily Grossman – I would like to be such a caring and spunky lecturer as you are. Being your instructional assistant was so rewarding and fun. I strive to have students that see me the way that your students see you. You are so down-to-earth with your students that it fosters such a brave space for students.

I would also like to thank some friends that have helped support me: Eleazar Martinez and Laura Bustos, Aaron JJ Lemus, Miranda Luque, Armen Khanbabaei, and Leonardo Gama. All of you have hyped me up more times than I can count, knew that I could do it, and provided the support only friends can provide. And to Leon Martinez, my Godson, I know you cannot read or talk just yet, but thinking of you has always helped me push through so that

one day I can hear you call me Nina Dr. Neets. I hope to serve as the role model you deserve.

To my CSUN mentors Dr. Jonathan Kelber, Dr. Maria Elena Zavala, and Dr. Maria Elena de Bellard. Dr. Kelber and Dr. Zavala, you helped form the basis of my scientific pathway and Dr. de Bellard, you helped me continue it. To the CSU community, I have always felt supported by you, especially by CSUPERB and CSU CDIP. Having gone through the CSU system, I now understand the power that the system has and its strength in building a positive and diverse community. I am proud to be a CSUN and CSU alum.

I would also like to thank Dr. Hercilia Corona, without whom I certainly would not have made it through graduate school. You have always looked out for my best interest, listened to me, and understood me even when I did not. Thank you for all your time and conversation.

I would also like to thank my family for all the unconditional love and support. My parents, Juan, Waldo, Juli, and James have all been a great support and I could not thank them enough. You all have had the utmost confidence in me and never questioned that I would reach my goals. That unconditional love, support, and pride helped me keep going even when I thought I wouldn't be able to finish. Thank you so much for everything, and I love you all.

Lastly, I would like to thank Stormtrooper "Kitty" Aguayo and Laika Whitney Aguayo. Kitty, you are the best cat ever and although we do not always like the lizards you bring in,

we appreciate the gesture. And thank you for always letting me scratch your “lickey button.” Laika, my fur child and dog baby, I would like to thank you for all the times when I felt that no one else was around; You were always there to follow me, grunt at me, lick me, beg for pets or treatos, or remind me to go outside, slow down, and lie down in some grass. My favorite times are always when it is just me and you walking, playing, or lounging around. You are my best friend, and I could not have done it without you. What will our next adventure together be?

Chapter 1 is a literature review by the dissertation author. The author would like to thank all the scientists and scholars who investigated and documented all their findings so that the dissertation author could read, learn, and support her own work with them.

Chapter 2, in full, is a reprint of the material as it appears in PLOS Biology, 2023, Kandel, R; Jung, Jasmine; Syau, Della; Kuo, Tiffany; Songster, Livia; Horn, Casey; Chapman, Claire; Aguayo, Analine; Duttke, Sasha; Benner, Chris; Neal, Sonya E, PLOS Biology 2023. https://doi.org/10.1371/journal.pbio.3001950. The thesis author was a contributing author on this paper. The authors would like to thank Tom Rapoport (Harvard Medical School), Davis Ng (National University of Singapore), Randy Schekman (University of California, Berkeley), Susan Michaelis (John Hopkins University), and Jeff Brodsky (University of Pittsburgh) for providing plasmids and antibodies. We also thank the Neal lab members for their positive reinforcement, in depth discussions, and technical assistance. This work was supported by the National Institutes of Health (1R35GM133565 to SEN; R00GM135515 to SD), the National Science Foundation (2047391 to SEN), and the Pew Charitable Trusts (34089 to SEN). The funders had no role in study design, data collection and analysis, decision to publish, or preparation of the manuscript.

Chapter 3, in full, is a reprint of the material as it appears in Bhaduri, S., Aguayo, A., Ohno, Y., Proietto, M., Jung, J., Wang, I., Kandel, R., Singh, N., Ibrahim, I., Fulzele, A., Bennett, E. J., Kihara, A., & Neal, S. E. (2023). An ERAD-independent role for rhomboid pseudoprotease Dfm1 in mediating sphingolipid homeostasis. *The EMBO journal, 42*(4), e112275. https://doi.org/10.15252/embj.2022112275. The dissertation author was a primary investigator and a first author of this material. The authors would like to thank Peter

Espenshade (Johns Hopkins Medicine), Oliver Schmidt (Medical University of Innsbruck), David Teis (Medical University of Innsbruck), Teresa Dunn (National Institutes of Health), Jim Wilhelm (University of California, San Diego), and Peter Novick (University of California, San Diego) for providing plasmids, yeast strains, antibodies. We thank Dr. Oswald Quehenberger from the UCSD Lipidomic Core Facility for performing lipidomic analysis. We also thank Dr. Maho Niwa, Dr. David Teis, Dr. Oliver Schmidt, and the Neal lab members for in-depth discussions and technical assistance. These studies were supported by NIH grant 1R35GM133565-01, Pew Biomedical Award 34089, and NSF CAREER grant 2047391 (to S.E.N), NIH grants 5R01GM136994-02 and DP2GM119132 (to E.J.B), HHMI Gilliam Fellowship GT15096 (to S.E.N and A.A.), and KAKENHI grant JPSSH04986 (to A.K.).

For Chapter 4, the author would like to thank the Randolph Hampton (University of California, San Diego), and Jim Wilhelm (University of California, San Diego) Labs for providing plasmids and yeast strains, and the Andreas Ernst Lab (University of California, San Diego) for providing microscope and imaging support for this study. A special thanks to William R. Wegeng (Andreas Ernst; University of California, San Diego) for technical assistance, imaging discussions, and scientific feedback; to Christina R. Liem for positive reinforcement, in-depth scientific discussions, and technical assistance; and to the Neal Lab members who offered positive scientific discussions, feedback, and reinforcement. A special thanks to Dr. Rachel R. Kandel, Jasmine L. Jung, and Chloe J. Welch for supporting the writing of this study. The author would also like to thank Dr. Maho Niwa Rosen, Dr. Samara Reck-Peterson, and Dr. Randolph Hampton for scientific guidance. These studies were supported by NIH grant 1R35GM133565-01, Pew Biomedical Award 34089, and NSF CAREER grant 2047391 (to S.E.N), NIH grants 5R01GM136994-02 and DP2GM119132 (to

E.J.B), HHMI Gilliam Fellowship GT15096 (to S.E.N and A.A.), and CSU CDIP Fellowship (to A.A.). The funders had no role in study design, data collection and analysis, decision to publish, or preparation of this study.

VITA

2019 B.S. in Cellular and Molecular Biology, California State University Northridge

2024 Ph.D. in Biology, University of California San Diego

Thesis advisor: Sonya Neal

PUBLICATIONS

Bhaduri, S., **Aguayo, A.**, Ohno, Y., Proietto, M., Jung, J., Wang, I., Kandel, R., Singh, N., Ibrahim, I., Fulzele, A., Bennett, E., Kihara, A., Neal, S., An ERAD-independent role for rhomboid pseudoprotease Dfm1 in mediating sphingolipid homeostasis. *EMBO Journal* (2022)

Kandel, R., Jung, J., Syau, D., Kuo, T., Songster, L., Horn, C., Chapman, C., **Aguayo, A.**, Duttke, S., Benner, C., Neal, S., Yeast Derlin Dfm1 Employs a Chaperone-Like Function to Resolve Misfolded Membrane Protein Stress. *PLOS Biology* (2023)

ABSTRACT OF THE DISSERTATION

Small but mighty rhomboid pseudoprotease Dfm1 mediates a novel role in regulating lipid homeostasis and proteotoxic stress

by

Analine Aguayo

Doctor of Philosophy in Biology

University of California San Diego, 2024

Professor Sonya Neal, Chair

In biological systems, efficient folding and assembly is necessary for cell health and longevity. Nascent proteins are initially targeted to the endoplasmic reticulum (ER), where they are correctly folded and assembled before being delivered to their final cellular destinations. When proteins are not folded correctly, the proteostasis network (PN) acts to degrade the aberrant proteins, and thus, prevent cellular stress. The PN is a complex network of different proteins, multiple organelles, including the ER, Golgi, endolysosomal

system, lipids, and degradation pathways that work in concert to maintain protein homeostasis.

An ER-resident protein and member of the rhomboid protein family, Dfm1, has been found to be required for the identification and degradation of misfolded membrane proteins at the endoplasmic reticulum (ER), along with having various other functions including substrate binding, lipid thinning, and AAA-ATPase recruitment. Dfm1 is a well-studied protein; however, not all its biological functions are known. Using genetic, protein, and biochemical approaches in *Saccharomyces cerevisiae*, this dissertation describes our original work in demonstrating Dfm1 as a chaperone-like protein that does not require recruitment of the ATPase Cdc48, a finding distinct from Dfm1's previously identified function in dislocating misfolded membrane proteins to the cytosol for degradation in ER-associated degradation (ERAD). Additionally, we establish another independent and novel role of Dfm1 in the sphingolipid biosynthesis pathway. Here, Dfm1 facilitates sphingolipid homeostasis by exporting phosphorylated Orm2, a key sphingolipid biosynthesis regulating enzyme, from the ER which results in the degradation of Orm2 through Endosome and Golgi-Associated Degradation (EGAD). Additionally, it has been found that lipid and protein homeostasis are tightly linked, so this work aims to develop a holistic system for further investigation of Dfm1's role in regulating sphingolipid biosynthetic enzymes. Taken together, this dissertation highlights Dfm1's extensive role in chaperone-like regulation of membrane protein aggregation stress and its novel role in sphingolipid biosynthesis. Given that the accumulation of aberrant misfolded proteins and dysregulation of sphingolipids are associated with various pathologies, this study serves as a molecular foothold for understanding how dysregulation of proteins and sphingolipid metabolism leads to various diseases.

Chapter 1: Introduction

1.1 Protein homeostasis is essential for cell survival

Proteins exist in all living cells as macromolecules responsible for necessary cellular functions. These functions include participating in signaling cascades, enzymatic reactions, and providing structural integrity and functional support to the cell. It is estimated that at any given time, a *Saccharomyces cerevisiae*, or baker's yeast, cell can have 5×10^7 protein molecules (Futcher et al., 1999). The number of protein molecules in any given cell may change as proteins are constantly being made, degraded, recycled, and being transported in and out of the cell. Given that a cell's proteome changes constantly, especially during development or environmental stresses like nutrient starvation (Xia et al., 2022), cells are known to have several protein quality control (PQC) mechanisms to maintain proteostasis, or protein homeostasis. Other instances that may alter proteostasis include organellar stress like ER (Logue et al., 2013; Schröder et al., 2005; Yoshida et al., 2007) and Golgi stress (Eisenberg-Lerner et al., 2020; Kim et al., 2023; Schwabl and Teis et al., 2022), chemical stress (Lindquist and Kelly et al., 2011; Powers et al,, 2009), aging (Min et al., 2010), and faulty protein turnover (Basisty et al., 2018; Cuanalo-Contreras et al., 2013).

Collectively, these intrinsic PQC mechanisms are termed the proteostasis network (PN) (Jayaraj et al., 2020). PQC mechanisms act as cellular protein surveillance networks that monitor protein quality and quantity through the protein life cycle. These mechanisms function to regulate proteins from their initial biosynthesis by ribosomes, to their folding in the ER, processing and modifications at the Golgi apparatus, trafficking and conformational maintenance at their cellular function sites, and finally, their recycling or degradation (Webster et al., 2020). The PN acts as a continuous checkpoint and maintenance network for protein confirmation, amount, location, and degradation once a protein's role is fulfilled or is no longer needed (Jayaraj et al., 2020). The PN includes all cellular factors that are required to maintain protein homeostasis and amounts to about 2,000 components in eukaryotes - about 850 of which are part of the ubiquitin proteasome system (UPS) (Klaips et al., 2018). A significant role of PQC mechanisms, and one that this study focuses on, is the role that PQC mechanisms play in degradation of misfolded, or aberrant proteins. A cell's ability to act accordingly to aberrant proteins is essential, as unchecked proteins can aggregate and lead to detrimental proteotoxic stress, or the accumulation of impaired or misfolded proteins (Haeri et al., 2012; Rao et al., 2004). In humans, this can manifest as different maladies, including neurodegenerative diseases (Lindholm et al., 2006) like Alzheimer's Disease (AD), Parkinson's Disease (PD), and Huntington's Disease (HD) (Roussel et al., 2013; Shacham et al., 2019), as well as certain cancers (Tax et al., 2019).

Protein degradation within eukaryotes occurs primarily by ubiquitination events that target proteins to one of two broader degradation systems, the ubiquitin proteasomal system (UPS) or the autophagy-lysosomal pathway (ALP) (Jayaraj et al., 2020). This chapter will describe these pathways as they relate to different PQC mechanisms within the cell's various compartments.

1.1.1 Proteostasis network (PN) works through protein synthesis, maintenance, and degradation

Cells constantly synthesize proteins from polypeptide building blocks and must do so in an efficient manner. Studies show that ribosomes can condense polypeptides together at a rate of 5.6 amino acids per second to build polypeptide chains (Ingolia et al., 2011). This process of synthesizing proteins is in fact error-prone with a misincorporation rate of 1 in 10^4 amino acids (Zaher & Green et al., 2009). Errors in protein synthesis can be from transcriptional errors due to misincorporation or deletion events, or splicing errors due to defective messenger RNA. In times of mistranslation of proteins, ribosome-associated quality control (RQC) (Brandman & Hegde et al., 2016) will activate the UPS to degrade the mistranslated proteins, and thus, prevent the aggregation of non-functional proteins and subsequent proteotoxic stress (Choe et al., 2016). The proteostasis network can also work to combat cellular stress by halting or decreasing protein production at ribosomes, for example, when there is a lack of transfer RNA leading to an aggregation of synthesized proteins (Spriggs et al, 2010).

The proteostasis network also involves mechanisms that utilize chaperone and structural support proteins to help maintain protein structure and function. One of the most recognized family of proteins in the proteostasis network is the heat shock protein (HSPs) group, as they are well conserved and initiated during heat stress and sensitivity. Disaggregases are another type of PN proteins that work to dissolve protein aggregates through disassembly of the aggregates, allowing for subsequent mechanisms to access and degrade the proteins (Mogk et al., 2018). Hsp104 is a well-known disaggregase in yeast that has important implications in delaying neurodegenerative disease progression by fragmenting amyloidogenic aggregates in the brain (Knier et al., 2022). Hsp104 functions with Hsp40 and Hsp70 to reactivate denatured proteins, ultimately clearing aggregated proteins (Glover & Lindquist, 1998; Mogk et al., 2015).

A substantial portion of the PN consists of the mechanisms in the cell that work on maintaining steady-state proteomic levels, or when metabolic balance is reached and constant in living systems (Nelson et al., 2008). If a cell is not in proteostatic balance and has an over-abundance of misfolded or aggregated proteins, the PN will activate the ubiquitin proteasome system or the autophagy-lysosomal system accordingly. See section 1.3 and 1.4 for proteasomal and vacuolar degradation routes, respectively.

1.1.2 Combating proteotoxic stress via proteostasis network degradation pathways

When cells are unable to clear misfolded and aberrant proteins, they accumulate and proteotoxic stress builds. The cell has several protein quality control checkpoints within the cell apart from the ubiquitin proteasome system (UPS) and autophagy-lysosome pathway (ALP). This chapter will describe different PQC systems in different compartments including vacuolar protein sorting (VPS), adapter protein-3 (AP3), Golgi membrane-associated degradation (GOMED), and endosome and Golgi-associated degradation (EGAD) systems at the Golgi; inner nuclear membrane-associated degradation (INMAD) and San-1 dependent degradation at the nucleus and perinuclear cytoplasm; endoplasmic reticulum associated degradation (ERAD), unfolded protein response (UPR), and endoplasmic reticulum stress surveillance (ERSU) at the ER; autophagy at the vacuole; and the broader UPS and ALP systems.

1.2 Degradation routes of the cell

The total amount of proteins in any eukaryotic cell is tightly regulated, not only by the amount of synthesis, but also by how much protein degradation occurs (Cooper et al., 2022). It is specifically important for cells to degrade proteins in an elaborate, yet energy efficient manner, as reusing amino acids and polypeptides from degraded proteins saves the cell energy (Gustafsson et al., 2008). These degradation events may be especially important in alleviating cellular stress, since accumulated proteins meant for degradation may alter the internal functions of cells. Proteins marked for degradation can be due to their improper structure or misfolding, stress due to UV or chemical exposure, or a cell no longer requiring more of the specific protein. Additionally, orphan proteins, or proteins that have not been able to associate with their interacting proteins in complexes, may also need to be degraded as their function relies heavily on the complexes to which they are no longer a part of (Juszkiewicz & Hegde et al., 2018). Moreover, the tightly regulated process of protein degradation is particularly important in regulating cellular feedback loops, gene expression, quality control proteins, and proteins responsible for cell proliferation and division cycles. For example, Cyclin B, a member of the cyclin family and subunit of the M phase-promoting factor (MPF) complex responsible for nuclear segregation and DNA replication events of mitosis and meiosis, holds a significant role in both positive and negative feedback loops of cell division and proliferation. When cell division is no longer necessary, the Cyclin B-Cdk1 complex is ubiquitinated and degraded through the Anaphase-promoting complex or cyclosome (APC/C) branch of the proteasomal inner nuclear membrane-associated degradation (INMAD) pathway, negatively regulating M phase in cells (Tsai et al., 2014).

The route by which proteins are degraded varies vastly by the type of protein the degradation candidate is, its location, and where the degradation products will be needed or reused. Although there are various routes and pathways by which proteins are degraded in eukaryotic cells, there are two primary terminal degradation pathways by which all degradation pathways and products are ultimately degraded by: the ubiquitin proteasome system (UPS) and autophagy – in plants and animals, autophagy occurs in the lysosome, and in yeast, within the vacuole (Li et al., 2022).

1.2.1 Ubiquitin processing marks substrates for degradation

It is estimated that about 80-90% of proteins are degraded by the ubiquitin proteasome system, including misfolded, abnormal, denatured, short-lived, damaged (Rock et al., 1994) and soluble proteins (Groll et al., 2003; Klionsky et al., 2007). Autophagy is responsible for degrading the remainder of the proteins, including long-lived, aggregated proteins and certain organelles like the mitochondria, peroxisome, ribosomes, insoluble proteins, or infectious material like viruses that may enter a cell (Chen et al., 2019; Lilienbaum et al., 2013). Multi-vesicular bodies (MVB), or acidic endocytic organelles defined by numerous lumenal vesicles (Buzuk & Hellerschmied, 2023), all autophagy to degrade larger and aggregated proteins (Clague & Urbé et al., 2008) to be degraded. UPS, however, relies on Cdc48, an AAA-ATPase known to unfold smaller substrates and translocate them through its small core to the 20S chamber of proteasomes, for degradation and therefore, cannot degrade such large proteins (Yin et al., 2016).

Although these two pathways are distinct, they have some overlap in protein members, like ubiquitin ligating molecules and the small linking protein and marker of protein aggregates, p62 (Stolz et al., 2014). Of note, the two pathways overlap in terms of substrate ubiquitination, proteasomes themselves being degraded via autophagy (termed proteaphagy), and the way by which each pathway can serve as compensatory role for the other in times of stress or change in homeostatic state (Kocaturk et al., 2018). The proteasomal and autophagy-lysosome pathways have been known to compensate for one another specifically in times of nutrient starvation, ER stress, oxidative stress, and during dysregulation of mitochondrial dynamics (Dikic et al., 2017).

The major similarity between the two terminal degradation pathways in cells is the use of the molecule ubiquitin. Ubiquitin is a 76 amino acid polypeptide highly conserved in all eukaryotes (Hershko et al., 1998) and serves as the main degradation signal in cells when it attaches to a target protein's lysine or methionine residue (Ciechanover, 2005). Ubiquitin is covalently attached to substrates by multiple enzymatic reactions catalyzed by E1 ubiquitin activating enzymes, followed by ubiquitin conjugating enzymes (E2), and then E3 ubiquitin ligases that hydrolyze the addition of the ubiquitin molecule to the substrate targeted for degradation (Kandel et al., 2023; Zhao et al., 2022). More specifically, E1 activates ubiquitin in an ATP-dependent manner and then transfers the ubiquitin to the E2 molecule, which is then transferred to the substrate by an E3 (Molineaux, 2012). Interestingly, E3 ligases make up the largest group of proteins in the proteostasis network, with about ~850 proteins of the estimated 2000 total proteostasis network members (Li et al., 2008). E3 ligases are the most abundant of the ubiquitin cascade; there are over 600 E3 ligases (Liu et al., 2023), ~40 E2 ligases (Stewart et al., 2016), and only 8 E1 ligases in humans (Barghout et al., 2021). This trend is conserved across all eukaryotes.

Even before the degradation of ubiquitinated substrates, they must be identifiable. This happens when degrons - or stretches of proteins with chains of hydrophobic residues that are not normally exposed in cytoplasm - are exposed and recognized by E1 ligases (Hickey et al., 2021). Then the E1/E2/E3 ubiquitin cascade continues to target substrates for degradation.

Polyubiquitin events also occur where ubiquitin molecules are continuously added to a target protein and form ubiquitin chains. These polyubiquitin chains or branches are known to recruit specific ligases by their very distinct confirmations and amount of ubiquitin molecules involved (French et al., 2021; Morimoto et al., 2015; Xu et al., 2009). Polyubiquitin chains can stem from conjugations of ubiquitin at different lysine residues and a methionine residue. Polyubiquitin chains are named based on the residue of the ubiquitin molecule that is conjugated. Known polyubiquitin chains include K6, K11, K27, K29, K33, K48, K63, and M1 which is located at the N-terminal methionine (Fiil & Gyrd-Hansen, 2014; Tracz & Bialek, 2021). K48 and K63 are the most abundant ubiquitination conjugations. K48 ubiquitin chains are known signals for proteasomal degradation and account for about 80% in mammals, whereas K63 ubiquitin chains signal for lysosomal degradation and inflammatory response (Zhao et al., 2022).

When degradation of certain substates is not necessary anymore, deubiquitinating enzymes (DUBs) work to stabilize proteins by trimming or removing ubiquitin chains via hydrolysis of the isopeptide bond between polyubiquitin chains or between ubiquitin molecules and the given degradation substrate (Franić et al., 2021). This hydrolysis reaction in turn halts the degradation of substrates. There are 20 known DUBs in the yeast genome that reside in the ER, cytoplasm, and mitochondria, including Ubp6 and Rpn11, known to be associated with Cdc48 (Suresh et al., 2020). Deubiquitinases play a vital role in balancing the ubiquitome, regulating ubiquitin chain lengths, and modulating degradation within the UPS (Lee et al., 2011; Yao & Cohen, 2002). DUBs also have unique specificity as ubiquitinases do; DUBs show specificity towards the types of ubiquitin linkages they break down and whether they make single breaks in chains or break them down completely to monomeric ubiquitin for ubiquitin recycling (Clague et al., 2019; Kandel et al., 2023; Mevissen & Komander, 2017).

It is important to note that ubiquitin is not the only small protein known to mark proteins for degradation. Ubiquitin-like proteins (UBLs) are also expressed in mammals and serve similar roles, like the small-ubiquitin-related modifier (SUMO) and NEDD8 that play a role in SUMOylation and NEDDylation, respectively (van der Veen et al., 2012). Although UBL and SUMO molecules play a key role in protein degradation, this dissertation focuses on ubiquitin-mediated protein degradation alone.

1.3 Proteasomal degradation and associated pathways

The 26S proteasome is a specialized organelle and protein complex known to be responsible for degrading most cellular proteins (Gomes et al., 2005; Zong et al., 2013), and is made up of a 20S core comprised of 4 7-subunit rings (Groll et al., 1997) and 19S caps on either side of the 20S core (Hilt & Wolf, 1995). Unfolded proteins can only enter the 20S (Nandi et al., 2006) and provide the complex with trypsin-, chymotrypsin-, and caspase-like proteolytic activity (Groll et al., 1999). The 19S caps provide the ATPase activity necessary for protease cleavage into peptide fragments for the complex (Hough et al., 1987). The 19S caps are also responsible for changing the gate of the 20S core to an open conformation (Groll et al., 2000; Köhler et al., 2001; Smith et al., 2005). Proteasomes are primarily located in the cytoplasm and nucleus, and recently shown to associate closely with the Golgi (Benyair et al., 2022; Eisenberg-Lerner et al., 2020). Organelles have specific pathways for shuttling their degradation substrates to be degraded by proteasomes. The following sections cover the different routes by which substrates are transported to the proteasome for degradation.

1.3.1 Inner nuclear membrane-associated degradation (INMAD)

The nucleus, apart from the cytoplasm, is one of the main locations of cellular proteasomes and has its own PQC mechanisms (Nielsen et al., 2014) for upholding protein homeostasis. It has been shown that in yeast, during certain events like cell proliferation, most proteasomes are found near the nucleus (Russell et al., 1999). In yeast, the nuclear PQC pathways include inner nuclear membrane-associated degradation (INMAD) and San-1-mediated protein quality control (Franić et al., 2021).

In eukaryotic cells, the nuclear envelope (NE) is a double lipid bilayer consisting of the inner nuclear membrane (INM) and the outer nuclear membrane (ONM) that together enclose the nuclear contents (Franić et al., 2021). These two membranes are joined by nuclear pore complexes that consist of multiple proteins in a pore-like confirmation, that allow transport from the cytoplasm to the nucleus usually by passive transport (Wilson et al., 2010). The INM bilayer is lined with Lamin intermediate filaments and proteins, distinct from that of the plasma membrane (Gruenbaum et al., 2015; Schirmer et al., 2007).

The most prominent degradation pathway of the nucleus is INMAD, which relies heavily on the attachment of ubiquitin molecules to candidate degradation substrates. The main E3 ubiquitin ligases responsible for ubiquitinating substrates in INMAD are Asi1-3, Doa10, and APC/C (Franić et al., 2021). INMAD primarily degrades nuclear proteins normally embedded in the inner nuclear membrane, while San-1 dependent degradation, another nuclear degradation pathway, degrades cytosolic proteins within the nucleus.

There are three different complexes/pathways by which INMAD functions to degrade substrates: the Asi1-Asi3 complex, the Doa10 complex, and the APC/C complex. The Asi1-3 complex comprises E3 ligases Asi1 and Asi3, and Asi2, an adapter protein. It is the main complex that ubiquitinates INMAD substrates for subsequent degradation. Asi1 and Asi3 are homologous INM proteins with five transmembrane domains each and a C-terminal RING domain towards the nucleoplasm (Khmelinskii et al., 2014; Natarajan et al., 2020). Substrates normally targeted by INMAD include proteins mislocalized to the INM from other organelles or the cytoplasm, orphan subunits or complexes, and temperature sensitive mutants (Franić et al., 2021). For substrates that the Asi complex cannot degrade, like certain temperature sensitive proteins, the Doa10 complex may help degrade these substrates.

Doa10 (degradation of alpha2) is an integral membrane E3 ubiquitin ligase mostly known for its role in ERAD (Carvalho et al., 2006; Habeck et al., 2015; Hampton & Garza et al., 2009; Mehrtash & Hochstrasser et al., 2022; Neal et al., 2020; Schmidt, Vasic, & Stein, 2020; Wu et al., 2024), but also serves a large role in degrading INMAD substrates. Doa10 has known functional similarities to another E3 ligase involved in ERAD, Hrd1. Hrd1, however, does not localize to the INM and therefore does not serve a role in INMAD. Doa10 normally recognizes degrons in the cytoplasm or in the membrane spanning regions of transmembrane proteins, (Mehrtash & Hochstrasser et al., 2006; Ravid et al., 2006; Swanson et al., 2001) and has an N-terminal RING domain (Hassink et al., 2005). Doa10 substrates marked to be degraded also rely on subsequent degradation by the proteasome and assistance by the Cdc48 complex (Ravid et al., 2006).

The Anaphase-promoting complex or cyclosome (APC/C) (Koch et al., 2019) is an E3 ligase complex which functions by interacting with two co-activators, Cdc20 and Cdh1, to specifically degrade Msp3, a conserved integral INM protein known to associate with the spindle pole body. Msp3 is a yeast protein important in cell cycle progression, much like the centromere in vertebrates (Conrad et al., 2007; Friederichs et al., 2011; Jaspersen et al., 2002). APC/C functions primarily by recognizing its substrates by short linear sequence motifs like the D and KEN boxes (Davey et al., 2016).

After an INMAD substrate is passed through the Asi1-3, Doa10, or APC/C complex, the substrate is then translocated to the inner nuclear space where it is degraded by the resident nuclear proteasomes.

1.3.2 San-1-dependant degradation

San1 is a nuclear localized E3 ligase with a RING domain that degrades misfolded and aberrant proteins in the nucleus (Franić et al., 2021), primarily those with long chains of hydrophobic peptides that lead to high insolubility and aggregation (Frederickson et al., 2011; Frederickson et al., 2013). San1 substrates include truncated proteins, and temperature sensitive nuclear proteins like Sir4-9 and Cdc68-1 (Dasgupta et al., 2004; Evans et al., 1998; Gardner et al., 2005). San1 can bind a broad range of proteins due to its large unstructured N- and C- terminal domains (Rosenbaum et al., 2011) as these domains allow San1 to be flexible (Dunker et al., 2008). San1 however does not work alone, it has been shown to require chaperones Ssa1 and Ssa2. These chaperones facilitate interactions between San1 and degradation substrates by maintaining their solubility. Cdc48, also functions in a comparable manner with San1, to aid in substrate solubility and recognition (Gallagher et al., 2014; Guerriero et al., 2013).

San1 has also been shown to help degrade substrates from the cytoplasm, but the degradation mechanism is unknown. Studies show that another E3 ligase known to degrade cytoplasmic substrates, Ubr1, may aid in this degradative role (Varshavsky et al., 2011). Studies show *san1*Δ*ubr1*Δ yeast strains result in fully stable cytoplasmic misfolded protein, CPY*, highlighting the interplay between San1 and Ubr1 necessary for degrading cytoplasmic misfolded proteins (Heck et al., 2010; Wolf et al., 2006).

There are three distinct requirements for the degradation of misfolded nuclear and cytoplasmic proteins: either a nuclear export signal (NES) or nuclear localization signal (NLS) and a K11- or K48-linked ubiquitination chain (Samant et al., 2018). San1-dependent K48-mediated linkages are specifically needed for nuclear substrates.

Although San1 and INMAD are efficient at degrading cytoplasmic and nuclear substrates efficiently, at times this machinery can be overloaded, especially in times of extra proteotoxic stress – in which case, proteins become sequestered into intranuclear quality control compartments (INQ). In yeast, INQs were initially termed juxtanuclear quality control compartments (JUNQ), since they were originally said to be structures at the outer side of the nuclear envelope (Kaganovich et al., 2008). Since the distinction between JUNQ and INQ are still unclear, the structures are sometimes called JUNQ/INQ (Hill et al., 2016). JUNQ/INQ inclusions require the nuclear chaperone Btn2 and cytoplasmic chaperone Hsp42, a specific aggregase that promotes the formation of the inclusions in the nucleus and cytosol, respectively (Specht et al., 2011).

1.3.3 Endoplasmic reticulum associated degradation (ERAD)

The endoplasmic reticulum (ER) is one of the largest organelles, second only to the nucleus (Lodish et al., 2000). It has two components: the rough endoplasmic reticulum (RER) and the smooth endoplasmic reticulum (SER) (Shibata et al., 2006). The RER plays a role in the synthesis of proteins as ribosomes associate with it, and the SER plays a role in creation and storage of lipids and steroids (Schwarz & Blower et al., 2016). More specifically, the ER is responsible for calcium storage, controlling the turnover of lipid biosynthetic enzymes, and regulating lipid compositions, as well as sterol homeostasis (Krshnan et al., 2022). In humans, dysfunctions within the ER lead to neurodegenerative diseases (Lindholm et al., 2006) like Alzheimer's Disease (AD), Parkinson's Disease (PD), Huntington's DIsease (HD) (Roussel et al., 2013; Shacham et al., 2019), and certain cancers (Tax et al., 2019). To avoid such catastrophic consequences, the ER has quality control mechanisms to help alleviate effects of improper ER function. One such quality control pathway is endoplasmic reticulum associated degradation (ERAD).

ERAD functions to maintain proteostasis by degrading surplus protein complex proteins (Knopf et al., 2020), mislocalized orphan proteins (Juszkiewicz et al., 2018), and by eliminating misfolded proteins (Kandel & Neal, 2020). ERAD has also been shown to control ER to mitochondria contact sites (Zhou et al., 2020). ERAD's primary role is to degrade misfolded proteins in a four-step process, which includes: 1) recognition of misfolded proteins by ERAD machinery, 2) ubiquitination of misfolded proteins, 3) retrotranslocation of ubiquitinated substrate from the ER to the cytosol (a process known as retrotranslocation), and 4) degradation by the proteasome system (Vembar et al., 2008).

In yeast, there are three branches of ERAD, specified by where the lesion is located on the misfolded ER substrate whereas the mammalian system has been shown to have at least ten branches (Krshnan et al., 2022). The three ERAD branches in yeast are ERAD-M (lesion within the membrane), ERAD-C (lesion in a cytoplasmic domain), and ERAD-L (lesion in a luminal ER protein) (Zhang et al., 2019). The E3 ligases HRD1 and DOA10 mediate the degradation of ERAD-L/ERAD-M and ERAD-C substrates, respectively. Together, all branches of ERAD provide the mechanisms to sustain protein homeostasis at the ER. Recently, INMAD has also been seen as an extension of ERAD (Smoyer & Jaspersen, 2019) due to its location, similar mechanisms, and sharing of target substrates, like the yeast chitin synthase, Chs3 (Sanchez et al., 2023). This idea of identifying INMAD and ERAD as extensions of the same pathway, however, is still a debate due to their distinct mechanisms (Koch & Yu, 2019).

Rhomboids, a specific superfamily of proteins, have been known to fulfill a key role in ERAD. Dfm1, a pseudoprotease of the family, has several conserved motifs that allow for its function in ERAD. One of these motifs is the SHP box, which is a cytoplasmic tail consisting of two 8-residue sequences shown to be responsible for recruitment of the ATPase Cdc48 (Simões et al., 2018) and it is required for retrotranslocation of substrates (Neal et al., 2017; Sato & Hampton, 2016; Twomey et al., 2019). Two other features are conserved rhomboid protein-specific domains, the WR domain and the GX_3G domain (Bergbold et al., 2013; Fleig et al., 2012; Grennblatt et al., 2011; Lemberg & Adrain, 2016; Neal et al., 2018). Additionally, our lab recently identified four key polar residues in TMD2 of Dfm1 necessary for lipid thinning, and three residues in its first luminal loop necessary for substrate binding (Nejatfard et al., 2021). Although much is known about Dfm1's function in ERAD, our research highlighted in this dissertation provides insights into Dfm1's ERAD independent roles in proteotoxic stress (Chapter 2) and regulating sphingolipid synthesis (Chapters 3 and 4).

The Endoplasmic Reticulum Unfolded Protein Response (UPR^{ER}) pathway has also been noted as an ER quality control mechanism and has specific crosstalk with ERAD, (Hwang & Qi, 2018) but does not directly degrade any misfolded proteins itself. The UPR^{ER} can be seen as an upstream sensor for translation mechanisms and activator of ERAD. It has three different ER stress sensing branches, IRE1, ATF6, and PERK, which work to inhibit protein translation, and to induce the translation of chaperone proteins and ERAD members (Bravo et al., 2013; Hetz et al., 2020) to help alleviate ER stress from aggregated misfolded proteins (Ogen-Shtern et al., 2016).

1.3.4 Endosome and Golgi-associated degradation (EGAD)

The Golgi Apparatus or Golgi body is a stacked membranous organelle known to be responsible for protein trafficking and post-translational modifications (PTMs) (Buzuk & Hellerschmied, 2023; Viotti et al., 2016), as well as protein processing, sorting, and lipid biogenesis (Mohan et al., 2023). The Golgi also sorts secretory proteins that route through the endomembrane system, to the plasma membrane, and exit the cell. The composition of Golgi varies in complexity across different organisms. Multicellular eukaryotes like plants and *Drosophila* have multiple scattered Golgi stacks within their cytoplasm and mammals have ribbon-like structures that connect the different Golgi stacks, while single-celled eukaryotes tend to only possess a single stack (Lupashin et al., 2005). In budding yeast, cells only have a dispersed Golgi (Suda & Nakano, 2012).

To fulfill its roles efficiently, the Golgi is known to have a complex quality and quantity control process that monitors proper folding, PTMs, and shipment to other organelles (Sun & Brodsky, 2019). The UPS or ALS are activated when Golgi QC proteins sense pathways sense a misfolded or aberrant protein. This sub-section will further outline the proteasomal pathways of degradation within the Golgi.

The ER and Golgi are known to play complimentary roles in protein maturation, transportation, and secretion. Secretory proteins are first folded at the ER, then transported to the Golgi though ER exit sites (ERES), and then sent out to the extracellular milleu or as different components of the cellular surface (Benyair et al., 2022). Normally, aberrant proteins at the ER and Golgi will transport in such an anterograde manner; however, it has been shown that a mutant vacuolar carboxypeptidase Y (CPY*) is cycled between the ER and Golgi (Spear & Ng, 2003) to be degraded. CPY* first travels from the ER to the Golgi, where it is sensed as aberrant, then is translocated back to the ER to be degraded by ERAD (Caldwell et al., 2001; Vashist et al., 2001). The MHC molecule and IgMμ have also been shown to retrotranslocate in a similar manner (Hsu et al., 1991).

The Golgi's participation in degradation was thought to be primarily in assistance with ERAD, lysosomal degradation or autophagy, and the endosomal sorting complexes required for transport (ESCRT) pathway. Recently, however, an independent degradation pathway, endosome and Golgi-associated degradation (EGAD), was discovered (Schmidt et al., 2019) when investigating sterol regulatory element-binding protein degradation pathway (SREBP) (Stewart et al., 2011). In fission yeast, SREBP is canonically ubiquitinated by the E3 ligase Dsc complex, then proteolytically cleaved by Rhomboid2 and Cdc48. The C-terminal cleavage product is then transported back to the ER for degradation via ERAD (Kober et al., 2020), while the N-terminal product is transported to the nucleus to serve as a sterol transcription factor (Hwang et al., 2016). In the absence of Rhomboid2 proteolytic cleavage, SREBP is still degraded, but in an ERAD-independent, Dsc-dependent manner - this pathway was termed EGAD (Schmidt et al., 2019). EGAD substrates are ubiquitinated and then degraded in a proteasome-dependent fashion without the intervention of the ER or the lysosome. EGAD has also been investigated in budding yeast. Orm2, a negative regulator of the sphingolipid biosynthetic pathway and a member of the serine palmitoyl transferase (SPT) complex, is also an EGAD substrate (Schmidt et al., 2019).

1.3.5 Golgi apparatus-related degradation (GARD)

Shortly after identifying EGAD as an ER-independent proteasomal degradation route at the Golgi, researchers identified another similar pathway in mammals that is activated solely as a morphological stress response, known as Golgi apparatus-related degradation (GARD) (Eisenberg-Lerner et al., 2020). A prime distinction of GARD from other proteasomal pathways, is that when GARD is activated, proteasomes directly associate with the Golgi (Eisenberg-Lerner et al., 2020). The Golgi tethering factor GM130 normally maintains Golgi structure and morphology. When the Golgi structure is compromised, GM130 becomes ubiquitinated, allowing for compromised Golgi to be dispersed and fractionated, alleviating the stress on the cell. This process is uniquely reversible – normally, Golgi fractionation is irreversible – leading to the restoration of Golgi integrity and deubiquitinated GM130 serving to maintain Golgi morphology again (Benyair et al., 2022).

1.4 Vacuolar degradation

The plant vacuole was discovered by Antonie van Leeuwenhoek, known as the "Father of Microbiology" in 1676, and named for its appearance as an optically empty sac, or *vacuus* (de Marcos Lousa et al., 2016). Yeast vacuoles are remarkably like mammalian lysosomes in function (*lysis*- meaning digestive in Greek and *soma*- meaning body) but hold physical characteristic distinctions. For example, mammalian lysosomes tend to be numerous and small (50-1000 per cell at a six of 0.1-1μm), while yeast vacuoles are larger, about 5μm in size and account for about 20% of a cell's volume (Hecht et al., 2014). Yeast vacuoles are also usually unique or one of few within the yeast cells (Bergeland et al., 2001) and normally exist as multi-lobular organelles during log-phase growth (Wiemken et al., 1970). Only when in stationary phase, or during stress events, do yeast vacuole lobes fuse together to form a single vacuole, focused on hydrolyzing proteins for amino acid recycling (Thumm, 2000). Both organelles must be slightly more acidic than the cytoplasm to carry out their many hydrolytic functions. In yeast, the average vacuole has a pH of about 6.2, whereas yeast cytosol is known to have a pH of about 7 (Brett et al., 2011).

Vacuoles and lysosomes hold remarkably similar, if not the same, roles. As this dissertation focuses on yeast cells, vacuolar roles will also be highlighted. The vacuole's leading role is its degradation of macromolecules and proteins such as those that have become senescent, superfluous, or damaged (Hecht 2014). Proteins are transported to the vacuole by selective and non-selective pathways. The main degradation mechanism of the vacuole is autophagy in a cytoplasmic-to-vacuole mechanism (Teter & Klionsky, 2000). The vacuole also participates in golgi-to-vacuole transport, directly, either through AP3 (Stepp et al., 1997) signaling or indirectly by MVB intermediates during VPS (Bowers et al., 2005). These vacuolar degradation routes including autophagy will be explained further in this section.

Yeast vacuoles have also been shown to serve a function in nutrient storage, protein homeostasis, detoxification of the cell (Armstrong, 2010; Broach et al., 1991; Li and Kane, 2009), cell-cycle progression (Jin & Weisman et al., 2015), and cellular trafficking. To accomplish this, the vacuole is host to several enzymes like proteases, lipases, nucleases, within their lumen (Klionsky et al., 1990), and protein transporters. Interestingly, the yeast vacuole is known to have about seven distinct proteases, including three aminopeptidases, two carboxypeptidases, and two endopeptidases (Hecht et al., 2014)

1.4.1 Autophagy

The autophagy-lysosome pathway, also known as vacuolar degradation in yeast, includes two conserved pathways – macroautophagy and microautophagy (Yamaguchi et al., 2016) - that involve degradation of ubiquitinated components entering lytic organelles (vacuoles in yeast or lysosomes in higher eukaryotes). In macroautophagy, double-membrane compartments filled with non-specific cytoplasmic bulk cargo, termed autophagosomes, are delivered to the vacuole/lysosome, and then degraded by membrane invagination, fusion, and expulsion of cargo into the lytic compartment (Müller et al., 2000; Nakatagowa et al., 2009; Nedelsky et al., 2008). Macroautophagic compartments normally contain larger degradation substrates, like aggregates, complexes, and larger proteins, but can also degrade parts of or entire organelles. Organellar degradation processes under macroautophagy include mitophagy, nucleophagy, pexeophagy, reticulophagy, golgiphagy, xenophagy, and ribophagy - degradation of the mitochondria, parts of the nucleus, peroxisomes, endoplasmic reticulum, the Golgi, microorganisms, and ribosomes, respectively (Kundu and Tompson, 2008).

In microautophagy, small volumes of cytosol are directly engulfed by the vacuole or lysosome organelle via invagination of the membrane (Nedelsky et al., 2008). Mammals have a third type of autophagy facilitated by chaperones termed chaperone-mediated autophagy (CMA) that has not been characterized in yeast (Ghosh et al., 2020).. In CMA, degradation substrates associated with specific chaperone complexes, are translocated to lytic organelles through the LAMP-2A lysosomal receptor that recognizes a KFERQ-like motif, and then are degraded (Ghosh et al., 2020).

Atg proteins are the main proteins known to drive autophagy in mammals and yeast. Atg5 and Atg7 are known to be the most crucial in mammals, and Atg8 and Lc3 in yeast (Mizushima et al., 2011). Key autophagy regulating enzymes include Ulk1, Becn1, Ambra1, Vps34, Atg14, Vps15, and Wipi2 (Chen et al., 2019).

1.4.2 Dsc complex: VPS and AP3

The Dsc complex was originally discovered in fission yeast and contains six components – Tul1, Dsc2, Dsc3, Dsc4, Ubx3, and Cdc48 (Stewart et al., 2012). These components share sequence similarities to the ER-localized Hrd1 E3 ligase complex (Yang et al., 2018), suggesting similar protein quality control mechanisms. In fact, Tul1, the multi-spanning E3 ligase in the Dsc complex also has a RING domain, as Hrd1 and other similar E3 ligases. Dsc2, Dsc3, and Ubx3 are homologous to Hrd1 complex Der1, Usa1, and Ubx2, respectively (Stewart et al., 2011, 2012). Baker's yeast cells, however, do not have Dsc4 within this complex. (Dobzinski et al., 2015; Li et al., 2015; Tong et al., 2014).

The Dsc complex had been uncertainly debated to be localized at the Golgi, until Yang et al. found that the Dsc complex can be localized to the Golgi, endosomes, and the vacuole to fulfill its protein quality control roles through various mechanisms. This conclusion was centered around the discovery of two novel Dsc complex members, 31 kDa Golgi/endosome Localized Dsc protein 1 (Gld1) and the 27 kDa Vacuole Localized Dsc protein 1 (Vld1), which determine the localization of the Dsc complex and the subsequent pathway by which proteins will be degraded (Yang et al., 2018). Gld1 and Vld1 are both 4-pass transmembrane proteins that were found to compete at the ER during Dsc complex assembly, resulting in two distinct Dsc complexes cycled between the Golgi and endosomes or to the vacuole membrane, respectively. The Gld1-Dsc subcomplex utilizes the vacuolar protein sorting (VPS) pathway to the Golgi and is recycled to the endosome via the retromer complex (Yang et al., 2018). The Vld1-Dsc subcomplex utilizes the AP3 pathway to the vacuole membrane to perform its PQC role at a slightly more preferential rate (60% of Dsc subcomplexes) (Li et al., 2015). Through further studies, the Li group found that each of the Dsc subcomplexes is formed by a trimer core consisting of Dsc2, Ubx3, and Gld1 or Vld1 (Yang et al., 2018).

The vacuolar protein sorting pathway (VPS) also known as the carboxypeptidase (CPY) pathway, (and will be used interchangeably throughout this dissertation), transports either membrane-bound or soluble proteins through the Golgi and endomembrane system to their ultimate degradation at the vacuole, or lysosome in mammals. First, the protein is recruited into the Golgi lumen through binding of the Vps10 (Feyder et al., 2015) receptor. Then, the protein is loaded into vesicles via the AP-1 adapter and clathrin coating. The newly formed vesicles then bud out from the Golgi membrane toward endosomes. The vesicular membranes then fuse to the endosomal membranes, releasing the degradation cargo into the endosomal lumen. Vps10 is then sorted back to the Golgi by the retromer complex (Seaman, 2012) for recycling and subsequent use back to the Golgi, while the degradation cargo is packed into multivesicular bodies (MVBs) mediated by the endosomal sorting complex required for transport ESCRT machinery components ESCRT-0, ESCRT-1, ESCRT-2, and ESCRT-3 (Winter & Hauser, 2006). The MVBs membranes will then pinch off toward the vacuole, and release the cargo into the vacuolar lumen, by fusion of the membranes, for degradation.

The alkaline phosphatase pathway (ALP), also known as the AP3 pathway, (and will be used interchangeably throughout this dissertation), is a similar vacuolar degradation route from the Golgi to the VPS pathway but has a more direct route from the Golgi to the vacuole. At the Golgi, ALP degradation candidates are packaged into vesicles through the heterotrimeric adapter protein 3 (AP-3) and recruitment of clathrin (Schoppe et al., 2021). These vesicles then transport out of the Golgi, towards the vacuole, and then fuse membranes with the vacuole. The cargo is then ubiquitinated by a vacuolar resident Dsc complex and degraded (Yang et al., 2018). The ALP-targeted protein's route is like protein routes of VPS proteins but bypasses the endosome/MVB system and makes use of the Dsc ubiquitin ligase complex.

1.4.3 Golgi membrane-associated degradation (GOMED)

Another degradation pathway localized at the Golgi apparatus, is termed Golgi membrane-associated degradation (GOMED). GOMED was originally discovered in *atg5Δ* and *atg7Δ* yeast cells, two proteins necessary for lysosomal-autophagic degradation in mammals and known to serve similar roles in yeast (Yamaguchi et al., 2016). Yeast cells lacking either Atg proteins are viable as Atg5 and Atg7 have compensatory functions determined by the Golgi. This compensatory Atg5/Atg7 axis was initially termed alternative autophagy and is now known as GOMED (Nishida et al., 2009). GOMED has been shown to compensate for the autophagic pathway when autophagy is compromised, and Golgi-to-plasma membrane (PM) trafficking is disrupted. In this manner, GOMED clears undeliverable proteins when autophagy cannot. This occurs in a multi-step process, where first, the Golgi membrane becomes stacked, elongated, curved, and generates its own double membrane compartment, enclosing cytoplasm with the proteins or organelles to be degraded. Next, the newly formed Golgi compartments fuse to the vacuole and the bulk cargo is degraded (Noguchi et al., 2022; Yamaguchi et al., 2016).

1.5 Lipids in the proteostasis network

Normally, the proteostasis network is an efficient network that works to maintain the balance and integrity of the proteome; however, it has been shown, that the competence of the PN declines over the course of an organism or cell's age (Carvalhal Marques et al., 2015). When the PN begins to fail, it may manifest in humans as protein maladies, or proteopathies, like neurodegenerative diseases, attributed to proteotoxicity and age (Amaducci & Tesco, 1994; Hardy &Higgins, 1992).

The decline of the proteostasis network has been documented to primarily stem from the loss of function and efficiency of heat shock and chaperone proteins during the aging process. However, it has been recently noted that lipid assemblies, also known as lipid rafts or detergent-resistant membranes (DRMs) (Rouvinski et al., 2003), play a large part in the ability of the proteostasis network to maintain homeostasis (Roitenberg et al., 2019). Current literature suggests that diseases associated with abnormal protein aggregates also have a dysregulation of lipid metabolism (Jayaraj et al., 2020). Taken together, the relationship between protein homeostasis and lipid homeostasis is something to be further investigated to continue our knowledge of proteostasis- and lipid-based diseases.

1.5.1 Lipid assemblies

Lipids rafts, normally found in bi-layer membranes, are composed of lipid microdomains that originate from different cellular components (Rouvinski et al., 2003). Although lipid rafts are inherently difficult to study, as their composition is prone to instability outside of the biological system due to their high location- and function-specificity, they are known to be composed of portions originally from the plasma membrane, caveolae, and mitochondrial-associated endoplasmic reticulum membranes (MAMs). Caveolae are a specific subtype of lipid raft containing a polymerized mass of Caveolin-1, –2, and –3, and are highly conserved across organisms. Additionally, caveolae normally serve as platforms for the assembly of signaling complexes (Roitenberg et al., 2019). MAMs are known to be important in phospholipid exchange, trafficking, mitochondrial biogenesis, and autophagy (van Vilet et al., 2014), and have been linked to Alzheimer's Disease (Larner, 2013) and amyotrophic lateral sclerosis (ALS) (Al-Saif et al., 2011). Together, the components of lipid rafts serve various proteome-related functions, including acting as scaffolds for signaling complexes and receptors, participating in transport, and aiding with adhesion (Michel & Babovic, 2007; Roitenberg et al., 2019).

1.5.2 Lipid droplets and deposition sites for protein aggregates

When the cell has an overwhelming amount of protein aggregates that it is unable to clear by other PN degradation pathways, cellular deposition sites at the cytosol (Johnston et al., 1998), nucleus (Miller et al., 2015), and ER (Kamhi-Nesher et al., 2001) can function to harbor the excess aggregates in efforts of combating proteotoxic stress. Aided by the recruitment of chaperones, lipid and protein storage organelles from the ER known as lipid droplets (LDs), and proteasomes, deposition sites can protect the cell from stress associated with aggregated proteins (Ben-Gedalya & Cohen, 2012). Deposition sites are also known as aggresomes (Ben-Gedalya et al., 2011) and have been known to form as a cellular response to aggregated and undegraded proteins. It is important to note that not all aggresomes or deposition site membranes are exclusively made up of lipids, but also of different integral membrane proteins (Johnston et al., 1998).

1.5.3 Lipid dysregulation activates the UPR

Another modality by which lipids influence the proteostasis network is by activating the ER unfolded protein response ($UPR^{ER)}$ pathway. Hou and colleagues found that the loss of function of Mediator subunit *mdt-15 in C. elegans,* a subunit responsible for the expression of fatty acid metabolism, was able to disrupt the ER due to a decrease in fatty acid saturation and phosphatidylcholine, a membrane phospholipid, and activate the UPR^{ER} (Hou et al., 2014). This is significant as the imbalance of lipids was sufficient to activate the UPR^{ER} alone without any proteostasis imbalance, highlighting another direct link between lipids and the proteostasis network. Other groups have observed similar outcomes and have identified regions of UPR^{ER} sensors adjacent to transmembrane helices that sense membrane lipid disequilibrium (Garcia et al., 2023; Halbleib et al., 2017; Tam et al., 2018; Volmer and Ron, 2015).

1.5.4 Sphingolipid biosynthesis and the PN

Sphingolipids are an important class of lipids localized in cellular membranes known to provide structural support, serve as energy storage, and as signal and regulatory molecules (Dickson, 2008; Hannun & Obeid, 2008; Hepowit et al., 2023; Quinville et al., 2021). Sphingolipids are synthesized by the serine palmitoyl transferase (SPT) complex at the ER and modified into more complex molecules at the Golgi, before performing their functions at membranes (Garić, et al., 2019; Hannun & Obeid, 2018; Pralhada et al., 2013). Interestingly, Hepowit and colleagues, found that when the SPT complex function is inhibited by myriocin (Myr), sphingolipids are not generated *de novo* and cellular amino acid pools are reduced, and enter a quiescent state that aids in a prolonged cell life (Hepowit et al., 2023). Additionally, sphingolipids have been shown to be activators of the Endoplasmic Reticulum Stress Surveillance (ERSU) pathway, a pathway known to block yeast daughter cells from inheriting ER stress from their mother cell (Babour et al., 2010; Piña & Niwa, 2015; Piña et al., 2018). Combined, these studies highlight the role that sphingolipids play in maintaining the steady state processes in cells including amino acids, serving as an important effector of the proteostasis network.

1.5.5 Degradation of sphingolipid biosynthetic enzymes is complex and understudied

Although a lot of research has been conducted on sphingolipid metabolism, unfortunately the degradation routes by which they and their precursors are degraded has still yet to be studied. Recently, Christiano et al., established a protein turnover map (TMAP) in S. cerevisiae, that characterized the degradation routes and turnover rates of key phospholipid and sphingolipid metabolism enzymes (Christiano et al., 2020). Among these enzymes were Tsc10, Orm2, Aur1, Sur1, Csg2, and Ipt1, enzymes involved in sphingolipid metabolism, that were shown to be short and medium-lived proteins (Christiano et al., 2020). Their studies also highlighted the fact that sphingolipid enzymes, interestingly, are degraded in different organelles by different degradation pathways. For example, they found Csg2 and Sur1, enzymes involved in the synthesis of complex sphingolipids (Uemura et al., 2003) are degraded by ESCRT machinery in the vacuole. Additionally, Orm2, an SPT complex regulator (Bhaduri et al., 2023; Schmidt et al., 2019; Xie et al., 2024), is degraded by the proteasome at the Golgi and endolysosomal system, and Tsc3, an enzyme that regulates the SPT complex and lipid droplets (Currie et al., 2014), is degraded by Asi1. The degradation of Tsc3 occurs at the ER and nuclear junction by the Asi branch of ERAD or by INMAD. Other degradation profiles of key sphingolipid enzymes, for example, those of Sur2, Lcb2, could not be identified due to overlapping hits in vacuolar and ERAD degradation machinery, highlighting a need to further investigate such mechanisms.

1.6 Conclusion and Perspectives

Cells are full of phenomenal, interconnected networks, that even when disrupted or stressed, have other phenomenal and interconnected mechanisms at play to compensate and/or help re-establish homeostasis. The proteostasis network is one of these interconnected networks with several pathways and players that take part in maintaining appropriate cellular balance. Studies have shown that proper function of the proteostasis network is important in all organisms and heavily relies on degradation machinery when an accumulation of misfolded or aberrant proteins occurs. In humans, several diseases stem from improper maintenance of these mechanisms, so it is imperative to continue understanding the proteostatic network, its intricacies, and how it is regulated by other networks. This dissertation aims to further understand how Dfm1 – a known member of the rhomboid superfamily, rhomboid pseudoproteases, and protein traditionally involved in trafficking ERAD substrates out of ER membrane and into the cytosol – functions, if it has any other functions, and how it might interact with different lipid biosynthetic enzymes. In doing so, we aim to gain a better understanding of the proteostasis network, the mechanisms behind protein and lipid homeostasis, and how different proteopathies and lipid-based diseases develop. Findings from these studies might eventually serve as therapeutic targets and potential targeted mechanisms in treating such diseases.

1.7 Acknowledgements

Chapter 1 is a literature review by the dissertation author. The author would like to thank all the scientists and scholars who investigated and documented all their findings so that the dissertation author could read, learn, and support her own work with them.

1.8 References

Al-Saif, A., Al-Mohanna, F., & Bohlega, S. (2011). A mutation in sigma-1 receptor causes juvenile amyotrophic lateral sclerosis. *Annals of neurology*, 70(6), 913-919.

Amaducci, L., & Tesco, G. (1994). Aging as a major risk for degenerative diseases of the central nervous system: Editorial commentary. *Current opinion in neurology*, 7(4), 283-286.

Armstrong, J. (2010). Yeast vacuoles: more than a model lysosome. Trends in cell biology, 20(10), 580-585.

Babour, A., Bicknell, A. A., Tourtellotte, J., & Niwa, M. (2010). A surveillance pathway monitors the fitness of the endoplasmic reticulum to control its inheritance. *Cell*, 142(2), 256-269.

Barghout, S. H., & Schimmer, A. D. (2021). E1 enzymes as therapeutic targets in cancer. *Pharmacological reviews*, *73*(1), 1-58.

Basisty, N., Meyer, J. G., & Schilling, B. (2018). Protein turnover in aging and longevity. *Proteomics*, *18*(5-6), 1700108.

Buzuk, L., & Hellerschmied, D. (2023). Ubiquitin-mediated degradation at the Golgi apparatus. *Frontiers in Molecular Biosciences*, *10*, 1197921.

Ben-Gedalya, T., & Cohen, E. (2012). Quality control compartments coming of age. *Traffic*, 13(5), 635-642.

Ben-Gedalya, T., Lyakhovetsky, R., Yedidia, Y., Bejerano-Sagie, M., Kogan, N. M., Karpuj, M. V., ... & Cohen, E. (2011). Cyclosporin-A-induced prion protein aggresomes are dynamic quality-control cellular compartments. *Journal of cell science*, 124(11), 1891-1902.

Benyair, R., Eisenberg-Lerner, A., & Merbl, Y. (2022). Maintaining Golgi homeostasis: A balancing act of two proteolytic pathways. *Cells*, 11(5), 780.

Bergbold, N., & Lemberg, M. K. (2013). Emerging role of rhomboid family proteins in mammalian biology and disease. *Biochimica et Biophysica Acta (BBA)-Biomembranes*, *1828*(12), 2840-2848.

Bergeland, T., Widerberg, J., Bakke, O., & Nordeng, T. W. (2001). Mitotic partitioning of endosomes and lysosomes. *Current Biology*, 11(9), 644-651.

Bhaduri, S., Aguayo, A., Ohno, Y., Proietto, M., Jung, J., Wang, I., ... & Neal, S. E. (2023). An ERAD-independent role for rhomboid pseudoprotease Dfm1 in mediating sphingolipid homeostasis. *The EMBO Journal*, 42(4), e112275.

Bhaduri, S., Scott, N. A., & Neal, S. E. (2023). The role of the rhomboid superfamily in ER protein quality control: from mechanisms and functions to diseases. *Cold Spring Harbor Perspectives in Biology*, 15(2), a041248.

Brandman, O., & Hegde, R. S. (2016). Ribosome-associated protein quality control. *Nature structural & molecular biology*, *23*(1), 7-15.

Bravo, R., Parra, V., Gatica, D., Rodriguez, A. E., Torrealba, N., Paredes, F., ... & Lavandero, S. (2013). Endoplasmic reticulum and the unfolded protein response: dynamics and metabolic integration. *International review of cell and molecular biology*, 301, 215-290.

Brett, C. L., Kallay, L., Hua, Z., Green, R., Chyou, A., Zhang, Y., ... & Rao, R. (2011). Genome-wide analysis reveals the vacuolar pH-stat of Saccharomyces cerevisiae. *PloS one*, 6(3), e17619.

Broach, J. R., Pringle, J. R., & Jones, E. W. (1991). Molecular and cellular biology of the yeast Saccharomyces. *Cole Spring Harbor Laboratory Press*.

Bowers, K., & Stevens, T. H. (2005). Protein transport from the late Golgi to the vacuole in the yeast Saccharomyces cerevisiae. *Biochimica et Biophysica Acta (BBA)-Molecular Cell Research*, 1744(3), 438-454.

Buzuk, L., & Hellerschmied, D. (2023). Ubiquitin-mediated degradation at the Golgi apparatus. *Frontiers in Molecular Biosciences*, 10, 1197921.

Caldwell, S. R., Hill, K. J., & Cooper, A. A. (2001). Degradation of endoplasmic reticulum (ER) quality control substrates requires transport between the ER and Golgi. *Journal of Biological Chemistry*, 276(26), 23296-23303.

Carvalhal Marques, F., Volovik, Y., & Cohen, E. (2015). The roles of cellular and organismal aging in the development of late-onset maladies. *Annual Review of Pathology: Mechanisms of Disease*, 10(1), 1-23.

Carvalho, P., Goder, V., & Rapoport, T. A. (2006). Distinct ubiquitin-ligase complexes define convergent pathways for the degradation of ER proteins. *Cell*, *126*(2), 361-373.

Chen, R. H., Chen, Y. H., & Huang, T. Y. (2019). Ubiquitin-mediated regulation of autophagy. *Journal of Biomedical Science*, *26*, 1-12.

Choe, Y. J., Park, S. H., Hassemer, T., Körner, R., Vincenz-Donnelly, L., Hayer-Hartl, M., & Hartl, F. U. (2016). Failure of RQC machinery causes protein aggregation and proteotoxic stress. *Nature*, *531*(7593), 191-195.

Christiano, R., Arlt, H., Kabatnik, S., Mejhert, N., Lai, Z. W., Farese, R. V., & Walther, T. C. (2020). A systematic protein turnover map for decoding protein degradation. *Cell reports*, 33(6).

Ciechanover, A. (2005). Proteolysis: from the lysosome to ubiquitin and the proteasome. *Nature reviews Molecular cell biology*, *6*(1), 79-87.

Clague, M. J., & Urbé, S. (2008). Multivesicular bodies. *Current Biology*, 18(10), R402-R404.

Clague, M. J., Urbé, S., & Komander, D. (2019). Breaking the chains: deubiquitylating enzyme specificity begets function. *Nature reviews Molecular cell biology*, 20(6), 338-352.

Conrad, M. N., Lee, C. Y., Wilkerson, J. L., & Dresser, M. E. (2007). MPS3 mediates meiotic bouquet formation in Saccharomyces cerevisiae. *Proceedings of the National Academy of Sciences*, *104*(21), 8863-8868.

Cooper, G. M., & Adams, K. (2022). *The cell: a molecular approach*. Oxford University Press.

Cuanalo-Contreras, K., Mukherjee, A., & Soto, C. (2013). Role of protein misfolding and proteostasis deficiency in protein misfolding diseases and aging. *International journal of cell biology*, *2013*(1), 638083.

Currie, E., Guo, X., Christiano, R., Chitraju, C., Kory, N., Harrison, K., ... & Farese, R. V. (2014). High confidence proteomic analysis of yeast LDs identifies additional droplet proteins and reveals connections to dolichol synthesis and sterol acetylation [S]. *Journal of lipid research*, 55(7), 1465-1477.

Dasgupta, A., Ramsey, K. L., Smith, J. S., & Auble, D. T. (2004). Sir Antagonist 1 (San1) is a ubiquitin ligase. *Journal of Biological Chemistry*, 279(26), 26830-26838.

Davey, N. E., & Morgan, D. O. (2016). Building a regulatory network with short linear sequence motifs: lessons from the degrons of the anaphase-promoting complex. *Molecular cell*, *64*(1), 12-23.

de Marcos Lousa, C., & Denecke, J. (2016). Lysosomal and vacuolar sorting: not so different after all!. *Biochemical Society Transactions*, 44(3), 891-897.

Dickson, R. C. (2008). Thematic review series: sphingolipids. New insights into sphingolipid metabolism and function in budding yeast. *Journal of lipid research*, 49(5), 909-921.

Dikic, I. (2017). Proteasomal and autophagic degradation systems. *Annual review of biochemistry*, *86*, 193-224.

Dobzinski, N., Chuartzman, S. G., Kama, R., Schuldiner, M., & Gerst, J. E. (2015). Starvation-dependent regulation of golgi quality control links the TOR signaling and vacuolar protein sorting pathways. *Cell reports*, 12(11), 1876-1886.

Dunker, A. K., Oldfield, C. J., Meng, J., Romero, P., Yang, J. Y., Chen, J. W., ... & Uversky, V. N. (2008). The unfoldomics decade: an update on intrinsically disordered proteins. *BMC genomics*, 9, 1-26.

Eisenberg-Lerner, A., Benyair, R., Hizkiahou, N., Nudel, N., Maor, R., Kramer, M. P., ... & Merbl, Y. (2020). Golgi organization is regulated by proteasomal degradation. *Nature communications*, *11*(1), 409.

Evans, D. R., Brewster, N. K., Xu, Q., Rowley, A., Altheim, B. A., Johnston, G. C., & Singer, R. A. (1998). The yeast protein complex containing cdc68 and pob3 mediates core-promoter repression through the cdc68 N-terminal domain. *Genetics*, 150(4), 1393-1405.

Feyder, S., De Craene, J. O., Bär, S., Bertazzi, D. L., & Friant, S. (2015). Membrane trafficking in the yeast Saccharomyces cerevisiae model. *International journal of molecular sciences*, 16(1), 1509-1525.

Fiil, B. K., & Gyrd-Hansen, M. (2014). Met1-linked ubiquitination in immune signalling. *The FEBS journal*, 281(19), 4337-4350.

Fleig, L., Bergbold, N., Sahasrabudhe, P., Geiger, B., Kaltak, L., & Lemberg, M. K. (2012). Ubiquitin-dependent intramembrane rhomboid protease promotes ERAD of membrane proteins. *Molecular cell*, 47(4), 558-569.

Franić, D., Zubčić, K., & Boban, M. (2021). Nuclear ubiquitin-proteasome pathways in proteostasis maintenance. *Biomolecules*, *11*(1), 54.

Fredrickson, E. K., Gallagher, P. S., Candadai, S. V. C., & Gardner, R. G. (2013). Substrate recognition in nuclear protein quality control degradation is governed by exposed hydrophobicity that correlates with aggregation and insolubility. J*ournal of Biological Chemistry*, 288(9), 6130-6139.

Fredrickson, E. K., Rosenbaum, J. C., Locke, M. N., Milac, T. I., & Gardner, R. G. (2011). Exposed hydrophobicity is a key determinant of nuclear quality control degradation. *Molecular biology of the cell*, 22(13), 2384-2395.

French, M. E., Koehler, C. F., & Hunter, T. (2021). Emerging functions of branched ubiquitin chains. *Cell discovery*, *7*(1), 6.

Friederichs, J. M., Ghosh, S., Smoyer, C. J., McCroskey, S., Miller, B. D., Weaver, K. J., ... & Jaspersen, S. L. (2011). The SUN protein Mps3 is required for spindle pole body insertion into the nuclear membrane and nuclear envelope homeostasis. *PLoS genetics*, *7*(11), e1002365.

Futcher, B., Latter, G. I., Monardo, P., McLaughlin, C. S., & Garrels, J. I. (1999). A sampling of the yeast proteome. *Molecular and cellular biology*, *19*(11), 7357-7368.

Gallagher, P. S., Clowes Candadai, S. V., & Gardner, R. G. (2014). The requirement for Cdc48/p97 in nuclear protein quality control degradation depends on the substrate and correlates with substrate insolubility. *Journal of cell science*, 127(9), 1980-1991.

Garcia, G., Zhang, H., Moreno, S., Tsui, C. K., Webster, B. M., Higuchi-Sanabria, R., & Dillin, A. (2023). Lipid homeostasis is essential for a maximal ER stress response. *Elife*, 12, e83884.

Gardner, R. G., Nelson, Z. W., & Gottschling, D. E. (2005). Degradation-mediated protein quality control in the nucleus. *Cell*, 120(6), 803-815.

Garić, D., De Sanctis, J. B., Shah, J., Dumut, D. C., & Radzioch, D. (2019). Biochemistry of very-long-chain and long-chain ceramides in cystic fibrosis and other diseases: the importance of side chain. *Progress in lipid research*, 74, 130-144.

Ghosh, R., Vinod, V., Symons, J. D., & Boudina, S. (2020). Protein and mitochondria quality control mechanisms and cardiac aging. *Cells*, 9(4), 933.

Glover, J. R., & Lindquist, S. (1998). Hsp104, Hsp70, and Hsp40: a novel chaperone system that rescues previously aggregated proteins. *Cell*, 94(1), 73-82.

Gomes, A. V., Zong, C., Edmondson, R. D., Berhane, B. T., WANG, G. W., Le, S., ... & Ping, P. (2005). The murine cardiac 26S proteasome: an organelle awaiting exploration. *Annuals of the New York Academy of Sciences*, 1047(1), 197-207.

Greenblatt, E. J., Olzmann, J. A., & Kopito, R. R. (2011). Derlin-1 is a rhomboid pseudoprotease required for the dislocation of mutant α-1 antitrypsin from the endoplasmic reticulum. *Nature structural & molecular biology*, *18*(10), 1147-1152.

Groll, M., Bajorek, M., Köhler, A., Moroder, L., Rubin, D. M., Huber, R., ... & Finley, D. (2000). A gated channel into the proteasome core particle. *Nature structural biology*, 7(11), 1062-1067.

Groll, M., Ditzel, L., Löwe, J., Stock, D., Bochtler, M., Bartunik, H. D., & Huber, R. (1997). Structure of 20S proteasome from yeast at 2.4 Å resolution. *Nature*, 386(6624), 463-471.

Groll, M., Heinemeyer, W., Jäger, S., Ullrich, T., Bochtler, M., Wolf, D. H., & Huber, R. (1999). The catalytic sites of 20S proteasomes and their role in subunit maturation: a mutational and crystallographic study. *Proceedings of the National Academy of Sciences*, 96(20), 10976-10983.

Groll, M., & Huber, R. (2003). Substrate access and processing by the 20S proteasome core particle. *The international journal of biochemistry & cell biology*, *35*(5), 606-616.

Gruenbaum, Y., & Foisner, R. (2015). Lamins: nuclear intermediate filament proteins with fundamental functions in nuclear mechanics and genome regulation. *Annual review of biochemistry*, *84*, 131-164.

Guerriero, C. J., Weiberth, K. F., & Brodsky, J. L. (2013). Hsp70 targets a cytoplasmic quality control substrate to the San1p ubiquitin ligase. *Journal of Biological Chemistry*, 288(25), 18506-18520.

Gustafsson, Å. B., & Gottlieb, R. A. (2008). Recycle or die: the role of autophagy in cardioprotection. *Journal of molecular and cellular cardiology*, *44*(4), 654-661.

Habeck, G., Ebner, F. A., Shimada-Kreft, H., & Kreft, S. G. (2015). The yeast ERAD-C ubiquitin ligase Doa10 recognizes an intramembrane degron. *Journal of Cell Biology*, *209*(2), 261-273.

Haeri, M. & Knox, B. E. Endoplasmic reticulum stress and unfolded protein response pathways: Potential for treating age-related retinal degeneration. *Journal of Ophthalmic and Vision Research* vol. 7 45–59 (2012).

Halbleib, K. (2017). Activation of the unfolded protein response sensor Ire1 by lipid bilayer stress (*Doctoral dissertation*, Universitätsbibliothek Johann Christian Senckenberg).

Hampton, R. Y., & Garza, R. M. (2009). Protein quality control as a strategy for cellular regulation: lessons from ubiquitin-mediated regulation of the sterol pathway. *Chemical reviews*, *109*(4), 1561-1574.

Hannun, Y. A., & Obeid, L. M. (2008). Principles of bioactive lipid signalling: lessons from sphingolipids. *Nature reviews Molecular cell biology*, 9(2), 139-150.

Hannun, Y. A., & Obeid, L. M. (2018). Sphingolipids and their metabolism in physiology and disease. *Nature reviews Molecular cell biology*, 19(3), 175-191.

Hardy, J. A., & Higgins, G. A. (1992). Alzheimer's disease: the amyloid cascade hypothesis. *Science*, 256(5054), 184-185.

Hassink, G., Kikkert, M., VOORDEN, S. V., Lee, S. J., Spaapen, R., LAAR, T. V., ... & Wiertz, E. (2005). TEB4 is a C4HC3 RING finger-containing ubiquitin ligase of the endoplasmic reticulum. *Biochemical Journal*, *388*(2), 647-655.

Hecht, K. A., O'Donnell, A. F., & Brodsky, J. L. (2014). The proteolytic landscape of the yeast vacuole. *Cell Logist,* 4: e28023.

Heck, J. W., Cheung, S. K., & Hampton, R. Y. (2010). Cytoplasmic protein quality control degradation mediated by parallel actions of the E3 ubiquitin ligases Ubr1 and San1. *Proceedings of the National Academy of Sciences*, 107(3), 1106-1111.

Hepowit, N. L., Blalock, E., Lee, S., Bretland, K. M., MacGurn, J. A., & Dickson, R. C. (2023). Reduced sphingolipid biosynthesis modulates proteostasis networks to enhance longevity. *Aging (Albany NY)*, 15(2), 472.

Hershko, A., & Ciechanover, A. (1998). The ubiquitin system. *Annual review of biochemistry*, *67*(1), 425-479.

Hetz, C., Zhang, K., & Kaufman, R. J. (2020). Mechanisms, regulation and functions of the unfolded protein response. *Nature reviews Molecular cell biology*, 21(8), 421-438.

Hickey, C. M., Breckel, C., Zhang, M., Theune, W. C., & Hochstrasser, M. (2021). Protein quality control degron-containing substrates are differentially targeted in the cytoplasm and nucleus by ubiquitin ligases. *Genetics*, *217*(1), iyaa031.

Hill, S. M., Hanzén, S., & Nyström, T. (2017). Restricted access: spatial sequestration of damaged proteins during stress and aging. *EMBO reports*, 18(3), 377-391.

Hilt, W., & Wolf, D. H. (1995). Proteasomes of the yeast S. cerevisiae: genes, structure and functions. *Molecular biology reports*, 21, 3-10.

Hou, N. S., Gutschmidt, A., Choi, D. Y., Pather, K., Shi, X., Watts, J. L., ... & Taubert, S. (2014). Activation of the endoplasmic reticulum unfolded protein response by lipid disequilibrium without disturbed proteostasis in vivo. *Proceedings of the National Academy of Sciences*, 111(22), E2271-E2280.

Hough, R., Pratt, G., & Rechsteiner, M. (1987). Purification of two high molecular weight proteases from rabbit reticulocyte lysate. *Journal of Biological Chemistry*, 262(17), 8303-8313.

Hsu, V. W., Yuan, L. C., Nuchtern, J. G., Lippincott-Schwartz, J., Hammerling, G. J., & Klausner, R. D. (1991). A recycling pathway between the endoplasmic reticulum and the Golgi apparatus for retention of unassembled MHC class I molecules. *Nature*, 352(6334), 441-444.

Hwang, J., & Qi, L. (2018). Quality control in the endoplasmic reticulum: crosstalk between ERAD and UPR pathways. *Trends in biochemical sciences*, 43(8), 593-605.

Hwang, J., Ribbens, D., Raychaudhuri, S., Cairns, L., Gu, H., Frost, A., ... & Espenshade, P. J. (2016). A Golgi rhomboid protease Rbd2 recruits Cdc48 to cleave yeast SREBP. *The EMBO journal*, 35(21), 2332-2349.

Ingolia, N. T., Lareau, L. F., & Weissman, J. S. (2011). Ribosome profiling of mouse embryonic stem cells reveals the complexity and dynamics of mammalian proteomes. *Cell*, *147*(4), 789-802.

Jaspersen, S. L., Giddings Jr, T. H., & Winey, M. (2002). Mps3p is a novel component of the yeast spindle pole body that interacts with the yeast centrin homologue Cdc31p. *The Journal of cell biology*, *159*(6), 945-956.

Jayaraj, G. G., Hipp, M. S., & Hartl, F. U. (2020). Functional modules of the proteostasis network. *Cold Spring Harbor Perspectives in Biology*, *12*(1), a033951.

Jin, Y., & Weisman, L. S. (2015). The vacuole/lysosome is required for cell-cycle progression. *Elife*, 4, e08160.

Johnston, J. A., Ward, C. L., & Kopito, R. R. (1998). Aggresomes: a cellular response to misfolded proteins. *The Journal of cell biology*, 143(7), 1883-1898.

Juszkiewicz, S., & Hegde, R. S. (2018). Quality control of orphaned proteins. *Molecular cell*, *71*(3), 443-457.

Kalous, J., Jansová, D., & Šušor, A. (2020). Role of cyclin-dependent kinase 1 in translational regulation in the M-phase. *Cells*, 9(7), 1568.

Kamhi-Nesher, S., Shenkman, M., Tolchinsky, S., Fromm, S. V., Ehrlich, R., & Lederkremer, G. Z. (2001). A novel quality control compartment derived from the endoplasmic reticulum. *Molecular biology of the cell*, 12(6), 1711-1723.

Kandel, R., Jung, J., & Neal, S. (2023, September). Proteotoxic stress and the ubiquitin proteasome system. In *Seminars in cell & developmental biology*. Academic Press.

Kandel, R. R., & Neal, S. E. (2020). The role of rhomboid superfamily members in protein homeostasis: Mechanistic insight and physiological implications. *Biochimica et Biophysica Acta (BBA)-Molecular Cell Research*, 1867(10), 118793.

Kaganovich, D., Kopito, R., & Frydman, J. (2008). Misfolded proteins partition between two distinct quality control compartments. *Nature*, 454(7208), 1088-1095.

Khmelinskii, A., Blaszczak, E., Pantazopoulou, M., Fischer, B., Omnus, D. J., Le Dez, G., ... & Knop, M. (2014). Protein quality control at the inner nuclear membrane. *Nature*, *516*(7531), 410-413.

Kim, W. K., Choi, W., Deshar, B., Kang, S., & Kim, J. (2023). Golgi stress response: New insights into the pathogenesis and therapeutic targets of human diseases. *Molecules and cells*, *46*(4), 191-199.

Klaips, C. L., Jayaraj, G. G., & Hartl, F. U. (2018). Pathways of cellular proteostasis in aging and disease. *Journal of Cell Biology*, *217*(1), 51-63.

Klionsky, D. J. (2007). Autophagy: from phenomenology to molecular understanding in less than a decade. *Nature reviews Molecular cell biology*, *8*(11), 931-937.

Klionsky, D. J., Herman, P. K., & Emr, S. D. (1990). The fungal vacuole: composition, function, and biogenesis. *Microbiological reviews*, 54(3), 266-292.

Knier, A. S., Davis, E. E., Buchholz, H. E., Dorweiler, J. E., Flannagan, L. E., & Manogaran, A. L. (2022). The yeast molecular chaperone, Hsp104, influences transthyretin aggregate formation. *Frontiers in Molecular Neuroscience*, 15, 1050472.

Knopf, J. D., Landscheidt, N., Pegg, C. L., Schulz, B. L., Kühnle, N., Chao, C. W., ... & Lemberg, M. K. (2020). Intramembrane protease RHBDL4 cleaves oligosaccharyltransferase subunits to target them for ER-associated degradation. *Journal of cell science*, 133(6), jcs243790.

Kober, D. L., Xu, S., Li, S., Bajaj, B., Liang, G., Rosenbaum, D. M., & Radhakrishnan, A. (2020). Identification of a degradation signal at the carboxy terminus of SREBP2: A new role for this domain in cholesterol homeostasis. *Proceedings of the National Academy of Sciences*, 117(45), 28080-28091.

Kocaturk, N. M., & Gozuacik, D. (2018). Crosstalk between mammalian autophagy and the ubiquitin-proteasome system. *Frontiers in cell and developmental biology*, *6*, 128.

Koch, B. A., Jin, H., Tomko Jr, R. J., & Yu, H. G. (2019). The anaphase-promoting complex regulates the degradation of the inner nuclear membrane protein Mps3. *Journal of Cell Biology*, *218*(3), 839-854.

Koch, B., & Yu, H. G. (2019). Regulation of inner nuclear membrane associated protein degradation. *Nucleus*, 10(1), 169-180.

Köhler, A., Cascio, P., Leggett, D. S., Woo, K. M., Goldberg, A. L., & Finley, D. (2001). The axial channel of the proteasome core particle is gated by the Rpt2 ATPase and controls both substrate entry and product release. *Molecular cell*, *7*(6), 1143-1152.

Krshnan, L., van de Weijer, M. L., & Carvalho, P. (2022). Endoplasmic reticulum–associated protein degradation. *Cold Spring Harbor Perspectives in Biology*, 14(12), a041247.

Kundu, M., & Thompson, C. B. (2008). Autophagy: basic principles and relevance to disease. *Annu. Rev. Pathol. Mech. Dis.*, 3(1), 427-455.

Larner, A. J. (2013). Presenilin-1 mutations in Alzheimer's disease: an update on genotype-phenotype relationships. *Journal of Alzheimer's Disease*, 37(4), 653-659.

Lee, M. J., Lee, B. H., Hanna, J., King, R. W., & Finley, D. (2011). Trimming of ubiquitin chains by proteasome-associated deubiquitinating enzymes. *Molecular & Cellular Proteomics*, 10(5).

Lemberg, M. K., & Adrain, C. (2016, December). Inactive rhomboid proteins: new mechanisms with implications in health and disease. *In Seminars in cell & developmental biology* (Vol. 60, pp. 29-37). Academic Press.

Li, M., Koshi, T., & Emr, S. D. (2015). Membrane-anchored ubiquitin ligase complex is required for the turnover of lysosomal membrane proteins. *Journal of Cell Biology*, 211(3), 639-652.

Li, S. C., & Kane, P. M. (2009). The yeast lysosome-like vacuole: endpoint and crossroads. *Biochimica et Biophysica Acta (BBA)-Molecular Cell Research*, 1793(4), 650-663.

Li, W., Bengtson, M. H., Ulbrich, A., Matsuda, A., Reddy, V. A., Orth, A., ... & Joazeiro, C. A. (2008). Genome-wide and functional annotation of human E3 ubiquitin ligases identifies MULAN, a mitochondrial E3 that regulates the organelle's dynamics and signaling. *PloS one*, *3*(1), e1487.

Li, Y., Li, S., & Wu, H. (2022). Ubiquitination-proteasome system (UPS) and autophagy two main protein degradation machineries in response to cell stress. *Cells*, *11*(5), 851.

Lilienbaum, A. (2013). Relationship between the proteasomal system and autophagy. *International journal of biochemistry and molecular biology*, 4(1), 1.

Lindholm, D., Wootz, H. & Korhonen, L. ER stress and neurodegenerative diseases. *Cell Death and Differentiation* vol. 13 385–392 (2006).

Lindholm, D., Wootz, H., & Korhonen, L. J. C. D. (2006). ER stress and neurodegenerative diseases. *Cell Death & Differentiation*, 13(3), 385-392.

Lindquist, S. L., & Kelly, J. W. (2011). Chemical and biological approaches for adapting proteostasis to ameliorate protein misfolding and aggregation diseases–progress and prognosis. *Cold Spring Harbor perspectives in biology*, *3*(12), a004507.

Liu, Y., Yang, J., Wang, T., Luo, M., Chen, Y., Chen, C., ... & Han, L. (2023). Expanding PROTACtable genome universe of E3 ligases. *Nature Communications*, *14*(1), 6509.

Lodish, H., Berk, A., Zipursky, S. L., Matsudaira, P., Baltimore, D., & Darnell, J. (2000). Organelles of the Eukaryotic cell. In *Molecular Cell Biology*. 4th edition. WH Freeman.

Logue, S. E., Cleary, P., Saveljeva, S., & Samali, A. (2013). New directions in ER stress-induced cell death. *Apoptosis*, *18*, 537-546.

Lupashin, V., & Sztul, E. (2005). Golgi tethering factors. *Biochimica et Biophysica Acta (BBA)-Molecular Cell Research*, *1744*(3), 325-339.

Mehrtash, A. B., & Hochstrasser, M. (2022). Elements of the ERAD ubiquitin ligase Doa10 regulating sequential poly-ubiquitylation of its targets. *Iscience*, *25*(11).

Mehrtash, A. B., & Hochstrasser, M. (2019, September). Ubiquitin-dependent protein degradation at the endoplasmic reticulum and nuclear envelope. In *Seminars in cell & developmental biology* (Vol. 93, pp. 111-124). Academic Press.

Merrill Jr, A. H. (2011). Sphingolipid and glycosphingolipid metabolic pathways in the era of sphingolipidomics. *Chemical reviews*, 111(10), 6387-6422.

Mevissen, T. E., & Komander, D. (2017). Mechanisms of deubiquitinase specificity and regulation. *Annual review of biochemistry*, 86(1), 159-192.

Michel, V., & Bakovic, M. (2007). Lipid rafts in health and disease. *Biology of the Cell*, 99(3), 129-140.

Miller, S. B., Ho, C. T., Winkler, J., Khokhrina, M., Neuner, A., Mohamed, M. Y., ... & Bukau, B. (2015). Compartment-specific aggregases direct distinct nuclear and cytoplasmic aggregate deposition. *The EMBO journal*, 34(6), 778-797.

Min, J. N., & Patterson, C. (2011). Evaluating age-associated phenotypes in a mouse model of protein dyshomeostasis. *Methods*, *53*(3), 187-193.

Mizushima, N., Yoshimori, T., & Ohsumi, Y. (2011). The role of Atg proteins in autophagosome formation. *Annual review of cell and developmental biology*, 27(1), 107-132.

Mogk, A., Bukau, B., & Kampinga, H. H. (2018). Cellular handling of protein aggregates by disaggregation machines. *Molecular cell*, *69*(2), 214-226.

Mogk, A., Kummer, E., & Bukau, B. (2015). Cooperation of Hsp70 and Hsp100 chaperone machines in protein disaggregation. *Frontiers in molecular biosciences*, *2*, 22.

Mohan, A. G., Calenic, B., Ghiurau, N. A., Duncea-Borca, R. M., Constantinescu, A. E., & Constantinescu, I. (2023). The Golgi apparatus: A voyage through time, structure, function and implication in neurodegenerative disorders. *Cells*, *12*(15), 1972.

Molineaux, S. M. (2012). Molecular pathways: targeting proteasomal protein degradation in cancer. *Clinical Cancer Research*, *18*(1), 15-20.

Morimoto, D., Walinda, E., Fukada, H., Sou, Y. S., Kageyama, S., Hoshino, M., ... & Shirakawa, M. (2015). The unexpected role of polyubiquitin chains in the formation of fibrillar aggregates. *Nature communications*, *6*(1), 6116.

Müller, O., Sattler, T., Flötenmeyer, M., Schwarz, H., Plattner, H., & Mayer, A. (2000). Autophagic tubes: vacuolar invaginations involved in lateral membrane sorting and inverse vesicle budding. *The Journal of cell biology*, 151(3), 519-528.

Nakatogawa, H., Suzuki, K., Kamada, Y., & Ohsumi, Y. (2009). Dynamics and diversity in autophagy mechanisms: lessons from yeast. *Nature reviews Molecular cell biology*, 10(7), 458-467.

Nandi, D., Tahiliani, P., Kumar, A., & Chandu, D. (2006). The ubiquitin-proteasome system. *Journal of biosciences*, 31, 137-155.

Natarajan, N., Foresti, O., Wendrich, K., Stein, A., & Carvalho, P. (2020). Quality control of protein complex assembly by a transmembrane recognition factor. *Molecular cell*, *77*(1), 108-119.

Neal, S., Jaeger, P. A., Duttke, S. H., Benner, C., Glass, C. K., Ideker, T., & Hampton, R. Y. (2018). The Dfm1 Derlin is required for ERAD retrotranslocation of integral membrane proteins. *Molecular cell*, *69*(2), 306-320.

Neal, S., Mak, R., Bennett, E. J., & Hampton, R. (2017). A Cdc48 “retrochaperone” function is required for the solubility of retrotranslocated, integral membrane endoplasmic reticulum-associated degradation (ERAD-M) substrates. *Journal of Biological Chemistry*, *292*(8), 3112-3128.

Neal, S., Syau, D., Nejatfard, A., Nadeau, S., & Hampton, R. Y. (2020). HRD complex self-remodeling enables a novel route of membrane protein retrotranslocation. *Iscience*, *23*(9).

Nedelsky, N. B., Todd, P. K., & Taylor, J. P. (2008). Autophagy and the ubiquitin-proteasome system: collaborators in neuroprotection. *Biochimica et Biophysica Acta (BBA)-Molecular Basis of Disease,* 1782(12), 691-699.

Nejatfard, A., Wauer, N., Bhaduri, S., Conn, A., Gourkanti, S., Singh, N., ... & Neal, S. E. (2021). Derlin rhomboid pseudoproteases employ substrate engagement and lipid distortion function for retrotranslocation of ER multi-spanning membrane substrates. *bioRxiv*, 2021-06.

Nelson, D. L., Lehninger, A. L., & Cox, M. M. (2008). Lehninger principles of biochemistry. *Macmillan*.

Nielsen, S. V., Poulsen, E. G., Rebula, C. A., & Hartmann-Petersen, R. (2014). Protein quality control in the nucleus. *Biomolecules*, *4*(3), 646-661.

Nishida, Y., Arakawa, S., Fujitani, K., Yamaguchi, H., Mizuta, T., Kanaseki, T., ... & Shimizu, S. (2009). Discovery of Atg5/Atg7-independent alternative macroautophagy. *Nature*, 461(7264), 654-658.

Noguchi, S., & Shimizu, S. (2022). Molecular mechanisms and biological roles of GOMED. *The FEBS Journal*, 289(22), 7213-7220.

Ogen-Shtern, N., David, T. B., & Lederkremer, G. Z. (2016). Protein aggregation and ER stress. *Brain research*, 1648, 658-666.

Piña, F. J., & Niwa, M. (2015). The ER Stress Surveillance (ERSU) pathway regulates daughter cell ER protein aggregate inheritance. *Elife*, 4, e06970.

Piña, F., Yagisawa, F., Obara, K., Gregerson, J. D., Kihara, A., & Niwa, M. (2018). Sphingolipids activate the endoplasmic reticulum stress surveillance pathway. *Journal of Cell Biology*, 217(2), 495-505.

Powers, E. T., Morimoto, R. I., Dillin, A., Kelly, J. W., & Balch, W. E. (2009). Biological and chemical approaches to diseases of proteostasis deficiency. *Annual review of biochemistry*, *78*(1), 959-991.

Pralhada Rao, R., Vaidyanathan, N., Rengasamy, M., Mammen Oommen, A., Somaiya, N., & Jagannath, M. R. (2013). Sphingolipid metabolic pathway: an overview of major roles played in human diseases. *Journal of lipids*, 2013(1), 178910.

Quinville, B. M., Deschenes, N. M., Ryckman, A. E., & Walia, J. S. (2021). A comprehensive review: sphingolipid metabolism and implications of disruption in sphingolipid homeostasis. *International journal of molecular sciences*, 22(11), 5793.

Rao, R. v. & Bredesen, D. E. Misfolded proteins, endoplasmic reticulum stress and neurodegeneration. *Current Opinion in Cell Biology* vol. 16 653–662 (2004).

Ravid, T., Kreft, S. G., & Hochstrasser, M. (2006). Membrane and soluble substrates of the Doa10 ubiquitin ligase are degraded by distinct pathways. *The EMBO journal*, *25*(3), 533-543.

Rock, K. L., Gramm, C., Rothstein, L., Clark, K., Stein, R., Dick, L., ... & Goldberg, A. L. (1994). Inhibitors of the proteasome block the degradation of most cell proteins and the generation of peptides presented on MHC class I molecules. *Cell*, *78*(5), 761-771.

Rouvinski, A., Gahali-Sass, I., Stav, I., Metzer, E., Atlan, H., & Taraboulos, A. (2003). Both raft-and non-raft proteins associate with CHAPS-insoluble complexes: some APP in large complexes. *Biochemical and biophysical research communications*, 308(4), 750-758.

Roitenberg, N., & Cohen, E. (2019). Lipid assemblies at the crossroads of aging, proteostasis, and neurodegeneration. *Trends in Cell Biology*, 29(12), 954-963.

Rosenbaum, J. C., Fredrickson, E. K., Oeser, M. L., Garrett-Engele, C. M., Locke, M. N., Richardson, L. A., ... & Gardner, R. G. (2011). Disorder targets misorder in nuclear quality control degradation: a disordered ubiquitin ligase directly recognizes its misfolded substrates. *Molecular cell*, 41(1), 93-106.

Roussel, B. D., Kruppa, A. J., Miranda, E., Crowther, D. C., Lomas, D. A., & Marciniak, S. J. (2013). Endoplasmic reticulum dysfunction in neurological disease. *The Lancet Neurology*, 12(1), 105-118.

Russell, S. J., Steger, K. A., & Johnston, S. A. (1999). Subcellular localization, stoichiometry, and protein levels of 26 S proteasome subunits in yeast. *Journal of Biological Chemistry*, *274*(31), 21943-21952.

Samant, R. S., Livingston, C. M., Sontag, E. M., & Frydman, J. (2018). Distinct proteostasis circuits cooperate in nuclear and cytoplasmic protein quality control. *Nature*, 563(7731), 407-411.

Sanchez, N., de Leon, N., Valle, R., Fung, J. J., Khmelinskii, A., & Roncero, C. (2023). Multiple quality control mechanisms monitor yeast chitin synthase folding in the endoplasmic reticulum. *Molecular Biology of the Cell*, 34(13), ar132.

Sato, B. K., & Hampton, R. Y. (2006). Yeast Derlin Dfm1 interacts with Cdc48 and functions in ER homeostasis. *Yeast*, *23*(14-15), 1053-1064.

Schirmer, E. C., & Foisner, R. (2007). Proteins that associate with lamins: many faces, many functions. *Experimental cell research*, *313*(10), 2167-2179.

Schoppe, J., Schubert, E., Apelbaum, A., Yavavli, E., Birkholz, O., Stephanowitz, H., ... & Ungermann, C. (2021). Flexible open conformation of the AP-3 complex explains its role in cargo recruitment at the Golgi. Journal of Biological Chemistry, 297(5).

Schröder, M., & Kaufman, R. J. (2005). ER stress and the unfolded protein response. *Mutation Research/Fundamental and Molecular Mechanisms of Mutagenesis*, *569*(1-2), 29-63.

Schmidt, C. C., Vasic, V., & Stein, A. (2020). Doa10 is a membrane protein retrotranslocase in ER-associated protein degradation. *Elife*, *9*, e56945.

Schmidt, O., Weyer, Y., Baumann, V., Widerin, M. A., Eising, S., Angelova, M., ... & Teis, D. (2019). Endosome and Golgi-associated degradation (EGAD) of membrane proteins regulates sphingolipid metabolism. *The EMBO Journal*, 38(15), e101433.

Schwabl, S., & Teis, D. (2022). Protein quality control at the Golgi. *Current Opinion in Cell Biology*, *75*, 102074.

Schwarz, D. S., & Blower, M. D. (2016). The endoplasmic reticulum: structure, function and response to cellular signaling. *Cellular and molecular life sciences*, 73, 79-94.

Seaman, M. N. (2012). The retromer complex–endosomal protein recycling and beyond. *Journal of cell science*, 125(20), 4693-4702.

Shacham, T., Sharma, N., & Lederkremer, G. Z. (2019). Protein misfolding and ER stress in Huntington's disease. *Frontiers in molecular biosciences*, 6, 20.

Shibata, Y., Voeltz, G. K., & Rapoport, T. A. (2006). Rough sheets and smooth tubules. *Cell*, 126(3), 435-439.

Simões, T., Schuster, R., den Brave, F., & Escobar-Henriques, M. (2018). Cdc48 regulates a deubiquitylase cascade critical for mitochondrial fusion. *elife*, 7, e30015.

Smith, D. M., Kafri, G., Cheng, Y., Ng, D., Walz, T., & Goldberg, A. L. (2005). ATP binding to PAN or the 26S ATPases causes association with the 20S proteasome, gate opening, and translocation of unfolded proteins. *Molecular cell*, 20(5), 687-698.

Smoyer, C. J., & Jaspersen, S. L. (2019). Patrolling the nucleus: inner nuclear membrane-associated degradation. *Current genetics*, 65(5), 1099-1106.

Spear, E. D., & Ng, D. T. (2003). Stress tolerance of misfolded carboxypeptidase Y requires maintenance of protein trafficking and degradative pathways. *Molecular biology of the cell*, 14(7), 2756-2767.

Specht, S., Miller, S. B., Mogk, A., & Bukau, B. (2011). Hsp42 is required for sequestration of protein aggregates into deposition sites in Saccharomyces cerevisiae. *Journal of Cell Biology*, 195(4), 617-629.

Spriggs, K. A., Bushell, M., & Willis, A. E. (2010). Translational regulation of gene expression during conditions of cell stress. *Molecular cell*, *40*(2), 228-237.

Stepp, J. D., Huang, K., & Lemmon, S. K. (1997). The yeast adaptor protein complex, AP-3, is essential for the efficient delivery of alkaline phosphatase by the alternate pathway to the vacuole. *The Journal of cell biology*, 139(7), 1761-1774.

Stewart, E. V., Nwosu, C. C., Tong, Z., Roguev, A., Cummins, T. D., Kim, D. U., ... & Espenshade, P. J. (2011). Yeast SREBP cleavage activation requires the Golgi Dsc E3 ligase complex. *Molecular cell*, 42(2), 160-171.

Stewart, E. V., Lloyd, S. J. A., Burg, J. S., Nwosu, C. C., Lintner, R. E., Daza, R., ... & Espenshade, P. J. (2012). Yeast sterol regulatory element-binding protein (SREBP) cleavage requires Cdc48 and Dsc5, a ubiquitin regulatory X domain-containing subunit of the Golgi Dsc E3 ligase. *Journal of Biological Chemistry*, 287(1), 672-681.

Stewart, M. D., Ritterhoff, T., Klevit, R. E., & Brzovic, P. S. (2016). E2 enzymes: more than just middle men. *Cell research*, *26*(4), 423-440.

Stolz, A., Ernst, A., & Dikic, I. (2014). Cargo recognition and trafficking in selective autophagy. *Nature cell biology*, *16*(6), 495-501.

Suda, Y., & Nakano, A. (2012). The Yeast Golgi Apparatus. *Traffic*, *13*(4), 505-510.

Sun, Z., & Brodsky, J. L. (2019). Protein quality control in the secretory pathway. *Journal of Cell Biology*, *218*(10), 3171-3187.

Suresh, H. G., Pascoe, N., & Andrews, B. (2020). The structure and function of deubiquitinases: Lessons from budding yeast. *Open biology*, *10*(10), 200279.

Swanson, R., Locher, M., & Hochstrasser, M. (2001). A conserved ubiquitin ligase of the nuclear envelope/endoplasmic reticulum that functions in both ER-associated and Matα2 repressor degradation. *Genes & development*, *15*(20), 2660-2674.

Tam, A. B., Roberts, L. S., Chandra, V., Rivera, I. G., Nomura, D. K., Forbes, D. J., & Niwa, M. (2018). The UPR activator ATF6 responds to proteotoxic and lipotoxic stress by distinct mechanisms. *Developmental cell*, 46(3), 327-343.

Tax, G., Lia, A., Santino, A., & Roversi, P. (2019). Modulation of ERQC and ERAD: a broad-spectrum spanner in the works of cancer cells?. *Journal of oncology*, 2019(1), 8384913.

Teter, S. A., & Klionsky, D. J. (2000, June). Transport of proteins to the yeast vacuole: autophagy, cytoplasm-to-vacuole targeting, and role of the vacuole in degradation. *In Seminars in cell & developmental biology* (Vol. 11, No. 3, pp. 173-179). Academic Press.

Thumm, M. (2000). Structure and function of the yeast vacuole and its role in autophagy. *Microscopy research and technique*, 51(6), 563-572.

Tong, Z., Kim, M. S., Pandey, A., & Espenshade, P. J. (2014). Identification of candidate substrates for the Golgi Tul1 E3 ligase using quantitative diGly proteomics in yeast. *Molecular & Cellular Proteomics*, 13(11), 2871-2882.

Tracz, M., & Bialek, W. (2021). Beyond K48 and K63: non-canonical protein ubiquitination. *Cellular & molecular biology letters*, 26(1), 1.

Tsai, T. Y. C., Theriot, J. A., & Ferrell Jr, J. E. (2014). Changes in oscillatory dynamics in the cell cycle of early Xenopus laevis embryos. *PLoS biology*, 12(2), e1001788.

Twomey, E. C., Ji, Z., Wales, T. E., Bodnar, N. O., Ficarro, S. B., Marto, J. A., ... & Rapoport, T. A. (2019). Substrate processing by the Cdc48 ATPase complex is initiated by ubiquitin unfolding. *Science*, *365*(6452), eaax1033.

Uemura, S., Kihara, A., Inokuchi, J. I., & Igarashi, Y. (2003). Csg1p and newly identified Csh1p function in mannosylinositol phosphorylceramide synthesis by interacting with Csg2p. *Journal of Biological Chemistry*, 278(46), 45049-45055.

van der Veen, A. G., & Ploegh, H. L. (2012). Ubiquitin-like proteins. *Annual review of biochemistry*, 81(1), 323-357.

van Vliet, A. R., Verfaillie, T., & Agostinis, P. (2014). New functions of mitochondria associated membranes in cellular signaling. *Biochimica et Biophysica Acta (BBA)-Molecular Cell Research*, 1843(10), 2253-2262.

Varshavsky, A. (2011). The N-end rule pathway and regulation by proteolysis. *Protein science*, 20(8), 1298-1345.

Vashist, S., Kim, W., Belden, W. J., Spear, E. D., Barlowe, C., & Ng, D. T. (2001). Distinct retrieval and retention mechanisms are required for the quality control of endoplasmic reticulum protein folding. *The Journal of cell biology*, 155(3), 355-368.

Vembar, S. S., & Brodsky, J. L. (2008). One step at a time: endoplasmic reticulum-associated degradation. *Nature reviews Molecular cell biology*, 9(12), 944-957.

Viotti, C. (2016). ER to Golgi-dependent protein secretion: the conventional pathway. *Unconventional protein secretion: methods and protocols*, 3-29.

Volmer, R., & Ron, D. (2015). Lipid-dependent regulation of the unfolded protein response. *Current opinion in cell biology*, 33, 67-73.

Webster, B. M., Gildea, H. K., & Dillin, A. (2020). Protein homeostasis from the outside in. *Nature cell biology*, 22(8), 911-912.

Wiemken, A., Matile, P., & Moor, H. (1970). Vacuolar dynamics in synchronously budding yeast. *Archiv für Mikrobiologie*, 70, 89-103.

Wilson, K. L., & Berk, J. M. (2010). The nuclear envelope at a glance. *Journal of cell science*, *123*(12), 1973-1978.

Winter, V., & Hauser, M. T. (2006). Exploring the ESCRTing machinery in eukaryotes. *Trends in plant science*, 11(3), 115-123.

Wolf, D. H., & Schäfer, A. (2006). CPY* and the power of yeast genetics in the elucidation of quality control and associated protein degradation of the endoplasmic reticulum. Dislocation and Degradation of Proteins from the Endoplasmic Reticulum, 41-56.

Wu, K., Itskanov, S., Lynch, D. L., Chen, Y., Turner, A., Gumbart, J. C., & Park, E. (2024). Substrate recognition mechanism of the endoplasmic reticulum-associated ubiquitin ligase Doa10. *Nature Communications*, *15*(1), 2182.

Xia, J., Sánchez, B. J., Chen, Y., Campbell, K., Kasvandik, S., & Nielsen, J. (2022). Proteome allocations change linearly with the specific growth rate of Saccharomyces cerevisiae under glucose limitation. *Nature Communications*, *13*(1), 2819.

Xie, T., Dong, F., Han, G., Wu, X., Liu, P., Zhang, Z., ... & Gong, X. (2024). Collaborative regulation of yeast SPT-Orm2 complex by phosphorylation and ceramide. *Cell Reports*, 43(2).

Xu, P., Duong, D. M., Seyfried, N. T., Cheng, D., Xie, Y., Robert, J., ... & Peng, J. (2009). Quantitative proteomics reveals the function of unconventional ubiquitin chains in proteasomal degradation. *Cell*, *137*(1), 133-145.

Yamaguchi, H., Arakawa, S., Kanaseki, T., Miyatsuka, T., Fujitani, Y., Watada, H., ... & Shimizu, S. (2016). Golgi membrane-associated degradation pathway in yeast and mammals. *The EMBO journal*, 35(18), 1991-2007.

Yang, X., Arines, F. M., Zhang, W., & Li, M. (2018). Sorting of a multi-subunit ubiquitin ligase complex in the endolysosome system. *Elife*, 7, e33116.

Yao, T., & Cohen, R. E. (2002). A cryptic protease couples deubiquitination and degradation by the proteasome. *Nature*, 419(6905), 403-407.

Yin, Z., Pascual, C., & Klionsky, D. J. (2016). Autophagy: machinery and regulation. *Microbial cell*, *3*(12), 588.

Yoshida, H. (2007). ER stress and diseases. *The FEBS journal*, *274*(3), 630-658.

Zaher, H. S., & Green, R. (2009). Fidelity at the molecular level: lessons from protein synthesis. *Cell*, *136*(4), 746-762.

Zhang, Z. R. (2019). Mechanism of Quality Control of Nascent Membrane Proteins. *Advances in Membrane Proteins: Building, Signaling and Malfunction*, 111-130.

Zhao, L., Zhao, J., Zhong, K., Tong, A., & Jia, D. (2022). Targeted protein degradation: mechanisms, strategies and application. *Signal transduction and targeted therapy*, *7*(1), 113.

Zong, N. C., Li, H., Li, H., Lam, M. P., Jimenez, R. C., Kim, C. S., ... & Ping, P. (2013). Integration of cardiac proteome biology and medicine by a specialized knowledgebase. *Circulation research*, 113(9), 1043-1053.

Figure 1.2.1. Two terminal degradation paths of ubiquitinated misfolded proteins

A model depicting the **(1)** ubiquitination cascade as E1, E2, E3 ligases ubiquitinate degradation substrates in an ATP-dependent manner. Substrates are then degraded by **(2a)** the ubiquitin proteasome system or by the **(2b)** autophagy-lysosomal/vacuolar pathways. Created with BioRender.com.

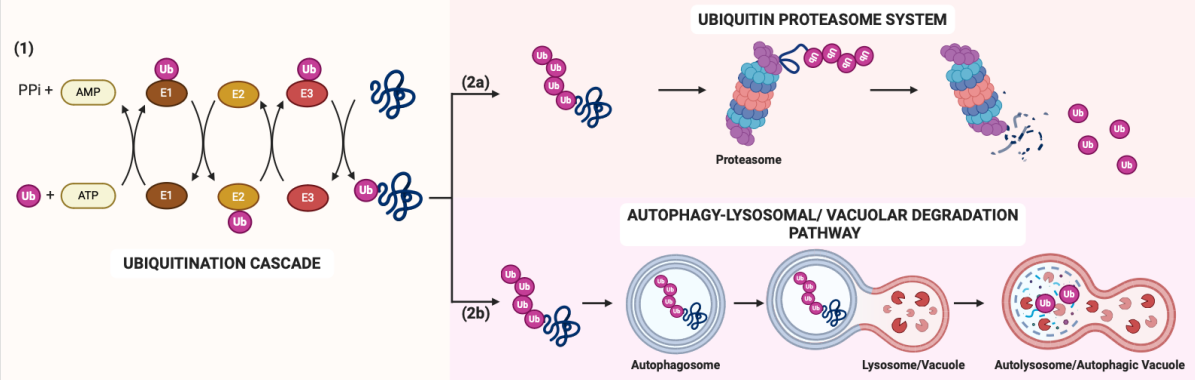


Figure 1.3.1. Overview of proteasomal degradation pathways in proteostasis network

A model depicting the degradation pathways within the proteasomal network that end with **(1)** proteasomal degradation. ERAD at the **(2a)** endoplasmic reticulum occurs via two distinct protein complexes, Hrd1 and Doa10, that help target and transport ubiquitinated degradation substrates from the membrane of the ER to the cytoplasm, where the ATPase Cdc48 helps transport the degradation substrate to proteasomes for degradation. At **(2b)** the nucleus, 3 distinct complexes, the Doa10, Asi1-3, and APC/C, function in the INMAD pathway to degrade INM substrates that are then transported to the cytosol, where Cdc48 transports the substrate to proteasomes for subsequent degradation. San1 works in a similar fashion at the nucleus as INMAD protein complexes, but on degradation substrates in the inner nuclear matrix. **(2c)** The Golgi has two proteasomal degradation routes, EGAD via Dsc complex involvement and GOMED during Golgi stress via GM130 involvement. Both pathways converge in the cytoplasm where substrates, with the aid of Cdc48, and the proteasome, are degraded. Created with BioRender.com.

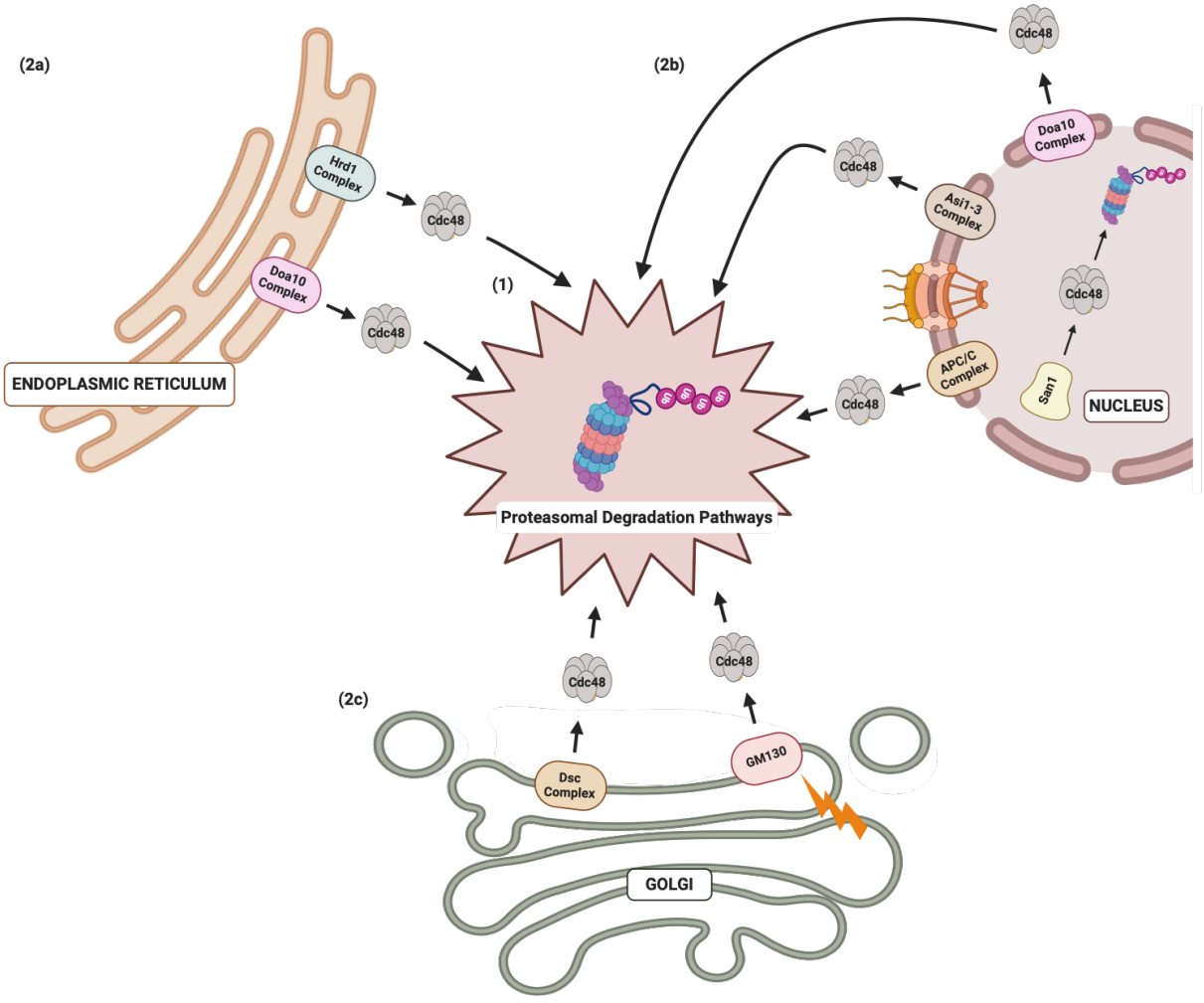
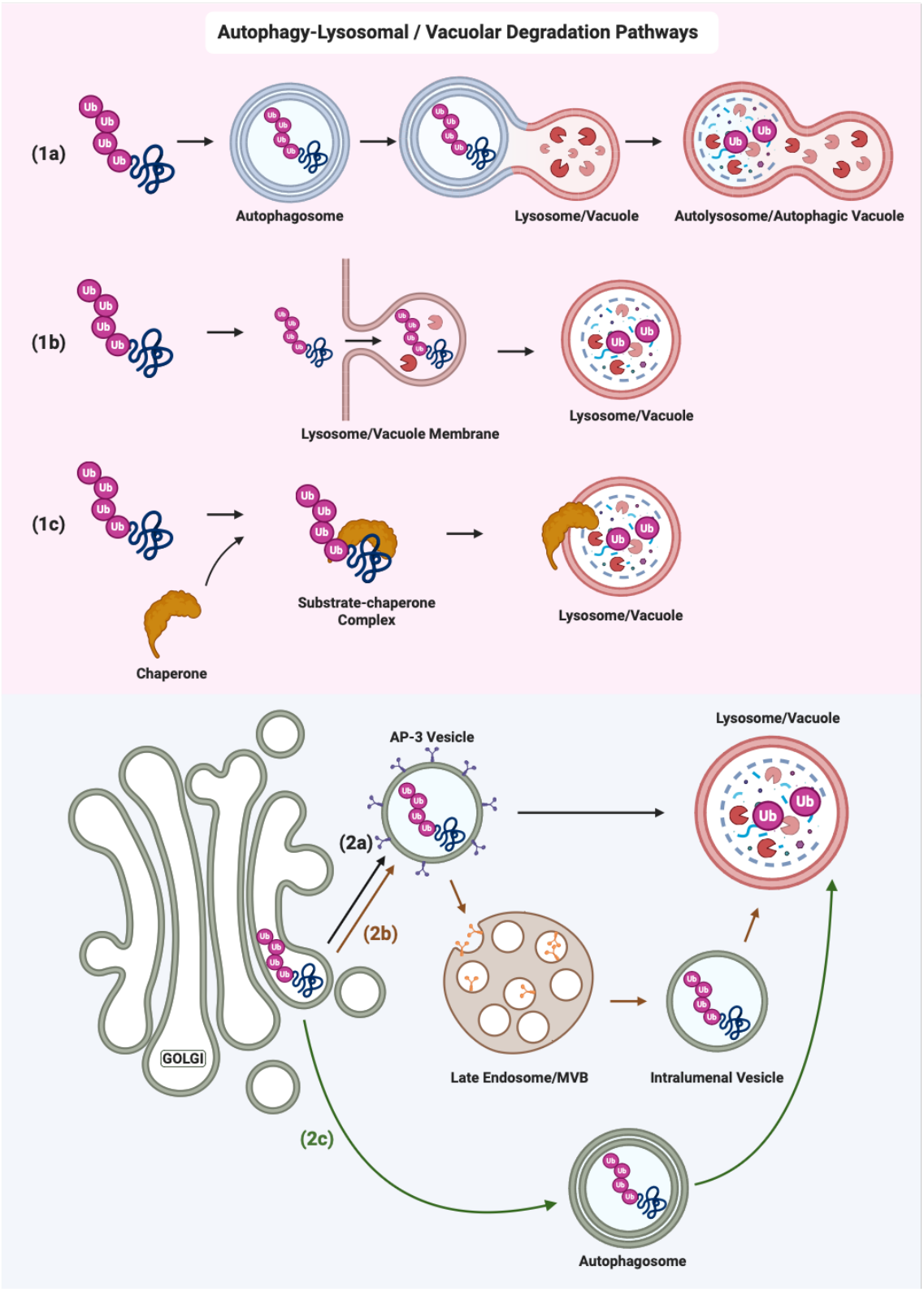


Figure 1.4.1. Overview of autophagy-lysosomal/vacuolar degradation pathways in proteostasis network

A model depicting vacuolar degradation routes. **(1a)** Marcoautophagy of large molecules begins with ubiquitination of misfolded membrane proteins, that are engulfed by double membrane vesicles called autophagosomes. Autophagosomes then fuse with vacuoles to form autophagic vacuoles where proteases break down the degradation substrate. **(1b)** in Microautophagy degradation substrates are engulfed directly by the vacuole where they are then degraded by proteases. **(1c)** In chaperone-mediated autophagy (not characterized in yeast), chaperones traffic substrates to the vacuole, and may in transport through the membrane, for degradation by proteases. At the Golgi, during **(2a)** AP-3 degradation, degradation substrates bud off into vesicles with AP-3 proteins as receptors and fuse to the vacuole for degradation. In **(2b)** CPY VPS degradation, Golgi degradation substrates bud off into vesicles and are trafficked to late endosomes. ESCRT proteins then assist in budding and transporting of intralumenal vesicles that fuse with the vacuole for degradation by proteasomes. In times of stress **(2c)** double-membraned Golgi vesicles, or autophagosomes, bud off from the Golgi and directly fuse to the vacuole for degradation by proteases in the GARD pathway. Created with BioRender.com.


Autophagy-Lysosomal / Vacuolar Degradation Pathways
(1a)
Autophagosome
Lysosome/Vacuole
Autolysosome/Autophagic Vacuole
(1b)
Lysosome/Vacuole Membrane
Lysosome/Vacuole
(1c)
Substrate-chaperone Complex
Lysosome/Vacuole
Chaperone
Lysosome/Vacuole
AP-3 Vesicle
(2a)
(2b)
GOLGI
Late Endosome/MVB
Intralumenal Vesicle
(2c)
Autophagosome

Chapter 2: Yeast Derlin Dfm1 Employs a Chaperone-Like Function to Resolve Misfolded Membrane Protein Stress

2.1. Introduction

Protein aggregates are a common feature of diseased and aged cells. Membrane proteins comprise a quarter of the proteome, and yet, it is not well understood how aggregation of membrane proteins is regulated and what effects these aggregates can have on cellular health. We have determined in yeast that the derlin Dfm1 has a chaperone-like activity that influences misfolded membrane protein aggregation. We establish that this function of Dfm1 does not require recruitment of the ATPase Cdc48, and it is distinct from Dfm1's previously identified function in dislocating misfolded membrane proteins from the endoplasmic reticulum (ER) to the cytosol for degradation. Additionally, we assess the cellular impacts of misfolded membrane proteins in the absence of Dfm1 and determine that misfolded membrane proteins are toxic to cells in the absence of Dfm1 and cause disruptions to proteasomal and ubiquitin homeostasis.

While misfolded proteins are recognized as a source of cellular stress, the mechanisms by which cells prevent this stress and how this stress impacts cells is not fully understood. Eukaryotic cells are equipped with protein quality control pathways for preventing the accumulation of aggregation-prone misfolded proteins. The endoplasmic reticulum (ER) is responsible for folding both secretory and membrane proteins and is well equipped with quality control pathways for refolding or eliminating misfolded proteins. One of the major pathways of protein quality control at the ER is ER-associated degradation (ERAD) (Hampton, 2002). ERAD utilizes the ubiquitin proteasome system (UPS) to selectively target and degrade misfolded or unassembled proteins at the ER (Werner et al., 1996).

ERAD is a well-conserved process from yeast to mammals. ERAD of membrane proteins requires 4 universal steps: (1) substrate recognition (Bhamidipati et al., 2005; Nakatasukasa et al., 2013; Sato et al., 2009; Stanley et al, 2011); (2) substrate ubiquitination (Bays et al., 2001); (3) retrotranslocation of substrate from the ER to the cytosol (Baldridge et al., 2016; Hampton et al., 1997; Neal et al., 2018; Sun et al., 2021; Swanson et al., 2001; Wahlman et al., 2007); and (4) degradation by the cytosolic proteasome (Farinha et al., 2005; Hampton et al., 1996; Werner et al., 1996). A hexameric cytosolic ATPase, Cdc48 in yeast and p97 in mammals, is required for retrotranslocation of all ERAD substrates (Rabinovich et al., 2002; Twomey et al., 2019; Ye et al., 2001). In the context of this paper, substrate refers to a protein that is targeted by the ERAD pathway.

In yeast, ER membrane substrates can be targeted by the DOA (degradation of alpha2) pathway or the HRD pathway (hydroxymethyl glutaryl-coenzyme A reductase degradation), utilizing the E3 ligases Doa10 and Hrd1, respectively. Additionally, the yeast derlin Dfm1 is specifically required for the retrotranslocation of misfolded membrane substrates, in both the HRD and DOA pathways (Neal et al., 2018). Dfm1 facilitates retrotranslocation of membrane proteins through several mechanisms including (1) recognition and binding to misfolded membrane proteins; (2) thinning the lipid bilayer to reduce the thermodynamic barrier to extraction; and (3) recruiting the ATPase Cdc48 to the ER (Neal et al., 2018; Nejatfard et al., 2021).

Dfm1 is a member of the derlin subclass of rhomboid proteins. Rhomboid proteins are a widely conserved family of proteins, found in all domains of life (Began et al., 2020; Freeman, 2014; Liu et al., 2020; Tichá et al., 2018). There are 2 major categories of

rhomboid proteins: active rhomboid proteases and inactive rhomboid pseudoproteases. While the inactive rhomboid pseudoproteases lack a catalytic site, they have been implicated in a wide variety of biological processes, including protein quality control, protein trafficking, and cell signaling (Adrian et al., 2020; Greenblatt et al., 2011; Kandel et al., 2020; Wu et al., 2020; Zettl et al., 2011). Derlin proteins, including Dfm1, are rhomboid pseudoproteases that are critical for ERAD of a wide variety of substrates, both in yeast and mammalian cells (Hoelen et al., 2015; Knop et al., 1996; Neal et al., 2018; Oda et al., 2006; Sun et al., 2006).

We have previously observed that in *dfm1*Δ cells, when a misfolded membrane protein is strongly expressed, the cells show a severe growth defect (Neal et al., 2020). This is seen specifically in the absence of Dfm1, and this growth defect is not observed in the absence of other ERAD components, indicating a specific function for Dfm1 in sensing and/or adapting cells to misfolded membrane protein stress (Fig. 2.2.1) (Neal et al., 2020). This is in line with a previous study linking Dfm1 to ER homeostasis (Sato et al., 2006).

In the present study, we determine that Dfm1 prevents membrane protein toxicity because of a previously unidentified chaperone-like function that is independent of Cdc48 recruitment. This function is distinct from Dfm1's role in protein retrotranslocation, while also relying on many of the same functions deployed by Dfm1 to promote retrotranslocation. We further determined that human homologs of Dfm1 have also retained this ability. This study is the first to demonstrate chaperone-like activity for any rhomboid protein. Many rhomboid proteins use similar functions to Dfm1 to promote retrotranslocation, and the rhomboid protease RHBDL4 has recently been characterized as acting on aggregation-prone substrates (Bock et al., 2022; Engberg et al., 2022; Fleig et al., 2012; Nejatfard et al., 2021;

Wu et al., 2020). It will be an interesting and important further line of inquiry to determine if a chaperone-like activity is a common ability of rhomboid proteins, both for pseudoproteases and proteases.

As a complement to our work on the function of Dfm1 in relieving misfolded membrane protein toxicity, we also sought to determine how misfolded membrane proteins cause toxicity. We determine that misfolded membrane proteins, but not other types of misfolded proteins, impact proteasome and ubiquitin homeostasis. We also identified several proteins that promote cellular health upon misfolded membrane protein by resolving the proteasome and ubiquitin stress that misfolded membrane proteins trigger. Intriguingly, we find that not all membrane protein aggregates are toxic. The combination required for toxicity appears to be both (1) aggregated misfolded membrane proteins; and (2) ubiquitinated misfolded membrane proteins. Either of these features alone is not sufficient for toxicity.

We propose a model in which upon accumulation of ubiquitinated misfolded membrane proteins in the absence of Dfm1, misfolded membrane proteins form toxic aggregates. In the presence of Dfm1, this toxicity is prevented by Dfm1's ability to solubilize membrane proteins, independent of its ability to retrotranslocate proteins.

2.2. Results

2.2.1. Absence of Dfm1 and expression of integral misfolded membrane proteins causes growth stress

Previous research from the Neal lab has revealed that accumulation of a misfolded membrane protein in the absence of Dfm1 causes a severe growth defect in the substrate-toxicity assay (Neal et al., 2020). In the substrate-toxicity assay, yeast strains with a misfolded protein under the control of a galactose inducible promoter are plated in a spot assay onto selection plates with either 2% galactose or 2% dextrose as a carbon source (Fig. 2.2.1) (Bhaduri & Neal, 2021). This allows for comparison of growth of yeast strains with different genetic perturbations with expression of misfolded substrates. This growth defect can be seen with strong expression of 3 misfolded membrane proteins in *dfm1*Δ cells: Hmg2, Pdr5*, and Ste6* (Fig. 2.2.1A - Fig. 2.2.1C). We have previously shown that this growth defect is specific to misfolded membrane proteins at the ER, as expression of a luminal ERAD substrate, CPY*, in *dfm1*Δ cells elicits no growth defect (Neal et al., 2020). Interestingly, this growth defect is not seen when membrane proteins accumulate in the absence of other ERAD components, such as the E3 ligases Hrd1 and Doa10 (Fig. 2.2.1A - Fig. 2.2.1C). In the case of *dfm1*Δ, *hrd1*Δ, and *doa10*Δ cells, misfolded membrane proteins accumulate at the ER due to defects in ERAD, but only in the case of *dfm1*Δ cells, is a growth defect observed with misfolded membrane protein expression. Altogether, we surmise that this growth defect triggered by the absence of Dfm1 along with expression of misfolded membrane protein is due to cellular stress caused by misfolded membrane protein toxicity. By utilizing the substrate-toxicity assay, we observed a growth defect in *dfm1*Δ cells and normal growth in *hrd1*Δ and *doa10*Δ cells upon expression of ERAD membrane substrates (Fig. 2.2.1A - Fig. 2.2.1C). The cellular difference among these ERAD knockout strains is that membrane substrates are ubiquitinated in *dfm1*Δ cells but not ubiquitinated in *hrd1*Δ and *doa10*Δ cells--due to the absence of the ER E3 ligases--as determined through western blot for ubiquitin (Fig. 2.2.7B). One possibility is that the growth stress is not specific to *dfm1*Δ cells and is solely dependent on the accumulation of ubiquitinated membrane

substrates. To rule out this possibility, we utilized a temperature-sensitive Cdc48 allele strain, *cdc48-2*, which, like *dfm1*Δ cells, results in accumulation of ubiquitinated ERAD membrane substrates (Neal et al., 2018). While we used *cdc48-2* cells at the permissive temperature of 30˚C, ERAD is still compromised for Hmg2, as previously reported, and we validated this using a cycloheximide chase that Pdr5* and Ste6*degradation is also impaired at 30˚C in *cdc48-2* cells (Supp. Fig. 2.2.1A and Supp. Fig. 2.2.1B) (Neal et al., 2017; Neal et al., 2018). The substrate-toxicity assay was employed on *cdc48-2* strains expressing membrane substrates Hmg2, Pdr5*, and Ste6* (Fig. 2.2.1D - Fig. 2.2.1F). These strains showed a growth defect while growing on galactose plates due to inherent slow growth of *cdc48-2* strains, but this was not worsened by expression of misfolded integral membrane proteins, despite the E3 ligases that ubiquitinate these proteins still being present. These results indicate that Dfm1 plays a specific role in the alleviation of misfolded membrane protein stress.

2.2.2. Disease-associated membrane proteins cause growth stress

Since a wide variety of misfolded membrane proteins elicit growth stress in dfm1Δ cells, we hypothesized that growth stress would also be observed with expression of clinically relevant human misfolded membrane proteins. We tested expression of WT cystic fibrosis transmembrane receptor (CFTR), CFTRΔF508, the most common disease-causing variant of CFTR, and the Z variant of alpha-1 proteinase inhibitor (A1PiZ), a protein variant that results in alpha-1 antitrypsin deficiency (AATD). All these substrates are targeted by ERAD when expressed in yeast, with CFTR and CFTRΔF508 being targeted by machinery for membrane proteins and A1PiZ being a soluble misfolded protein in the ER lumen (Palmer et al., 2003; Zhang et al., 2001). When these proteins were expressed in *dfm1*Δ cells, both CFTR and CFTRΔF508 resulted in a growth defect, while none was observed with expression on A1PiZ (Fig. 2.2.1G). Expression of any of the proteins in WT yeast cells resulted in no growth defect (Fig. 2.2.1G). It was not wholly surprising that WT CFTR also elicited growth stress in *dfm1*Δ cells. Previous studies have shown that while virtually all CFTRΔF508 is targeted to ERAD, about 80% of WT CFTR is degraded via ERAD in yeast and mammals (Cheng et al., 1990; Gnann et al., 2004; Zhang et al., 2001).

2.2.3. Dfm1 has a dual role in ER protein stress and ERAD retrotranslocation

Previous work from the Hampton lab establishing a role for Dfm1 in misfolded membrane protein retrotranslocation also identified several motifs of Dfm1 that are essential for its retrotranslocation function (Neal et al., 2018). Additionally, by employing an unbiased genetic screen, our lab recently identified 5 residues of Dfm1 that are required for retrotranslocation (Nejatfard et al., 2021). Here, we tested whether these residues, critical for Dfm1's retrotranslocation function, are required for alleviating the growth stress in *dfm1*Δ cells expressing Hmg2.

Fig. 2.2.2A shows a schematic of Dfm1, with the regions of the protein important for retrotranslocation function highlighted, and a list of specific motifs and residues that are mutated listed in a table (Neal et al., 2018; Nejatfard et al., 2021). Dfm1 contains 2 motifs that are well conserved among the rhomboid superfamily, the WR motif in Loop 1 and the GxxxG (Gx3G) motif in transmembrane domain (TMD) 6 (Greenblatt et al., 2011; Neal et al., 2018). Both of these motifs are required for Dfm1-mediated retrotranslocation (Neal et al., 2018; Nejatfard et al., 2021). We first tested the requirement of the conserved rhomboid motif mutants by expressing Hmg2 with WR mutants (WA and AR) and Gx3G mutants (Ax3G and Gx3A) and observed no restoration in growth (Fig. 2.2.2B). Our previous work determined that Loop 1 mutants (F58S, L64V, and K67E) obliterated Dfm1's ability to bind misfolded membrane substrates, and TMD 2 mutants (Q101R and F107S) reduce the lipid thinning ability of Dfm1, a function that aids in Dfm1's retrotranslocation function (Nejatfard et al., 2021). Accordingly, we utilized these mutants in our growth assay and did not observe a rescue of the growth defect (Fig. 2.2.2C). We have previously shown that alteration of the 5 signature residues of the Dfm1 SHP box to alanine (Dfm1- 5Ashp) ablates its ability to recruit Cdc48 (Fig. 2.2.2D). We also established, Dfm1's Cdc48 recruitment function is required for Dfm1's retrotranslocation function, whereas the Dfm1-5Ashp mutant impairs its retrotranslocation function (Neal et al., 2018). Notably, in contrast to the other mutants tested, Dfm1-5Ashp was still able to alleviate the growth defect like WT Dfm1 (Fig. 2.2.2E). These results suggest that Dfm1's substrate engagement and lipid thinning function is required for alleviating membrane substrate-induced stress, whereas Dfm1's Cdc48 recruitment function is dispensable for alleviating the growth stress. We validated that expression of WT Dfm1 and all Dfm1 mutants were comparable using western blot (Supp. Fig. 2.2.1C).

2.2.4. Human derlins relieve growth stress

Dfm1 is a rhomboid pseudoprotease and a member of the derlin subclass of rhomboid proteins. The human genome encodes 3 derlins, Derlin-1, Derlin-2, and Derlin-3. Yeast Dfm1 is the closest homolog of the mammalian derlins (Greenblatt et al., 2011). All 3 are ER-localized proteins that are implicated in ERAD and adaptation to ER stress (Hoelen et al., 2015; Oda et al., 2006; Lilley et al., 2004; Lilley et al., 2005; Ren et al., 2018; Ye et al., 2004). We expressed human Derlin-1 and Derlin-2 in *dfm1*Δ+Hmg2 cells. We opted to only test Derlin-1 and Derlin-2, as they are more structurally similar to Dfm1 and also contain cytoplasmic SHP box motifs (Nejatfrad et al., 2021). Both human derlins were able to rescue growth in these cells in the substrate-toxicity assay (Fig. 2.2.2F). This was surprising, as we had previously found that mammalian derlins cannot complement the retrotranslocation function of Dfm1 in yeast cells for self-ubiquitinating substrate (SUS)- GFP, a similar ERAD substrate to Hmg2 (Nejatfard et al., 2021).

2.2.5. Dfm1 solubilizes misfolded membrane protein aggregates independent of Cdc48 recruitment

The above studies show that Dfm1 residues critical for retrotranslocation—through substrate binding and its lipid thinning function—are also important for alleviating membrane substrate-induced stress. Conversely, add-back of a Dfm1 Shp box mutant (Dfm1-5Ashp) (Fig. 2.2.2D), which does not recruit Cdc48 and cannot retrotranslocate proteins, is able to restore growth in the substrate-toxicity assay. We surmise that Dfm1's actions—independent of its Cdc48 recruitment function—may be directly acting on misfolded membrane substrates to prevent growth stress. One possibility is that Dfm1 may directly act on misfolded membrane substrates by functioning as a chaperone-like protein to prevent misfolded membrane protein toxicity. We hypothesize that Dfm1 acts as either a holdase, preventing the aggregation of misfolded membrane substrates, or as a disaggregase, separating proteins in existing protein aggregates. To address this hypothesis, we employed a detergent solubility assay in *dfm1*Δ + Hmg2 cells with add-back of WT DFM1 or DFM1 mutants. ER microsomes were isolated and incubated in 1% dodecyl maltoside (DDM) and subjected to centrifugation to separate aggregated substrate (pellet fraction) from non-aggregated substrate (soluble fraction). As shown in Fig. 2.2.3A, nearly all Hmg2-GFP in *dfm1*Δ cells was pelleted (aggregated). Conversely, with Dfm1 and Dfm1-5Ashp add-back cells, nearly all Hmg2-GFP was solubilized (non-aggregated). This striking all-or-nothing phenotype of Hmg2 aggregation demonstrates an important role for Dfm1 in influencing membrane protein aggregation. As a control for these studies, we examined Hmg2 in both WT, *hrd1*Δ cells, and *hrd1*Δ+Hrd1 cells. Nearly all protein was soluble in all 3 strains (Fig. 2.2.4A). We also tested a properly folded ER membrane protein, Sec61-GFP in *dfm1*Δ cells. In contrast to Hmg2-GFP, majority of Sec61-GFP was in the detergent-solubilized supernatant fraction and there was no change in Sec61-GFP detergent solubility with Dfm1 or Dfm1-5Ashp add-back in dfm1Δ cells (Fig. 2.2.4B).

It appears Dfm1—independent of its Cdc48 recruitment function—functions as a chaperone-like protein to influence the aggregation of misfolded membrane proteins. We next explored additional Dfm1 residues that are required for solubilizing membrane substrates. Accordingly, mutants in the conserved rhomboid motifs (AR and Ax3G) were employed in the detergent solubility assay. DFM1-AR and DFM1-Ax3G add-back resulted in aggregated HMG2 (Fig. 2.2.3A). Similarly, retrotranslocation defective Dfm1 mutants in Loop 1 (F58S, L64V, and K67E) and TMD 2 mutants (Q101R and F107S) in the detergent solubility assay were not capable of solubilizing Hmg2 (Fig. 2.2.3B). This all-or-nothing effect that Dfm1's presence has on aggregation led us to determine whether Dfm1 binds to Hmg2 even after solubilization with DDM. Indeed, using co-immunoprecipitation, we found that Dfm1 physically interacts with solubilized Hmg2 (Fig. 2.2.3C). Altogether, Dfm1 is critical in influencing the aggregation state of its ERAD membrane substrate (Fig. 2.2.3D). Although the ability to recruit Cdc48 is vital for Dfm1's retrotranslocation function, it is not required for this newly established chaperone-like function.

The chaperone-like function of Dfm1 is generalizable to other misfolded membrane proteins but not non-membrane misfolded proteins. We tested other membrane ERAD membrane substrates targeted by the HRD (Pdr5*) or DOA (Ste6*) pathways, and they were both completely solubilized in the presence of Dfm1 in the detergent solubility assay (Fig. 2.2.4C and Fig. 2.2.4D). In contrast, the misfolded ER luminal protein, CPY*, was completely solubilized regardless of the presence or absence of Dfm1 (Fig. 2.2.4E). Notably, we also observed that Derlin-1 and Derlin-2 were able to prevent aggregation of Hmg2 in *dfm1*Δ cells, indicating that other derlin proteins have a conserved chaperone-like function (Fig. 2.2.4F). We also investigated whether Hmg2-GFP appeared in puncta in *dfm1*Δ cells through confocal microscopy. We found no significant difference between the percentage of GFP in puncta or the number of puncta with add-back of WT DFM1 or any of the DFM1 mutants in *dfm1*Δ cells (Supp. Fig. 2.2.1D–Supp. Fig. 2.2.1F). This is in line with the view of some in the field that toxic aggregates are generally below the visible detection limit for confocal microscopy and that puncta identified through microscopy tend to be representative of sequestrosomes, a cellular adaptation to the accumulation of aggregation prone proteins (Mogk et al., 2018).

2.2.6. Misfolded membrane proteins do not activate the unfolded protein response

The canonical ER stress pathway triggered by the accumulation of misfolded proteins is the unfolded protein response (UPR) (Hwang et al., 2018). The UPR is known to be induced by the accumulation of misfolded soluble proteins within the ER lumen. To test if misfolded membrane protein accumulation at the ER activates UPR, we used a fluorescence-based flow cytometry assay. In this assay, yeast cells encoding both a galactose inducible misfolded protein or empty vector (EV) and UPR reporter 4xUPRE-GFP were treated with or without 0.2% galactose and 2 µg/mL of the ER stress inducing drug tunicamycin or DMSO as the vehicle control. GFP expression was measured by flow cytometry for 5 hours following galactose treatment. We found that GFP expression did not increase by 5 hours post-galactose addition in *dfm1*Δ cells compared to *pdr5*Δ cells expressing any of the following substrates tested: Hmg2, Ste6*, or EV (Fig. 2.2.5A - Fig. 2.2.5D, Fig. 2.2.5G and Fig. 2.2.5H). *Dfm1*Δ cells can activate UPR, as addition of tunicamycin to these cells allowed them to activate the UPR at similar levels as *pdr5*Δ cells (Fig. 2.2.5A - Fig. 2.2.5H). As expected, expression of the ER luminal substrate CPY* activated the UPR in *dfm1*Δ cells and *pdr5*Δ cells (Fig. 2.2.5E and Fig. 2.2.5F).

Our findings from flow cytometry experiments were further corroborated by measuring Hac1 splicing via polymerase chain reaction (PCR) (Supp. Fig. 2.2.2A and Supp. Fig. 2.2.2B). When the UPR is active, the mRNA of the transcription factor Hac1 is spliced to create a transcript 252bp shorter than the full-length transcript (Cox et al., 1996). Samples with a band for both spliced and unspliced Hac1 indicated UPR activation, while a single band of the unspliced variant indicated no UPR activation. The results from these experiments agreed with the flow cytometry-based assay; we found no HAC1 splicing with misfolded membrane protein overexpression in *dfm1*Δ cells (Supp. Fig. 2.2.2A and Supp. Fig. 2.2.2B).

2.2.7. Accumulation of misfolded membrane proteins up-regulates proteasome components

After determining the UPR is not activated in *dfm1*Δ cells expressing Hmg2, we next sought to determine the transcriptional changes that occur with misfolded membrane protein stress. To address this question, we utilized RNA sequencing (RNA-seq). We prepared and sequenced cDNA libraries from mRNA extracted from *pdr5*Δ cells, *hrd1*Δ*pdr5*Δ cells, and *dfm1*Δ *pdr5*Δ cells containing galactose inducible Hmg2 or EV, 2 hours post-galactose treatment. These yeast strains were generated from a yeast knockout collection with the BY4742 strain background, and *pdr5*Δ cells are commonly used as the wild-type background for the knockout collection. We validated using the substrate-toxicity assay that *dfm1*Δ *pdr5*Δ+Hmg2 strains in this background also display a growth defect (Supp. Fig. 2.2.3A). We used principal component analysis (PCA) to determine genes that were up-regulated and down-regulated most in *dfm1*Δ cells expressing Hmg2 versus the control strains; WT+EV, WT+Hmg2, *hrd1*Δ+EV, *hrd1*Δ+Hmg2, and *dfm1*Δ+EV (S1 Data; Available online). Principal component 1 (PC1) value of all replicate strains except for *dfm1*Δ+Hmg2 cells clustered closer to each other than they did to either replicate of the *dfm1*Δ +Hmg2 cells, indicating that these strains were transcriptionally distinct from the others sequenced (Supp. Fig. 2.2.3B). Additionally, the *dfm1*Δ+Hmg2 replicates were fairly distinct from each other, so while there were genes up-regulated in both replicates, there were also variable transcriptional changes (Supp. Fig. 2.2.3B). This variability is likely representative of biological variability in these strains rather than experimental variability as it was only observed between these replicates and not replicates of the other strains tested.

Up-regulated (+PC1 values) and down-regulated (-PC1 values) genes in dfm1Δ+Hmg2 cells were used for gene ontology (GO) analysis. The most overrepresented group of up-regulated genes were those classified as being involved in “Proteasomal Ubiquitin-Independent Protein Catabolic Processes,” “Regulation of Endopeptidase Activity,” and “Proteasome Regulatory Particle Assembly” (Supp. Fig. 2.2.3D). Several proteasome subunits were represented in this list of up-regulated genes. The most overrepresented group of down-regulated genes in this dataset were those classified as being involved in “rRNA Export from Nucleus,” “rRNA Transport,” and “Translational Termination” (Supp. Fig. 2.2.3E). Because a down-regulation of the mRNA for genes encoding ribosomal proteins is a general feature of stressed yeast cells (Gasch et al., 2000), we focused on the up-regulation of proteasome components. Plotting the PC1 and PC2 values for *dfm1*Δ +Hmg2 cells for the highest PC1 value genes, we observed a large overlap between genes in this dataset and those that are targets of the transcription factor Rpn4 (Supp. Fig. 2.2.3C, highlighted in red).

2.2.8. The transcription factor Rpn4 is involved in misfolded membrane protein stress

Rpn4 is a transcription factor that up-regulates genes with a proteasome-associated control element (PACE) in their promoters (Mannhaupt et al., 1999). From our RNA-seq data, there was a remarkably high overlap between the genes that were observed to be up-regulated in *dfm1*Δ cells expressing Hmg2 and those that are known Rpn4 targets (Mannhaupt et al., 1999). We reasoned that Rpn4 may be involved in adapting cells to misfolded membrane protein stress and predicted *rpn4*Δ cells should phenocopy *dfm1*Δ cells by exhibiting a growth defect induced by ERAD membrane substrates. Using the substrate-toxicity assay, we found expression of misfolded membrane proteins in *rpn4*Δ cells resulted in a growth defect equivalent to that seen in *dfm1*Δ cells (Fig. 6A and Supp. Fig. 2.2.4A), indicating that Rpn4 is also required for alleviating misfolded membrane protein stress. As with *dfm1*Δ cells, this effect was specific to membrane protein expression, as expression of CPY* in *rpn4*Δ cells did not result in a growth defect (Supp. Fig. 2.2.4B). This is in line with previous research demonstrating Rpn4 is activated in response to misfolded membrane protein accumulation and that misfolded membrane protein expression can result in proteasome impairment, even in WT cells (Boyle Metzger et al., 2009; Burns et al., 2021). Finally, we tested a transcription factor that can regulate Rpn4 and that has many overlapping transcriptional targets with Rpn4 and Pdr1 (Owsianik et al., 2002). We did not observe any growth defect in *pdr1*Δ+Hmg2 cells (Supp. Fig. 2.2.4C).

As a readout for Rpn4 activity, we measured the abundance of a GFP-tagged version of the proteasome component Pre6-GFP in *dfm1*Δ+Hmg2 cells 0- and 5-hours after galactose induction through flow cytometry. Pre6 is a component of the 20S core of the proteasome that can be transcriptionally up-regulated by Rpn4, and Pre6-GFP has been used by others as a marker for the proteasome (Enenkel et al., 1998; Xie et al., 2001). In comparison to WT control strains and other substrates tested, *dfm1*Δ+Hmg2 had a significant increase in Pre6-GFP after 5 hours (Fig. 2.2.6B and Fig. 2.2.6C).

2.2.9. Misfolded membrane protein stress in *dfm1*Δ cells leads to proteasome impairment

Because Rpn4 appears to be active in membrane protein-stressed *dfm1*Δ cells, we hypothesized that proteasome function is impacted in *dfm1*Δ cells expressing an integral membrane protein. We tested this using an MG132 sensitivity assay developed by the Michaelis lab (Boyle Metzger et al., 2009). MG132 is a drug that reversibly inhibits proteasome function (Lee et al., 1998). For this assay, cells in liquid culture were treated with MG132, plated, and counted the number of colony-forming units (CFUs) resulting from each strain. Due to the risk of the retrotranslocation defect being suppressed in *dfm1*Δ cells with constitutive expression of a misfolded membrane protein, and thus possibly artificially increasing the number of CFUs resulting from treatment of dfm1Δ cells with MG132, we opted to instead test *dfm1*Δ *hrd1*Δ*pdr5*Δ cells. These cells are unable to suppress the retrotranslocation defect of *dfm1*Δ cells, due to the absence of Hrd1, which has been characterized to function as an alternative retrotranslocon for membrane substrates when Dfm1 is absent (Neal et al., 2020). We utilized the engineered misfolded membrane protein SUS-GFP as the substrate for these experiments. SUS-GFP contains the RING domain of Hrd1 and catalyzes its own ubiquitination, thus still causing the stress that is elicited by ubiquitinated misfolded membrane proteins in *dfm1*Δ cells (Garza et al., 2009). We predicted that cells with compromised proteasome function would be more sensitive to MG132 treatment, resulting in fewer CFUs. Strikingly, no CFUs resulted from MG132 treated *dfm1*Δ*hrd1*Δ*pdr5*Δ cells constitutively expressing SUS-GFP (Fig. 2.2.6F). All others strains and treatments tested did not show as dramatic of a change in the number of CFUs, either with MG132 or DMSO treatment (Fig. 2.2.6D - Fig. 2.2.6F). These results demonstrate that proteasome function is impacted in dfm1Δ cells with misfolded membrane protein accumulation.

2.2.10. Misfolded membrane protein stress does not cause proteasome sequestration

One hypothesis that we explored to understand the mechanism by which proteasomes are impaired with misfolded membrane protein stress was direct sequestration of proteasomes at the ER. Using *dfm1*Δ cells expressing EV or Hmg2, we used western blotting to detect ER recruitment of Pre6, a proteasome component (Fig. 2.2.6G). Proteasome recruitment was similar between both strains. We also tested aggregation versus solubility of Pre6 at the ER in both strains and this was also not affected in either strain (Fig. 2.2.6G). These results indicate an indirect mechanism for proteasome impairment in membrane protein-stressed cells.

2.2.11. Growth defect in *dfm1*Δ cells is ubiquitination dependent

The observation that a growth defect triggered by misfolded membrane proteins is only seen in the absence of Dfm1, and not in cells lacking either of the ER E3 ligases Hrd1 and Doa10, led us to hypothesize that this growth defect is dependent upon ubiquitination of the misfolded membrane proteins. The substrate-toxicity assay results using *cdc48-2* cells indicate that the growth defect is not solely due to defective ERAD or the accumulation of ubiquitinated misfolded membrane proteins. Nonetheless, we still explored the possibility that misfolded membrane protein-induced toxicity is dependent on substrate ubiquitination.

We examined whether growth defects were seen in either *dfm1*Δ*hrd1*Δ or *dfm1*Δ*doa10*Δ cells expressing either Hmg2 (an Hrd1 target) or Ste6* (a Doa10 target), respectively (Fig. 2.2.7A). These results showed no growth defect in the double mutants for which the membrane protein expressed was not ubiquitinated by the absent E3 ligase: *dfm1*Δ*hrd1*Δ cells expressing Hmg2 and *dfm1*Δdoa10Δ cells expressing Ste6* (Fig. 2.2.7A). We validated that substrates were indeed not ubiquitinated in E3 ligase knockouts via western blot for ubiquitin (Fig. 2.2.7B). In contrast, a growth defect was observed in the double mutants for which the absent E3 ligase did not participate in ubiquitination of the expressed membrane protein: *dfm1*Δ*hrd1*Δ expressing Ste6* and *dfm1*Δ*doa10*Δ expressing Hmg2. This indicates that growth stress in *dfm1*Δ cells is dependent upon ubiquitination of the accumulated misfolded membrane protein.

As an alternative approach to determine if membrane proteins must be ubiquitinated to cause toxicity in the absence of Dfm1, we tested the expression of well-characterized, stabilized Hmg2 mutants. These mutants, Hmg2 (K6R), Hmg2 (K357R), and Hmg2 (K6R, K357R), were previously identified by the Hampton lab in a genetic screen for stabilized Hmg2 mutants (Gardner et al., 1999). Both K➔R stabilized mutations disrupt Hmg2 ubiquitination, and these sites are hypothesized to be Hmg2 ubiquitination sites. While the Hampton lab has shown that ubiquitination levels of both substrates are nearly undetectable with western blot, they also showed that the K6R mutant is not further stabilized in an ERAD deficient background, while the K357R mutant is slightly more stable in an ERAD deficient background than in a WT background (Gardner et al., 1999). We propose that because of this slight level of degradation in the K357R mutant, some fraction of this mutant must be ubiquitinated and targeted to the Hrd1 ERAD pathway. Our model predicts that toxicity of misfolded membrane proteins is ubiquitination dependent. Thus, we would expect that the fully stabilized Hmg2-K6R with negligible ubiquitination should not elicit a growth defect, whereas Hmg2-K357R, which is a poor ERAD substrate but can still be targeted for degradation, should elicit a growth defect in *dfm1*Δ cells. Indeed, we observed no growth defect in *dfm1*Δ cells expressing the K6R mutant, while the K357R mutant still showed a growth defect. Moreover, the growth defect is still observed in the double mutant Hmg2-(K6R, K357R), which phenocopies Hmg2-K6R, in that it is completely stabilized, consistent with the model that growth stress in the absence of Dfm1 is dependent on the accumulation of ubiquitinated membrane substrates (Fig. 2.2.7C).

2.2.12. Ubiquitin homeostasis is disrupted with misfolded membrane protein accumulation

There is increasing evidence that suggests ubiquitin homeostasis and maintenance of the free ubiquitin pool is critical for cellular survival under normal and stress conditions (Anderson et al., 2005; Carter et al., 2009; Hanna et al., 2007; Wu et al., 2020). Because we observed that growth defect in *dfm1*Δ cells is dependent on ubiquitination of membrane substrates, we hypothesized that ubiquitin conjugation to accumulating membrane proteins reduces the availability of free ubiquitin, impacting cell viability.

One hypothesis that would explain substrate ubiquitination dependency of the growth defect in dfm1Δ cells is that the pool of monomeric ubiquitin is depleted by accumulation of misfolded membrane proteins. If this hypothesis is correct, exogenous ubiquitin should rescue the growth defect seen from substrate-induced stress in *dfm1*Δ cells. To that end, *dfm1*Δ +Hmg2 cells harboring a plasmid containing ubiquitin under the control of the copper inducible promoter CUP1 (Koller et al., 2000) were tested in the substrate-toxicity assay. These cells were plated on 2% galactose and 50 μM copper to induce expression of Hmg2 and ubiquitin in *dfm1*Δ cells, respectively. Notably, supplementation of ubiquitin restored the growth defect (Fig. 2.2.7D). We blotted for monomeric ubiquitin to determine whether this pool is depleted in *dfm1*Δ+Hmg2 cells and found that it was reduced compared to WT and *hrd1*Δ strains with Hmg2 (Fig. 2.2.7E and Fig. 2.2.7F). In contrast, *dfm1*Δ without overexpressed Hmg2 do not show a decrease in monomeric ubiquitin (Supp. Fig. 2.2.5A and Supp. Fig. 2.2.5B).

2.2.13. Deubiquitinases prevent or resolve misfolded membrane protein stress

The deubiquitinase (DUB) Ubp6 is a peripheral subunit of the proteasome and recycles ubiquitin from substrates prior to proteasome degradation (Hanna et al., 2007). Accordingly, *ubp6*Δ cells were employed in the substrate-toxicity assay to determine whether this protein is involved in alleviating misfolded membrane protein stress by replenishing the free ubiquitin pool. By utilizing the substrate-toxicity assay, we found Hmg2 or Ste6* expression causes a growth defect in *ubp6*Δ cells (Fig. 7F and Supp. Fig. 2.2.5C). Like *dfm1*Δ and *rpn4*Δ cells, this growth defect was specific to misfolded membrane proteins and was not observed with CPY* (Supp. Fig. 2.2.6D). To confirm whether this effect was specific to Ubp6, we also tested DUB Doa4, another regulator of free ubiquitin, in the substrate-toxicity assay. Unexpectedly, we found that *doa4*Δ cells phenocopy *ubp6*Δ cells with Hmg2 expression (Supp. Fig. 2.2.6A). From this observation, we tested a collection of DUB KOs in the substrate-toxicity assay. Of the 14 yeast DUBs tested (out of 22 DUBs total), we observed a growth defect with both *ubp9*Δ and *ubp14*Δ cells (Fig. 7H and Supp. Fig. 2.2.6B). Interestingly, Ubp6, Doa4, and Ubp14 have all previously been implicated in ubiquitin homeostasis and, to date, no research has been conducted into the specific role of Ubp9 (Suresh et al., 2020). Interestingly, when a misfolded cytosolic substrate, ΔssCPY*, is expressed in *ubp6*Δ, *doa4*Δ, *ubp9*Δ, and *ubp14*Δ cells, there is no growth defect observed (Supp. Fig. 2.2.6C).

2.2.14. Absence of deubiquitinases and RPN4 in combination with DFM1 do not exacerbate toxicity

We tested double knockouts of *dfm1*Δ*rpn4*Δ, *dfm1*Δ*ubp6*Δ, and *rpn4*Δ*ubp6*Δ cells expressing Hmg2 in the substrate-toxicity assay to determine whether these genetic backgrounds display the same or different growth defect than either of the single knockouts. Expression of either Hmg2 or Ste6* in either *dfm1*Δ*rpn4*Δ or*F020dfm1*Δ*ubp6*Δ cells resulted in a growth defect that phenocopied that observed in any of the single knockouts (Supp. Fig.2.2.7A and Supp. Fig. 2.2.7B Fig), whereas expression of CPY* showed no growth defect (Supp. Fig. 2.2.7C). In contrast, *rpn4*Δ*ubp6*Δ cells showed a growth defect in the absence of substrates, whereas *rpn4*Δ and *ubp6*Δ displayed normal growth. Moreover, *rpn4*Δ*ubp6*Δ cells along with expression of Hmg2 or Ste6* resulted in synthetic lethality (Supp. Fig. 2.2.7A–Supp. Fig. 2.2.7C). This indicates that there is an exacerbation of stress in *rpn4*Δ*ubp6*Δ background, whereas there is no increase in toxicity when RPN4 or UBP6 are knocked out in combination with DFM1. It is likely that there are several parallel pathways contributing to preventing stress from misfolded membrane proteins and resolving this stress, and Dfm1 appears to be one of the major mediators of misfolded membrane stress prevention.

We also tested expression of previously described Hmg2 mutants K6R and K357R in *rpn4*Δ and *ubp6*Δ cells (Supp. Fig. 2.2.7D). As with *dfm1*Δ cells expressing these mutants, expression of Hmg2-K6R does not cause toxicity while Hmg2-K357R does cause toxicity in both *rpn4*Δ and *ubp6*Δ. Thus, ubiquitination of misfolded membrane proteins influences toxicity in *dfm1*Δ, *rpn4*Δ, and *ubp6*Δ cells.

2.2.15. Misfolded protein aggregation toxicity requires protein ubiquitination

We originally hypothesized that ubiquitination of membrane proteins was promoting those proteins to become aggregated. To test this hypothesis, we measured aggregation versus solubility of Hmg2-K6R in *dfm1*Δ cells in the detergent solubility assay (Fig. 2.2.7I). Surprisingly, Hmg2-K6R phenocopied Hmg2 in *dfm1*Δ cells, with virtually all the protein being in the aggregated fraction. This demonstrates ubiquitin does not influence aggregation and not all misfolded membrane protein aggregates are toxic.

2.2.16. Increased expression of Dfm1 relieves misfolded membrane protein stress in *rpn4*Δ and *ubp6*Δ cells

Using the substrate-toxicity assay, we examined whether increasing expression of Dfm1 could relieve growth stress in *rpn4*Δ and *ubp6*Δ cells expressing Hmg2. We utilized the substrate-toxicity assay with the addition of galactose inducible Dfm1 to address this question. Increasing Dfm1 in both *rpn4*Δ+Hmg2 and *ubp6*Δ+Hmg2 cells restored normal growth (Supp. Fig. 2.2.7E). Importantly, endogenous Dfm1 is already present in these cells, but increasing expression level relieves toxicity caused by misfolded membrane proteins.

2.3. Discussion

Proper protein folding and efficient elimination of misfolded proteins is imperative for maintaining cellular health. Accumulation of misfolded proteins, which is a widespread phenomenon in aging and diseased cells, is deleterious to cells and can impact cellular function. Despite membrane proteins accounting for one-quarter of proteins in the cell, there is a dearth of research into the mechanisms cells use to prevent misfolded membrane protein toxicity. In this study, we sought to understand how cells prevent toxicity from misfolded proteins and how they are impacted by misfolded membrane protein stress. By employing our genetically tractable substrate-toxicity assay, we found that the source of cellular toxicity was aggregation of ubiquitinated misfolded membrane proteins and that Dfm1's rhomboid motifs, lipid thinning function, and substrate engagement function are required for its chaperone-like function towards aggregation-prone membrane substrates. We propose a model in which ubiquitinated misfolded membrane proteins in dfm1Δ cells form aggregates, resulting in a reduction in monomeric ubiquitin and compromised proteasome function. Overall, our studies unveil a new role for rhomboid pseudoproteases in mitigating the stress state caused by ERAD membrane substrates, a function that is independent of their retrotranslocation function.

Our results above (Fig. 2.2.2B - Fig. 2.2.2D) indicate differential requirements for Dfm1's role in membrane substrate retrotranslocation, versus its role in stress alleviation. These results are fascinating, because of all the retrotranslocation-deficient mutants tested, we were able to identify a mutant that was still able to rescue the growth defect observed in dfm1Δ+Hmg2 cell. This indicates a bifurcated role of Dfm1 in retrotranslocation and membrane protein stress alleviation. The retrotranslocation defective mutants that did not

restore growth were mutations of conserved rhomboid protein motifs (WR and Gx3G), mutants that obliterate substrate engagement (Loop 1 mutants: F58S, L64V, and K67E), and mutants that reduce the ability of Dfm1 to distort the ER membrane (TMD 2 mutants: Q101R and F107S). This indicates the substrate binding and lipid distortion roles of Dfm1 that are imperative for retrotranslocation are also imperative for alleviation of misfolded membrane protein stress. In contrast, the SHP box mutant, which prevents Cdc48 binding to Dfm1, restores growth in *dfm1*Δ+Hmg2 cells (Fig. 2.2.2D). While Cdc48 binding to Dfm1 is critical for retrotranslocation, this is not a requirement for Dfm1's role in preventing membrane proteotoxicity. Previous work from our lab indicates transient interactions between membrane substrates and Dfm1 still occurs even when Dfm1's Cdc48 recruitment activity is impaired (Nejatfard et al., 2021). This suggests that this level of physical interaction is sufficient for Dfm1 to directly act on substrates to prevent membrane substrate-induced stress.

Our results from both this study and previous work from the lab on Dfm1's function indicate Dfm1 acts directly on misfolded membrane proteins to promote influence aggregation (Nejatfard et al., 2021). Firstly, all the L1 mutants of Dfm1, which have previously been shown to ablate binding of Dfm1 to misfolded membrane proteins, such as Hmg2, are not able to restore nonaggregated Hmg2. Secondly, we demonstrate here that DDM solubilized (non-aggregated) Hmg2 still interacts with Dfm1, as shown through co-immunoprecipitation (Fig. 2.2.3C). Lastly, both human Derlin-1 and Derlin-2 are able to restore non-aggregated Hmg2 in dfm1Δ cells (Fig. 2.2.4F). It seems unlikely that if Dfm1 was influencing solubility of Hmg2 through an indirect route that mammalian derlins, which have diverged significantly from Dfm1, would still influence aggregation.

We previously demonstrated that expression of integral membrane ERAD substrate induces toxicity in yeast cells when Dfm1's function is impaired. Remarkably, this strong growth defect phenotype is unique to *dfm1*Δ strains: other equally strong ERAD deficient mutants, both upstream or downstream of Dfm1 (*hrd1*Δ or *cdc48-2*), show no growth stress upon similar elevation of ERAD integral membrane substrates. Thus, the growth effects above suggest the intriguing possibility that Dfm1 has a unique role in this novel ER stress.

Our data on the ability of Dfm1 to influence misfolded membrane protein aggregation provides evidence that this is the mechanism by which Dfm1 prevents misfolded membrane protein toxicity. We find that both WT Dfm1 and Dfm1-5Ashp expression result in nonaggregated Hmg2 (Fig. 2.2.3A and 2.2.3B). In contrast, the retrotranslocation defective Dfm1 rhomboid motif mutants, L1 mutants, and TMD2 mutants are not able to influence Hmg2 aggregation. This agrees with our observation that both WT Dfm1 and Dfm1-5Ashp can restore normal growth in *dfm1*Δ cells in the S-T assay, but the rhomboid motifs mutants cannot (Fig. 2.2.2B and Fig. 2.2.2D). The exact mechanism by which Dfm1 results in non-aggregated Hmg2 is unclear. We propose two possible models that will be important to distinguish between in future works. In one model, Dfm1 functions as a disaggregase to physically separate misfolded membrane proteins from existing protein aggregates. In another model, Dfm1 functions as a holdase to maintain misfolded membrane proteins in a non-aggregated state. We believe present data indicates a holdase function is more likely, as Dfm1 interacts with solubilized Hmg2 (Fig. 2.2.3C), potentially preventing it from forming aggregates, but this hypothesis will need to be tested more mechanistically in future studies. While the ability of Dfm1-5Ashp to influence Hmg2 aggregation in *dfm1*Δ cells indicates that Dfm1's chaperone-like ability is likely ATP-independent, we cannot exclude the possibility

that Dfm1 recruits another ATPase besides Cdc48, independent of the SHP box motif. Another possibility is that Dfm1 itself can bind and hydrolyze ATP. There are a growing number of identified ATP-independent disaggregases (Huang et al., 2021), including 1 membrane protein dissagregase identified in plants (Jaru-Ampornpan et al., 2010). Understanding how Dfm1 influences the aggregation of membrane substrates will be an important future line of inquiry.

By analyzing the transcriptome upon triggering this unique membrane substrate-induced stress state, we find that many proteasomal subunits are up-regulated. Interestingly, Rpn4—a transcription factor known to induce proteasome subunit expression—up-regulates many of the proteasomal subunits up-regulated in our transcriptome analysis. One interpretation of our data is that accumulation of integral membrane proteins results in reduced proteasome efficiency, which triggers Rpn4-mediated up-regulation of proteasome subunits. Indeed, we and others have shown that *rpn4*Δ cells phenocopy *dfm1*Δ cells by exhibiting a growth defect upon expression of ERAD integral membrane substrates and not ERAD lumenal substrates (Boyle Metzger et al., 2009). This was also supported by our above studies showing ERAD membrane substrates exacerbate cellular growth defects when proteasome function is compromised with treatment of proteasome inhibitor, MG132 (Fig. 2.2.6D - Fig. 2.2.6F). These data indicate that cells require optimal proteasome activity to avoid the proteotoxicity associated with integral membrane ERAD substrates.

The facile and genetically tractable substrate-toxicity assay allowed us to ascertain how membrane substrates cause the growth defect phenotype when Dfm1 is absent. Intriguingly, no growth defect was observed in *dfm1*Δ cells expressing the K6R Hmg2 mutant

(with negligible ubiquitination), while the K357R Hmg2 mutant (with slight ubiquitination) still showed a growth defect, suggesting the source of Dfm1-mitigated stress is ubiquitination of the substrates. We reasoned that accumulation of ubiquitinated ERAD membrane substrates disrupts the ubiquitin pool through excessive ubiquitination of substrates and concomitant reduction of the ubiquitin pool. Indeed, a collection of DUB mutants (*ubp6*Δ, *doa4*Δ, *ubp14*Δ)—known for their role in replenishing the ubiquitin pool through their deubiquitinating function—is unable to mitigate the proteotoxic effect of integral membrane substrates, and proteotoxic stress is rescued with exogenous addition of ubiquitin molecules in *dfm1*Δ+Hmg2 cells (Fig. 2.2.7D, Fig. 2.2.7G and Fig. 2.2.7H). This observation is extended in mammalian studies in which a mouse line with a loss-of-function mutation in Usp14, the mammalian homolog of Ubp6, reduces the free ubiquitin pool in neurons and results in ataxia that can be rescued with exogenous ubiquitin expression (Anderson et al., 2005). The reduction we observed in monomeric ubiquitin in *dfm1*Δ+Hmg2 cells was approximately half of that observed in WT+Hmg2 cells (Fig. 2.2.6E). The hypothesis that this reduction is enough to contribute to toxicity in these cells is supported both by our experiment demonstrating the exogenous ubiquitin restores growth in the substrate-toxicity assay (Fig. 2.2.7D) and by the observation that ataxic Usp14-deficient mice only show about a 25% reduction in monomeric ubiquitin in most tissues (Anderson et al., 2005). Perhaps what is most fascinating is that the stress state is only induced by excessive ubiquitination of integral membrane substrates and not soluble proteins residing in the cytosol (Supp. Fig. 2.2.6C), suggesting the source of stress is due to excessive ubiquitination of substrates at the ER membrane.

There is an emerging body of evidence that protein aggregation is not inherently toxic (De Groot et al., 2012; Li et al., 2012; Li et al., 2008). We propose a model in which two

conditions need to be met for misfolded membrane protein accumulation to become toxic; (1) the misfolded membrane proteins must become aggregated; and (2) the misfolded membrane proteins must be ubiquitinated (Fig. 2.2.8). If only one of these conditions is met, there is no toxicity observed in the substrate-toxicity assay. For example, Dfm1-5Ashp restores growth and results in non-aggregated Hmg2, even without restoring retrotranslocation (Figs 2E and 3A). These accumulated membrane proteins would still be expected to be ubiquitinated, but no toxicity is observed without aggregated Hmg2 in this circumstance. Conversely, the non-ubiquitinated Hmg2-K6R does not cause toxicity, even though virtually all the protein is aggregated in *dfm1*Δ cells (Fig. 2.2.7I). Additionally, the ability to influence aggregation of misfolded membrane proteins appears specific to Dfm1 among ERAD machinery, as cdc48-2 cells with an overexpressed misfolded membrane protein do not display growth stress, and nearly all Hmg2 non-aggregated in *hrd1*Δ cells in the detergent solubility assay (Figs 1E, 1F and 4A).

Molecular chaperones have long been identified for their role in protein quality control systems, including ERAD, for their ability to triage terminally misfolded proteins to degradation machinery. In recent years, more studies have shown a dual function of protein quality control machinery in directly controlling degradation and being chaperones (Neal et al., 2017; Wang et al., 2011). We have now provided evidence for rhomboid pseudoproteases, a subclass of proteins widely recognized as involved in protein quality control, having chaperone-like function. This raises the question of whether chaperone ability is more widespread among other protein quality control components, specifically those known to bind to membrane proteins. Previous work from the Brodsky lab demonstrated that aggregation-prone ER proteins are more likely to be targeted by ERAD and are

disaggregated by the ATP-dependent cytoplasmic disaggregase Hsp104, which aids in retrotranslocation (Preston et al., 2018). Our results demonstrate that a component of membrane protein retrotranslocation machinery, Dfm1, also has a chaperone-like function to aid in retrotranslocation. The Carvalho group has demonstrated that the Asi complex involved in inner nuclear membrane protein quality control in yeast and the mammalian ERAD factor membralin are able to recognize TMDs of misfolded proteins (Natarajan et al., 2020; van de Weijer et al., 2020). It is possible that chaperone function has arisen more than once evolutionarily among proteins involved in membrane protein quality control.

Rhomboid pseudoproteases have been recognized for over a decade as being involved in a diverse array of cellular processes, from protein quality control to cell signaling to adaptations to cellular stress (Christova et al., 2013; Lee et al., 2015; Lilley et al., 2004; Oda et al., 2006; Zettl et al., 2011). Our lab and others have made progress towards understanding how these proteins are able to function in such diverse cellular processes without an enzymatic function. With the knowledge that several derlin proteins are chaperone-like proteins, it will be of extreme interest to determine if this function is conserved among all rhomboid pseudoproteases, and even among the active rhomboid proteases. Two specific areas of interest include determining the conservation of this chaperone-like function and identifying the repertoire of substrates that can be solubilized by rhomboid pseudoproteases. There are 2 subclasses of rhomboid pseudoproteases, iRhoms and derlins (Lemberg et al., 2007). Both of these classes are evolutionarily distinct, and it will be of interest to determine if chaperone-like ability is only specific to derlins and not to iRhoms. Derlins are known to function in retrotranslocation of a wide variety of substrates, including disease-associated membrane substrates. In this study, we observed accumulation of both

WT and the disease-causing CFTRΔF508 resulted in growth stress in dfm1Δ cells (Greenblatt et al., 2011; Knop et al., 1996; Lilley et al., 2004; Ye et al., 2004). Surprisingly, we found that heterologous expression of both human Derlin-1 and Derlin-2 restores growth in yeast dfm1Δ+Hmg2 cell and results in non-aggregated Hmg2, implying the chaperone-like function is a conserved feature among derlin rhomboid pseudoproteases. Moreover, research from our lab demonstrated that Derlin-1 and Derlin-2 do not support ERAD-M retrotranslocation in dfm1Δ cells (Nejatfard et al., 2021). This indicates that Derlin-1 and Derlin-2 relieve toxicity in dfm1Δ+Hmg2 cells, without restoring retrotranslocation, through a conserved chaperone-like function.

Our studies provide the first evidence that the derlin subclass of rhomboid pseudoproteases function as chaperone-like proteins by influencing aggregation of misfolded membrane substrates. Findings gleaned from our studies hold great promise for foundational and translational arenas of cell biology, since fundamental understanding of a membrane protein chaperone will aid in understanding a plethora of diseases associated with misfolded membrane proteins such as cystic fibrosis, retinal degeneration, and neurodegenerative diseases.

2.4. Materials and Methods

Plasmids and strains

Plasmids used in this study are listed in Supp. Table 2.4.1. Plasmids for this work were generated using standard molecular biological cloning techniques via PCR of genes from yeast genomic DNA or plasmid followed by ligation into a specific restricted digested site within a construct and verified by sequencing (Eton Bioscience and Plasmidsaurus). Primer information is available upon request. A complete list of yeast strains and their corresponding genotypes are listed in Supp. Table 2.4.2 Table. All strains used in this work were derived from S288C or Resgen. Yeast strains were transformed with DNA or PCR fragments using the standard LiOAc method in which null alleles were generated by using PCR to amplify a selection marker flanked by 30 base pairs of the 50 and 30 regions, which are immediately adjacent to the coding region of the gene to be deleted. The selectable markers used for making null alleles were genes encoding resistance to G418 or CloNat/nourseothricin or HIS3. After transformation, strains with drug markers were plated onto YPD followed by replica-plating onto YPD plates containing 500 µg/mL G418 or 200 µg/mL nourseothricin, or minimal media (-His) plates. All gene deletions were confirmed by PCR.

Galactose induction

For strains with plasmids containing galactose inducible promoters, protein expression was achieved by growing proteins overnight in appropriate selection media containing 2% raffinose as carbon source. The following day, samples were diluted between 0.10 and 0.20 OD at 600 nm (diluted absorbance was assay dependent). Cells in log phase were induced by adding 0.2% galactose to media. Minimum time requirement for robust protein expression was determined for strains using flow cytometry and was 2 or 3 hours for every strain used.

Flow cytometry

Yeast were grown in minimal medium with 2% raffinose and 0.2% galactose and appropriate amino acids into log phase (OD600 < 0.2). The BD Biosciences FACS Calibur flow cytometer measured the individual fluorescence of 10,000 cells. Experiments were analyzed using GraphPad Prism v8.

Unfolded protein response activation assay

Strains were inoculated overnight in minimal media (-His) with 2% raffinose. The following day, samples were diluted to 0.20 OD in of minimal media (-His) and allowed to grow to log phase. Samples were then diluted to 0.30 OD before adding 20% galactose to a

final concentration of 0.2% galactose or an equal volume of dH2O. Timer was started after galactose addition and samples were measured using flow cytometry, as described above, every hour, starting from the 0-hour mark, and ending at the 5-hour mark. At the 1-hour time point, samples were treated with either 2 µg/mL tunicamycin or an equal volume of DMSO.

Hac1 splicing PCR

Strains were prepared the same as for the UPR activation assay, except they were grown in minimal media (-Ura -His) with 2% raffinose. After 5 hours of incubation with 0.2% galactose and 2 µg/mL tunicamycin, samples were pelleted and washed with dH2O. RNA from samples was extracted using Qiagen RNeasy Mini Kit. Samples were ethanol precipitated by adding 1 uL of Glycoblue (Thermo Fisher), 50 uL of 7.5 M ammonium acetate, and 700 uL of chilled 100% ethanol. Tubes were then stored at −80˚C for between 3 hours to overnight. Samples were then centrifuged at 13,000 × g for 30 minutes at 4˚C and supernatant was removed. Pellets were washed twice with 75% ethanol and centrifuged at room temperature at 13,000xg for 30 seconds. After drying the pellet, it was resuspended in 15 uL of molecular grade water. A total of 250 ng of RNA from each sample was used to generate cDNA using a standard protocol for ProtoscriptII Reverse Transcriptase (NEB), except with 1 uL of Oligo (dT)12-18 (Thermo Fisher Scientific) used for primer. Wizard SV Gel and PCR Clean-Up System (ProMega) was used on cDNA samples. Hac1 mRNA was amplified using forward primer 5’ ACTTGGCTATCCCTACCAACT 3’ and reverse primer 5’ ATGAATTCAAACCTGACTGC 3’. PCR products were resolved on a 2% agarose gel.

MG132 sensitivity assay

MG132 sensitivity assay was performed using a protocol adapted from (Boyle Metzger et al., 2009). In brief, cultures grown minimal media (-his) with 2% dextrose. Cultures in log phase were split and treated with either 50 μM MG132 in DMSO or an equal volume of DMSO alone and incubated for 8 hours at 30˚C. Cultures were diluted 1:500 and 100 μL of sample was plated onto minimal media (-His) plates and grown at 30˚C for 3 days. Two technical replicates and 3 biological replicates were done for each strain. CFUs were counted for using the ProMega Colony Counter application for iPhone.

Spot dilution assay (substrate-toxicity assay)

Yeast strains were grown in minimal selection media (-His) supplemented with 2% dextrose to log phase (OD600 0.2 to 0.3) at 30˚C. Approximately 0.10 OD cells were pelleted and resuspended in 1 mL dH2O. A total of 250 μL of each sample was transferred to a 96-well plate where a 5-fold serial dilution in dH2O of each sample was performed to obtain a gradient of 0.1–0.0000064 OD cells. The 8 × 6 pinning apparatus was used to pin cells onto synthetic complete agar plates supplemented with 2% dextrose or 2% galactose. Plates were incubated at 30˚C and removed from the incubator for imaging after 3 days and again after 7 days. All experiments were done in biological triplicates with technical replicates.

RNA sequencing

RNA was isolated using a Qiagen RNeasy kit using standard protocol for yeast. Samples were eluted twice with 30 µL of molecular grade water. To cleanup samples, 1 µL of DNase was added to each sample and was incubated at 37˚C for 25 minutes. Approximately 6 µL of DNase inactivation buffer was added to samples and was incubated for 2 minutes. Samples were spun down at 10,000xg for 1.5 minutes and supernatant was transferred to a new microfuge tube. Samples were ethanol precipitated by adding 1 µL of Glycoblue (Thermo Fisher), 50 µL of 7.5 M ammonium acetate, and 700 µL of chilled 100% ethanol. Tubes were then stored at −80˚C for between 3 hours to overnight. Samples were then centrifuged at 13,000 × g for 30 minutes at 4˚C and supernatant was removed. Pellets were washed twice with 75% ethanol and centrifuged at room temperature at 13,000xg for 30 seconds. After drying the pellet, it was resuspended in 15 µL of molecular grade water. Samples were measured for RNA concentration and an equal concentration of each sample was measured out into a total of 50 µL of molecular grade water and RNA-seq was performed as previously described (Link et al., 2018) or as follows. Poly A-enriched mRNA was fragmented, in 2× Superscript III Mg2+ containing first-strand buffer with 10 mM DTT (Invitrogen), by incubation at 94˚C for 9 minutes, then immediately chilled on ice before the next step. The 10 µL of fragmented mRNA, 0.5 µL of Random primer (Invitrogen), 0.5 µL of Oligo dT primer (Invitrogen), 0.5 µL of SUPERase-In (Ambion), 1 µL of dNTPs (10 mM), and 1 µL of DTT (10 mM) were heated at 50˚C for 3 minutes. At the end of incubation, 5.8 µL of water, 1 µL of DTT (100 mM), 0.1 µL Actinomycin D (2 µg/µL), 0.2 µL of 1% Tween-20 (Sigma), and 0.2 µL of Superscript III (Invitrogen) were added and incubated in a PCR machine using the following conditions: 25˚C for 10 minutes, 50˚C for 50 minutes, and a 4˚C

hold. The product was then purified with Agentcourt RNAClean XP beads (Beckman Coulter) according to manufacturer's instruction and eluted with 10 µL nuclease-free water. The RNA/cDNA double-stranded hybrid was then added to 1.5 µL of Blue Buffer (Enzymatics), 1.1 µL of dUTP mix (10 mM dATP, dCTP, dGTP, and 20 mM dUTP), 0.2 µL of RNAse H (5 U/µL), 1.05 µL of water, 1 µL of DNA polymerase I (Enzymatics), and 0.15 µL of 1% Tween-20. The mixture was incubated at 16˚C for 1 hour. The resulting dUTP-marked dsDNA was purified using 28 µL of Sera-Mag Speedbeads (Thermo Fisher Scientific), diluted with 20% PEG8000, 2.5 M NaCl to final of 13% PEG, eluted with 40 µL EB buffer (10 mM Tris-Cl (pH 8.5)), and frozen −80˚C. The purified dsDNA (40 µL) underwent end repair by blunting, A-tailing and adapter ligation using barcoded adapters (NextFlex, Bioo Scientific). Libraries were PCR-amplified for 9 to 14 cycles, size selected by gel extraction, quantified by Qubit dsDNA HS Assay Kit (Thermo Fisher Scientific) and sequenced on a NextSeq 500.

RNA sequencing data analysis

Data was analyzed by normalizing reads per million and using principal components analysis to determine genes with the highest PC1 (+) scores and lowest PC1 (-) scores between dfm1Δ +GALpr-Hmg2-GFP and every other strain tested. From this list, we used the top 100 genes with the highest (+) and lowest (-) PCA1 values, and cross referenced those to the normalized transcript per million reads value for each gene and removed genes that were not expressed at either a higher (for +PCA1 values) or lower (for -PCA1 values) reads per million level than all other conditions that were sequenced. Then, this list of up-regulated and down-regulated genes was used for GO analysis using http://geneontology.org/.

Fluorescence microscopy

To prepare cells, overnight cultures were diluted to approximately 0.20 OD in minimal media lacking uracil (-URA). After growing approximately 3 hours, samples were pelleted and washed with dH2O before being resuspended in 80 uL of media to be used for imaging. Fluorescence microscopy was accomplished using a CSU-X1 Spinning Disk (Yokogawa) confocal microscope at the Nikon Imaging Center on the UCSD campus. Samples were analyzed to measure the fraction of GFP in puncta.

Microscopy quantification and analysis

Microscopy images (16-bit) were analyzed using the Fiji distribution of ImageJ2 (Schindelin et al., 2012) and data was compiled in the RStudio integrated development environment of R (RStudio Team, 2020). Briefly, cell outlines were segmented by uploading brightfield images of each field of view to the online YeastSpotter tool (Lu et al., 2019); available at http://yeastspotter.csb.utoronto.ca/. Then, fluorescent micrographs from the 488 channel were maximum-projected for all z-slices. To identify Hmg2 puncta in the 488 channel, a 20-pixel median filter was subtracted from each max-Z projected image. Then, any fluorescent Hmg2 signal above a gray value of 750 was thresholded as a “puncta.” This threshold value was applied to all fields of view, regardless of genotype, and was determined after manually comparing the puncta calls for representative images of each genotype using different threshold values. The fraction of Hmg2 in these bright puncta relative to total Hmg2 in the cell was quantified by summing the integrated density of all puncta in a cell and

dividing by the total integrated density of the cell. All ImageJ macros and Rscripts used in this analysis, as well as more detailed methods, are available in a GitHub repository from 3 March 2022 (https://github.com/LiviaSongster/yeast-fluor-percent-puncta). All statistical analysis was performed using GraphPad Prism v8.

Detergent solubility assay

ER microsomes were isolated by centrifuging and pelleting 15 OD of yeast in log phase growth. Pellets were resuspended in MF buffer (20 mM Tris (pH 7), 100 mM NaCl, 300 mM sorbitol) with protease inhibitors (PIs) (1 mM phenylmethylsulfonyl fluoride, 260 µM 4-(2-aminoethyl) benzenesulfonyl fluoride hydrochloride, 100 µM leupeptin hemisulfate, 76 µM pepstatin A, 5 mM aminocaproic acid, 5 mM benzamidine, and 142 µM N-tosyl-l-phenylalanine chloromethyl ketone) and 0.5 mM lysis beads were added to each sample. Samples were vortexed 6 times in 1-minute intervals, with 1-minute on ice in between. Lysed cells were transferred to new microcentrifuge tube and samples were clarified by spinning at 1,500× for 5 minutes at 4˚C. Microsomes were separated by centrifuging clarified lysate at 14,000 × g for 1 minute. Fractions were incubated on ice in the presence or absence of 1% DDM for 1 hour. The mixture was then centrifuged at 14,000 × g for 30 minutes at 4˚C, and the detergent soluble fraction (i.e., the supernatant) was precipitated with 20% trichloroacetic acid (TCA) on ice for 30 minutes and then centrifuged at 14,000 × g for 30 minutes to get a pellet of the soluble protein. Proteins from both the soluble and insoluble fractions were resuspended in sample buffer and resolved by SDS-PAGE.

Co-Immunoprecipitation

Yeast were grown to mid log phase in minimal media, and 15 OD equivalents were pelleted, washed in water, and resuspended in 240 µl lysis buffer (0.24 M sorbitol, 1 mM EDTA, 20 mM KH2PO4/K2HPO4 (pH 7.5)) with PIs. Acid-washed glass beads were added up to the meniscus. Cells were lysed on a multivortexer at 4˚C for six to eight 1-minute intervals with 1 minute on ice in between each lysis step. The lysates were transferred to a new tube, and lysates cleared with 5-second pulses of centrifugation. Microsomes were pelleted from cleared lysates by centrifugation at 14,000 × g for 5 minutes. Microsome pellets were washed once in XL buffer (1.2 M sorbitol, 5 mM EDTA, 0.1 M KH2PO4/K2HPO4 (pH 7.5)) and resuspended in XL buffer. Samples were then solubilized by the addition of detergent solution at 10× the desired final concentration in XL buffer (final concentration of 1% DDM). Preparations with detergent were incubated at 4˚C for 1 hour with rocking and then repeatedly pipetted up and down. Finally, samples were cleared by centrifugation in a benchtop microcentrifuge for 15 minutes at 16,000 g. The supernatants were then separated by ultracentrifugation at 89,000 RPM for 15 minutes, and the supernatant was incubated overnight with 10 µL of equilibrated GFP-Trap agarose (ChromoTek, Hauppauge, New York) at 4˚C. The next day, the GFP-Trap agarose beads were combined to 1 tube, washed once with non-detergent IP buffer, washed once more with IP wash buffer, and resuspended in 100 µL of 2xUSB. Samples were resolved on 8% SDS-PAGE and immunoblotted for Hmg2-GFP with anti-GFP, Dfm1-HA with anti-HA, and anti-Sec61 antibody.

Cycloheximide-chase assay

Cycloheximide chase assays were performed as previously described (Sato et al., 2009). Cells were grown to log-phase (OD600 0.2 to 0.3) and cycloheximide was added to a final concentration of 50 µg/ mL. At each time point, a constant volume of culture was removed and lysed. Lysis was initiated with addition of 100 µL SUME with PIs and glass beads, followed by vortexing for 4 minutes. Approximately 100 µL of 2xUSB was added followed by incubation at 55˚C for 10 minutes. Samples were clarified by centrifugation and analyzed by SDS-PAGE and immunoblotting.

In vivo ubiquitination assay

Cells were grown to log phase (OD600 0.3 to 0.6) and 15 ODs of cells were pelleted. Cells were resuspended in H20, centrifuged and lysed with the addition of 0.5 mM glass beads and 400 µL of XL buffer (1.2 M sorbitol, 5 mM EDTA, 0.1 M KH2PO4, final pH 7.5) with PIs followed by vortexing in 1-minute intervals for 6 to 8 minutes at 4˚C. Lysates were combined and clarified by centrifugation at 2,500 g for 5 minutes. Approximately 100 µL clarified lysate was resuspended in 100 µL SUME (1% SDS, 8 M Urea, 10 mM MOPS (pH 6.8), 10 mM EDTA) with PIs and 5 mM N-ethyl maleimide (NEM, Sigma) followed by addition of 600 µL immunoprecipitation buffer (IPB) (15 mM Na2HPO4, 150 mM NaCl, 2% Triton X-100, 0.1% SDS, 0.5% deoxycholate, and 10 mM EDTA (pH 7.5)) with PIs and NEM. A total of 15 µL of rabbit polyclonal anti-GFP antisera (C. Zuker, University of California, San Diego) was added to the samples for immunoprecipitation (IP) of Hmg2-GFP. Samples were

incubated on ice for 5 minutes, clarified at 14,000 g for 5 minutes, and removed to a new eppendorf tube and incubated overnight at 4˚C. Approximately 100 µL of equilibrated Protein A-Sepharose in IPB (50% w/v) (Amersham Biosciences) was added and incubated for 2 hours at 4˚C. Proteins A beads were washed twice with IPB and washed once more with IP wash buffer (50 mM NaCl, 10 mM Tris), aspirated to dryness, resuspended in 2× urea sample buffer (8 M urea, 4% SDS, 1 mM DTT, 125 mM Tris (pH 6.8)), and incubated at 55˚C for 10 minutes. IPs were resolved by 8% SDS-PAGE, transferred to nitrocellulose, and immunoblotted with monoclonal anti-ubiquitin (Fred Hutchinson Cancer Center, Seattle) and anti-GFP (Clontech, Mountain View, California). Goat anti-mouse (Jackson ImmunoResearch, West Grove, Pennsylvania) and goat anti-rabbit (Bio-Rad) conjugated with horseradish peroxidase (HRP) recognized the primary antibodies. Western Lightning Plus (Perkin Elmer, Watham, Massachusetts) chemiluminescence reagents were used for immunodetection.

Western blot quantification

Western blot images were quantified using ImageJ/Fiji. Band intensities were measured from high resolution TIF files of western blot images acquired from a BioRad Chemidoc Imager. Data analysis was done using GraphPad Prism v8.

2.5. Acknowledgements

Chapter 2, in full, is a reprint of the material as it appears in PLOS Biology, 2023, Kandel, R; Jung, Jasmine; Syau, Della; Kuo, Tiffany; Songster, Livia; Horn, Casey; Chapman, Claire; Aguayo, Analine; Duttke, Sasha; Benner, Chris; Neal, Sonya E, PLOS Biology 2023. https://doi.org/10.1371/journal.pbio.3001950. The thesis author was a contributing author on this paper. The authors would like to thank Tom Rapoport (Harvard Medical School), Davis Ng (National University of Singapore), Randy Schekman (University of California, Berkeley), Susan Michaelis (John Hopkins University), and Jeff Brodsky (University of Pittsburgh) for providing plasmids and antibodies. We also thank the Neal lab members for their positive reinforcement, in depth discussions, and technical assistance. This work was supported by the National Institutes of Health (1R35GM133565 to SEN; R00GM135515 to SD), the National Science Foundation (2047391 to SEN), and the Pew Charitable Trusts (34089 to SEN). The funders had no role in study design, data collection and analysis, decision to publish, or preparation of the manuscript.

2.6. References

Adrain, C., & Cavadas, M. (n.d.). *The complex life of rhomboid pseudoproteases*. https://doi.org/10.1111/febs.15548

Anderson, C., Crimmins, S., Wilson, J. A., Korbel, G. A., Ploegh, H. L., & Wilson, S. M. (2005). Loss of Usp14 results in reduced levels of ubiquitin in ataxia mice. *Journal of Neurochemistry*, *95*(3), 724–731. https://doi.org/10.1111/j.1471-4159.2005.03409.x

Baldridge, R. D., & Rapoport, T. A. (2016). Autoubiquitination of the Hrd1 Ligase Triggers Protein Retrotranslocation in ERAD. *Cell*, *166*(2), 394–407. https://doi.org/10.1016/J.CELL.2016.05.04

Bays, N. W., Gardner, R. G., Seelig, L. P., Joazeiro, C. A., & Hampton, R. Y. (2001). Hrd1p/Der3p is a membrane-anchored ubiquitin ligase required for ER-associated degradation. *Nature Cell Biology*, *3*(1), 24–29. https://doi.org/10.1038/35050524

Began, J., Cordier, B., Březinová, J., Delisle, J., Hexnerová, R., Srb, P., Rampírová, P., Kožíšek, M., Baudet, M., Couté, Y., Galinier, A., Veverka, V., Doan, T., & Strisovsky, K. (2020). Rhomboid intramembrane protease YqgP licenses bacterial membrane protein quality control as adaptor of FtsH AAA protease . *The EMBO Journal*, e102935. https://doi.org/10.15252/embj.2019102935

Bhaduri, S., & Neal, S. E. (2021). Assays for studying normal versus suppressive ERAD-associated retrotranslocation pathways in yeast. *STAR Protocols*, *2*(3), 100640. https://doi.org/10.1016/j.xpro.2021.100640

Bhamidipati, A., Denic, V., Quan, E. M., & Weissman, J. S. (2005). Exploration of the topological requirements of ERAD identifies Yos9p as a lectin sensor of misfolded glycoproteins in the ER lumen. *Molecular Cell*, *19*(6), 741–751. https://doi.org/10.1016/J.MOLCEL.2005.07.027

Bock, J., Kühnle, N., Knopf, J. D., Landscheidt, N., Lee, J. G., Ye, Y., & Lemberg, M. K. (2022). Rhomboid protease RHBDL4 promotes retrotranslocation of aggregation-prone proteins for degradation. *Cell Reports*, *40*(6), 111175. https://doi.org/10.1016/J.CELREP.2022.111175

Boyle Metzger, M., & Michaelis, S. (2008). Analysis of Quality Control Substrates in Distinct Cellular Compartments Reveals a Unique Role for Rpn4p in Tolerating Misfolded Membrane Proteins. *Molecular Biology of the Cell*, *20*(1006–1019).

Burns, G. D., Hilal, O. E., Sun, Z., Reutter, K. R., Preston, G. M., Augustine, A. A., Brodsky, J. L., & Guerriero, C. J. (2021). Distinct classes of misfolded proteins differentially affect the growth of yeast compromised for proteasome function. *FEBS Letters*, *595*(18), 2383–2394. https://doi.org/10.1002/1873-3468.14172

Cartier, A. E., Djakovic, S. N., Salehi, A., Wilson, S. M., Masliah, E., & Patrick, G. N. (2009). Regulation of synaptic structure by ubiquitin C-terminal hydrolase L1. *Journal of Neuroscience*, *29*(24), 7857–7868. https://doi.org/10.1523/JNEUROSCI.1817-09.2009

Cheng, S. H., Gregory, R. J., Marshall, J., Paul, S., Souza, D. W., White, G. A., O'Riordan, C. R., & Smith, A. E. (1990). Defective intracellular transport and processing of CFTR is the molecular basis of most cystic fibrosis. *Cell*, *63*(4), 827–834. https://doi.org/10.1016/0092-8674(90)90148-8

Christova, Y., Adrain, C., Bambrough, P., Ibrahim, A., & Freeman, M. (2013). Mammalian iRhoms have distinct physiological functions including an essential role in TACE regulation. *EMBO Reports*, *14*(10), 884–890. https://doi.org/10.1038/embor.2013.128

Cox, J. S., & Walter, P. (1996). A Novel Mechanism for Regulating Activity of a Transcription Factor That Controls the Unfolded Protein Response. *Cell*, *87*(3), 391–404. https://doi.org/10.1016/S0092-8674(00)81360-4

De Groot, N. S., Torrent, M., Villar-Piqué, A., Lang, B., Ventura, S., Gsponer, J., & Babu, M. M. (2012). Evolutionary selection for protein aggregation. *Biochemical Society Transactions*, *40*(5), 1032–1037. https://doi.org/10.1042/BST20120160

Enenkel, C., Lehmann, A., & Kloetzel, P. M. (1998). Subcellular distribution of proteasomes implicates a major location of protein degradation in the nuclear envelope-ER network in yeast. *The EMBO Journal*, *17*(21), 6144. https://doi.org/10.1093/EMBOJ/17.21.6144

Engberg, O., Ulbricht, D., Döbel, V., Siebert, V., Frie, C., Penk, A., Lemberg, M. K., & Huster, D. (2022). Rhomboid-catalyzed intramembrane proteolysis requires hydrophobic matching with the surrounding lipid bilayer. *Science Advances*, *8*(38), eabq8303. https://doi.org/10.1126/SCIADV.ABQ8303/SUPPL_FILE/SCIADV.ABQ8303_SM.PDF

Farinha, C. M., & Amaral, M. D. (2005). Most F508del-CFTR Is Targeted to Degradation at an Early Folding Checkpoint and Independently of Calnexin. *Molecular and Cellular Biology*, *25*(12), 5242–5252. https://doi.org/10.1128/MCB.25.12.5242-5252.2005/ASSET/2C5A297B-2994-4706-95BB-76C171C07C02/ASSETS/GRAPHIC/ZMB0120550950009.JPEG

Fleig, L., Bergbold, N., Sahasrabudhe, P., Geiger, B., Kaltak, L., & Lemberg, M. K. (2012). Ubiquitin-Dependent Intramembrane Rhomboid Protease Promotes ERAD of Membrane Proteins. *Molecular Cell*, *47*(4), 558–569. https://doi.org/10.1016/j.molcel.2012.06.008

Freeman, M. (2014). The rhomboid-like superfamily: molecular mechanisms and biological roles. *Annual Review of Cell and Developmental Biology*, *30*(1), 235–254. https://doi.org/10.1146/annurev-cellbio-100913-012944

Gardner, R. G., & Hampton, R. Y. (1999). A "distributed degron" allows regulated entry into the ER degradation pathway. *EMBO Journal*, *18*(21), 5994–6004. https://doi.org/10.1093/emboj/18.21.5994

Garza, R. M., Sato, B. K., & Hampton, R. Y. (2009). In vitro analysis of Hrd1p-mediated retrotranslocation of its multispanning membrane substrate 3-hydroxy-3-methylglutaryl (HMG)-CoA reductase. *The Journal of Biological Chemistry*, *284*(22), 14710–14722. https://doi.org/10.1074/jbc.M809607200

Gasch, A. P., Spellman, P. T., Kao, C. M., Carmel-Harel, O., Eisen, M. B., Storz, G., Botstein, D., & Brown, P. O. (2000). Genomic Expression Programs in the Response of Yeast Cells to Environmental Changes. *Molecular Biology of the Cell*, *11*, 4241–4257. https://doi.org/https://doi.org/10.1091/mbc.11.12.4241

Gnann, A., Riordan, J. R., & Wolf, D. H. (2004). Cystic Fibrosis Transmembrane Conductance Regulator Degradation Depends on the Lectins Htm1p/EDEM and the Cdc48 Protein Complex in Yeast. *Mol Biol Cell*, *15*(September), 4125–4135. https://doi.org/10.1091/mbc.E04

Greenblatt, E. J., Olzmann, J. a, & Kopito, R. R. (2011). Derlin-1 is a rhomboid pseudoprotease required for the dislocation of mutant α-1 antitrypsin from the endoplasmic reticulum. *Nature Structural & Molecular Biology*, *18*(10), 1147–1152. https://doi.org/10.1038/nsmb.2111

Hampton, R. Y. (2002). ER-associated degradation in protein quality control andcellular regulation. *Current Opinion in Cell Biology*, *14*, 476–482.

Hampton, R. Y., & Bhakta, H. (1997). Ubiquitin-mediated regulation of 3-hydroxy-3-methylglutaryl-CoA reductase. *Proceedings of the National Academy of Sciences of the United States of America*, *94*(24), 12944–12948. https://doi.org/10.1073/PNAS.94.24.12944/ASSET/9FCCF2C8-649B-4B42-8C6B-B1827811DE12/ASSETS/GRAPHIC/PQ2473110004.JPEG

Hampton, R. Y., Gardner, R. G., & Rine, J. (1996). Role of 26S proteasome and HRD genes in the degradation of 3-hydroxy-3-methylglutaryl-CoA reductase, an integral endoplasmic reticulum membrane protein. *Molecular Biology of the Cell*, *7*(12), 2029. https://doi.org/10.1091/MBC.7.12.2029

Hanna, J., Meides, A., Zhang, D. P., & Finley, D. (2007). A Ubiquitin Stress Response Induces Altered Proteasome Composition. *Cell*, *129*(4), 747–759. https://doi.org/10.1016/j.cell.2007.03.042

Hoelen, H., Zaldumbide, A., van Leeuwen, W. F., Torfs, E. C. W., Engelse, M. A., Hassan, C., Lebbink, R. J., de Koning, E. J., Resssing, M. E., de Ru, A. H., van Veelen, P. A., Hoeben, R. C., Roep, B. O., & Wiertz, E. J. H. J. (2015). Proteasomal Degradation of Proinsulin Requires Derlin-2, HRD1 and p97. *PLOS ONE*, *10*(6), e0128206. https://doi.org/10.1371/JOURNAL.PONE.0128206

Huang, L., Agrawal, T., Zhu, G., Yu, S., Tao, L., Lin, J. B., Marmorstein, R., Shorter, J., & Yang, X. (2021). DAXX represents a new type of protein-folding enabler. *Nature*, *597*(7874), 132–137. https://doi.org/10.1038/s41586-021-03824-5

Hwang, J., & Qi, L. (2018). Quality Control in the Endoplasmic Reticulum: Crosstalk between ERAD and UPR pathways. *Trends in Biochemical Sciences*, *43*(8), 593–605. https://doi.org/10.1016/j.tibs.2018.06.005

Jaru-Ampornpan, P., Shen, K., Lam, V. Q., Ali, M., Doniach, S., Jia, T. Z., & Shan, S. O. (2010). ATP-independent reversal of a membrane protein aggregate by a chloroplast SRP subunit. *Nature Structural and Molecular Biology*, *17*(6), 696–702. https://doi.org/10.1038/nsmb.1836

Kandel, R. R., & Neal, S. E. (2020). The role of rhomboid superfamily members in protein homeostasis: Mechanistic insight and physiological implications. In *Biochimica et Biophysica Acta - Molecular Cell Research* (Vol. 1867, Issue 10, p. 118793). Elsevier B.V. https://doi.org/10.1016/j.bbamcr.2020.118793

Knop, M., Finger, A., Braun, T., Hellmuth, K., & Wolf, D. H. (1996). Der1, a novel protein specifically required for endoplasmic reticulum degradation in yeast. *The EMBO Journal*, *15*(4), 753–763. https://doi.org/10.1002/j.1460-2075.1996.tb00411.x

Koller, A., Valesco, J., & Subramani, S. (2000). The CUP1 promoter of Saccharomyces cerevisiae is inducible by copper in Pichia pastoris. *Yeast*, *16*(7), 651–656. https://doi.org/10.1002/(SICI)1097-0061(200005)16:7<651::AID-YEA580>3.0.CO;2-F

Lee, D. H., & Goldberg, A. L. (1998). Proteasome Inhibitors Cause Induction of Heat Shock Proteins and Trehalose, Which Together Confer Thermotolerance in Saccharomyces cerevisiae . *Molecular and Cellular Biology*, *18*(1), 30–38. https://doi.org/10.1128/mcb.18.1.30

Lee, W., Kim, Y., Park, J., Shim, S., Lee, J., Hong, S. H., Ahn, H. H., Lee, H., & Jung, Y. K. (2015). IRhom1 regulates proteasome activity via PAC1/2 under ER stress. *Scientific Reports*, *5*. https://doi.org/10.1038/srep11559

Lemberg, M. K., & Freeman, M. (2007). Functional and evolutionary implications of enhanced genomic analysis of rhomboid intramembrane proteases. *Genome Research*, *17*(11), 1634–1646. https://doi.org/10.1101/gr.6425307

Li, J., McQuade, T., Siemer, A. B., Napetschnig, J., Moriwaki, K., Hsiao, Y. S., Damko, E., Moquin, D., Walz, T., McDermott, A., Chan, F. K. M., & Wu, H. (2012). The RIP1/RIP3 necrosome forms a functional amyloid signaling complex required for programmed necrosis. *Cell*, *150*(2), 339–350. https://doi.org/10.1016/j.cell.2012.06.019

Li, Z. F., Wu, X., Jiang, Y., Liu, J., Wu, C., Inagaki, M., Izawa, I., Mizisin, A. P., Engvall, E., & Shelton, G. D. (2008). Non-pathogenic protein aggregates in skeletal muscle in MLF1 transgenic mice. *Journal of the Neurological Sciences*, *264*(1–2), 77–86. https://doi.org/10.1016/j.jns.2007.07.027

Lilley, B. N., & Ploegh, H. L. (2004). A membrane protein required for dislocation of misfolded proteins from the ER. *Nature*, *429*(6994), 834–840. https://doi.org/10.1038/nature02592

Lilley, B. N., & Ploegh, H. L. (2005). Multiprotein complexes that link dislocation, ubiquitination, and extraction of misfolded proteins from the endoplasmic reticulum membrane. *Proceedings of the National Academy of Sciences of the United States of America*, *102*(40), 14296–14301. https://doi.org/10.1073/pnas.0505014102

Link, V. M., Duttke, S. H., Chun, H. B., Holtman, I. R., Westin, E., Hoeksema, M. A., Abe, Y., Skola, D., Romanoski, C. E., Tao, J., Fonseca, G. J., Troutman, T. D., Spann, N. J., Strid, T., Sakai, M., Yu, M., Hu, R., Fang, R., Metzler, D., Ren, B., & Glass, C. K. (2018). Analysis of Genetically Diverse Macrophages Reveals Local and Domain-wide Mechanisms that Control Transcription Factor Binding and Function. *Cell*, *173*(7), 1796-1809.e17. https://doi.org/10.1016/j.cell.2018.04.018

Liu, G., Beaton, S. E., Grieve, A. G., Evans, R., Rogers, M., Strisovsky, K., Armstrong, F. A., Freeman, M., Exley, R. M., & Tang, C. M. (2020). Bacterial rhomboid proteases mediate quality control of orphan membrane proteins. *The EMBO Journal*, *39*(10), e102922. https://doi.org/10.15252/EMBJ.2019102922

Mannhaupt, G., Schnall, R., Karpov, V., Vetter, I., & Feldmann, H. (1999). Rpn4p acts as a transcription factor by binding to PACE, a nonamer box found upstream of 26S proteasomal and other genes in yeast. *FEBS Letters*, *450*(1–2), 27–34. https://doi.org/10.1016/S0014-5793(99)00467-6

Mogk, A., Bukau, B., & Kampinga, H. H. (2018). Cellular Handling of Protein Aggregates by Disaggregation Machines. *Molecular Cell*, *69*(2), 214–226. https://doi.org/10.1016/j.molcel.2018.01.004

Nakatsukasa, K., Brodsky, J. L., & Kamura, T. (2013). A stalled retrotranslocation complex reveals physical linkage between substrate recognition and proteasomal degradation during ER-associated degradation. *Molecular biology of the cell*, 24(11), 1765-1775.

Natarajan, N., Foresti, O., Wendrich, K., Stein, A., & Carvalho, P. (2020). Quality Control of Protein Complex Assembly by a Transmembrane Recognition Factor. *Molecular Cell*, *77*(1), 108-119.e9. https://doi.org/10.1016/j.molcel.2019.10.003

Neal, S., Jaeger, P. A., Duttke, S. H., Benner, C. K., Glass, C., Ideker, T., & Hampton, R. (2018). The Dfm1 Derlin Is Required for ERAD Retrotranslocation of Integral Membrane Proteins. *Molecular Cell*, *69*(2). https://doi.org/10.1016/j.molcel.2017.12.012

Neal, S., Mak, R., Bennett, E. J., & Hampton, R. (2017). A Cdc48 “retrochaperone” function is required for the solubility of retrotranslocated, integral membrane Endoplasmic Reticulum-associated Degradation (ERAD-M) substrates. *Journal of Biological Chemistry*, *292*(8). https://doi.org/10.1074/jbc.M116.770610

Neal, S., Syau, D., Nejatfard, A., Nadeau, S., & Hampton, R. Y. (2020). HRD Complex Self-Remodeling Enables a Novel Route of Membrane Protein Retrotranslocation. *IScience*, *23*(9). https://doi.org/10.1016/j.isci.2020.101493

Nejatfard, A., Wauer, N., Bhaduri, S., Conn, A., Gourkanti, S., Singh, N., Kuo, T., Kandel, R., Amaro, R. E., & Neal, S. E. (2021). Derlin rhomboid pseudoproteases employ substrate engagement and lipid distortion to enable the retrotranslocation of ERAD membrane substrates. *Cell Reports*, *37*(3), 109840. https://doi.org/10.1016/j.celrep.2021.109840

Oda, Y., Okada, T., Yoshida, H., Kaufman, R. J., Nagata, K., & Mori, K. (2006). Derlin-2 and Derlin-3 are regulated by the mammalian unfolded protein response and are required for ER-associated degradation. *Journal of Cell Biology*, *172*(3), 383–393. https://doi.org/10.1083/JCB.200507057

Owsianik, G., Balzi, L., & Ghislain, M. (2002). Control of 26S proteasome expression by transcription factors regulating multidrug resistance in Saccharomyces cerevisiae. *Molecular Microbiology*, *43*(5), 1295–1308. https://doi.org/10.1046/j.1365-2958.2002.02823.x

Palmer, E. A., Kruse, K. B., Fewell, S. W., Buchanan, S. M., Brodsky, J. L., & McCracken, A. A. (2003). Differential requirements of novel A1PiZ degradation deficient (ADD) genes in ER-associated protein degradation. *Journal of Cell Science*, *116*(11), 2361–2373. https://doi.org/10.1242/jcs.00439

Preston, G. M., Guerriero, C. J., Metzger, M. B., Michaelis, S., & Brodsky, J. L. (2018). Substrate Insolubility Dictates Hsp104-Dependent Endoplasmic-Reticulum-Associated Degradation. *Molecular Cell*, *70*(2), 242-253.e6. https://doi.org/10.1016/j.molcel.2018.03.016

Rabinovich, E., Kerem, A., Fröhlich, K.-U., Diamant, N., & Bar-Nun, S. (2002). AAA-ATPase p97/Cdc48p, a cytosolic chaperone required for endoplasmic reticulum-associated protein degradation. *Molecular and Cellular Biology*, *22*(2), 626–634. http://www.pubmedcentral.nih.gov/articlerender.fcgi?artid=139744&tool=pmcentrez&rendertype=abstract

Ren, G., Tardi, N. J., Matsuda, F., Koh, K. H., Ruiz, P., Wei, C., Altintas, M. M., Ploegh, H., & Reiser, J. (2018). Podocytes exhibit a specialized protein quality control employing derlin-2 in kidney disease. *American Journal of Physiology - Renal Physiology*, *314*(3), F471–F482. https://doi.org/10.1152/ajprenal.00691.2016

Sato, B. K., & Hampton, R. Y. (2006). Yeast Derlin Dfm I interacts with Cdc48 and functions in ER homeostasis. *Yeast*, *23*(14–15), 1053–1064. https://doi.org/10.1002/yea.1407

Sato, B. K., Schulz, D., Do, P. H., & Hampton, R. Y. (2009). Misfolded Membrane Proteins Are Specifically Recognized by the Transmembrane Domain of the Hrd1p Ubiquitin Ligase. *Molecular Cell*, *34*(2), 212–222. https://doi.org/10.1016/j.molcel.2009.03.010

Stanley, A. M., Carvalho, P., & Rapoport, T. (2011). Recognition of an ERAD-L substrate analyzed by site-specific in vivo photocrosslinking. *FEBS Letters*, *585*(9), 1281–1286. https://doi.org/10.1016/J.FEBSLET.2011.04.009

Sun, F., Zhang, R., Gong, X., Geng, X., Drain, P. F., & Frizzell, R. A. (2006). Derlin-1 promotes the efficient degradation of the cystic fibrosis transmembrane conductance regulator (CFTR) and CFTR folding mutants. *Journal of Biological Chemistry*, *281*(48), 36856–36863. https://doi.org/10.1074/jbc.M607085200

Sun, Z., Guerriero, C. J., & Brodsky, J. L. (2021). Substrate ubiquitination retains misfolded membrane proteins in the endoplasmic reticulum for degradation. *Cell Reports*, *36*(12), 109717. https://doi.org/10.1016/J.CELREP.2021.109717

Suresh, H. G., Pascoe, N., & Andrews, B. (2020). The structure and function of deubiquitinases: Lessons from budding yeast: Mechanism and function of DUBs. *Open Biology*, *10*(10). https://doi.org/10.1098/rsob.200279rsob200279

Swanson, R., Locher, M., & Hochstrasser, M. (2001). A conserved ubiquitin ligase of the nuclear envelope/endoplasmic reticulum that functions in both ER-associated and Matα2 repressor degradation. *Genes & Development*, *15*(20), 2660–2674. https://doi.org/10.1101/GAD.933301

Tichá, A., Collis, B., & Strisovsky, K. (2018). The Rhomboid Superfamily: Structural Mechanisms and Chemical Biology Opportunities. In *Trends in Biochemical Sciences* (Vol. 43, Issue 9, pp. 726–739). Elsevier Ltd. https://doi.org/10.1016/j.tibs.2018.06.0

Twomey, E. C., Ji, Z., Wales, T. E., Bodnar, N. O., Ficarro, S. B., Marto, J. A., Engen, J. R., & Rapoport, T. A. (2019). *Substrate processing by the Cdc48 ATPase complex is initiated by ubiquitin unfolding*. https://doi.org/10.1126/science.aax1033

Van de Weijer, M. L., Krshnan, L., Liberatori, S., Guerrero, E. N., Robson-Tull, J., Hahn, L., Lebbink, R. J., Wiertz, E. J. H. J., Fischer, R., Ebner, D., & Carvalho, P. (2020). Quality Control of ER Membrane Proteins by the RNF185/Membralin Ubiquitin Ligase Complex. *Molecular Cell*, *79*(5), 768-781.e7. https://doi.org/10.1016/j.molcel.2020.07.009

Wahlman, J., DeMartino, G. N., Skach, W. R., Bulleid, N. J., Brodsky, J. L., & Johnson, A. E. E. (2007). Real-Time Fluorescence Detection of ERAD Substrate Retrotranslocation in a Mammalian In Vitro System. *Cell*, *129*(5), 943–955. https://doi.org/10.1016/J.CELL.2007.03.046

Wang, Q., Liu, Y., Soetandyo, N., Baek, K., Hegde, R., & Ye, Y. (2011). A Ubiquitin Ligase-Associated Chaperone Holdase Maintains Polypeptides in Soluble States for Proteasome Degradation. *Molecular Cell*, *42*(6), 758–770. https://doi.org/10.1016/j.molcel.2011.05.010

Werner, E. D., Brodsky, J. L., & McCracken, A. A. (1996). Proteasome-dependent endoplasmic reticulum-associated protein degradation: An unconventional route to a familiar fate. *Proceedings of the National Academy of Sciences of the United States of America*, *93*(24), 13797–13801. https://doi.org/10.1073/pnas.93.24.13797

Wu, H., Ng, D. T. W., Cheong, I., & Matsudaira, P. (2020). The degradation-promoting roles of deubiquitinases Ubp6 and Ubp3 in cytosolic and ER protein quality control. *PLoS ONE*, *15*(5), 1–37. https://doi.org/10.1371/journal.pone.0232755

Wu, X., Siggel, M., Ovchinnikov, S., Mi, W., Svetlov, V., Nudler, E., Liao, M., Hummer, G., & Rapoport, T. A. (2020). Structural basis of ER-associated protein degradation mediated by the Hrd1 ubiquitin ligase complex. *Science*, *368*(6489), 1–13. https://doi.org/10.1126/SCIENCE.AAZ2449

Xie, Y., & Varshavsky, A. (2001). RPN4 is a ligand, substrate, and transcriptional regulator of the 26S proteasome: A negative feedback circuit. *Proceedings of the National Academy of Sciences of the United States of America*, *98*(6), 3056–3061. https://doi.org/10.1073/PNAS.071022298/ASSET/90604D55-2029-41EA-853B-728FBABABC48/ASSETS/GRAPHIC/PQ0710222004.JPEG

Ye, Y., Meyer, H. H., & Rapoport, T. A. (2001). The AAA ATPase Cdc48/p97 and its partners transport proteins from the ER into the cytosol. *Nature*, *414*(6864), 652–656. https://doi.org/10.1038/414652a

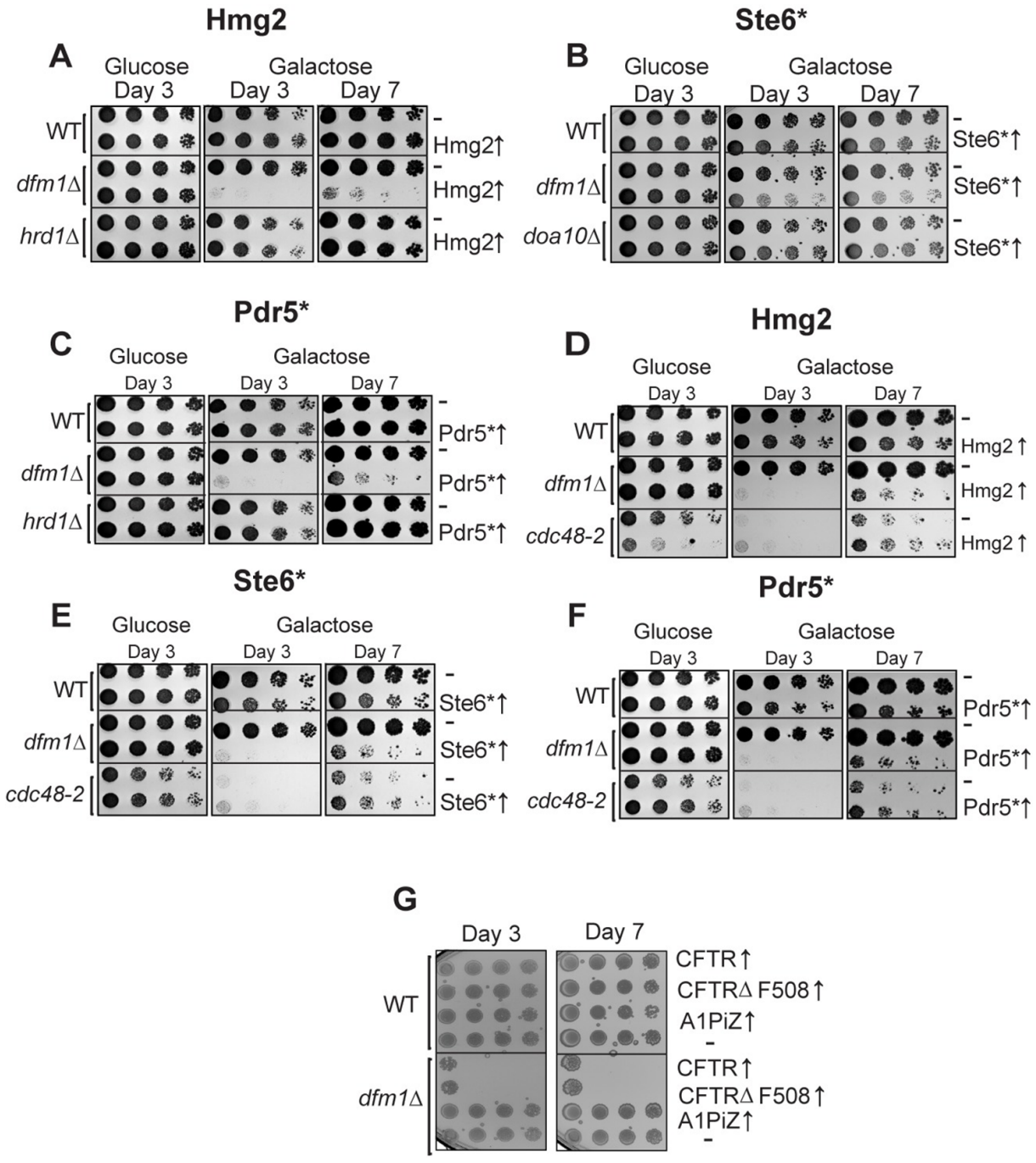
Ye, Y., Shibata, Y., Yun, C., Ron, D., & Rapoport, T. A. (2004). A membrane protein complex mediates retro-translocation from the ER lumen into the cytosol. *Nature*, *429*(6994), 841–847. https://doi.org/10.1038/nature02656

Zettl, M., Adrain, C., Strisovsky, K., Lastun, V., & Freeman, M. (2011). Rhomboid Family Pseudoproteases Use the ER Quality Control Machinery to Regulate Intercellular Signaling. *Cell*, *145*(1), 79–91. https://doi.org/10.1016/J.CELL.2011.02.047

Zhang, Y., Nijbroek, G., Sullivan, M. L., McCracken, A. A., Watkins, S. C., Michaelis, S., & Brodsky, J. L. (2001). Hsp70 molecular chaperone facilitates endoplasmic reticulum-associated protein degradation of cystic fibrosis transmembrane conductance regulator in yeast. *Molecular Biology of the Cell*, *12*(5), 1303–1314.

Figure 2.2.1. Integral membrane protein overexpression causes a growth defect in *dfm1*Δ cells in an ERAD independent manner

(A) WT, *dfm1*Δ, and *hrd1*Δ cells containing either GAL_{pr}-HMG2-GFP or EV were compared for growth by dilution assay. Each strain was spotted 5-fold dilutions on glucose or galactose-containing plates to drive HMG2-GFP overexpression, and plates were incubated at 30°C. **(B)** Dilution assay as described in (A) except using WT, *dfm1*Δ, and *doa10*Δ cells containing either GAL_{pr}-STE6*-GFP or EV. **(C)** Dilution assay as described in (A) except using WT, *dfm1*Δ, and *hrd1*Δ cells containing either GAL_{pr}-PDR5*-HA or EV. **(D)** Dilution assay as described in (A) except using WT, *dfm1*Δ, and *cdc48-2* cells. **(E)** Dilution assay as described in (B) except using WT, *dfm1*Δ, and *cdc48-2* cells. **(F)** Dilution assay as described in (C) except using WT, *dfm1*Δ, and *cdc48-2* cells. **(G)** Dilution assay as described in (A) except using WT or *dfm1*Δ cells expressing human CFTR, CFTRΔF508, or A1PiZ and plated only on glucose-containing plates. All dilution growth assays were performed in 3 biological and 2 technical replicates (*N* = 3). CFTR, cystic fibrosis transmembrane receptor; ERAD, endoplasmic reticulum-associated degradation; EV, empty vector.

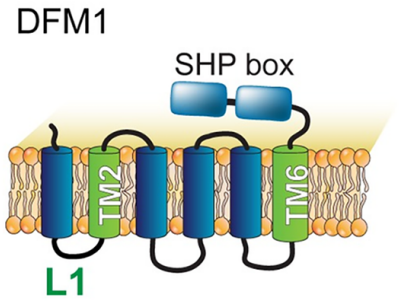

Hmg2
A
Glucose
Day 3
Galactose
Day 3
Day 7
WT
dfm1Δ
hrd1Δ
-
Hmg2↑
Ste6*
B
doa10Δ
Ste6*↑
Pdr5*
C
Pdr5*↑
D
cdc48-2
Hmg2 ↑
E
F

G
Day 3
Day 7
WT
dfm1Δ
CFTR↑
CFTRΔ F508↑
A1PiZ↑
-

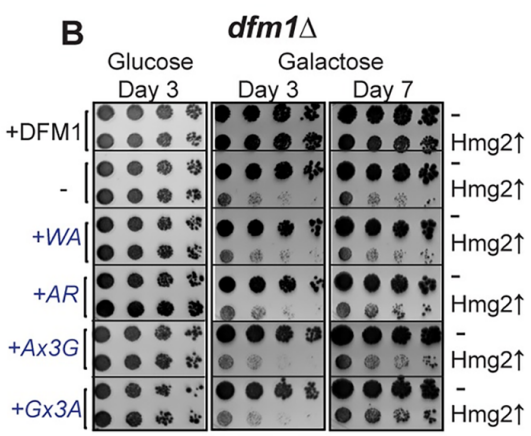
Figure 2.2.2. Dfm1 retrotranslocation defective mutants show differing abilities to restore growth

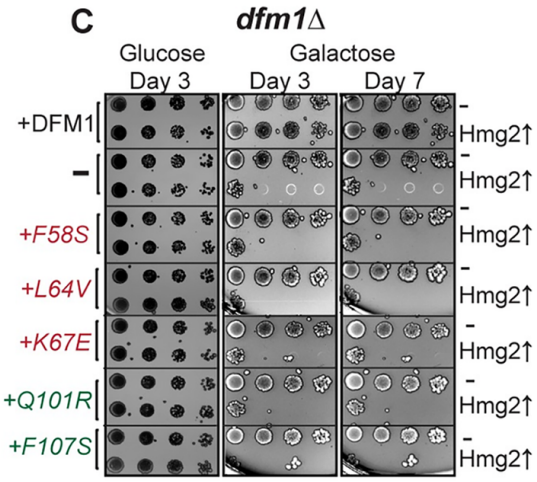
(A) Depiction of Dfm1, which highlights L1, TM2, TM6, and its SHP box domain. The table indicates the Dfm1 region, amino acid mutation, and the corresponding function that is specifically impaired. All mutants have been previously identified as being required for retrotranslocation and when mutated did not restore growth in *dfm1*Δ cells expressing an integral membrane protein (GAL_{pr}-HMG2-GFP). **(B)** *dfm1*Δ cells with an add-back of either WT DFM1-HA, EV, DFM1-WA-HA, DFM1-AR-HA, DFM1-Ax3G-HA, or DFM1-Gx3A-HA containing either GAL_{pr}-HMG2-GFP or EV were compared for growth by dilution assay. Each strain was spotted 5-fold dilutions on glucose or galactose-containing plates to drive Hmg2-GFP overexpression, and plates were incubated at 30°C. **(C)** Dilution assay as described in (B) except using an add-back of either WT Dfm1-HA, EV, Dfm1-F57S-HA, Dfm1-L64V-HA, Dfm1-K67E-HA, Dfm1-Q101R-HA, or Dfm1-F107S-HA. **(D)** Depiction of Dfm1 and Dfm1-5Ashp. Dfm1 is an ER-localized membrane proteins with 6 TMDs. Both versions of Dfm1 have a cytoplasmic shp box, but the 5Ashp mutant is unable to recruit the cytosolic ATPase Cdc48. **(E)** Dilution assay as described in (B) except using add-back of either EV, WT DFM1-HA, or DFM1-5Ashp-HA mutant. **(F)** Dilution assay as described in (B) except with add-back of human Derlin-1-Myc or Derlin-2-Myc. All dilution growth assays were performed in 3 biological replicates and 2 technical replicates ($N = 3$). ER, endoplasmic reticulum EV, empty vector; TMD, transmembrane domain.

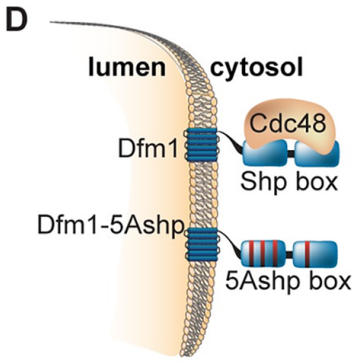
A

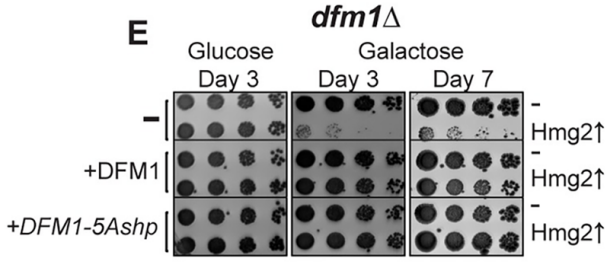


Dfm1 region	mutation	function impacted
L1: WR motif	W63A/R64A	substrate binding
L1	F58S	substrate binding
L1	L64V	substrate binding
L1	K67E	substrate binding
TM2	Q101R/F107S	lipid thinning
TM6:Gx3G motif	G206A/G210A	structural integrity









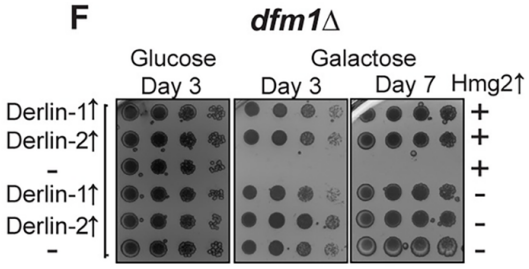
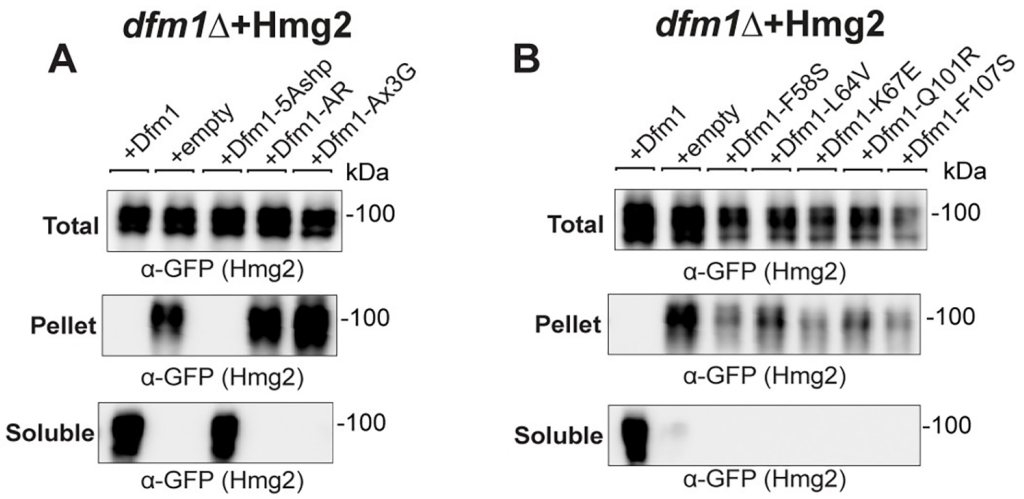
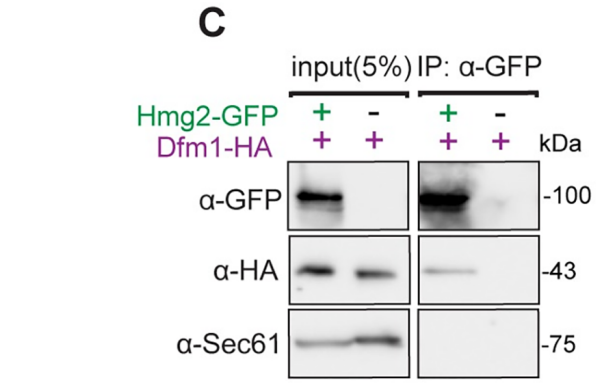


Figure 2.2.3. Dfm1 reduces misfolded membrane protein toxicity through a chaperone-like activity

(A) Western blot of aggregated (pelleted) versus non-aggregated (soluble) membrane proteins at the ER. Lysates from *dfm1*Δ cells containing HMG2-GFP, with either add-back of WT DFM1-HA, EV, DFM1-5Ashp-HA, DFM1-AR-HA, and DFM1-AxxxG-HA were blotted using anti-GFP to detect Hmg2. Top: Total fraction. Middle: ER pelleted fraction. Bottom: ER DDM solublilized fraction. **(B)** Western blot of aggregated versus non-aggregated membrane proteins at the ER as in (A) but with add-back of either WT DFM1-HA, EV, DFM1-F58S-HA, DFM1-L64V-HA, DFM1-K67E-HA, DFM1-Q101R-HA, and DFM1-F107S-HA. **(C)** DDM solubilized Hmg2-GFP binding to Dfm1-HA was analyzed by Co-IP, using anti-GFP to detect Hmg2 and anti-HA to detect Dfm1-HA. As negative control, cells not expressing Hmg2-GFP were used. Sec61 was analyzed as another negative control for nonspecific binding using anti-Sec61 (3 biological replicates, *N* = 3). **(D)** Graphic depicting integrated model of Dfm1's function in misfolded membrane protein stress. Top: Misfolded membrane proteins in the absence of Dfm1 forming aggregates within the ER membrane. Bottom: Cells with WT Dfm1 or 5Ashp-Dfm1 promoting non-aggregated misfolded membrane proteins and preventing cellular toxicity. Data Information: All detergent solubility assays were performed with 3 biological replicates (*N* = 3). DDM, dodecyl maltoside; ER, endoplasmic reticulum; EV, empty vector.


A
dfm1Δ+Hmg2
+Dfm1
+empty
+Dfm1-5Ashp
+Dfm1-AR
+Dfm1-Ax3G
kDa
Total
-100
α-GFP (Hmg2)
Pellet
-100
α-GFP (Hmg2)
Soluble
-100
α-GFP (Hmg2)
B
dfm1Δ+Hmg2
+Dfm1
+empty
+Dfm1-F58S
+Dfm1-L64V
+Dfm1-K67E
+Dfm1-Q101R
+Dfm1-F107S
kDa
Total
-100
α-GFP (Hmg2)
Pellet
-100
α-GFP (Hmg2)
Soluble
-100
α-GFP (Hmg2)


C
input(5%)
IP: α-GFP
Hmg2-GFP
Dfm1-HA
kDa
α-GFP
-100
α-HA
-43
α-Sec61
-75

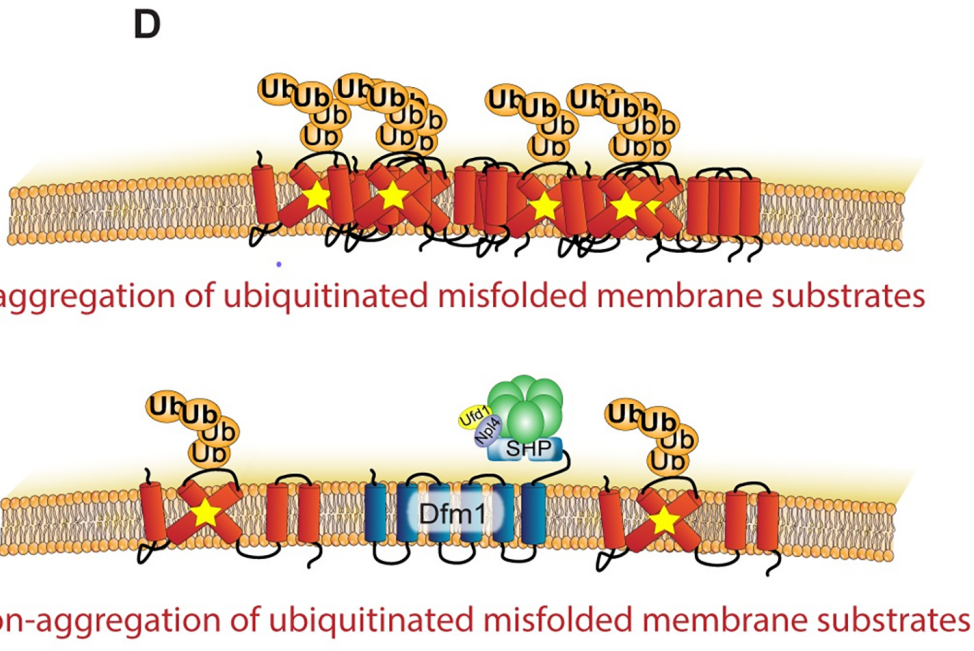

D
aggregation of ubiquitinated misfolded membrane substrates
Ufd1
Npl4
SHP
Dfm1
non-aggregation of ubiquitinated misfolded membrane substrates

Figure 2.2.4. Dfm1 specifically influences solubility of misfolded membrane proteins

(A) Western blot of aggregated versus non-aggregated membrane proteins at the ER. Lysates from WT, *hrd1*Δ, or *hrd1*Δ+HRD1 cells containing HMG2-GFP were blotted using anti-GFP to detect Hmg2. T is total protein, P is pellet (ER aggregated) fraction, and S is soluble (ER non-aggregated) fraction. **(B)** Western blot of aggregated versus non-aggregated membrane proteins at the ER as in (A) except with *dfm1*Δ cells containing SEC61-GFP with add-back of EV, WT DFM1-HA, or DFM1-5Ashp-HA. Anti-GFP was used to detect SEC61-GFP. **(C)** Western blot of aggregated versus non-aggregated membrane proteins at the ER as in (A) except with *dfm1*Δ cells containing PDR5*-HA with add-back of WT DFM1-HA or EV. Anti-HA was used to detect PDR5*-HA. **(D)** Western blot of aggregated versus non-aggregated membrane proteins at the ER as in (A) except with *dfm1*Δ cells containing STE6*-GFP with add-back of WT DFM1-HA or EV. Anti-GFP was used to detect STE6*-GFP. **(E)** Western blot of aggregated versus non-aggregated membrane proteins at the ER as in (A) except with *dfm1*Δ cells containing CPY*-GFP with add-back of EV or WT DFM1-HA. Anti-GFP was used to detect CPY*-GFP. **(F)** Western blot of aggregated versus non-aggregated membrane proteins at the ER as in (A) except with *dfm1*Δ cells containing HMG2-GFP with add-back of EV, DERLIN-1-Myc, and DERLIN-2-Myc. Anti-Myc was used to detect DERLIN-1-Myc and DERLIN-2-Myc. Data information: All detergent solubility assays were performed with 3 biological replicates (N = 3). ER, endoplasmic reticulum; EV, empty vector.

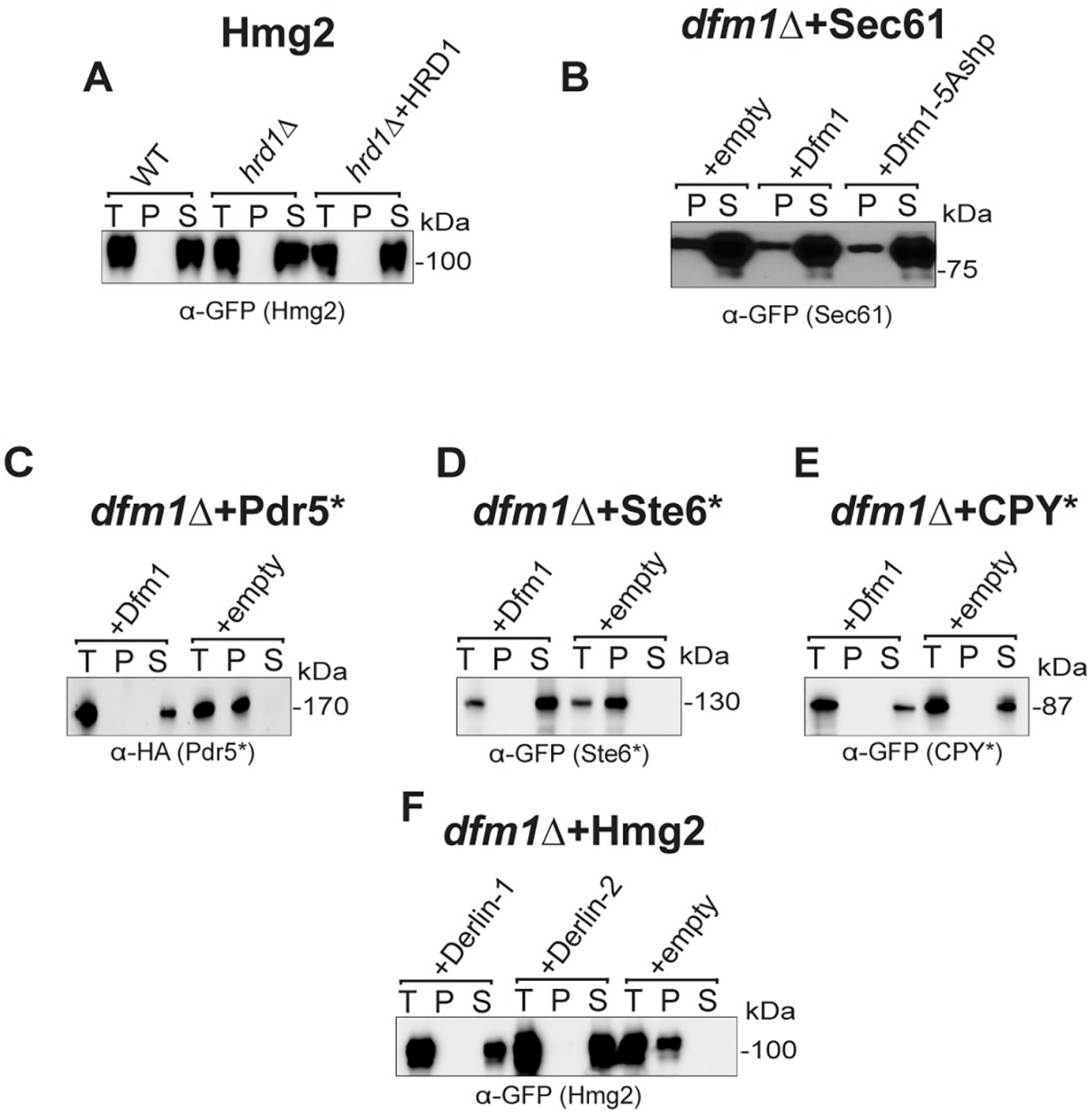

A
Hmg2
WT
hrd1Δ
hrd1Δ+HRD1
T P S T P S T P S
kDa
-100
α-GFP (Hmg2)
B
dfm1Δ+Sec61
+empty
+Dfm1
+Dfm1-5Ashp
P S P S P S
kDa
-75
α-GFP (Sec61)
C
dfm1Δ+Pdr5*
+Dfm1
+empty
T P S T P S
kDa
-170
α-HA (Pdr5*)
D
dfm1Δ+Ste6*
+Dfm1
+empty
T P S T P S
kDa
-130
α-GFP (Ste6*)
E
dfm1Δ+CPY*
+Dfm1
+empty
T P S T P S
kDa
-87
α-GFP (CPY*)
F
dfm1Δ+Hmg2
+Derlin-1
+Derlin-2
+empty
T P S T P S T P S
kDa
-100
α-GFP (Hmg2)

Figure 2.2.5. Misfolded membrane protein stress in *dfm1*Δ cells does not activate the UPR

(A) UPR activation for indicated strains with overexpression of a misfolded integral membrane protein. *pdr5*Δ cells containing GAL_{pr}-Hmg2-6MYC and 4xUPRE-GFP (a reporter that expresses GFP with activation of the UPR) were measured for GFP expression using flow cytometry every hour for 5 hours starting at the point of galactose induction and tunicamycin or equivalent volume of DMSO was added at the 1-hour timepoint. Figure depicts the GFP fluorescence in arbitrary units (A.U.) for indicated conditions 5 hours post-galactose addition. In figure legend, “Gal” indicates addition of 0.2% galactose to cultures and “Raf” indicates addition of 0.2% raffinose to culture, and “Tm" indicates tunicamycin presence (+) or absence (-) of 2ug/mL tunicamycin **(B)** Flow cytometry based UPR activation assay as described in (A) except using *dfm1*Δ cells. **(C) (E)** and **(G)** Flow cytometry based UPR activation assay as described in (A) except using cells containing GAL_{pr}-Ste6*-GFP, GAL_{pr}-CPY*-HA, or EV, respectively. **(D) (F)** and **(H)** Flow cytometry based UPR activation assay as described in (B) except using cells containing GAL_{pr}-Ste6*-GFP, GAL_{pr}-CPY*-HA, or EV, respectively. Data information: All data are measured mean ± SEM; N=3 biological replicates.

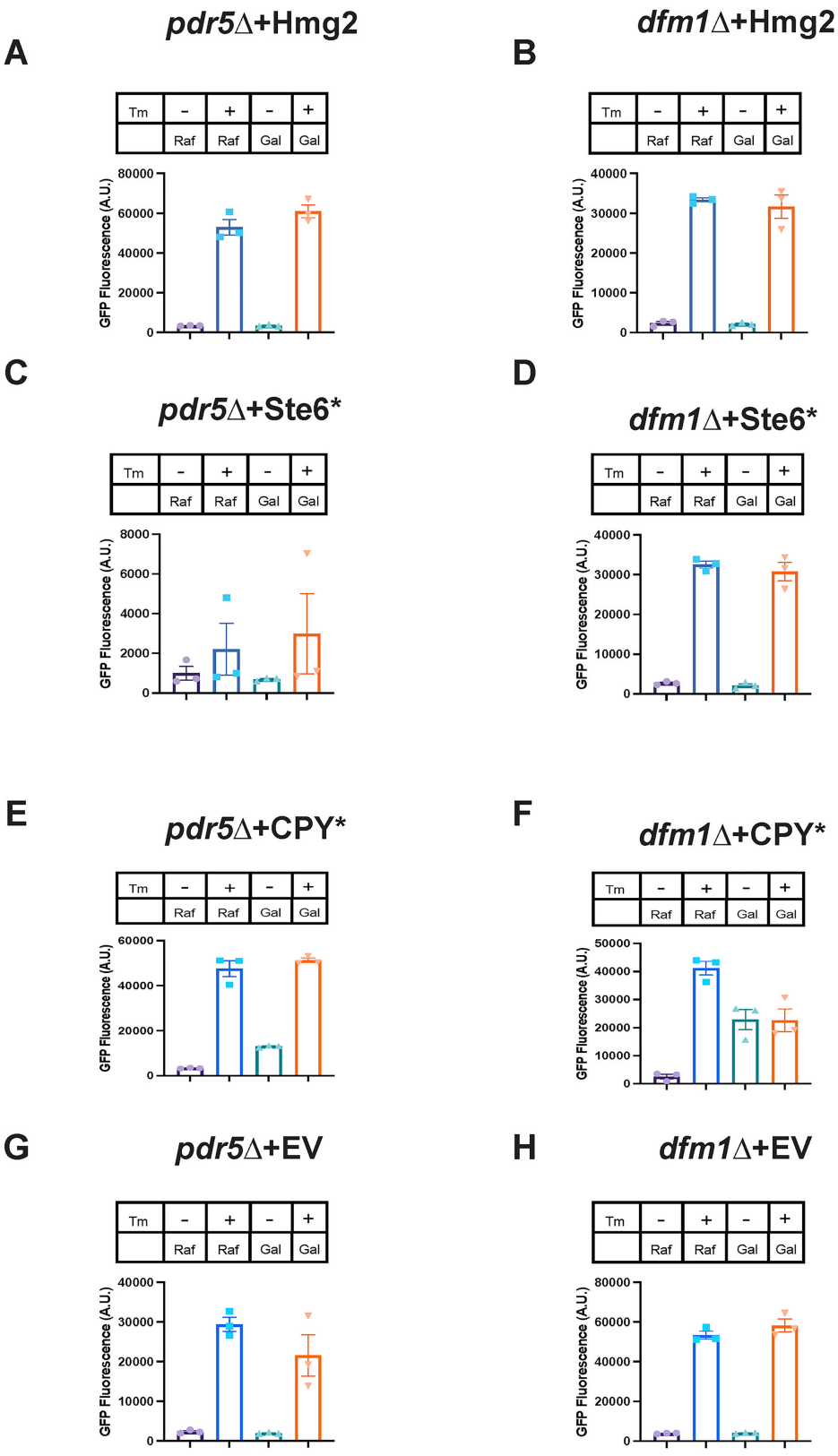

A
pdr5Δ+Hmg2
Tm - + - +
Raf Raf Gal Gal
GFP Fluorescence (A.U.)
80000
60000
40000
20000
0
B
dfm1Δ+Hmg2
Tm - + - +
Raf Raf Gal Gal
GFP Fluorescence (A.U.)
40000
30000
20000
10000
0
C
pdr5Δ+Ste6*
Tm - + - +
Raf Raf Gal Gal
GFP Fluorescence (A.U.)
8000
6000
4000
2000
0
D
dfm1Δ+Ste6*
Tm - + - +
Raf Raf Gal Gal
GFP Fluorescence (A.U.)
40000
30000
20000
10000
0
E
pdr5Δ+CPY*
Tm - + - +
Raf Raf Gal Gal
GFP Fluorescence (A.U.)
60000
40000
20000
0
F
dfm1Δ+CPY*
Tm - + - +
Raf Raf Gal Gal
GFP Fluorescence (A.U.)
50000
40000
30000
20000
10000
0
G
pdr5Δ+EV
Tm - + - +
Raf Raf Gal Gal
GFP Fluorescence (A.U.)
40000
30000
20000
10000
0
H
dfm1Δ+EV
Tm - + - +
Raf Raf Gal Gal
GFP Fluorescence (A.U.)
80000
60000
40000
20000
0

Figure 2.2.6. Misfolded membrane protein toxicity results in proteasome impairment

(A) WT, *dfm1*Δ, and *rpn4Δ* cells containing either GAL_{pr}-HMG2-GFP or EV were compared for growth by dilution assay. Each strain was spotted 5-fold dilutions on glucose or galactose-containing plates to drive Hmg2-GFP overexpression, and plates were incubated at 30°C. Three biological replicates and 2 technical replicates (*N* = 3). **(B)** PRE6-GFP levels as measured by flow cytometry at 0 versus 5 hours post-galactose induction in WT cells containing either EV, GAL_{pr}-CPY*-HA, or GAL_{pr}-HMG2-GFP. **(C)** Pre6-GFP levels as in (B) except in *dfm1*Δ cells. **(D)** Quantification of CFUs formed on appropriate selection plates from proteasome sensitivity inhibition assay. *pdr5*Δ cells containing SUS-GFP or EV in log phase were treated with 25 uM of proteasome inhibitor MG132 or equivalent volume of DMSO for 8 hours and samples were diluted 1:500 and 50 uL of each sample was plated. **(E)** Proteasome sensitivity assay as in (D) except using *hrd1*Δ*pdr5*Δ cells. **(F)** Proteasome sensitivity assay as in (D) except using *dfm1*Δ*hrd1*Δ*pdr5*Δ cells. Data information: For (B) and (C), all data are mean ± SEM, with 7 biological replicates (*N* = 7). For (D), (E), and (F), all data are mean ± SEM, 3 biological replicates and 2 technical replicates (*N* = 3); statistical significance is displayed as two-tailed unpaired *t* test, **P* < 0.05, ns, not significant. **(G)** Western blot of Pre6 in cytosol versus ER (top panel) and aggregated (pelleted) versus non-aggregated (soluble) Pre6 at the ER (bottom panel). Lysates from *dfm1*Δ, cells containing Pre6-GFP and HMG2-6Myc or EV were blotted using anti-GFP to detect Pre6. T is total protein, ER is endoplasmic reticulum protein fraction, C is cystolosic protein fraction, P is pellet (ER aggregated) fraction, and S is soluble (ER non-aggregated) fraction. The data underlying this figure can be found in Table I–K in S1 Data (Sheet 2; Available online). CFU, colony-forming unit; EV, empty vector.

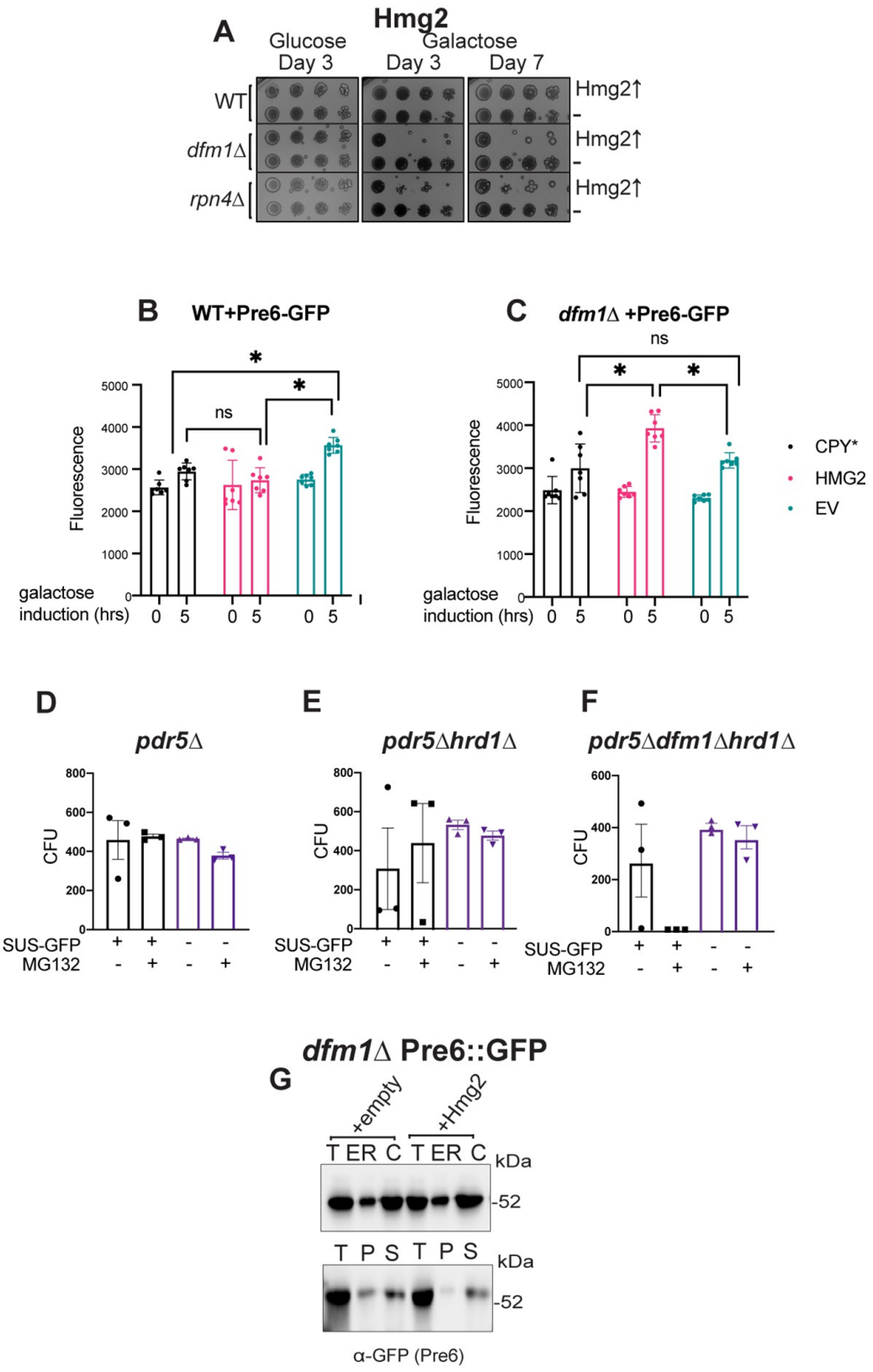

A
Hmg2
Glucose
Day 3
Galactose
Day 3
Day 7
WT
dfm1Δ
rpn4Δ
Hmg2↑
-
Hmg2↑
-
Hmg2↑
-
B
WT+Pre6-GFP
Fluorescence
galactose
induction (hrs)
0 5 0 5 0 5
ns
*
*
C
dfm1Δ +Pre6-GFP
ns
*
*
Fluorescence
galactose
induction (hrs)
0 5 0 5 0 5
CPY*
HMG2
EV
D
pdr5Δ
CFU
SUS-GFP
MG132
E
pdr5Δhrd1Δ
CFU
SUS-GFP
MG132
F
pdr5Δdfm1Δhrd1Δ
CFU
SUS-GFP
MG132
G
dfm1Δ Pre6::GFP
+empty
+Hmg2
T ER C T ER C
kDa
-52
T P S T P S
kDa
-52
α-GFP (Pre6)

Figure 2.2.7. Ubiquitin stress contributes to misfolded membrane protein toxicity

(A) WT, *dfm1*Δ, *dfm1*Δ*hrd1*Δ, and *dfm1*Δ*doa10*Δ cells containing either GAL_{pr}-Hmg2-GFP, GAL_{pr}-STE6*-GFP, or EV were compared for growth by dilution assay. Each strain was spotted 5-fold dilutions on glucose or galactose-containing plates to drive Hmg2-GFP overexpression, and plates were incubated at 30°C. **(B)** Indicated strains expressing either Hmg2-GFP or Ste6*-GFP were grown to log-phase, lysed, and microsomes were collected and immunoprecipitated with α-GFP conjugated to agarose beads. Samples were then subjected to SDS-PAGE and immunoblotted by α-Ubiquitin and α-GFP. Three biological replicates (*N* = 3). **(C)** Dilution assay as described in (A) except using WT and *dfm1*Δ cells containing either GAL_{pr}-Hmg2-GFP, GAL_{pr}-Hmg2-K6R-GFP, GAL_{pr}-Hmg2-K357R-GFP, GAL_{pr}-Hmg2- (K6R and K357R)-GFP, or EV. **(D)** WT and *dfm1*Δ cells containing either $CUP1_{pr}$-Ub or EV and GAL_{pr}-HMG2-GFP or EV were compared for growth by dilution assay. Each strain was spotted 5-fold dilutions on glucose or galactose-containing plates to drive Hmg2-GFP overexpression, and plates were incubated at 30°C. Galactose plates containing 50 μM Cu2+ were used to allow expression of Ub driven by the CUP1 promoter. **(E)** Western blot of monomeric ubiquitin in WT, *dfm1*Δ, and *hrd1*Δ expressing HMG2-GFP. Anti-ubiquitin was used to blot for ubiquitin and anti-PGK1 was used to blot for PGK1 as a loading control. **(F)** Quantification of western blots from (E). Each strain was normalized to PGK1 and the monomeric ubiquitin quantification of WT+HMG2-GFP was used to normalize all strains. **(G)** Dilution assay as described in (A) *dfm1*Δ, *ubp9Δ*, *ubp14Δ*, and *doa4Δ* cells. **(H)** Dilution assay as described in (A) except using WT, *dfm1*Δ, and *ubp6Δ* cells containing either GAL_{pr}-HMG2-GFP or EV. **(I)** Western blot of aggregated versus soluble membrane proteins at the ER. Lysates from *dfm1*Δ cells containing HMG2-GFP or HMG2-K6R-GFP with EV or DFM1-HA were blotted using anti-GFP to detect Hmg2. T is total fraction, P is pellet (ER aggregated) fraction, and S is soluble (ER non-aggregated) fraction. Data information: All dilution growth assays were performed in 3 biological replicates and 2 technical replicates (*N* = 3). For (F), all data are mean ± SEM, 3 biological replicates (*N* = 3); statistical significance is displayed as two-tailed unpaired *t* test, **P* < 0.05, ns, not significant. Detergent solubility assay in (H) was performed with 3 biological replicates (*N* = 3). The data underlying this figure can be found in Table L in S1 Data (Sheet 3; Available online). ER, endoplasmic reticulum; EV, empty vector.

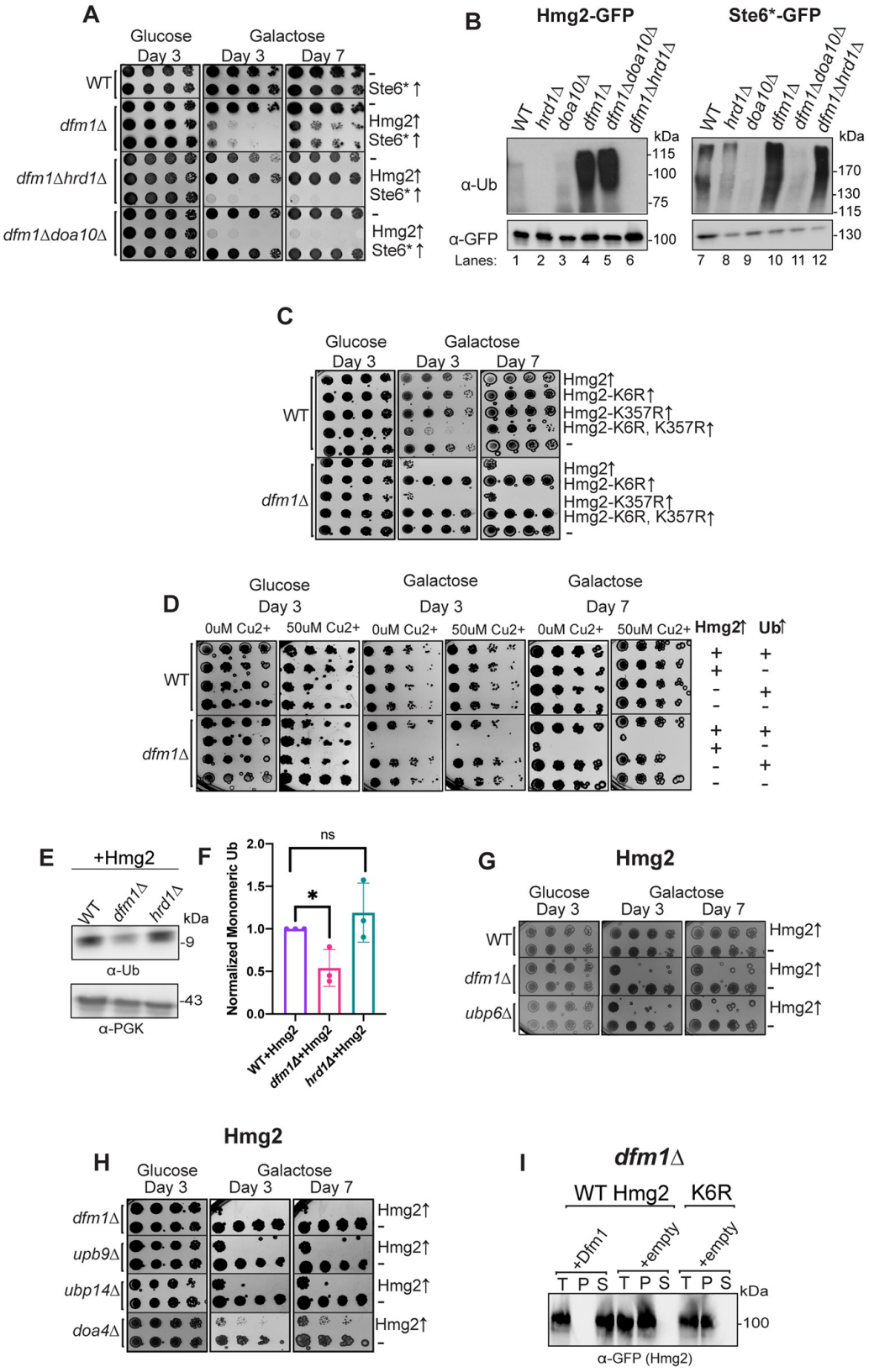
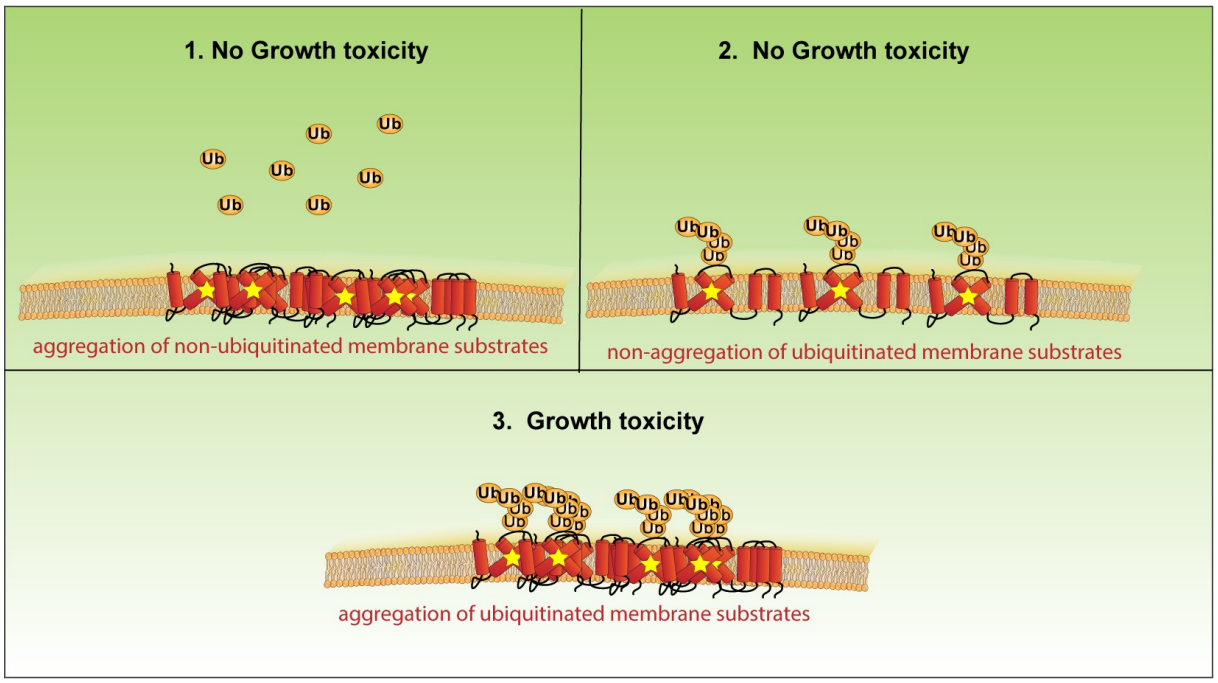

A
Glucose
Day 3
Galactose
Day 3
Day 7
WT
dfm1Δ
dfm1Δhrd1Δ
dfm1Δdoa10Δ
Ste6*↑
Hmg2↑
Ste6*↑
B
Hmg2-GFP
Ste6*-GFP
WT
hrd1Δ
doa10Δ
dfm1Δ
dfm1Δdoa10Δ
dfm1Δhrd1Δ
kDa
α-Ub
α-GFP
Lanes: 1 2 3 4 5 6
7 8 9 10 11 12
C
Hmg2↑
Hmg2-K6R↑
Hmg2-K357R↑
Hmg2-K6R, K357R↑
D
0uM Cu2+
50uM Cu2+
Hmg2↑
Ub↑
E
+Hmg2
α-Ub
α-PGK
F
Normalized Monomeric Ub
ns
*
WT+Hmg2
dfm1Δ+Hmg2
hrd1Δ+Hmg2
G
Hmg2
ubp6Δ
H
upb9Δ
ubp14Δ
doa4Δ
I
dfm1Δ
WT Hmg2
K6R
+Dfm1
+empty
T P S
α-GFP (Hmg2)

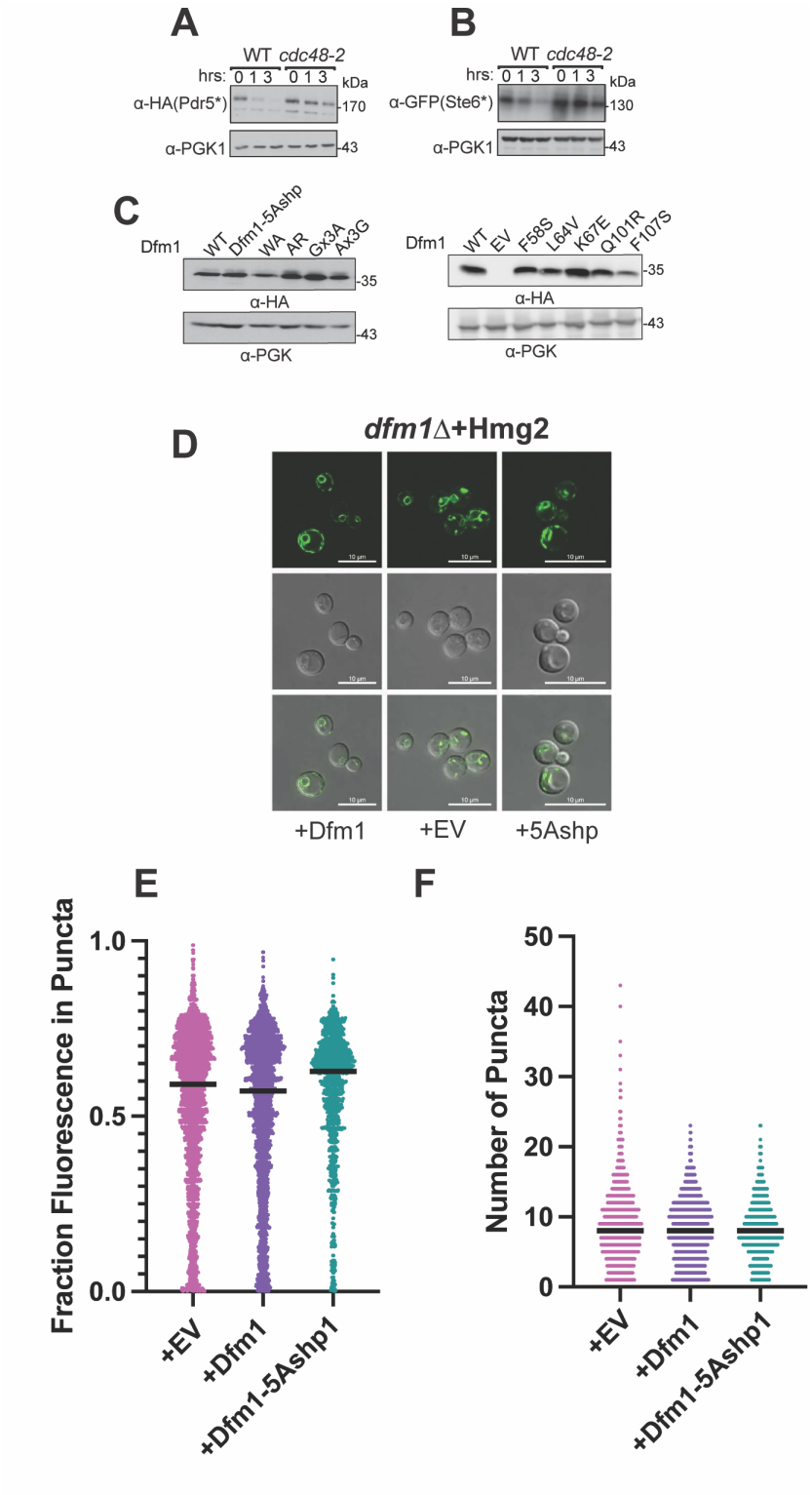
Figure 2.2.8. Model for misfolded membrane protein-induced toxicity

A model depicting how accumulation of ER-resident misfolded membrane proteins would induce growth toxicity. (1) No growth toxicity is observed when misfolded membrane proteins aggregate but are not ubiquitinated. (2) No growth toxicity is observed when misfolded membrane proteins are ubiquitinated, but not aggregated. (3) Growth toxicity is observed when misfolded membrane proteins are both ubiquitinated and aggregated. ER, endoplasmic reticulum.



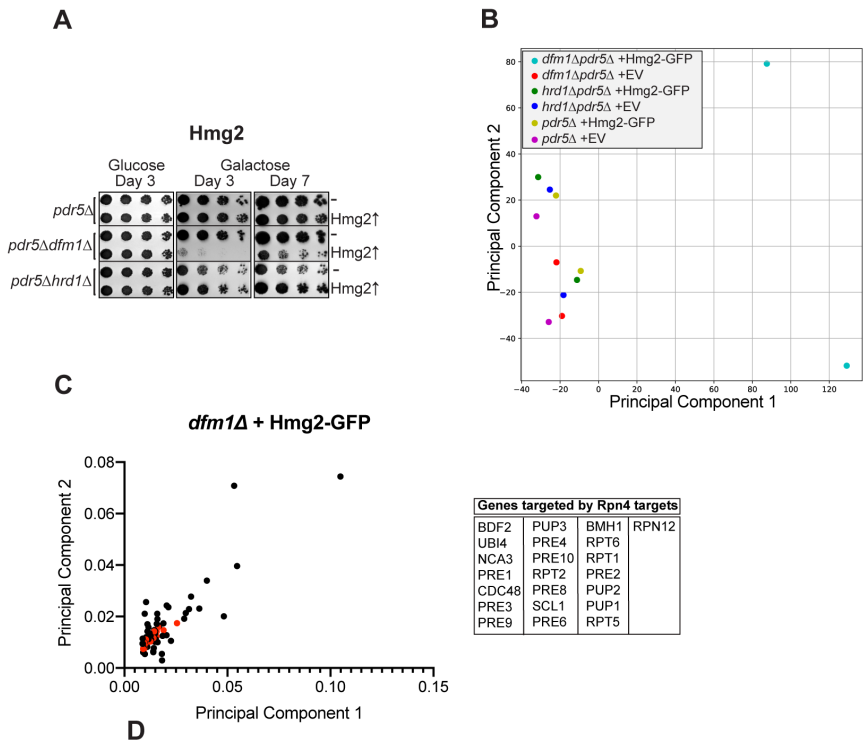
Supplemental Figure 2.2.1. Hmg2-GFP microscopy puncta are unaffected by Dfm1

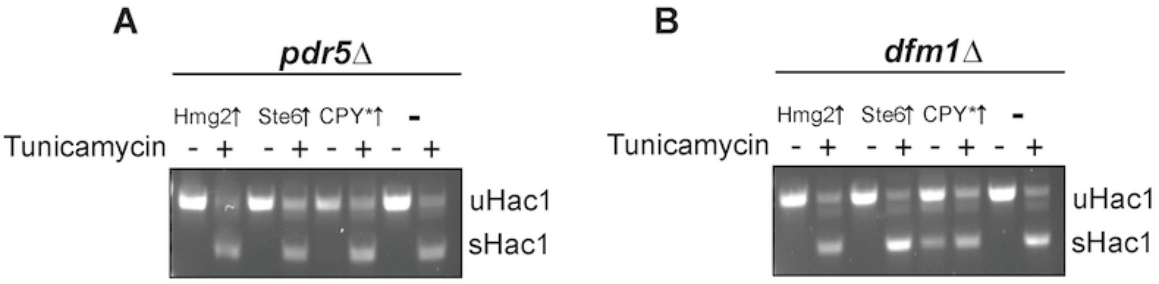
(A and B) WT and *cdc48-2* strains were grown into log-phase at 30°C and degradation was measured by cycloheximide chase (CHX). After CHX addition, cells were lysed at the indicated times, and analyzed by SDS-PAGE and immunoblotted for Pdr5*-HA with α-HA and Ste6*-GFP with α-GFP. Three biological replicates (*N* = 3). **(C)** Steady-state levels of Dfm1 and corresponding Dfm1 mutants from *dfm1*Δ cells containing GAL_{pr}-HMG2-GFP that were used for growth assays in Fig. 2.2.2. Cells were analyzed by SDS-PAGE and immunoblotted with α-HA. Three biological replicates (*N* = 3). **(D)** Representative confocal microscopy images of Hmg2-GFP in *dfm1*Δ cells with add-back of EV, WT DFM1, and DFM1-5Ashp. Five biological replicates were imaged, and 3 images were taken of each strain (*N* = 5). **(E)** Fraction of Hmg2-GFP in puncta for *dfm1*Δ cells with add-back of WT DFM1, EV, and DFM1-5Ashp. Each dot represents an individual cell. **(F)** Number of puncta per cell for *dfm1*Δ cells with add-back of WT DFM1, EV, and DFM1-5Ashp. Each dot represents an individual cell. Data information: The data underlying this figure can be found in Table M and N in S1 Data (Sheet 4; Available online).


A
WT cdc48-2
hrs: 0 1 3 0 1 3
kDa
α-HA(Pdr5*)
170
α-PGK1
43
B
WT cdc48-2
hrs: 0 1 3 0 1 3
kDa
α-GFP(Ste6*)
130
α-PGK1
43
C
Dfm1
WT
Dfm1-5Ashp
WA
AR
Gx3A
AX3G
35
α-HA
43
α-PGK
Dfm1
WT
EV
F58S
L64V
K67E
Q101R
F107S
35
α-HA
43
α-PGK
D
dfm1Δ+Hmg2
+Dfm1
+EV
+5Ashp
E
Fraction Fluorescence in Puncta
1.0
0.5
0.0
+EV
+Dfm1
+Dfm1-5Ashp1
F
Number of Puncta
50
40
30
20
10
0
+EV
+Dfm1
+Dfm1-5Ashp1

Supplemental Figure 2.2.2. Transcriptional changes in membrane protein-stressed *dfm1*Δ cells

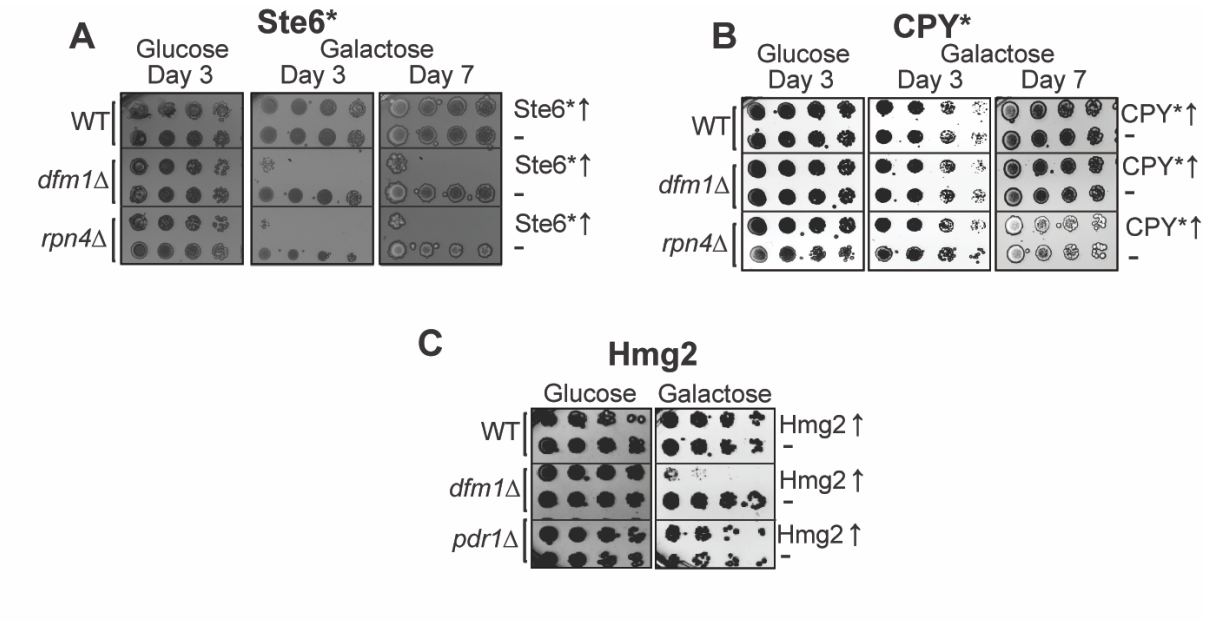
(A) *pdr5*Δ, *pdr5*Δ*dfm1*Δ, and *pdr5*Δ*hrd1*Δ cells containing either GAL_{pr}-HMG2-GFP or EV were compared for growth by dilution assay. Each strain was spotted 5-fold dilutions on glucose or galactose-containing plates to drive HMG2-GFP overexpression, and plates were incubated at 30°C. Three biological replicates and 2 technical replicates (N = 3). **(B)** Principal component 1 (PC1) and principal component 2 (PC2) values of each of the 2 biological replicates (N = 2) of RNA-seq samples for *pdr5Δ*, *dfm1Δpdr5Δ*, and *hrd1Δpdr5Δ* cells containing either GAL_{pr}-HMG2-GFP or EV. **(C)** PC1 and PC2 of sorted top 100 highest PC1 value genes from both replicates of *dfm1Δpdr5Δ* cells containing GAL_{pr}-HMG2-GFP. Red dots indicate Rpn4 target genes. Table indicates up-regulated genes that are targeted by Rpn4. **(D)** Top 10 GO terms and their enrichment factor for the set of 100 up-regulated genes with the highest PC1 scores. (**E)** Top 10 GO terms and their enrichment factor for the set of 100 down-regulated genes with the lowest PC1 scores. Data information: The data underlying this figure can be found in Table O–Q in S1 Data (Sheet 5; Available online) and Table R (Sheet 6; Available online).


A
Hmg2
Glucose
Day 3
Galactose
Day 3
Day 7
pdr5Δ
pdr5Δdfm1Δ
pdr5Δhrd1Δ
Hmg2↑
B
dfm1Δpdr5Δ +Hmg2-GFP
dfm1Δpdr5Δ +EV
hrd1Δpdr5Δ +Hmg2-GFP
hrd1Δpdr5Δ +EV
pdr5Δ +Hmg2-GFP
pdr5Δ +EV
Principal Component 2
Principal Component 1
C
dfm1Δ + Hmg2-GFP
Principal Component 2
Principal Component 1
Genes targeted by Rpn4 targets
BDF2 PUP3 BMH1 RPN12
UBI4 PRE4 RPT6
NCA3 PRE10 RPT1
PRE1 RPT2 PRE2
CDC48 PRE8 PUP2
PRE3 SCL1 PUP1
PRE9 PRE6 RPT5
D
Top 10 upregulated GO terms
Proteasomal Ubiquitin-Independent Protein Catabolic Process
Regulation of Endopeptidase Activity
Proteasome Regulatory Particle Assembly
Proteasome Assembly
Regulation of Peptidase Activity
Positive Regulation of Proteolysis
Protein Refolding
'De Novo' Protein Folding
Proteasome-Mediated Ubiquitin-Dependent Protein Catabolic Proccess
Regulation of Proteolysis
Fold Enrichment
E
Top 10 downregulated GO terms
rRNA Export from Nucleus
rRNA Transport
Translational Termination
Cellular Protein Complex DIsassembly
Cytoplasmic Translation
Protein Containing Complex Disassembly
ncRNA Export from Nucleus
Cellular Componenent Dissassembly
Ribosomal Small Subunit Biogenesis
Translation
Fold Enrichment



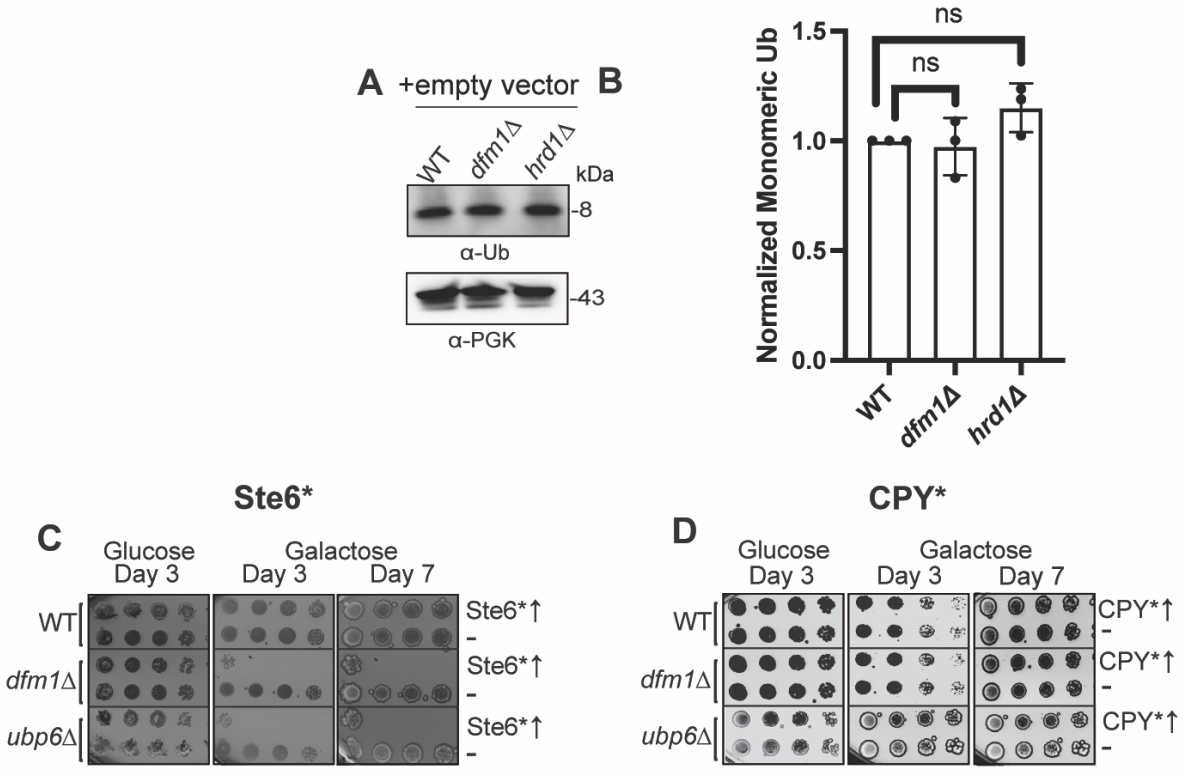
Supplemental Figure 2.2.3. Misfolded membrane protein stress in *dfm1*Δ cells does not affect Hac1 splicing

(A) PCR products of spliced and unspliced Hac1 transcripts. *pdr5*Δ cells containing GAL_{pr}-Hmg2-6MYC, GAL_{pr}-Ste6*-GFP, GAL_{pr}-CPY*-HA, or EV were treated with 0.2% galactose and 2 µg/mL tunicamycin (+) or an equivalent volume of DMSO (-). RNA was extracted from cells and cDNA was generated and used as a template for PCR. uHac1 represents unspliced Hac1 transcripts and sHac1 represents spliced Hac1. **(B)** Hac1 splicing assay as in (A) except using *dfm1*Δ cells. Data information: Images are representative of 3 biological replicates (*N* = 3).



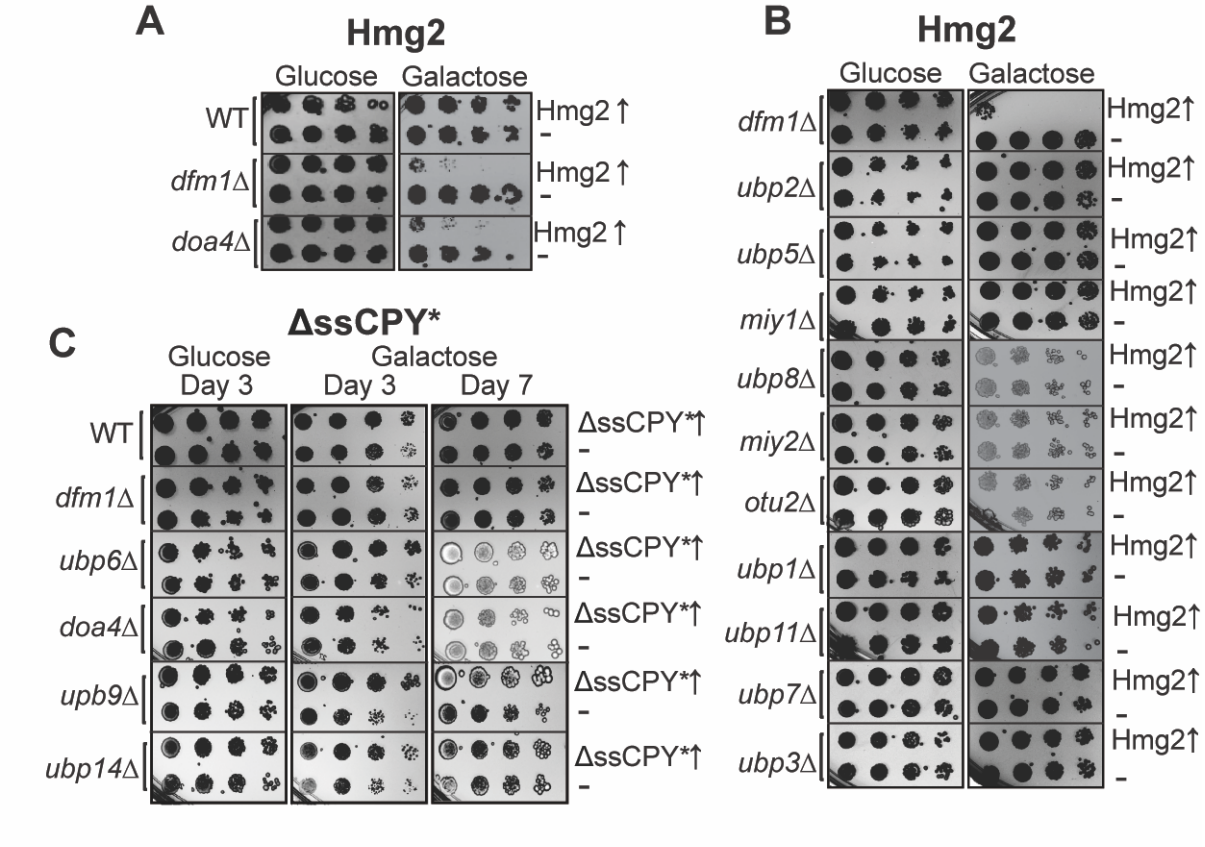
Supplemental Figure 2.2.4. *Rpn4Δ* toxicity is Specific to misfolded membrane proteins

(A) WT, *dfm1*Δ, and *rpn4Δ* cells containing either GAL_{pr}-STE6*-GFP or EV were compared for growth by dilution assay. Each strain was spotted 5-fold dilutions on glucose or galactose-containing plates to drive Ste6*-GFP overexpression, and plates were incubated at 30°C. **(B)** Dilution assay as depicted in (A) except using cells containing GAL_{pr}-CPY*-HA or EV. **(C)** Dilution assay as described in (A) except using WT, *dfm1*Δ, and *pdr1Δ* cells containing either GAL_{pr}-HMG2-GFP or EV. Data information: All dilution growth assays were performed in 3 biological and 2 technical replicates (N = 3).



Supplemental Figure 2.2.5. *Ubp6*Δ toxicity is Specific to misfolded membrane proteins

(A) Western blot of monomeric ubiquitin in WT, *dfm1*Δ, and *hrd1*Δ cells. Anti-ubiquitin was used to blot for ubiquitin and anti-PGK1 was used to blot for PGK1 as a loading control. **(B)** Quantification of western blots from (A). Each strain was normalized to PGK1 and the monomeric ubiquitin quantification of WT was used to normalize all strains. **(C)** WT, *dfm1*Δ, and *ubp6Δ* cells containing either GAL_{pr}-STE6*-GFP or EV were compared for growth by dilution assay. Each strain was spotted 5-fold dilutions on glucose or galactose-containing plates to drive Ste6*-GFP overexpression, and plates were incubated at 30°C. **(D)** Dilution assay as depicted in (C) except using cells containing GAL_{pr}-CPY*-HA or EV. Data information: All dilution growth assays were performed in 3 biological and 2 technical replicates (N = 3). For (B), all data are mean ± SEM, 3 biological replicates (N = 3); statistical significance is displayed as two-tailed unpaired t test, ns, not significant. The data underlying this figure can be found in Table S (Sheet 7).

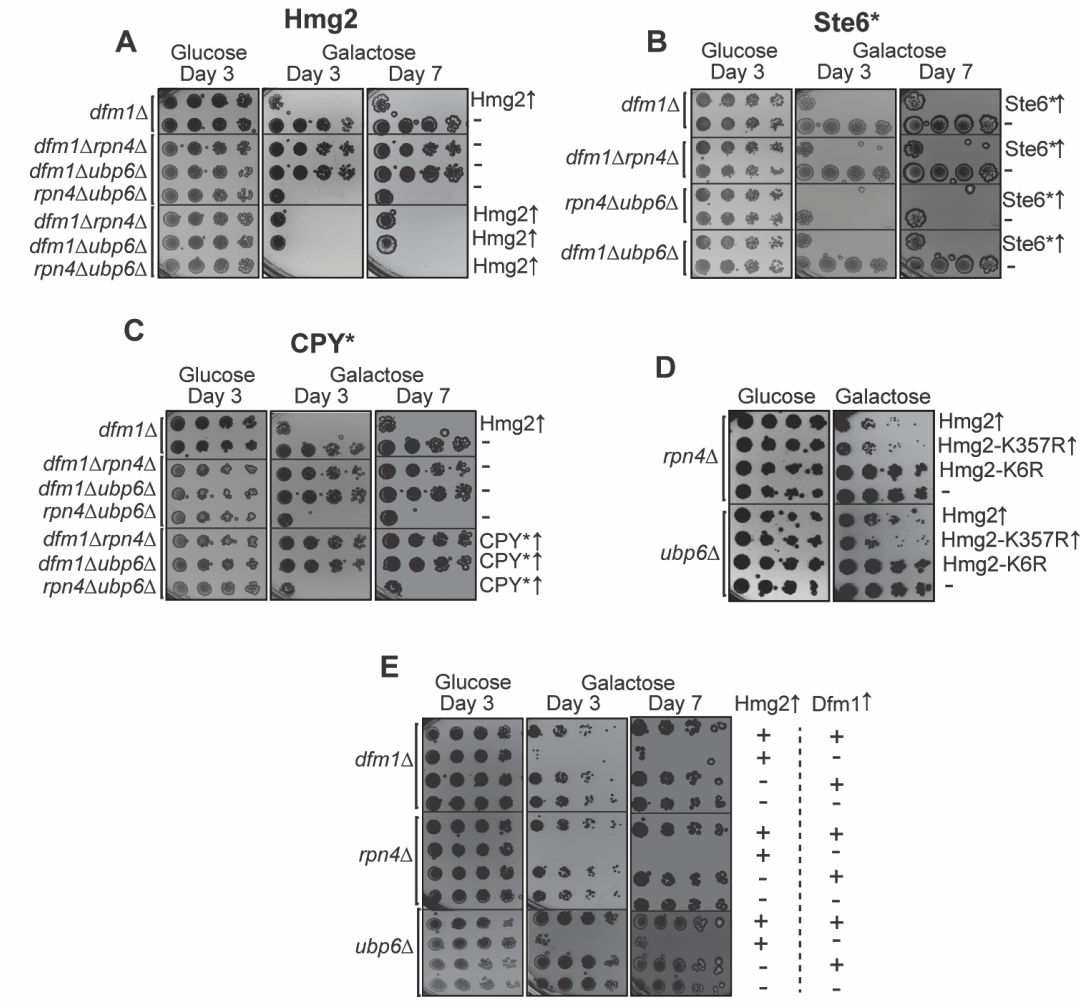


Supplemental Figure 2.2.6. Not all deubiquitinates mediate misfolded membrane toxicity and toxicity is specific to misfolded membrane proteins

(A) WT, *dfm1*Δ, and *doa4Δ* cells containing either GAL_{pr}-HMG2-GFP or EV were compared for growth by dilution assay. Each strain was spotted 5-fold dilutions on glucose or galactose-containing plates to drive Hmg2-GFP overexpression, and plates were incubated at 30°C. **(B)** Dilution assay as in **(A)** except in *dfm1*Δ, *ubp2*Δ, *ubp5*Δ, *miy1*Δ, *ubp8*Δ, *miy2*Δ, *otu2*Δ, *ubp1*Δ, *ubp11*Δ, *ubp7*Δ, and *ubp3*Δ cells. **(C)** WT, *dfm1*Δ, *ubp6Δ*, *doa4Δ*, *ubp9Δ*, and *ubp14Δ* cells containing either GAL_{pr}-ΔssCPY*-Myc or EV were compared for growth by dilution assay. Each strain was spotted 5-fold dilutions on glucose or galactose-containing plates to drive Hmg2-GFP overexpression, and plates were incubated at 30°C. Data information: All dilution growth assays were performed in 3 biological and 2 technical replicates (N = 3).

Supplemental Figure 2.2.7. Genetic interactions between Dfm1, Rpn4, and Ubp6 in resolving misfolded membrane protein toxicity

(A) *dfm1*Δ, *dfm1*Δ*rpn4Δ*, *dfm1*Δ*ubp6Δ*, and *rpn4Δubp6Δ* cells containing either GAL_{pr}-HMG2-GFP or EV were compared for growth by dilution assay. Each strain was spotted 5-fold dilutions on glucose or galactose-containing plates to drive Hmg2-GFP overexpression, and plates were incubated at 30°C. **(B)** Dilution assays as depicted in **(A)** except using cells containing GAL_{pr}-STE6*-GFP. **(C)** Dilution assays as depicted in (A) except using cells containing GAL_{pr}-CPY*. **(D)** *dfm1*Δ, *rpn4Δ*, and *ubp6Δ* cells containing either GAL_{pr}-Hmg2-GFP or EV and GAL_{pr}-Dfm1-10xHis or EV were compared for growth by dilution assay. Each strain was spotted 5-fold dilutions on glucose or galactose-containing plates to drive Hmg2-GFP and Dfm1-10xHis overexpression, and plates were incubated at 30°C. **(E)** Dilution assay as described in **(A)** except using *rpn4*Δ and *ubp6*Δ cells containing either GAL_{pr}-Hmg2-GFP, GAL_{pr}-Hmg2 (K6R)-GFP, GAL_{pr}-Hmg2 (K357R)-GFP, GAL_{pr}-Hmg2 (K6R and K357R)-GFP, or EV. Data information: All dilution growth assays were performed in 3 biological and 2 technical replicates (N = 3).


Hmg2
A
Glucose
Day 3
Galactose
Day 3
Day 7
dfm1Δ
dfm1Δrpn4Δ
dfm1Δubp6Δ
rpn4Δubp6Δ
dfm1Δrpn4Δ
dfm1Δubp6Δ
rpn4Δubp6Δ
Hmg2↑
-
-
-
-
Hmg2↑
Hmg2↑
Hmg2↑
Ste6*
B
Glucose
Day 3
Galactose
Day 3
Day 7
dfm1Δ
dfm1Δrpn4Δ
rpn4Δubp6Δ
dfm1Δubp6Δ
Ste6*↑
-
Ste6*↑
-
Ste6*↑
-
Ste6*↑
-
C
CPY*
Glucose
Day 3
Galactose
Day 3
Day 7
dfm1Δ
dfm1Δrpn4Δ
dfm1Δubp6Δ
rpn4Δubp6Δ
dfm1Δrpn4Δ
dfm1Δubp6Δ
rpn4Δubp6Δ
Hmg2↑
-
-
-
-
CPY*↑
CPY*↑
CPY*↑
D
Glucose
Galactose
rpn4Δ
ubp6Δ
Hmg2↑
Hmg2-K357R↑
Hmg2-K6R
-
Hmg2↑
Hmg2-K357R↑
Hmg2-K6R
-
E
Glucose
Day 3
Galactose
Day 3
Day 7
Hmg2↑
Dfm1↑
dfm1Δ
rpn4Δ
ubp6Δ
+ +
+ -
- +
- -
+ +
+ -
- +
- -
+ +
+ -
- +
- -

Supplemental Table 2.4.1. Plasmid List

Plasmid	Gene		
pRH1120	YCp	URA3	pGAL1-HMG2-GFP
pRH3113	YCp	URA3	pGAL1-PDR5*-HA
pRH3112	YCp	URA3	pGAL1-CPY*-HA
pRH3144	YCp	URA3	pGAL1- Ste6-166p-3HA-GFP
pRH317	YCp	URA3	
pRH316	YCp	LEU2	
pRH1945	YIp	ADE2 URA3	4xUPRE-GFP
pRH2890	YCp	LEU2	pDFM1-DFM1-3HA-5aShp
pRH1997	YCp	LEU2	pDFM1-DFM1-3HA
pRH2812	YCp	LEU2	pDFM1-DFM1-3HA-AxxxG
pRH2813	YCp	LEU2	pDFM1-DFM1-3HA-GxxxA
pRH2826	YCp	LEU2	pDFM1-DFM1-3HA-WA
pRH2827	YCp	LEU2	pDFM1-DFM1-3HA-AR

Supplemental Table 2.4.1. Plasmid List (Continued)

Plasmid	Gene		
pRH2013	YCp	LEU2	pDFM1-DFM1-3HA
pSN12	YIp	ADE2 HIS3	
pSN11	YCp	URA3	
pSN103	YIp	ADE2 HIS3	pGAL1-HMG2-GFP-K357R
pSN104	YIp	ADE2 HIS3	pGAL1-HMG2-GFP-K6R
pSN105	YIp	ADE2 HIS3	pGAL1-HMG2-GFP
pSN59	YCp	LEU2	pDFM1-DFM1-3HA-F107S
pSN60	YCp	LEU2	pDFM1-DFM1-3HA-L64V
pSN93	YCp	LEU2	pDFM1-DFM1-3HA-K67E
pSN94	YCp	LEU2	pDFM1-DFM1-3HA-Q101R
pSN95	YCp	LEU2	pDFM1-DFM1-3HA-F57S
pSN168	YCp	ADE2 HIS3	pGAL1-HMG2-GFP-K6R-K357R
pSN86	YIp	ADE2 HIS3	pGAL1-STE6-166p-3HA-GFP
pSN88	YIp	ADE2 HIS3	pGAL1-HMG2-6MYC

Supplemental Table 2.4.1. Plasmid List (Continued)

Plasmid	Gene		
pSN100	YIp	ADE2 HIS3	pGAL1-CPY*-HA
pSN195	YCp	URA3	CFTR-HA
pSN196	YCp	URA3	CFTR-HA-ΔF508
pSN197	YCp	URA3	A1PiZ
pSN199	YCp	URA3	pGAL1-DFM1-6HIS
pSN5	YCp	URA3	
pSN193	YIp	ADE2 LEU2	pADH1-Derlin-1-MYC
pSN194	YIp	ADE2 LEU2	pADH1-Derlin-2-MYC
pSN39	YIp	ADE2 LEU2	
pSN190	YCp	URA3	pCUP1-HBT-Ubiquitin
pRH613	YIp	ADE2	pTDH3-HMG2-GFP
pRH2312	YCp	HIS3	pPGK1-PDR5*-HA
pRH2058	YCp	URA3	pPGK1-STE6-166p-3HA-GFP
pRH311	YIp	TRP1	

Supplemental Table 2.4.1. Plasmid List (Continued)

Plasmid	Gene		
pRH1862	YIp	ADE2 URA3	pTDH3-HMG2-GFP-K6R
pRH469	YIp	URA3	HMG2-GFP
pSN177	YCp	URA3	CPY*-GFP
pRH2513	YIp	TRP1	pHRD1-Hrd1-5MYC
pSN189	YCp	URA3	pGAL-ΔssCPY-MYC
pRH2880	YIp	TRP1	pTDH3-SEC61-GFP

Supplemental Table 2.4.2. Yeast Strains Used in this Study

Strain	Genotype	Reference
RHY10520	Mata *ADE2 met15Δ0 LYS2(LYS+) ura3Δ0 TRP1 leu2Δ0 his3Δ1 pdr5Δ::KanMX* *CEN::URA3*	This study
RHY10519	*Mata ADE2 met15Δ0 LYS2(LYS+) ura3Δ0 TRP1 leu2Δ0 his3Δ1 pdr5Δ::KanMX* *CEN::URA3::GAL1pr-HMG2-GFP*	This study
RHY10518	*Mata ADE2 met15Δ0 LYS2(LYS+) ura3Δ0 TRP1 leu2Δ0 his3Δ1 dfm1Δ::KanMX* *CEN::URA3*	This study
RHY10517	*Mata ADE2 met15Δ0 LYS2(LYS+) ura3Δ0 TRP1 leu2Δ0 his3Δ1* *dfm1Δ::KanMX* *CEN::URA3::GAL1pr-HMG2-GFP*	This study
RHY10655	*Mata ADE2 met15Δ0 LYS2(LYS+) ura3Δ0 TRP1 leu2Δ0 his3Δ1hrd1Δ::KanMX* *CEN::URA3*	This study
RHY10654	*Mata ADE2 met15Δ0 LYS2(LYS+) ura3Δ0 TRP1 leu2Δ0 his3Δ1 hrd1Δ::KanMX* *CEN::URA3::GAL1pr-HMG2-GFP*	This study
RHY11580	*Mata ADE2 met15Δ0 LYS2(LYS+) ura3Δ0 TRP1 leu2Δ0 his3Δ1 pdr5Δ::KanMX* *CEN::URA3::GAL1pr-PDR5*-HA*	This study
RHY11581	*Mata ADE2 met15Δ0 LYS2(LYS+) ura3Δ0 TRP1 leu2Δ0 his3Δ1 dfm1Δ::KanMX* *CEN::URA3::GAL1pr-PDR5*-HA*	This study
RHY11583	*Mata ADE2 met15Δ0 LYS2(LYS+) ura3Δ0 TRP1 leu2Δ0 his3Δ1 hrd1Δ::KanMX* *CEN::URA3::GAL1pr-PDR5*-HA*	This study

Supplemental Table 2.4.2. Yeast Strains Used in this Study (Continued)

Strain	Genotype	Reference
RHY11576	*Mata ADE2 met15Δ0 LYS2(LYS+) ura3Δ0 TRP1 leu2Δ0 his3Δ1 pdr5Δ::KanMX* *CEN::URA3::GAL1pr-CPY*-HA*	This study
RHY11577	*Mata ADE2 met15Δ0 LYS2(LYS+) ura3Δ0 TRP1 leu2Δ0 his3Δ1 dfm1Δ::KanMX* *CEN::URA3::GAL1pr-CPY*-HA*	Neal et al., 2020
RHY11579	*Mata ADE2 met15Δ0 LYS2(LYS+) ura3Δ0 TRP1 leu2Δ0 his3Δ1 hrd1Δ::KanMX* *CEN::URA3::GAL1pr-CPY*-HA*	Neal et al., 2020
RHY11817	*Mata ADE2 MET2 lys2-801 ura3Δ0 TRP1 leu2Δ0 his3Δ200 dfm1Δ::KanMX hrd1Δ::CloNAT CEN::URA3*	Neal et al., 2020
RHY11818	*Mata ADE2 MET2 lys2-801 ura3Δ0 TRP1 leu2Δ0 his3Δ200* *dfm1Δ::KanMX hrd1Δ::CloNAT* *CEN::URA3::GAL1pr-HMG2-GFP*	This study
RHY 11867	*Mata ADE2 met15Δ0 LYS2(LYS+) ura3Δ0 TRP1 leu2Δ0 his3Δ1 pdr5Δ::KanMX* *CEN::URA3::GAL1pr-STE6-166p-3HA-GFP*	Neal et al., 2018
RHY 11868	*Mata ADE2 met15Δ0 LYS2(LYS+) ura3Δ0 TRP1 leu2Δ0 his3Δ1 dfm1Δ::KanMX* *CEN::URA3::GAL1pr-STE6-166p-3HA-GFP*	Neal et al., 2018
RHY 11869	*Mata ADE2 met15Δ0 LYS2(LYS+) ura3Δ0 TRP1 leu2Δ0 his3Δ1 hrd1Δ::KanMX* *CEN::URA3::GAL1pr-STE6-166p-3HA-GFP*	Neal et al., 2020
RHY 1826	*Mata ADE2 MET2 lys2-801 ura3Δ0 TRP1 leu2Δ0 his3Δ200* *dfm1Δ::KanMX hrd1Δ::CloNAT* *CEN::URA3::GAL1pr-STE6-166p-3HA-GFP*	This study

Supplemental Table 2.4.2. Yeast Strains Used in this Study (Continued)

Strain	Genotype	Reference
RHY 11873	*Mata ADE2 met15Δ0 LYS2(LYS+) ura3-52 trp1::hisG leu2Δ his3Δ1 dfm1Δ::CloNAT doa10Δ::HphMx* *CEN::URA3::GAL1pr-STE6-166p-3HA-GFP*	This study
RHY 11908	*Mata ADE2 met15Δ0 LYS2(LYS+) ura3-52 trp1::hisG leu2Δ his3Δ1 doa10Δ::HphMx* *CEN::URA3::GAL1pr-STE6-166p-3HA-GFP*	This study
RHY 11906	*Mata ADE2 met15Δ0 LYS2(LYS+) ura3-52 trp1::hisG leu2Δ his3Δ1 doa10Δ::HphMx* *CEN::URA3*	Neal et al., 2020
RHY 11907	*Mata ADE2 met15Δ0 LYS2(LYS+) ura3-52 trp1::hisG leu2Δ his3Δ1 doa10Δ::HphMx* *CEN::URA3::GAL1pr-HMG2-GFP*	Neal et al., 2020
RHY 11914	*Mata ADE2 met15Δ0 LYS2(LYS+) ura3-52 trp1::hisG leu2Δ his3Δ1 dfm1Δ::CloNAT doa10Δ::HphMx* *CEN::URA3*	This study
RHY 11915	*Mata ADE2 met15Δ0 LYS2(LYS+) ura3-52 trp1::hisG leu2Δ his3Δ1 dfm1Δ::CloNAT doa10Δ::HphMx* *CEN::URA3::GAL1pr-HMG2-GFP*	This study
RHY 11226	*Mata ADE2 met15Δ0 LYS2(LYS+) ura3Δ0 TRP1 leu2Δ0 his3Δ1 dfm1Δ::KanMX* *CEN::URA3 CEN::LEU2::pDFM1-DFM1-3HA*	Neal et al., 2018
RHY 11227	*Mata ADE2 met15Δ0 LYS2(LYS+) ura3Δ0 TRP1 leu2Δ0 his3Δ1 dfm1Δ::KanMX* *CEN::URA3:: GAL1pr-HMG2-GFP CEN::LEU2::pDFM1-DFM1-3HA*	Neal et al., 2018
RHY 11216	*Mata ADE2 met15Δ0 LYS2(LYS+) ura3Δ0 TRP1 leu2Δ0 his3Δ1 dfm1Δ::KanMX* *CEN::URA3 CEN::LEU2*	Neal et al., 2018

Supplemental Table 2.4.2. Yeast Strains Used in this Study (Continued)

Strain	Genotype	Reference
RHY12217	*Mata ADE2 met15Δ0 LYS2(LYS+) ura3Δ0 TRP1 leu2Δ0 his3Δ1 dfm1Δ::KanMX* *CEN::URA3:: GAL1pr-HMG2-GFP CEN::LEU2*	Neal et al., 2018
RHY11222	*Mata ADE2 met15Δ0 LYS2(LYS+) ura3Δ0 TRP1 leu2Δ0 his3Δ1 dfm1Δ::KanMX* *CEN::URA3 CEN::LEU2::pDFM1-DFM1-3HA-WA*	Neal et al., 2018
RHY11223	*Mata ADE2 met15Δ0 LYS2(LYS+) ura3Δ0 TRP1 leu2Δ0 his3Δ1 dfm1Δ::KanMX* *CEN::URA3:: GAL1pr-HMG2-GFP CEN::LEU2::pDFM1-DFM1-3HA-WA*	Neal et al., 2018
RHY11224	*Mata ADE2 met15Δ0 LYS2(LYS+) ura3Δ0 TRP1 leu2Δ0 his3Δ1 dfm1Δ::KanMX* *CEN::URA3 CEN::LEU2::pDFM1-DFM1-3HA-AR*	Neal et al., 2018
RHY11225	*Mata ADE2 met15Δ0 LYS2(LYS+) ura3Δ0 TRP1 leu2Δ0 his3Δ1 dfm1Δ::KanMX* *CEN::URA3:: GAL1pr-HMG2-GFP CEN::LEU2::pDFM1-DFM1-3HA-AR*	Neal et al., 2018
RHY11218	*Mata ADE2 met15Δ0 LYS2(LYS+) ura3Δ0 TRP1 leu2Δ0 his3Δ1 dfm1Δ::KanMX* *CEN::URA3 CEN::LEU2::pDFM1-DFM1-3HA-AxxxG*	Neal et al., 2018
RHY11219	*Mata ADE2 met15Δ0 LYS2(LYS+) ura3Δ0 TRP1 leu2Δ0 his3Δ1 dfm1Δ::KanMX* *CEN::URA3:: GAL1pr-HMG2-GFP CEN::LEU2::pDFM1-DFM1-3HA-AxxxG*	Neal et al., 2018
RHY11220	*Mata ADE2 met15Δ0 LYS2(LYS+) ura3Δ0 TRP1 leu2Δ0 his3Δ1 dfm1Δ::KanMX* *CEN::URA3 CEN::LEU2::pDFM1-DFM1-3HA-GxxxA*	Neal et al., 2018
RHY11221	*Mata ADE2 met15Δ0 LYS2(LYS+) ura3Δ0 TRP1 leu2Δ0 his3Δ1 dfm1Δ::KanMX* *CEN::URA3:: GAL1pr-HMG2-GFP CEN::LEU2::pDFM1-DFM1-3HA-GxxxA*	Neal et al., 2018

Supplemental Table 2.4.2. Yeast Strains Used in this Study (Continued)

Strain	Genotype	Reference
RHY11073	*Mata ADE2 met15Δ0 LYS2(LYS+) ura3Δ0 TRP1 leu2Δ0 his3Δ1 dfm1Δ::KanMX* *CEN::URA3 CEN::LEU2::pDFM1-DFM1-3HA-5aShp*	Neal et al., 2018
RHY11074	*Mata ADE2 met15Δ0 LYS2(LYS+) ura3Δ0 TRP1 leu2Δ0 his3Δ1 dfm1Δ::KanMX* *CEN::URA3:: GAL1pr-HMG2-GFP CEN::LEU2::pDFM1-DFM1-3HA-5aShp*	Neal et al., 2018
SEN141	Mata *ade2::ADE2::HIS3::pGAL1::Hmg2-GFP met2 lys2-801 ura3-52 trp1::hisG leu2Δ his3Δ200*	This study
SEN142	Mata *ade2::ADE2::HIS3 met2 lys2-801 ura3-5, trp1::hisG leu2Δ his3Δ200*	This study
SEN149	Mata *ade2::ADE2::HIS3 met2 lys2-801 ura3-52 trp1::hisG leu2Δ his3Δ200 dfm1Δ::KanMX*	This study
SEN165	Mata *ade2::ADE2::HIS3::pGAL1::Hmg2-GFP met2 lys2-801 ura3-52, trp1::hisG leu2Δ his3Δ200 dfm1Δ::KanMX*	This study
SEN407	Mata *ade2-101 met2 lys2-801 ura3-5, trp1::hisG leu2Δ his3Δ200* *CEN::ADE2::HIS3::pGAL1-Hmg2-GFP-K6R-K357R*	This study
SEN408	Mata *ade2-101 met2 lys2-801 ura3-5, trp1::hisG leu2Δ his3Δ200 dfm1Δ::KanMX* *CEN::ADE2::HIS3::pGAL1-Hmg2-GFP-K6R-K357R*	This study
SEN139	Mata *ade2::ADE2::HIS3::pGAL1::Hmg2-GFP-K357R met2 lys2-801 ura3-52 trp1::hisG leu2Δ his3Δ200*	This study
SEN147	Mata *ade2::ADE2::HIS3::pGAL1::Hmg2-GFP-K357R met2 lys2-801 ura3-52 trp1::hisG leu2Δ his3Δ200 dfm1Δ::KanMX*	This study
SEN140	Mata *ade2::ADE2::HIS3::pGAL1::Hmg2-GFP-K6R met2 lys2-801 ura3-52 trp1::hisG leu2Δ his3Δ200*	This study
SEN148	Mata *ade2::ADE2::HIS3::pGAL1::Hmg2-GFP-K6R met2 lys2-801 ura3-52 trp1::hisG leu2Δ his3Δ200 dfm1Δ::KanMX*	This study

Supplemental Table 2.4.2. Yeast Strains Used in this Study (Continued)

Strain	Genotype	Reference
SEN182	Mata *ade2::ADE2::HIS3 met2 lys2-801 ura3-52 trp1::hisG leu2Δ his3Δ200 dfm1Δ::KanMX* *CEN::LEU2::pDFM1-DFM1-3HA*	This study
SEN183	Mata *ade2::ADE2::HIS3 met2 lys2-801 ura3-52 trp1::hisG leu2Δ his3Δ200 dfm1Δ::KanMX CEN::LEU2*	This study
SEN192	Mata *ade2::ADE2::HIS3::pGAL1::Hmg2-GFP met2 lys2-801 ura3-52, trp1::hisG leu2Δ his3Δ200 dfm1Δ::KanMX* *CEN::LEU2::pDFM1-DFM1-3HA*	This study
SEN193	Mata *ade2::ADE2::HIS3::pGAL1::Hmg2-GFP met2 lys2-801 ura3-52, trp1::hisG leu2Δ his3Δ200 dfm1Δ::KanMX* *CEN::LEU2*	This study
SEN250	Mata *ade2::ADE2::HIS3 met2 lys2-801 ura3-52 trp1::hisG leu2Δ his3Δ200 dfm1Δ::KanMX* *CEN::LEU2::pDFM1-DFM1-3HA-F107S*	This study
SEN251	Mata *ade2::ADE2::HIS3 met2 lys2-801 ura3-52 trp1::hisG leu2Δ his3Δ200 dfm1Δ::KanMX* *CEN::LEU2::pDFM1-DFM1-3HA-L64V*	This study
SEN252	Mata *ade2::ADE2::HIS3 met2 lys2-801 ura3-52 trp1::hisG leu2Δ his3Δ200 dfm1Δ::KanMX* *CEN::LEU2::pDFM1-DFM1-3HA-K67E*	This study
SEN253	Mata *ade2::ADE2::HIS3 met2 lys2-801 ura3-52 trp1::hisG leu2Δ his3Δ200 dfm1Δ::KanMX* *CEN::LEU2::pDFM1-DFM1-3HA-Q101R*	This study
SEN254	Mata *ade2::ADE2::HIS3 met2 lys2-801 ura3-52 trp1::hisG leu2Δ his3Δ200 dfm1Δ::KanMX* *CEN::LEU2::pDFM1-DFM1-3HA-F58S*	This study
SEN256	Mata *ade2::ADE2::HIS3::pGAL1::Hmg2-GFP met2 lys2-801 ura3-52, trp1::hisG leu2Δ his3Δ200 dfm1Δ::KanMX* *CEN::LEU2::pDFM1-DFM1-3HA-F107S*	This study

Supplemental Table 2.4.2. Yeast Strains Used in this Study (Continued)

Strain	Genotype	Reference
SEN257	Mata *ade2::ADE2::HIS3::pGAL1::Hmg2-GFP met2 lys2-801 ura3-52, trp1::hisG leu2Δ his3Δ200 dfm1Δ::KanMX* *CEN::LEU2::pDFM1-DFM1-3HA-L64V*	This study
SEN258	Mata *ade2::ADE2::HIS3::pGAL1::Hmg2-GFP met2 lys2-801 ura3-52, trp1::hisG leu2Δ his3Δ200 dfm1Δ::KanMX* *CEN::LEU2::pDFM1-DFM1-3HA-K67E*	This study
SEN259	Mata *ade2::ADE2::HIS3::pGAL1::Hmg2-GFP met2 lys2-801 ura3-52, trp1::hisG leu2Δ his3Δ200 dfm1Δ::KanMX* *CEN::LEU2::pDFM1-DFM1-3HA-Q101R*	This study
SEN260	Mata *ade2::ADE2::HIS3::pGAL1::Hmg2-GFP met2 lys2-801 ura3-52, trp1::hisG leu2Δ his3Δ200 dfm1Δ::KanMX* *CEN::LEU2::pDFM1-DFM1-3HA-F58S*	This study
SEN103	Mata *ade2::ADE2::URA3::4xUPRE-GFP met15Δ0 LYS2 (LYS+) ura3Δ0 TRP1 leu2Δ0 his3Δ1 pdr5Δ::KanMX* *pGAL1::CPY*-HA*	This study
SEN111	Mata *ade2::ADE2::URA3::4xUPRE-GFP met15Δ0 LYS2 (LYS+) ura3Δ0 TRP1 leu2Δ0 his3Δ1 dfm1Δ:: KanMX* *pGAL1::CPY*-HA*	This study
SEN73	Mata *ade2::ADE2::URA3::4xUPRE-GFP met15Δ0 LYS2 (LYS+) ura3Δ0 TRP1 leu2Δ0 his3Δ1 pdr5Δ::KanMX* *pGAL1::STE6-166p-3HA-GFP*	This study
SEN75	Mata *ade2::ADE2::URA3::4xUPRE-GFP met15Δ0 LYS2 (LYS+) ura3Δ0 TRP1 leu2Δ0 his3Δ1 dfm1Δ:: KanMX* *pGAL1::STE6-166p-3HA-GFP*	This study
SEN76	Mata *ade2::ADE2::URA3::4xUPRE-GFP met15Δ0 LYS2 (LYS+) ura3Δ0 TRP1 leu2Δ0 his3Δ1 ADE2::HIS3 pdr5Δ::KanMX*	This study
SEN68	Mata *ade2::ADE2::URA3::4xUPRE-GFP met15Δ0 LYS2 (LYS+) ura3Δ0 TRP1 leu2Δ0 his3Δ1 ADE2::HIS3 dfm1Δ::KanMX*	This study

Supplemental Table 2.4.2. Yeast Strains Used in this Study (Continued)

Strain	Genotype	Reference
SEN70	Mata *ade2::ADE2::URA3::4xUPRE-GFP met15Δ0 LYS2 (LYS+) ura3Δ0 TRP1 leu2Δ0 his3Δ1 dfm1Δ::KanMX pGAL1::HMG2-6MYC*	This study
SEN71	Mata *ade2::ADE2::URA3::4xUPRE-GFP met15Δ0 LYS2 (LYS+) ura3Δ0 TRP1 leu2Δ0 his3Δ1 ADE2::HIS3 dfm1Δ::KanMX*	This study
SEN155	Mata *ADE2::HIS3 met15Δ0 LYS2 (LYS+) ura3Δ0 TRP1 leu2Δ0 his3Δ1 rpn4Δ::KanMX*	This study
SEN166	Mata *ADE2::HIS3::pGAL::Hmg2-GFP met15Δ0 LYS2 (LYS+) ura3Δ0 TRP1 leu2Δ0 his3Δ1 rpn4Δ::KanMX*	This study
SEN196	Mata *ADE2::HIS3 met15Δ0 LYS2 (LYS+) ura3Δ0 TRP1 leu2Δ0 his3Δ1 ubp6Δ::KanMX*	This study
SEN197	Mata *ADE2::HIS3::pGAL1::Hmg2-GFP met15Δ0 LYS2 (LYS+) ura3Δ0 TRP1 leu2Δ0 his3Δ1 ubp6Δ::KanMX*	This study
SEN411	Mata *ade2::ADE2::HIS3::pGAL1::STE6-166-3HA-GFP met2 lys2-801 ura3-52 trp1::hisG leu2Δ his3Δ200*	This study
SEN412	Mata *ADE2::HIS3::pGAL1::STE6-166p-3HA-GFP met15Δ0 LYS2 (LYS+) ura3Δ0 TRP1 leu2Δ0 his3Δ1 rpn4Δ::KanMX*	This study
SEN413	Mata *ade2::ADE2::HIS3:: pGAL1::STE6-166p-3HA-GFP met2 lys2-801 ura3-52 trp1::hisG leu2Δ his3Δ200 dfm1Δ::KanMX*	This study
SEN414	Mata *ADE2::HIS3::pGAL1::STE6-166p-3HA-GFP met15Δ0 LYS2 (LYS+) ura3Δ0 TRP1 leu2Δ0 his3Δ1 ubp6Δ::KanMX*	This study
SEN269	Mata *ADE2::HIS3::pGAL1::CPY*-HA met15Δ0 LYS2 (LYS+) ura3Δ0 TRP1 leu2Δ0 his3Δ1 ubp6Δ::KanMX*	This study
SEN415	Mata *ade2::ADE2::HIS3::pGAL1::CPY*-HA met2 lys2-801 ura3-52 trp1::hisG leu2Δ his3Δ200*	This study
SEN416	Mata *ADE2::HIS3::pGAL1::CPY*-HA met15Δ0 LYS2 (LYS+) ura3Δ0 TRP1 leu2Δ0 his3Δ1 rpn4Δ::KanMX*	This study
SEN417	Mata *ade2::ADE2::HIS3:: pGAL1::CPY*-HA met2 lys2-801 ura3-52 trp1::hisG leu2Δ his3Δ200 dfm1Δ::KanMX*	This study

Supplemental Table 2.4.2. Yeast Strains Used in this Study (Continued)

Strain	Genotype	Reference
SEN270	Mata *ADE2::HIS3::pGAL1::CPY*-HA met15Δ0 LYS2 (LYS+) ura3Δ0 TRP1 leu2Δ0 his3Δ1 rpn4Δ::KanMX dfm1Δ::CloNAT*	This study
SEN271	Mata *ADE2::HIS3::pGAL1::CPY*-HA met15Δ0 LYS2 (LYS+) ura3Δ0 TRP1 leu2Δ0 his3Δ1 rpn4Δ::KanMX ubp6Δ::CloNAT*	This study
SEN272	Mata *ADE2::HIS3::pGAL1::CPY*-HA met15Δ0 LYS2 (LYS+) ura3Δ0 TRP1 leu2Δ0 his3Δ1 ubp6Δ::KanMX dfm1Δ::CloNAT*	This study
SEN499	Mata *ADE2::HIS3::pGAL1::STE6-166p-3HA-GFP met15Δ0 LYS2 (LYS+) ura3Δ0 TRP1 leu2Δ0 his3Δ1 rpn4Δ::KanMX dfm1Δ::CloNAT*	This study
SEN500	Mata *ADE2::HIS3::pGAL1::STE6-166p-3HA-GFP met15Δ0 LYS2 (LYS+) ura3Δ0 TRP1 leu2Δ0 his3Δ1 rpn4Δ::KanMX ubp6Δ::CloNAT*	This study
SEN501	Mata *ADE2::HIS3::pGAL1::STE6-166p-3HA-GFP met15Δ0 LYS2 (LYS+) ura3Δ0 TRP1 leu2Δ0 his3Δ1 ubp6Δ::KanMX dfm1Δ::CloNAT*	This study
SEN273	Mata *ADE2::HIS3::pGAL1::HMG2-GFP met15Δ0 LYS2 (LYS+) ura3Δ0 TRP1 leu2Δ0 his3Δ1 rpn4Δ::KanMX dfm1Δ::CloNAT*	This study
SEN276	Mata *ADE2::HIS3 met15Δ0 LYS2 (LYS+) ura3Δ0 TRP1 leu2Δ0 his3Δ1 rpn4Δ::KanMX dfm1Δ::CloNAT*	This study
SEN274	Mata *ADE2::HIS3::pGAL1::HMG2-GFP met15Δ0 LYS2 (LYS+) ura3Δ0 TRP1 leu2Δ0 his3Δ1 rpn4Δ::KanMX ubp6Δ::CloNAT*	This study
SEN277	Mata *ADE2::HIS3 met15Δ0 LYS2 (LYS+) ura3Δ0 TRP1 leu2Δ0 his3Δ1 rpn4Δ::KanMX ubp6Δ::CloNAT*	This study
SEN275	Mata *ADE2::HIS3::pGAL1::HMG2-GFP met15Δ0 LYS2 (LYS+) ura3Δ0 TRP1 leu2Δ0 his3Δ1 ubp6Δ::KanMX dfm1Δ::CloNAT*	This study
SEN278	Mata *ADE2::HIS3 met15Δ0 LYS2 (LYS+) ura3Δ0 TRP1 leu2Δ0 his3Δ1 ubp6Δ::KanMX dfm1Δ::CloNAT*	This study

Supplemental Table 2.4.2. Yeast Strains Used in this Study (Continued)

Strain	Genotype	Reference
SEN487	Mata *ade2::ADE2::HIS3::pGAL1::Hmg2-GFP met2 lys2-801 ura3-52, trp1::hisG leu2Δ his3Δ200 dfm1Δ::KanMX* *CEN::URA3::pGAL1::DFM1-6HIS*	This study
SEN488	Mata *ade2::ADE2::HIS3::pGAL1::Hmg2-GFP met2 lys2-801 ura3-52, trp1::hisG leu2Δ his3Δ200 dfm1Δ::KanMX* *CEN::URA3*	This study
SEN489	Mata *ade2::ADE2::HIS3 met2 lys2-801 ura3-52, trp1::hisG leu2Δ his3Δ200 dfm1Δ::KanMX* *CEN::URA3::pGAL1::DFM1-6HIS*	This study
SEN490	Mata *ade2::ADE2::HIS3 met2 lys2-801 ura3-52, trp1::hisG leu2Δ his3Δ200 dfm1Δ::KanMX CEN::URA3*	This study
SEN491	Mata *ADE2::HIS3::pGAL::Hmg2-GFP met15Δ0 LYS2 (LYS+) ura3Δ0 TRP1 leu2Δ0 his3Δ1 rpn4Δ::KanMX* *CEN::URA3::pGAL1::DFM1-6HIS*	This study
SEN492	Mata *ADE2::HIS3::pGAL::Hmg2-GFP met15Δ0 LYS2 (LYS+) ura3Δ0 TRP1 leu2Δ0 his3Δ1 rpn4Δ::KanMX* *CEN::URA3*	This study
SEN493	Mata *ADE2::HIS3 met15Δ0 LYS2 (LYS+) ura3Δ0 TRP1 leu2Δ0 his3Δ1 rpn4Δ::KanMX* *CEN::URA3::pGAL1::DFM1-6HIS*	This study
SEN494	Mata *ADE2::HIS3 met15Δ0 LYS2 (LYS+) ura3Δ0 TRP1 leu2Δ0 his3Δ1 rpn4Δ::KanMX CEN::URA3*	This study
SEN517	Mata *ADE2::HIS3::pGAL::Hmg2-GFP met15Δ0 LYS2 (LYS+) ura3Δ0 TRP1 leu2Δ0 his3Δ1 ubp6Δ::KanMX* *CEN::URA3::pGAL1::DFM1-6HIS*	This study
SEN518	Mata *ADE2::HIS3::pGAL::Hmg2-GFP met15Δ0 LYS2 (LYS+) ura3Δ0 TRP1 leu2Δ0 his3Δ1 ubp6Δ::KanMX* *CEN::URA3*	This study

Supplemental Table 2.4.2. Yeast Strains Used in this Study (Continued)

Strain	Genotype	Reference
SEN519	Mata *ADE2::HIS3 met15Δ0 LYS2 (LYS+) ura3Δ0 TRP1 leu2Δ0 his3Δ1 ubp6Δ::KanMX* *CEN::URA3::pGAL1::DFM1-6HIS*	This study
SEN520	Mata *ADE2::HIS3 met15Δ0 LYS2 (LYS+) ura3Δ0 TRP1 leu2Δ0 his3Δ1 ubp6Δ::KanMX CEN::URA3*	This study
SEN249	Mata *ade2-101 met2 lys2-801 ura3-52 trp1::hisG::TRP1:: pTDH3-Hmg1p-MYC-Hrd1p-3HA-GFP leu2Δ his3Δ200 hrd1Δ::KanMX dfm1Δ::CloNAT pdr5Δ::HIS3*	This study
SEN378	Mata *ade2-101 met2 lys2-801 ura3-52 trp1::hisG::TRP1 leu2Δ his3Δ200 hrd1Δ::KanMX pdr5Δ::HIS3*	This study
SEN229	Mata *ade2-101 met2 lys2-801 ura3-52 trp1::hisG::TRP1:: pTDH3-Hmg1p-MYC-Hrd1p-3HA-GFP leu2Δ his3Δ200 hrd1Δ::KanMX pdr5Δ::HIS3*	This study
SEN228	Mata *ade2-101 met2 lys2-801 ura3-52 trp1::hisG::TRP1:: pTDH3-Hmg1p-MYC-Hrd1p-3HA-GFP leu2Δ his3Δ200 pdr5Δ::HIS3*	This study
SEN377	Mata *ade2-101 met2 lys2-801 ura3-52 trp1::hisG::TRP1 leu2Δ his3Δ200 pdr5Δ::HIS3*	This study
SEN379	Mata *ade2-101 met2 lys2-801 ura3-52 trp1::hisG::TRP1 leu2Δ his3Δ200 hrd1Δ::KanMX dfm1Δ::CloNAT pdr5Δ::HIS3*	This study
SEN401	Mata *ADE2::HIS3::pGAL1::Hmg2-GFP met15Δ0 LYS2 (LYS+) ura3Δ0 TRP1 leu2Δ0 his3Δ1 ubp9Δ::KanMX*	This study
SEN424	Mata *ADE2::HIS3 met15Δ0 LYS2 (LYS+) ura3Δ0 TRP1 leu2Δ0 his3Δ1 ubp9Δ::KanMX*	This study
SEN446	Mata *ADE2 met15Δ0 LYS2 (LYS+) ura3Δ0 TRP1 leu2Δ0 his3Δ1 ubp9Δ::KanMX CEN::URA3:: ΔssCPY*-MYC*	This study
SEN459	Mata *ADE2 met15Δ0 LYS2 (LYS+) ura3Δ0 TRP1 leu2Δ0 his3Δ1 ubp14Δ::KanMX CEN::URA3*	This study

Supplemental Table 2.4.2. Yeast Strains Used in this Study (Continued)

Strain	Genotype	Reference
SEN460	Mata *ADE2 met15Δ0 LYS2 (LYS+) ura3Δ0 TRP1 leu2Δ0 his3Δ1 doa4Δ::KanMX CEN::URA3*	This study
SEN461	Mata *ade2-101 met2 lys2-801 ura3-52 trp1::hisG leu2Δ his3Δ200 CEN::URA3:: ΔssCPY*-MYC*	This study
SEN463	Mata *ade2-101 met2 lys2-801 ura3-52 trp1::hisG leu2Δ his3Δ200 dfm1Δ::KanMX CEN::URA3:: ΔssCPY*-MYC*	This study
SEN464	Mata *ADE2 met15Δ0 LYS2 (LYS+) ura3Δ0 TRP1 leu2Δ0 his3Δ1 ubp14Δ::KanMX CEN::URA3:: ΔssCPY*-MYC*	This study
SEN449	Mata *ADE2 met15Δ0 LYS2 (LYS+) ura3Δ0 TRP1 leu2Δ0 his3Δ1 ubp6Δ::KanMX CEN::URA3*	This study
SEN450	Mata *ADE2 met15Δ0 LYS2 (LYS+) ura3Δ0 TRP1 leu2Δ0 his3Δ1 ubp14Δ::KanMX CEN::URA3*	This study
SEN451	Mata *ade2-101 met2 lys2-801 ura3-52 trp1::hisG leu2Δ his3Δ200 dfm1Δ::KanMX CEN::URA3*	This study
SEN215	*Mata ADE2::URA3::pTDH3-HMG2-GFPx met15Δ0 LYS2(LYS+) ura3Δ0 TRP1 leu2Δ0 his3Δ1 dfm1Δ::KanMX CEN::LEU2::pDFM1-DFM1-3HA-L64V*	Nejatfard, et al., 2021
SEN216	*Mata ADE2::URA3::pTDH3-HMG2-GFPx met15Δ0 LYS2(LYS+) ura3Δ0 TRP1 leu2Δ0 his3Δ1 dfm1Δ::KanMX CEN::LEU2::pDFM1-DFM1-3HA-F107S*	Nejatfard, et al., 2021
SEN217	*Mata ADE2::URA3::pTDH3-HMG2-GFPx met15Δ0 LYS2(LYS+) ura3Δ0 TRP1 leu2Δ0 his3Δ1 dfm1Δ::KanMX CEN::LEU2::pDFM1-DFM1-3HA-K67E*	Nejatfard, et al., 2021

Supplemental Table 2.4.2. Yeast Strains Used in this Study (Continued)

Strain	Genotype	Reference
SEN218	*Mata ADE2::URA3::pTDH3-HMG2-GFPx met15Δ0 LYS2(LYS+) ura3Δ0 TRP1 leu2Δ0 his3Δ1 dfm1Δ::KanMX CEN::LEU2::pDFM1-DFM1-3HA-Q101R*	Nejatfard, et al., 2021
SEN219	*Mata ADE2::URA3::pTDH3-HMG2-GFPx met15Δ0 LYS2(LYS+) ura3Δ0 TRP1 leu2Δ0 his3Δ1 dfm1Δ::KanMX CEN::LEU2::pDFM1-DFM1-3HA-F58S*	Nejatfard, et al., 2021
SEN529	*Mata ADE2::URA3::pTDH3-HMG2-GFPx met15Δ0 LYS2(LYS+) ura3Δ0 TRP1 leu2Δ0 his3Δ1 dfm1Δ::KanMX CEN::LEU2*	Nejatfard, et al., 2021
SEN530	*Mata ADE2::URA3::pTDH3-HMG2-GFPx met15Δ0 LYS2(LYS+) ura3Δ0 TRP1 leu2Δ0 his3Δ1 dfm1Δ::KanMX CEN::LEU2::pDFM1-DFM1-3HA-AR*	Nejatfard, et al., 2021
SEN532	*Mata ADE2::URA3::pTDH3-HMG2-GFPx met15Δ0 LYS2(LYS+) ura3Δ0 TRP1 leu2Δ0 his3Δ1 dfm1Δ::KanMX CEN::LEU2::pDFM1-DFM1-3HA-AxxxG*	Nejatfard, et al., 2021
SEN534	*Mata ADE2::URA3::pTDH3-HMG2-GFPx met15Δ0 LYS2(LYS+) ura3Δ0 TRP1 leu2Δ0 his3Δ1 dfm1Δ::KanMX CEN::LEU2::pDFM1-DFM1-3HA*	Nejatfard, et al., 2021
SEN535	*Mata ADE2::URA3::pTDH3-HMG2-GFPx met15Δ0 LYS2(LYS+) ura3Δ0 TRP1 leu2Δ0 his3Δ1 dfm1Δ::KanMX CEN::LEU2::pDFM1-DFM1-3HA-5aShp*	Nejatfard, et al., 2021
SEN506	Mata *ade2::ADE2::HIS3 met2 lys2-801 ura3-52, trp1::hisG leu2::LEU2::ADE2:: pADH1-Derlin-1-MYC his3Δ200 dfm1Δ::KanMX*	This study
SEN507	Mata *ade2::ADE2::HIS3 met2 lys2-801 ura3-52, trp1::hisG leu2::LEU2::ADE2:: pADH1-Derlin-1-MYC his3Δ200*	This study
SEN510	Mata *ade2::ADE2::HIS3 met2 lys2-801 ura3-52, trp1::hisG leu2::LEU2::ADE2:: pADH1-Derlin-2-MYC his3Δ200*	This study

Supplemental Table 2.4.2. Yeast Strains Used in this Study (Continued)

Strain	Genotype	Reference
SEN512	Mata *ade2::ADE2::HIS3::pGAL1::Hmg2-GFP met2 lys2-801 ura3-52, trp1::hisG leu2::LEU2::ADE2::pADH1-Derlin-2-MYC his3∆200 dfm1∆::KanMX*	This study
SEN515	Mata *ade2::ADE2::HIS3::pGAL1::Hmg2-GFP met2 lys2-801 ura3-52, trp1::hisG leu2::LEU2::ADE2 his3∆200 dfm1∆::KanMX*	This study
SEN516	Mata *ade2::ADE2::HIS3::pGAL1::Hmg2-GFP met2 lys2-801 ura3-52, trp1::hisG leu2::LEU2::ADE2 his3∆200*	This study
SEN470	Mata *ade2::ADE2::HIS3 met2 lys2-801 ura3-5, trp1::hisG leu2∆ his3∆200 CEN::URA3::CFTR-HA*	This study
SEN472	Mata *ade2::ADE2::HIS3 met2 lys2-801 ura3-52, trp1::hisG leu2::LEU2::ADE2 his3∆200 dfm1∆::KanMX* *CEN::URA3::CFTR-HA*	This study
SEN474	Mata *ade2::ADE2::HIS3 met2 lys2-801 ura3-5, trp1::hisG leu2∆ his3∆200 CEN::URA3::CFTR-HA-∆F508*	This study
SEN476	Mata *ade2::ADE2::HIS3 met2 lys2-801 ura3-52, trp1::hisG leu2::LEU2::ADE2 his3∆200 dfm1∆::KanMX* *CEN::URA3::CFTR-HA-∆F508*	This study
SEN478	Mata *ade2::ADE2::HIS3 met2 lys2-801 ura3-5, trp1::hisG leu2∆ his3∆200 CEN::URA3::A1PiZ*	This study
SEN480	Mata *ade2::ADE2::HIS3 met2 lys2-801 ura3-52, trp1::hisG leu2::LEU2::ADE2 his3∆200 dfm1∆::KanMX* *CEN::URA3::A1PiZ*	This study
SEN452	Mata *ade2::ADE2::HIS3 met2 lys2-801 ura3-52, trp1::hisG leu2::LEU2::ADE2 his3∆200 dfm1∆::KanMX* *CEN::URA3*	This study
SEN455	Mata *ade2::ADE2::HIS3 met2 lys2-801 ura3-52, trp1::hisG leu2::LEU2::ADE2 his3∆200 CEN::URA3*	This study

Supplemental Table 2.4.2. Yeast Strains Used in this Study (Continued)

Strain	Genotype	Reference
SEN365	ata *ADE2::HIS3::pGAL1::Hmg2-GFP met15Δ0 LYS2 (LYS+) ura3Δ0 TRP1 leu2Δ0 his3Δ1 pdr1Δ::KanMX*	This study
SEN366	Mata *ADE2::HIS3 met15Δ0 LYS2 (LYS+) ura3Δ0 TRP1 leu2Δ0 his3Δ1 pdr1Δ::KanMX*	This study
SEN395	Mata *ADE2::HIS3::pGAL1::Hmg2-GFP met15Δ0 LYS2 (LYS+) ura3Δ0 TRP1 leu2Δ0 his3Δ1 ubp8Δ::KanMX*	This study
SEN418	Mata *ADE2::HIS3 met15Δ0 LYS2 (LYS+) ura3Δ0 TRP1 leu2Δ0 his3Δ1 ubp8Δ::KanMX*	This study
SEN396	Mata *ADE2::HIS3::pGAL1::Hmg2-GFP met15Δ0 LYS2 (LYS+) ura3Δ0 TRP1 leu2Δ0 his3Δ1 miy2Δ::KanMX*	This study
SEN419	Mata *ADE2::HIS3 met15Δ0 LYS2 (LYS+) ura3Δ0 TRP1 leu2Δ0 his3Δ1 miy2Δ::KanMX*	This study
SEN397	Mata *ADE2::HIS3::pGAL1::Hmg2-GFP met15Δ0 LYS2 (LYS+) ura3Δ0 TRP1 leu2Δ0 his3Δ1 otu2Δ::KanMX*	This study
SEN420	Mata *ADE2::HIS3 met15Δ0 LYS2 (LYS+) ura3Δ0 TRP1 leu2Δ0 his3Δ1 otu2Δ::KanMX*	This study
SEN398	Mata *ADE2::HIS3::pGAL1::Hmg2-GFP met15Δ0 LYS2 (LYS+) ura3Δ0 TRP1 leu2Δ0 his3Δ1 ubp2Δ::KanMX*	This study
SEN421	Mata *ADE2::HIS3 met15Δ0 LYS2 (LYS+) ura3Δ0 TRP1 leu2Δ0 his3Δ1 ubp2Δ::KanMX*	This study
SEN399	Mata *ADE2::HIS3::pGAL1::Hmg2-GFP met15Δ0 LYS2 (LYS+) ura3Δ0 TRP1 leu2Δ0 his3Δ1 ubp5Δ::KanMX*	This study
SEN422	Mata *ADE2::HIS3 met15Δ0 LYS2 (LYS+) ura3Δ0 TRP1 leu2Δ0 his3Δ1 ubp5Δ::KanMX*	This study
SEN400	Mata *ADE2::HIS3::pGAL1::Hmg2-GFP met15Δ0 LYS2 (LYS+) ura3Δ0 TRP1 leu2Δ0 his3Δ1 miy1Δ::KanMX*	This study
SEN423	Mata *ADE2::HIS3 met15Δ0 LYS2 (LYS+) ura3Δ0 TRP1 leu2Δ0 his3Δ1 miy1Δ::KanMX*	This study
SEN402	Mata *ADE2::HIS3::pGAL1::Hmg2-GFP met15Δ0 LYS2 (LYS+) ura3Δ0 TRP1 leu2Δ0 his3Δ1 ubp1Δ::KanMX*	This study
SEN425	Mata *ADE2::HIS3 met15Δ0 LYS2 (LYS+) ura3Δ0 TRP1 leu2Δ0 his3Δ1 ubp1Δ::KanMX*	This study

Supplemental Table 2.4.2. Yeast Strains Used in this Study (Continued)

Strain	Genotype	Reference
SEN403	Mata *ADE2::HIS3::pGAL1::Hmg2-GFP met15Δ0 LYS2 (LYS+) ura3Δ0 TRP1 leu2Δ0 his3Δ1 ubp11Δ::KanMX*	This study
SEN426	Mata *ADE2::HIS3 met15Δ0 LYS2 (LYS+) ura3Δ0 TRP1 leu2Δ0 his3Δ1 ubp11Δ::KanMX*	This study
SEN405	Mata *ADE2::HIS3::pGAL1::Hmg2-GFP met15Δ0 LYS2 (LYS+) ura3Δ0 TRP1 leu2Δ0 his3Δ1 ubp7Δ::KanMX*	This study
SEN428	Mata *ADE2::HIS3 met15Δ0 LYS2 (LYS+) ura3Δ0 TRP1 leu2Δ0 his3Δ1 ubp7Δ::KanMX*	This study
SEN406	Mata *ADE2::HIS3::pGAL1::Hmg2-GFP met15Δ0 LYS2 (LYS+) ura3Δ0 TRP1 leu2Δ0 his3Δ1 ubp3Δ::KanMX*	This study
SEN429	Mata *ADE2::HIS3 met15Δ0 LYS2 (LYS+) ura3Δ0 TRP1 leu2Δ0 his3Δ1 ubp3Δ::KanMX*	This study
SEN453	Mata *ade2::ADE2::HIS3 met2 lys2-801 ura3-52, trp1::hisG leu2Δ his3Δ200* *CEN::URA3::pCUP1-HBT-Ubiquitin*	This study
SEN454	Mata *ade2::ADE2::HIS3 met2 lys2-801 ura3-52, trp1::hisG leu2Δ his3Δ200* *CEN::URA3*	This study
SEN457	Mata *ade2::ADE2::HIS3 met2 lys2-801 ura3-52, trp1::hisG leu2Δ his3Δ200* *CEN::URA3::pCUP1-HBT-Ubiquitin*	This study
SEN455	Mata *ade2::ADE2::HIS3 met2 lys2-801 ura3-52, trp1::hisG leu2Δ his3Δ200* *CEN::URA3*	This study
SEN481	Mata *ade2::ADE2::HIS3::pGAL1::Hmg2-GFP met2 lys2-801 ura3-52, trp1::hisG leu2Δ his3Δ200 dfm1Δ::KanMX* *CEN::URA3::pCUP1-HBT-Ubiquitin*	This study
SEN456	Mata *ade2::ADE2::HIS3::pGAL1::Hmg2-GFP met2 lys2-801 ura3-52, trp1::hisG leu2Δ his3Δ200 dfm1Δ::KanMX* *CEN::URA3*	This study

Supplemental Table 2.4.2. Yeast Strains Used in this Study (Continued)

Strain	Genotype	Reference
SEN482	Mata *ade2::ADE2::HIS3 met2 lys2-801 ura3-52, trp1::hisG leu2Δ his3Δ200 dfm1Δ::KanMX* *CEN::URA3::pCUP1-HBT-Ubiquitin*	This study
SEN452	Mata *ade2::ADE2::HIS3 met2 lys2-801 ura3-52, trp1::hisG leu2Δ his3Δ200 dfm1Δ::KanMX CEN::URA3*	This study
SEN122	*ade2::ADE2::HIS3 met2 lys2-801 ura3-52::URA3::4xUPRE::GFP TRP1 leu2Δ his3Δ200 der1Δ::CloNat*	This study
SEN123	*ade2::ADE2::HIS3::pGAL::Hmg2-6MYC met2 lys2-801 ura3-52::URA3::4xUPRE::GFP TRP1 leu2Δhis3Δ200 der1Δ::CloNat*	This study
RHY11923	Mata *ade2-101 met2 lys2-801 ura3-5, trp1::hisG::pGAL::Hmg2-GFP leu2Δ his3Δ200 pdr5Δ::HIS3*	This study
RHY11924	Mata *ade2-101 met2 lys2-801 ura3-5, trp1::hisG::pGAL::Hmg2-GFP leu2Δ his3Δ200 pdr5Δ::HIS3 hrd1Δ::KanMX*	This study
RHY11925	Mata *ade2-101 met2 lys2-801 ura3-5, trp1::hisG::pGAL::Hmg2-GFP leu2Δ his3Δ200 pdr5Δ::HIS3 dfm1Δ::CloNAT*	This study
RHY11916	Mata *ade2-101 met2 lys2-801 ura3-5, trp1::hisG::TRP1 leu2Δ his3Δ200 pdr5Δ::HIS3*	This study
RHY11917	Mata *ade2-101 met2 lys2-801 ura3-5, trp1::hisG::TRP1 leu2Δ his3Δ200 pdr5Δ::HIS3 hrd1Δ::KanMX*	This study

Supplemental Table 2.4.2. Yeast Strains Used in this Study (Continued)

Strain	Genotype	Reference
RHY11918	Mata *ade2-101 met2 lys2-801 ura3-5, trp1::hisG::TRP1 leu2Δ his3Δ200 pdr5Δ::HIS3* *dfm1Δ::CloNAT*	This study
SEN409	Mata *ade2 met2 lys2-801 ura3-52 trp1::hisG leu2Δ his3Δ200 dfm1Δ::KanMX* *CEN::URA3::CPY*-GFP*	Nejatfard, et al., 2021
SEN410	Mata *ade2 met2 lys2-801 ura3-52 trp1::hisG leu2Δ his3Δ200 dfm1Δ::KanMX* *CEN::URA3::CPY*-GFP* *CEN::LEU2::pDFM1-DFM1-3HA*	Nejatfard, et al., 2021
SEN206	*Mata ADE2 met15Δ0 LYS2(LYS+) ura3Δ0 TRP1 leu2Δ0 his3Δ1 hrd1Δ::KanMX* *CEN::HIS3::PDR5*-HA* *CEN::LEU2::pDFM1-DFM1-3HA*	Nejatfard, et al., 2021
SEN264	*Mata ADE2 met15Δ0 LYS2(LYS+) ura3Δ0 TRP1 leu2Δ0 his3Δ1 hrd1Δ::KanMX CEN::HIS3::PDR5*-HA* *CEN::LEU2*	Nejatfard, et al., 2021
SEN554	*ade2-101 met2 lys2-801 ura3-52::URA3::HMG2-GFP trp1::hisG leu2Δ his3Δ200 pdr5Δ::KanMX*	This study
SEN555	*ade2-101 met2 lys2-801 ura3-52::URA3::HMG2-GFP trp1::hisG::TRP1 leu2Δ his3Δ200 hrd1Δ::KanMX*	This study
SEN556	*ade2-101 met2 lys2-801 ura3-52::URA3::HMG2-GFP trp1::hisG::TRP1::pHrd1::Hrd1-5MYC leu2Δ his3Δ200 hrd1Δ::KanMX*	This study
RHY10584	Mata *ADE2::ADE2::URA3::TDH3p-HMG2-GFP-K6R met15Δ0 LYS2 (LYS+) ura3Δ0 TRP1 leu2Δ0 his3Δ1 dfm1Δ::KanMX*	This study

Supplemental Table 2.4.2. Yeast Strains Used in this Study (Continued)

Strain	Genotype	Reference
RHY12239	*ade2-101 met2 lys2-801 ura3-52::URA3::HMG2-GFP trp1::hisG::TRP1 leu2Δ his3Δ200 dfm1Δ::KanMX* *CEN::LEU2*	This study
RHY12240	*ade2-101 met2 lys2-801 ura3-52 trp1::hisG::TRP1::TDH3-SEC61-GFP leu2Δ his3Δ200 dfm1Δ::KanMX* *CEN::LEU2::pDFM1-DFM1-3HA*	This study
RHY12241	*ade2-101 met2 lys2-801 ura3-52 trp1::hisG::TRP1::TDH3-SEC61-GFP leu2Δ his3Δ200 dfm1Δ::KanMX* *CEN::LEU2::pDFM1-5ASHP-3HA*	This study

Chapter 3: An ERAD-independent role for rhomboid pseudoprotease Dfm1 in mediating sphingolipid homeostasis

3.1. Introduction

Nearly one-third of nascent proteins are initially targeted to the endoplasmic reticulum (ER) where they are correctly folded and assembled before being delivered to their final cellular destinations. To prevent the accumulation of misfolded membrane proteins, ER-associated-degradation (ERAD) removes these clients from the ER membrane to the cytosol in a process known as retrotranslocation. Our previous work demonstrated that rhomboid pseudoprotease, Dfm1, is involved in the retrotranslocation of ubiquitinated integral membrane ERAD substrates. To survey for potential interaction partners of Dfm1, we performed protein-proximity labeling by BioID (proximity-dependent biotin identification) followed by mass spectrometry and identified several interacting proteins known to play a role in the sphingolipid biosynthesis pathway. Specifically, we found that Dfm1 associates with the SPOTS complex, which is composed of serine palmitoyltransferase (SPT) enzymes and accessory components and is critical for catalyzing the first rate-limiting step of the sphingolipid biosynthesis pathway. Herein, we found that Dfm1 binds directly to phosphorylated Orm2, a major antagonizer of SPT activity, to facilitate Orm2 export from the ER and its subsequent degradation by EGAD (ER Golgi Associated Degradation). Moreover, recruitment of Cdc48 by Dfm1, which is critical for its role in ERAD retrotranslocation, is dispensable for Dfm1's role in controlling Orm2 export. Given that the accumulation of human Orm2 homologs, ORMDLs, are associated with many maladies, our study serves as a molecular foothold for understanding how dysregulation of sphingolipid metabolism leads to various diseases.

The endoplasmic reticulum (ER) carries out a vast range of functions including protein synthesis and transport, protein folding, lipid and steroid synthesis, carbohydrate

metabolism, and calcium storage. Almost all eukaryotic membrane and secreted proteins are co-translationally imported into the ER where they are subsequently folded (Sicari et al., 2019; Wang and Dehesh, 2018). Proteins frequently fail to fold or assemble properly, at which point they are eliminated by ER-Associated-Degradation (ERAD) (Mehrtash and Hochstrasser, 2019; Ruggiano et al., 2014; Sun and Brodsky, 2019).

ERAD describes a range of pathways that target and ubiquitinate a large repertoire of secretory and membrane substrates for proteasomal degradation. To date, most of the knowledge about ERAD is obtained in yeast and mammals. In yeast, ERAD substrates are classified according to the location of their lesions and are referred as ERAD-L (lesion in luminal domain), ERAD-M (lesion within the transmembrane domain), and ERAD-C (lesion in the cytosolic domain). The HMG-CoA reductase degradation (HRD) pathway utilizes the E3 ligase, Hrd1, to target ERAD-M and ERAD-L substrates, and the degradation of alpha 2 (DOA) pathway utilizes the E3 ligase, Doa10, to target ERAD-C substrates (Carvalho et al., 2006; Foresti et al., 2013; Hampton et al., 1996; Hiller et al., 1996; Laney and Hochstrasser, 2003). Moreover, unassembled ER subunits escaping to the inner nuclear membrane (INM) are targeted by the Asi complex (Foresti et al., 2014; Natarajan et al., 2020). ERAD pathways are much more diverse in mammalians cells due to the complexity of lesions or degrons within ERAD substrates (Leto et al., 2019). Although there are no Asi homologs present in mammals, there are at least 20 ER-localized ubiquitin ligases characterized that contribute to ERAD (Fenech et al.; Leto et al., 2019). A common theme for all ERAD pathways is the removal or retrotranslocation of ubiquitinated substrates from the ER membrane or INM followed by degradation by the proteasome (Hampton and Sommer, 2012). Retrotranslocation has been well-characterized in yeast, with two derlins, Der1 and

Dfm1, serving as major mediators of retrotranslocation for ERAD-L and ERAD-M substrates, respectively (Neal et al., 2018; Wu et al., 2020). Moreover, previous structural studies suggest that the multi-membrane spanning yeast E3 ligases, Hrd1 and Doa10, function as channels for the retrotranslocation of luminal and single-spanning membrane substrates, respectively (Schmidt et al., 2020; Wu et al., 2020). No analogous channel for multi-spanning membrane substrates had been determined, until Neal and colleagues identified the yeast derlin, Dfm1, as a major retrotranslocation factor for a subset of membrane substrates (Neal et al., 2018).

Dfm1 is an ER-resident multi-spanning membrane protein and is classified as a rhomboid pseudoprotease. Recently, we showed that Dfm1 utilizes its conserved rhomboid protein residues for substrate engagement and its lipid thinning properties to allow retrotranslocation of multi-spanning membrane substrates (Nejatfard et al., 2021a). To identify interacting partners of Dfm1 that may assist with retrotranslocation, we employed proximity-based labeling followed by mass spectrometry. Remarkably, we identified several proteins enriched with Dfm1, which are known to play a role in the sphingolipid biosynthesis pathway. Sphingolipids constitute a major class of lipids defined by their amino-alcohol backbone with mainly eighteen-carbon and are synthesized in the ER from non-sphingolipid precursors (Hannun and Obeid, 2018). Modification of this basic structure gives rise to the vast family of sphingolipids, which have essential roles in cell signaling and function. Serine palmitoyltransferase (SPT) is the first rate-limiting enzyme in the de novo synthesis of sphingolipids, and its sole function is to catalyze the initial step in sphingolipid biosynthesis by converting serine and palmitoyl-CoA into a sphingolipid precursor, 3-keto-sphinganine (Hanada, 2003). SPT is essential for the viability of all eukaryotic cells, and mutations of SPT

are linked to hereditary sensory neuropathy type 1 (HSAN1) and early onset amyotrophic lateral sclerosis (ALS) (Bode et al., 2015; Mohassel et al.). Accordingly, SPT serves as the key point for regulation of sphingolipid biosynthesis. SPT forms the SPOTS complex, comprised of Orm1 and Orm2 (members of the orosomucoid (ORM) gene family), Tsc3, and Sac1. The SPOTS complex is highly conserved from yeast to mammals (Breslow et al., 2010). Functionally, Orm1, Orm2, and phosphoinositide phosphatase Sac1 are evolutionarily conserved negative regulators of SPT, while Tsc3 is a positive regulator.

Previous studies have demonstrated that levels of several SPOT complex members and sphingolipid biosynthesis enzymes are regulated through protein degradation pathways in order to control sphingolipid levels. For example, the TORC2-Ypk1 signaling axis phosphorylates Orm2, triggering its export from the ER to the Golgi, where it is selectively ubiquitinated by the Dsc complex before being retrotranslocated and degraded by the cytosolic proteasome. This pathway is known as ER Golgi-Associated Degradation (EGAD)(Schmidt et al., 2019, 2020). Another study analyzing systematic turnover of proteins in yeast revealed that several enzymes and regulators involved in the de novo sphingolipid biosynthesis pathway are degraded in separate organelles, such as the Golgi and vacuole (Christiano et al., 2020). Although many enzymes and regulators associated with sphingolipid biosynthesis reside in the ER, an ER-localized regulator for sphingolipid homeostasis has not yet been identified. In this study, we report a novel role for the ER-resident Dfm1 in maintaining sphingolipid homeostasis. We find that Dfm1 physically and genetically interacts with SPOTS complex components. This includes a genetic interaction with TSC3, a positive regulator of SPT, whose function is essential for stimulating SPT activity at 37^{o}C. Specifically, loss of Dfm1 rescues the growth lethality of *tsc3*Δ cells by

increasing ceramide and complex sphingolipid levels. DFM1 also genetically interacts with ORM1, a negative regulator of SPT activity, in which *orm1*Δ*dfm1*Δ cells have an exacerbated growth defect due to increased flux in sphingolipid biosynthesis. Finally, we provide the first evidence that Dfm1 is required for Orm2 degradation, a function that is independent of Dfm1's classical ERAD-M retrotranslocation function. We confirm the independence of Dfm1's ERAD function and demonstrate that the EGAD-client, Orm2, does not require ERAD nor Inner Nuclear Membrane Associated Degradation (INMAD) pathways, which is in agreement with an earlier study (Schmidt et al., 2019). To better understand the role of Dfm1 in Orm2 degradation, we show that loss of Dfm1 results in accumulation of phosphorylated Orm2 at the ER, suggesting a novel role for Dfm1 in controlling Orm2 export from the ER and its subsequent degradation by EGAD. We further show that Dfm1 does not directly function with COPII dynamics and trafficking, but functions upstream of ER export where Dfm1 interacts with Ypk1-dependent phosphorylated Orm2. Overall, our work identifies the highly conserved derlin Dfm1 as a critical mediator of sphingolipid homeostasis and provides a new therapeutic target for maladies associated with dysregulation in sphingolipid homeostasis.

3.2. Results

3.2.1. Derlin Dfm1 interacts with members of the sphingolipid biosynthetic pathway

To identify potential Dfm-1 interacting proteins, Proximity-dependent biotin identification (BioID) was employed. Briefly, BirA-3xFLAG was fused to Dfm1 to survey for potential interacting partners (Fig. 3.2.1A). Because Dfm1 included an added BirA-3xFLAG epitope at the C-terminus, we wished to confirm that the tag did not affect the expression and function of Dfm1. To this end, tagged-DFM1 was placed under a galactose inducible promoter (GAL_{pr}) and cells expressing GAL-driven Dfm1-BirA-3xFLAG were grown in the presence of 2% galactose. Under these conditions, induced expression of Dfm1 was observed at the expected molecular weight of ~60 kDa (Fig. 3.2.1B). BirA-3xFLAG alone expressed at both the expected size of ~25 kDa and at a larger size, which most likely represents BirA aggregates (marked by asterisks, Fig. 3.2.1B). To test whether Dfm1-BirA-3xFLAG function is still intact, we performed cycloheximide (CHX)-chase of a well-characterized Dfm1 substrate, Hmg2 (Hampton et al., 1996). We observed Hmg2-GFP degradation upon addback of Dfm1-BirA-3xFLAG while Hmg2-GFP degradation was stabilized with both empty vector and BirA-3xFLAG alone (Fig. 3.2.1C). To validate the identification of Dfm1 interactors via biotinylation, cells were treated with biotin and biotinylated proteins were enriched with streptavidin beads. As expected, the ATPase Cdc48, which has previously been shown to bind directly to Dfm1 (Neal et al., 2018; Sato and Hampton, 2006), was enriched in the biotin-treated samples, whereas neither Cdc48 nor Dfm1 were enriched in untreated or BirA-3xFLAG alone cells (Fig. 3.2.1D). Next, proteins that were enriched with streptavidin beads were digested to obtain tryptic peptides and analyzed by LC/MS/MS. Quantified proteins were mapped on volcano plots based on the

significance and the ratio between biotin-treated Dfm1-BirA-3xFLAG and untreated control cells. High-confidence interacting proteins were identified using DEP and Maxquant analysis (Fig. 3.2.1E and Supp. Dataset EV1; Available online) (Zuzow et al., 2018). By applying gene ontology (GO) enrichment analyses for the sets of Dfm1 interacting proteins identified, we found GO terms related to “Ceramide Metabolic Process” to be the most enriched (Fig. 3.2.1F). The interactions were validated by the presence of several ERAD components (Hrd1, Cdc48, proteasome subunits: Rpt2 and Pre9). Interestingly, closer analysis revealed unexpected interactions with SPOTS complex members (Orm1, Tsc3, and Lcb2). Taken together, these results suggest that our data have a high level of confidence and represent a rich source of Dfm1 interactome proteins, which include members of the sphingolipid biosynthesis pathway.

To validate the interaction of Dfm1 with SPOTS complex members, we performed co-immunoprecipitation (co-IP). Cells co-expressing Dfm1-GFP and members of the SPOTS complex (Lcb1-RFP, and Orm2-RFP) were subjected to immunoprecipitation via GFP Trap. Notably, Lcb1-RFP and Orm2-RFP co-immunoprecipitated with Dfm1-GFP, whereas no detectable association was seen in control cells without Dfm1-GFP (Fig. 3.2.2A). These interactions were also validated by fluorescence microscopy, in which the majority of Dfm1-GFP co-localized with Lcb1-RFP and Orm2-RFP at the ER (Fig. 3.2.2B).

3.2.2. DFM1 genetically interacts with TSC3

We next examined whether Dfm1 genetically interacts with SPOTS complex members. The SPOTS complex consists of the SPT enzymes, Lcb1 and Lcb2, and the smaller subunit, Tsc3, which has been required to positively regulate SPT at high temperatures (Gable et al., 2000). Furthermore, SPT activity is negatively regulated by two yeast paralogs, Orm1 and Orm2, through direct interactions, and by Sac1, which negatively regulates SPT through an unknown mechanism (Breslow et al., 2010; Han et al., 2010). To survey for gene interactions, we generated double mutant yeast strains of *dfm1*Δ along with respective SPOTS complex members and performed serial dilution growth assays to test whether double knockout cells confer any distinct growth phenotypes compared with WT and single knockouts. To test the involvement of essential enzymes Lcb1/Lcb2 and non-essential regulator Sac1, we utilized *Lcb1-DaMP*, *Lcb2-DamP*, and *sac1*Δ mutants and observed no genetic interactions, since growth of *dfm1*Δ*Lcb1-DaMP*, *dfm1*Δ*Lcb2-DaMP*, and *dfm1*Δ*sac1*Δ was similar to that of WT cells at 25^{o}C, 30^{o}C, and 37^{o}C (Supp. Fig. 3.2.1A). A small subunit of the SPT, Tsc3, directly interacts with Lcb1/Lcb2 to stimulate their activity and increase synthesis of the sphingolipid precursor, 3-ketosphinganine. The stimulatory function of Tsc3 is essential at the higher temperature where the *tsc3*Δ temperature-sensitive phenotype is lethal due to lack of phytosphingosine (PHS) production ((Gable et al., 2000) and Fig. 3.2.3A). In line with this observation, we observed a growth defect and lethality from *tsc3*Δ cells at 30^{o}C and 37^{o}C, respectively (Fig. 3.2.3A, *filled triangle*), and rescue of lethality when PHS was supplied to *tsc3*Δ cells (Fig. 3.2.3B, *right panel; filled triangle*). Remarkably, removal of DFM1 in this background – *dfm1*Δ*tsc3*Δ – completely rescued the lethality at 37^{o}C (Fig. 3.2.3A, *open circle*). Thus, removal of DFM1 suppresses *tsc3*Δ lethality at 37^{o}C.

3.2.3. *dfm1*Δ*tsc3*Δ cells have increased steady-state levels of ceramides and complex sphingolipids

We predicted that removal of DFM1 was able to reverse the temperature-sensitive lethality in *tsc3*Δ as a result of increased production of sphingolipid precursors. Notably, myriocin is a potent inhibitor of SPT, the first committed step in the sphingolipid biosynthesis pathway, and treatment with myriocin reduces sphingolipid levels in both *S. cerevisiae* and mammals (Breslow, 2013). Because SPT activity is essential, myriocin treatment exacerbates growth due to decreased flux in the sphingolipid biosynthesis pathway. We therefore wanted to test whether *dfm1*Δ*tsc3*Δ cells are resistant to myriocin inhibition. To this end, a sublethal dose of myriocin was used in the serial growth assay to reduce sphingolipid synthesis without impairing cell growth. As expected, *tsc3*Δ cells were sensitive to myriocin treatment at 30^{o}C since these cells already have decreased sphingolipid levels (Fig. 3.2.3B, *left panel; filled triangle*). By contrast, the *dfm1*Δ*tsc3*Δ cells were resistant to myriocin treatment, suggesting that these cells have higher levels of sphingolipids (Fig. 3.2.3B, *left panel; open circle*). Indeed, when grown at 30^{o}C, lipidomic analysis demonstrated that *dfm1*Δ*tsc3*Δ cells significantly produced higher levels of ceramides (Type A, C, & D) and complex sphingolipid inositolphosphorylceramide (IPC) (Type B & C) in comparison to WT cells (Fig. 3.2.3C). Altogether, *dfm1*Δ*tsc3* cells appear to produce higher steady-state levels of ceramide and complex sphingolipids.

3.2.4. DFM1 genetically interacts with ORM1

Because removal of DFM1 leads to higher levels of ceramides and complex sphingolipids in *tsc3*Δ cells, we hypothesized that Dfm1 is antagonizing the sphingolipid biosynthesis pathway. If this hypothesis is correct, *dfm1*Δ cells should phenocopy both *orm1*Δ and *orm2*Δ cells, which are established negative regulators of the SPT enzymes, in the growth assays. To test this hypothesis, *orm1*Δ*tsc3*Δ and *orm2*Δ*tsc3*Δ cells were generated and employed in the growth assays at 25°C, 30°C, and 37°C (Fig. 3.2.3D). Under these conditions, both *orm1*Δ and *orm2*Δ phenocopied *dfm1*Δ; both *orm1*Δ*tsc3*Δ and *orm2*Δ*tsc3*Δ cells were able to rescue the temperature-sensitive lethality displayed by *tsc3*Δ cells (Fig. 3.2.3D). Because *dfm1*Δ cells phenocopy both *orm1*Δ and *orm2*Δ cells, we next examined whether DFM1 genetically interacts with either ORM1 or ORM2. Although no growth defect was observed for *dfm1*Δ*orm2*Δ cells, we did observe a growth defect in *dfm1*Δ*orm1*Δ cells at room temperature, 30°C, and 37°C, suggesting that DFM1 functions with ORM1 in a parallel pathway (Fig. 3.2.4A, *filled triangle*). Furthermore, lipidomic analysis confirmed that *dfm1*Δ*orm2*Δ cells showed no increase in ceramides compared with WT cells. This was in contrast to *dfm1*Δ*orm1*Δ cells where there were significant changes in ceramides levels compared to WT cells (discussed below) (Fig. 3.2.4B and Supp. Fig. 3.2.1B). Orm1 and Orm2 have been shown to coordinate lipid homeostasis with ER protein quality control. This was demonstrated through growth sensitivity of *orm1*Δ*orm2*Δ cells to agents that increase protein misfolding in the ER (Han et al., 2010). Because DFM1 genetically interacts with ORM1, we surmise that *dfm1*Δ*orm1*Δ cells should also exhibit growth sensitivity to ER protein misfolding agents (Supp. Fig. 3.2.1C). We performed growth assays on plates containing tunicamycin, an inhibitor of N-linked glycosylation. Growth sensitivity to tunicamycin was observed for *orm1*Δ, *orm2*Δ, and *dfm1*Δ cells whereas exasperated growth

defects were observed for *dfm1*Δ*orm1*Δ and *orm1*Δ*orm2*Δ, but not *dfm1*Δ*orm2*Δ cells, further confirming that DFM1 genetically interacts with ORM1 and not ORM2. Cells lacking ORM1 and ORM2 exhibit a growth defect (Fig. 3.2.4A, *bottom panel*) due to an increased flux in de novo sphingolipid synthesis and the knockout cells were more resistant to myriocin inhibition (Breslow et al., 2010; Han et al., 2010). Given the growth defect seen in *dfm1*Δ*orm1*Δ cells, we reasoned that the flux in sphingolipid synthesis should be similarly increased. Notably, *dfm1*Δ*orm1*Δ cells were resistant to myriocin treatment (Fig. 3.2.4B, *left panel; open circle*) and sensitive to exogenously-added PHS (Fig. 3.2.4B, *right panel; open circle*), since *dfm1*Δ*orm1*Δ cells already exhibit higher levels of sphingolipids. Both dihydrosphingosine (DHS) and phytosphingosine (PHS) are early precursors of the sphingolipid biosynthesis pathway and are derivatives of long-chain bases (LCBs). Lipidomic analysis via mass spectrometry showed that C18-DHS levels were significantly higher in *dfm1*Δ*orm1*Δ cells than in WT cells. Also, C18-PHS levels were significantly higher in both *dfm1*Δ and *dfm1*Δ*orm1*Δ cells in comparison to WT cells, suggesting there is increased flux in sphingolipid biosynthesis in *dfm1*Δ*orm1*Δ cells (Fig. 3.2.4C). In contrast, the levels of ceramides and complex sphingolipids varied in *dfm1*Δ*orm1*Δ cells. There were higher levels of ceramide and complex sphingolipids (Type D) and lower levels of ceramide (Type A,B,&C) and complex sphingolipids (Type B) in *dfm1*Δ*orm1*Δ cells in comparison to WT cells (Fig. 3.2.4E). Notably, *orm1*Δ*orm2*Δ control cells also exhibited similar fluctuating levels of the varying types of ceramides and complex sphingolipids (Fig. 3.2.4E). Despite varying levels of ceramides and complex sphingolipids, *dfm1*Δ*orm1*Δ cells have higher LCB levels and are resistant to myriocin treatment, which suggests that the major physiological effect of *dfm1*Δ*orm1*Δ cells is from increased SPT activity (Fig. 3.2.4B and Fig. 3.2.4C).

3.2.5. Orm2 is targeted by Dfm1 for degradation

Given the myriad biological processes carried out by sphingolipids, it is not surprising that disruptions to sphingolipid homeostasis have deleterious effects and must be tightly regulated. One possible mode of regulation is through regulated degradation of key enzymes and regulators of sphingolipid biosynthesis in a manner analogous to the regulated degradation of Orm2 by EGAD to establish sphingolipid homeostasis. We therefore tested whether key enzymes or regulators within the sphingolipid biosynthesis pathway are targeted for Dfm1-mediated degradation by performing cycloheximide (CHX)-chase assays on candidate substrates (Lcb1, Lcb2, Orm1, Orm2, Sac1, Tsc3, Ypk1, and Tsc10), which function in either SPT synthesis or regulation (Supp. Fig. 3.2.2A). Of these, Orm2 was rapidly degraded in wild-type strains and its degradation was completely prevented in *dfm1*Δ cells (Fig. 3.2.5A). The yeast paralog of Dfm1, Der1, has a strong broad role in retrotranslocating ERAD-L substrates (Wu et al., 2020). We therefore directly tested the role of Der1 in Orm2 degradation using the CHX-chase assay and found that in both WT and *der1*Δ cells, Orm2 was still degraded (Fig. 3.2.5B). These results imply that the degradation of Orm2 is specifically dependent on derlin Dfm1 and not Der1.

3.2.6. Derlin Dfm1's Cdc48 recruitment function is not required for Orm2 degradation

We have previously identified specific motifs and residues of Dfm1 that are critical for its ERAD retrotranslocation function. Accordingly, we wished to test the importance of these motifs/residues for Orm2 degradation by performing CHX-chase assays. Dfm1 possesses a unique C-terminal SHP box motif, which recruits the ATPase, Cdc48, directly to the ER

surface (Neal et al., 2018). Cdc48 functions as an energy source for membrane substrate retrotranslocation and as a retrochaperone where it acts to maintain the solubility of retrotranslocated membrane substrates prior to proteasome degradation (Neal et al., 2017). We previously demonstrated that mutations within the SHP box, Dfm1-5Ashp, ablates Cdc48 recruitment and the retrotranslocation function of Dfm1 (Fig. 3.2.5C) (Neal et al., 2018). We also demonstrated that a Der1-SHP chimera, which consists of Der1, the paralog of Dfm1, fused to the cytoplasmic SHP tail of Dfm1, supports Cdc48 recruitment via binding of Cdc48 to the chimera's SHP tail, but does not support retrotranslocation through Der1's transmembrane segment (Fig. 3.2.5C) (Neal et al., 2018). We utilized these retrotranslocation-deficient variants in our CHX-chase assay to test whether Dfm1's Cdc48 recruitment function is required for Orm2 degradation. Addback of Der1-SHP in *dfm1*Δ cells impaired Orm2 degradation whereas Dfm1-5Ashp addback still enabled Orm2 degradation (Fig. 3.2.5D). These results suggest that recruitment of Cdc48 by Dfm1 is dispensable for Orm2 degradation. In addition, the inability of Der1-SHP to facilitate degradation of Orm2 implies the involvement of additional residues within the transmembrane segments of Dfm1.

Dfm1 contains the highly conserved WR motif in loop 1 (L1) and a Gx3G motif in transmembrane 6 (TM6). Both motifs have previously been substituted for alanine residues (WA and Gx3A) and such mutants are unable to support retrotranslocation (Fig. 3.2.5E and Fig. 3.2.5F) (Neal et al., 2018). In addition, we have previously identified that the L1 and TM2 regions of Dfm1 are critical for its retrotranslocation function (Fig. 3.2.5E and Fig. 3.2.5F). Specifically, L1 mutants (F58S, L64V, and K67E) impaired membrane substrate binding to Dfm1 and TM2 mutants (R98L, S99V, S100V, and Q101L) impaired Dfm1's lipid thinning distortion function (Nejatfard et al., 2021). The lipid distortion function of Dfm1 increases lipid

permeability to aid the extraction of integral membrane substrates from the lipid bilayer. All mutants are well characterized to date where they show robust Dfm1 expression (Supp. Fig. 3.2.2B) (Neal et al., 2018; Nejatfard et al., 2021). Accordingly, the effect of these retrotranslocation-deficient mutants on Orm2 degradation was directly tested with the CHX-chase assay. All Dfm1 mutants, with the exception of Dfm1-5Ashp, completely stabilized Orm2 (Fig. 3.2.5G). Furthermore, we employed the substrate binding co-IP assay to analyze the association of Dfm1 L1 mutants with Orm2-GFP. Orm2-GFP was immunoprecipitated with GFP Trap and immunoblotted for Dfm1 with α-HA. There was no detectable association of Orm2 with Dfm1 L1 mutants, implying that all three L1 residues are required for Orm2 binding (Fig. 3.2.5H). Overall, the conserved rhomboid motifs, WR and Gx3G, the L1 region for substrate binding, and the TM2 region for lipid thinning, are all required for Orm2 degradation. We employed another functional assay for Dfm1 to test whether the retrotranslocation-deficient Dfm1 mutants can restore growth in *dfm1*Δ*orm1*Δ cells, which normally have impaired growth at 37^{o}C due to increased flux in sphingolipid synthesis. To this end, adding back empty vector or wild-type DFM1 to *dfm1*Δ*orm1*Δ cells resulted in the expected impairment and rescue of normal growth, respectively (Supp. Fig. 3.2.2C and Supp. Fig. 3.3.3D). Introduction of Dfm1 mutants to *dfm1*Δ*orm1*Δ cells did not rescue growth defects, with the exception of Dfm1-5Ashp, which was able to rescue the growth defect in a manner similar to that of WT Dfm1 (Supp. Fig. 3.3.2C). Taken together, these data suggest that the substrate binding, lipid distortion function, and conserved rhomboid motifs, but not Cdc48 recruitment function, of Dfm1 are required for Orm2 degradation.

3.2.7. Orm2 degradation is dependent on EGAD, but not ERAD or INMAD

Given that the Cdc48 recruitment function of Dfm1 is dispensable for Orm2 degradation, it seems likely that Dfm1's retrotranslocation function in ERAD is not required for Orm2 degradation. Accordingly, we wished to survey for all protein degradation pathways in which Dfm1 may participate. The secretory pathway possesses several protein quality-control pathways including the INM-associated degradation (INMAD), ERAD, and EGAD, which govern both regulated and quality-control degradation of INM proteins, ER proteins, and Endosomal/Golgi proteins, respectively (Sicari et al., 2019; Sun and Brodsky, 2019). All pathways employ dedicated E3 ligases that determine substrate specificity and ubiquitination. Specifically, the Asi and Doa10 E3 ligases mediate INMAD, the Hrd1 and Doa10 E3 ligases mediate ERAD, and Tul1 E3 ligase mediates EGAD. A unifying theme for all protein degradation pathways is that they require the hexameric AAA ATPase, Cdc48, and the proteasome for retrotranslocation and degradation of all substrates. We utilized the CHX-chase assay to test the requirement for all E3 ligases, Cdc48, and the proteasome for degradation of Orm2. In line with previous studies (Schmidt et al., 2019), Orm2 was still degraded with similar kinetics to wild-type strains in *hrd1Δ, doa10Δ*, and *asi1Δ* (Fig. 3.2.6A). These results indicate that Orm2 degradation does not require either the INMAD or ERAD pathways. As expected, Orm2 degradation was completely inhibited in *tu1lΔ* cells, *cdc48-2* cells, and proteasome subunit mutant, *hrd2-1* (Fig. 3.2.6B) (Schmidt et al., 2019). These observations are in accordance with previous studies and demonstrate that Orm2 ubiquitination, extraction, and proteasome degradation is mediated solely by EGAD (Schmidt et al., 2019). To further confirm that Orm2 degradation is independent of ERAD and INMAD, we performed *in vivo* ubiquitination assays on WT, *asi1Δ*, *hrd1Δ*, *doa10Δ*, *tul1Δ*, *cdc48-2*, and *hrd2-1* strains. Strains were lysed and subjected to immunoprecipitation (IP) using anti-

RFP antibodies, followed by immunoblotting (IB) with anti-ubiquitin and anti-RFP antibodies. As suggested by CHX-chase experiments conducted by our lab and others (Schmidt et al., 2019), the degree of Orm2 ubiquitination in *asi1Δ*, *hrd1Δ*, and *doa10Δ* was similar to that seen in WT strains, demonstrating that the E3 ligases Asi, Hrd1, and Doa10 are not involved in the polyubiquitination of Orm2 (Fig. 3.2.6C, *lanes 1, 2, 3, 4*). In line with a previous study, the amount of Orm2 ubiquitination is increased in *cdc48-2* and *hrd2-1* cells, suggesting that Orm2 is on pathway for retrotranslocation and proteasome degradation (Fig. 3.2.6C, *lanes 8, 9*) (Schmidt et al., 2019).

As expected, Orm2 ubiquitination was decreased in *tul1Δ* strains, indicating that Orm2 is ubiquitinated by Tul1-dependent EGAD (Fig. 3.2.6C, lane 5). To further confirm that Orm2 degradation is independent of EGAD and INMAD, we next tested whether any of the ERAD components besides Dfm1, genetically interacted with Tsc3 and Orm1. Specifically, we examined whether any ERAD mutants phenocopy *dfm1Δtsc3Δ* cells, which rescues lethality at 37^{o}C, or *dfm1Δorm1Δ*, which exhibits a growth defect at 37^{o}C. To this end, double mutants were generated in which *tsc3Δ* or *orm1*Δ was knocked out, along with the following HRD and DOA pathway components: *hrd1Δ*, *hrd3*Δ, *der1*Δ, and *doa10*Δ. In all cases, the HRD and DOA pathway mutants did not phenocopy *dfm1*Δ: *hrd1Δtsc3Δ*, *hrd3Δtsc3Δ*, *der1Δtsc3Δ*, and *doa1Δtsc3Δ* were unable to rescue the temperature-sensitive lethality of *tsc3*Δ (Fig. 3.2.6D); and *hrd1Δorm1Δ, doa10Δorm1Δ, hrd2-1orm1Δ,* and *cdc48-2Δorm1Δ* did not exhibit an exacerbated growth defect at 30^{o}C (Supp. Fig. 3.2.2E). Hence, the DOA and HRD ERAD pathways do not genetically interact with Tsc3 or Orm1. In summary, CHX-chase, genetics, and *in vivo* ubiquitination assays confirmed that Orm2 is degraded solely by the EGAD pathway and not by INMAD or ERAD.

3.2.8. Dfm1 does not function at the post-ubiquitination step of Orm2 degradation pathway

To determine the step at which Dfm1 functions in Orm2 degradation, the ubiquitination status of Orm2 in *dfm1Δ* strains was analyzed. We have previously demonstrated that Dfm1 functions at the post-ubiquitination step of ERAD, with an increased degree of polyubiquitination of ERAD-M substrates observed in *dfm1Δ* strains (Neal et al., 2018). This was caused by the inability of Dfm1 to retrotranslocate its substrates, resulting in build-up of polyubiquitinated membrane substrates along the ER membrane. Surprisingly, in *dfm1Δ* strains, the level of Orm2 ubiquitination was the same as in WT strains and did not phenocopy retrotranslocation-deficient strains, *cdc48-2*, or the proteasomal mutant *hrd2-1* (Fig. 3.2.6C, lanes 7,8,9). Hence, Dfm1 does not function in the post-ubiquitination step of EGAD. We also tested the requirement of Der1 for Orm2 ubiquitination and saw no change in Orm2 ubiquitination levels in *der1Δ* strains compared with WT strains (Fig. 3.2.6C, lanes 1 & 7). Taken together, these data suggest that Dfm1 does not function at the post-ubiquitination step of the Orm2 degradation pathway.

3.2.9. Dfm1 does not directly function in EGAD

Given the requirement for Dfm1 in Orm2 degradation, it is surprising that the Dfm1-dependent ERAD pathway is not involved with Orm2 degradation. It is possible that Dfm1 directly functions in EGAD. To test this hypothesis, we examined the interaction of Dfm1 with the Dsc complex (E3 ligase Tul1 and Dsc2), which mediates substrate detection and ubiquitination within the Golgi in the EGAD pathway. Dfm1-GFP was immunoprecipitated

with GFP Trap antibodies followed by SDS-PAGE and immunoblotting for endogenous Tul1 and Dsc2 with anti-Tul1 and anti-Dsc2, respectively. In all cases, no association of Dfm1 with Tul1 and Dsc2 was observed, while Dfm1 was able to associate with Cdc48, as expected (Supp. Fig. 3.2.3). Moreover, fluorescence microscopy demonstrated that Dfm1 is solely localized in the ER and does not co-localize with Golgi-associated markers (Fig. 3.2.2B). Finally, there were no significant interactions between Dfm1 and any EGAD components identified from our proteomic analysis (Fig. 3.2.1E, Dataset EV1; Available online).

3.2.10. Dfm1 is required for Orm2 export from the ER to the Golgi

The observation that Dfm1-5Ashp can still facilitate Orm2 degradation suggeststhat Dfm1-mediated degradation of Orm2 is independent of its canonical retrotranslocation role in ERAD. Hence, we sought to identify the specific step at which Dfm1 functions within the Orm2 degradation pathway. EGAD-mediated degradation of Orm2 is most well characterized in yeast in which it consists of five steps: 1) phosphorylation of Orm2 by Ypk1 in the ER, 2) COPII-mediated export of phosphorylated Orm2 from ER to Golgi and endosome, 3) polyubiquitination of Orm2 by the E3 ligase Dsc2, 4) retrotranslocation of substrates from the Golgi/endosome to the cytosol, and 5) degradation of the ubiquitinated substrates by the cytosolic proteasome (Schmidt et al., 2019). To determine which step was blocked in Dfm1-deficient cells, we analyzed the phosphorylation status of Orm2 in *dfm1*Δ cells. In *dfm1*Δ, Orm2 phosphorylation was increased to levels similar to those in the Dsc complex mutant *tul1*Δ, a knockout that blocks Orm2 degradation and leads to accumulation of phosphorylated Orm2 (Fig. 3.2.7A). This indicates *dfm1*Δ cells result in defective trafficking of Orm2 to the Golgi. To validate this in a cellular context, we next utilized live cell imaging fluorescence

microscopy to determine the cellular compartment in which Orm2 was accumulating in *dfm1*Δ cells. In line with a previous study, Orm2 accumulated mainly in the early endosomes in *tul1*Δ cells (Schmidt et al., 2019), indicating that Orm2 was being routed to the Golgi/endosomes for degradation. By contrast, in *dfm1*Δ cells, Orm2 accumulated mainly at the ER and Orm2 co-localized with an ER, but not an endosome marker (Fig. 3.2.7B). In parallel, we utilized a phospho-mimetic Orm2 variant (Orm2-3D), which has been shown to mimic Ypk1-dependent constitutive phosphorylation and is continuously exported from the ER and degraded via EGAD. Indeed, we and others show that in WT cells, Orm2-3D is rapidly degraded (Fig. 3.2.7C) (Schmidt et al., 2019, 2020). Remarkably, by employing a CHX-chase assay, we found that Orm2-3D degradation was completely prevented in *dfm1*Δ cells (Fig. 3.2.7C). Using microscopy, we confirmed that Orm2-3D remained exclusively in the ER in *dfm1*Δ cells (Fig. 3.2.7E). By contrast, degradation of an Orm2 phosphonull variant (Orm2-3A) was completely prevented in WT cells (Fig. 3.2.7C) and we and others showed that Orm2-3A was not exported to the ER (Supp. Fig. 3.2.4)(Schmidt et al., 2019). Because *orm2*Δ cells can rescue *tsc3*Δ lethality, we wanted to test whether Orm2-3D or Orm2-3A elicits the same effect. To test this, either phosphonull Orm2-3A or phosphomimetic Orm2-3D were added to *tsc3*Δ*orm2*Δ cells and the growth assay was employed. As controls, Orm2-3A alone and Orm2-3D cells grew similarly as WT cells whereas *tsc3*Δ cells exhibited the expected growth lethality at 37ºC. Notably, *tsc3*Δ*orm2*Δ cells containing Orm2-3D alleviated *tsc3*Δ lethality whereas *tsc3*Δ*orm2*Δ cells containing Orm2-3A did not rescue *tsc3*Δ lethality (Fig. 3.2.7D). These results suggest that two conditions are sufficient in rescuing *tsc3*Δ lethality: 1) absence of Orm2 (*orm2*Δ) or 2) continuous phosphorylation and degradation of Orm2 via EGAD (Orm2-3D). In summary, based on CHX-chase, live image florescence microscopy, and genetic interaction assays, we demonstrate that Dfm1 is required for the export of

phosphorylated Orm2 from the ER to Golgi. The physiological consequence for Dfm1 dysfunction is retention of Orm2 in the ER, which prevents its subsequent degradation.

Our data demonstrate that Dfm1-deficient cells accumulate phosphorylated Orm2 within the ER, the negative regulator of sphingolipid biosynthesis, which raises the question of why increased levels of LCBs, ceramides, and complex sphingolipids were observed in *dfm1*Δ and *dfm1*Δ*tsc3*Δ cells? Our results contrast our initial expectation that accumulation of Orm2 would decrease levels of LCB and ceramides, since Orm2 antagonizes the sphingolipid biosynthesis pathway. One possibility is that in *dfm1*Δ cells, ER-localized phosphorylated Orm2 is no longer able to repress SPT activity. To test this possibility, we measured steady-state levels of PHS in WT and *dfm1*Δ cells either expressing phosphomimic Orm2-3D or phosphonull Orm3A. As expected, in both WT and *dfm1*Δ cells, Orm2-3A leads to low steady-state levels of PHS whereas in WT cells with Orm2-3D, which is constitutively degraded by EGAD, leads to significantly higher levels of PHS (Fig. 3.2.7F). Notably, *dfm1*Δ cells with Orm2-3D, which is phosphomimic Orm2 accumulating in the ER, leads to significantly higher levels of PHS (Fig. 3.2.7F). This finding suggests accumulation of phosphorylated Orm2 at the ER does indeed increase SPT activity.

3.2.11. Loss of Dfm1 does not affect COPII-mediated trafficking

Because loss of Dfm1 resulted in accumulation of Orm2 in the ER, we directly interrogated the role of Dfm1 in COPII-mediated trafficking. To test whether Dfm1 has a direct function in COPII-mediated trafficking, we analyzed the steady-state levels of COPII

cargo substrate, carboxypeptidase Y (CPY), and found that in *dfm1*Δ cells, the mature form of CPY accumulated at similar levels as WT cells (*m*; Supp. Fig. 3.2.4B). As a control for a deficiency in COPII-mediated export, when *sec12-1* cells were shifted to nonpermissive growth temperature at 37^{o}C, there was the expected buildup of the premature form (*P*; Supp. Fig. 3.2.4B). Finally, we did not identify significant interactions between Dfm1 and any COPII trafficking components from our proteomic analysis (Fig. 3.2.1C and Dataset EV1; Available online). Taken together, our data suggests that Dfm1 does not directly function in COPII-dependent trafficking.

3.2.12. Dfm1 interacts with Ypk1-dependent phosphorylated Orm2

Because Dfm1 isn't functioning in ER exit, we hypothesized that Dfm1 is functioning directly with the SPOTs complex where it specifically interacts with phosphorylated Orm2. To interrogate this, we used co-IP to test interactions of Dfm1 with either phosphomimic Orm2-3D or phospho-null Orm2-3A. As a negative control, a strain containing empty vector (instead of Dfm1-HA) was included. We also tested the binding of Dfm1 to an ER membrane protein, Sec61, that isn't normally associated with SPOTS complex members and Dfm1. Notably, Dfm1 associated with both WT Orm2 or phosphomimic Orm2-3D and not phospho-null Orm2-3A (Fig. 3.2.8A). In strains expressing Orm2-3A, Dfm1 no longer interacted with Orm1, Lcb1, and Lcb2, which implicates that Dfm1 interacts with SPOTs complex members through binding of Orm2. We confirmed this using co-IP in *orm2*Δ cells in which Dfm1 no longer interacted with Orm1, Lcb1, and Lcb2 (Fig. 3.2.8B). In yeast, TORC2-Ypk1 signaling axis is required for Orm2 phosphorylation, which triggers Orm2 degradation by EGAD whereas TORC1-Npr1 signaling axis is required for Orm2 phosphorylation at distinct sites to

stimulate synthesis of complex sphingolipids (Schmidt et al., 2020; Shimobayashi et al., 2013). We were interested in investigating the effect of Ypk1-mediated *versus* Npr1-mediated Orm2 phosphorylation on Dfm1 interaction. To address this, co-IP was performed in *ypk1*Δ and *npr1*Δ cells. In *npr1*Δ cells, the SPOTs complex remain intact where Orm2 associated with Dfm1, Lcb1, Lcb2, and Orm1 (Fig. 3.2.8C). In contrast, in *ypk1*Δ cells, Orm2 no longer associated with Dfm1, but remain associated with Lcb1, Lcb2, and Orm1 (Fig. 3.2.8C). Interestingly, in cells lacking either Npr1 or Ypk1, Orm2 still associated with other SPOTs complex members indicating phosphorylation status of Orm2 doesn't affect its interactions with the SPOTs complex. Overall, our findings indicate that Dfm1 specifically interacts with Ypk1-dependent phosphorylated Orm2.

3.3. Discussion

In this study, we describe a novel role for the derlin rhomboid pseudoprotease, Dfm1, in maintaining sphingolipid homeostasis. The function of Dfm1 in ERAD-M retrotranslocation of misfolded membrane protein substrates has been well established in our laboratory and this study uncovers an additional biological function of Dfm1. The role of Dfm1 in maintaining sphingolipid homeostasis appears to be separate from its role in ERAD-M retrotranslocation. Our study indicates that Dfm1 is required to facilitate the export of phosphorylated Orm2 from the ER and that this function requires substrate bindingand lipid thinning activity, but not its Cdc48 recruitment function. Specifically, Dfm1 functions immediately downstream of Ypk1-dependent Orm2 phosphorylation where Dfm1 associates with the SPOTs complex through binding of phosphorylated Orm2 and not unphosphorylated Orm2 (Fig. 3.2.8D). Overall, our studies reveal a novel role for rhomboid pseudoproteases in maintaining sphingolipid homeostasis, a function that is independent of their role in ERAD.

To identify Dfm1 interacting partner proteins, we performed proximity-dependent biotinylation (BioID) coupled with mass spectrometry. Several proteins found in close proximity to Dfm1 were involved in the sphingolipid biosynthesis pathway. The first committed step of the sphingolipid biosynthetic pathway is catalyzed by the serine palmitoyl transferase (SPT) complex, which consists of Lcb1, Lcb2, and Tsc3. This step is strictly regulated by Orm1/Orm2 and Sac1, which negatively regulates SPT, and Tsc3, and enhances SPT activity 100-fold. Indeed, we confirmed a physical interaction between Dfm1 and the SPOTS complex members Orm2 and Lcb1. To further explore the relationship between Dfm1 and SPOTS complex members, we examined the genetic interactions between *dfm1*Δ and knockout of SPOTS complex members or sphingolipid biosynthetic

enzymes. We exploited the *tsc3*Δ growth lethality phenotype at 37°C, which is due to Tsc3 being required for enhancing SPT activity at 37°C. Growth assays and lipidomic analyses indicated that *dfm1*Δ cells phenocopy established negative regulators of the SPT enzymes, *orm1*Δ and *orm2*Δ, where all three are able to reverse the temperature-sensitive lethality of *tsc3*Δ by increasing ceramide and complex sphingolipid levels. Therefore, we propose that Dfm1 antagonizes the sphingolipid biosynthesis pathway.

The mechanism associated with Dfm1-dependent Orm2 export from the ER remains to be elucidated. Our data suggests that Dfm1 functions at the post-phosphorylation step of Orm2 where loss of Dfm1 blocks ER export of phosphorylated Orm2. Moreover, Dfm1 does not directly function in COPII export since its absence does not abrogate export of a COPII cargo, CPY. Instead, Dfm1 directly binds to Ypk1-dependent phosphorylated Orm2, which is followed by its exit from the ER and degradation by EGAD. Our laboratory has recently identified a chaperone-like Dfm1 function where it influences the solubility of aggregate-prone misfolded membrane substrates along the ER membrane (Kandel et al., 2022). Similar to Dfm1's function as a mediator in sphingolipid homeostasis, its chaperone-like role requires Dfm1's substrate binding and lipid thinning function, but not its Cdc48 recruitment function. Based on the solubility assay, Dfm1 doesn't significantly enhance the solubility of Orm2 since a majority of it remains solubilized in the presence and absence of Dfm1 (Supp. Fig. 3.2.4C). In this case, Dfm1 may not be required for influencing the solubility of Orm2, but instead is utilizing another chaperone-like activity to prime Orm2 for delivery to the COPII machinery for ER export (Fig. 3.2.8D). The extent to which the chaperone-like activity of Dfm1 is required for Orm2 export from the ER warrants future investigations.

Based on lipidomic analysis, *dfm1*Δ cells accumulate phosphorylated Orm2, which no longer inhibits SPT activity. This was shown through marked increase in PHS steady-state levels in *dfm1*Δ cells expressing phosphomimic Orm2-3D. This raises the question of why accumulation of a negative regulator wouldn't inhibit sphingolipid biosynthesis. A possible explanation stems from a previous study in which Orms have been found to directly regulate the localization and oligomerization state of SPT at the ER in a manner that is dependent upon their phosphorylation state. Specifically, phosphorylated Orm2 shifts SPT to the monomeric state, which contributes to sustained SPT activity (Han et al., 2019). This model is supported by our co-IP experiment, in which phosphorylated Orm2 still associated with the SPOTs complex (Fig. 3.2.8A). In this context, phosphorylated Orm2 may have a direct influence on increasing SPT activity. Investigating how phosphorylated Orm2 leads to increased SPT activity will be a fruitful line of inquiry to address in the future.

The ER hosts metabolic pathways that synthesize a variety of lipids such as phospholipids, cholesterol, and sphingolipids. Thus, it is critical for the ER to sense and respond to fluctuations in lipid composition in order to maintain cellular homeostasis (Fun and Thibault, 2020; Piña et al., 2018; Tam et al., 2018). Several pathways are employed to maintain the flux of the lipid biosynthetic pathway. One such pathway is the targeting and degradation of lipid biosynthetic enzymes through ERAD-mediated degradation. For example, cholesterol synthesis is downregulated through regulated ERAD of the rate-controlling cholesterol biosynthetic enzymes Hmg-CoA reductase and squalene monooxygenase (Wangeline et al., 2017). Maintenance of lipid homeostasis is also critical for protein synthesis, as dysregulated lipid levels negatively impact ER protein quality-control machineries. This is supported by studies demonstrating that increased flux of sphingolipids

induces UPR and sensitivity of cells to ER stress (Han et al., 2010). This is also in alignment with our observations where *dfm1*Δ*orm1*Δ cells are sensitive to ER stress due to dysregulated sphingolipid metabolism (Supp. Fig. 3.2.1A). Previous studies from our lab and others have demonstrated that lipid thinning by the ERAD machinery facilitates the removal of misfolded substrates from the ER (Neal et al., 2018; Wu et al., 2020). Because lipids play a large role in ERAD retrotranslocation, fine-tuning lipid levels is critical to ensure that ERAD remains intact and functional. Our findings implicate Dfm1 as a mediator in sphingolipid homeostasis. Interestingly, by utilizing homology modeling and bioinformatic analysis, we identified sphingolipid-binding motifs on TM1 and TM6 of Dfm1, suggesting that Dfm1 may directly detect sphingolipid levels and fine-tune the control of sphingolipid production by modulating the export of Orm2 (unpublished data). Similarly, cholesterol has been shown to directly regulate levels of the E3 ligase MARCH6 levels, with increased MARCH6 levels leading to ubiquitination and degradation of the key cholesterol enzyme, squalene monoozygenase (Zelcer et al., 2014). Future studies on the lipid-sensing function of Dfm1 and how it de-represses SPT activity via Orm2 export from the ER will require additional experimentation.

The Orm family proteins are well conserved and all three human ORMDLs associate with SPT and directly regulate SPT activity. However, unlike their yeast counterparts, they do not appear to be phosphorylated since they lack the homologous N-terminal domains that are phosphorylated by Npr1, Ypk1, and Ypk2 in yeast. Instead, ORMDL protein levels are regulated directly by ceramide levels (Davis et al., 2019). Consistent with this finding, altered protein levels of ORMDLs are associated with the pathophysiology of a range of diseases, including colorectal cancer, inflammation, obesity, and diabetes (Davis et al., 2018).

Moreover, single nucleotide polymorphisms near ORMDL3, which lead to its increased expression, are associated with childhood asthma. Accordingly, our observation that yeast Dfm1 alters Orm2 protein levels and impacts sphingolipid metabolism raises the possibility that derlins have a causative role in these diseases. Defining the mechanism of Dfm1-mediated regulation of Orm2 levels should illuminate new treatment paradigms for patients with dysregulated sphingolipid metabolism.

In summary, we have performed proteomic analyses to enable the identification of Dfm1 interacting factors. These studies have demonstrated that several key regulators of sphingolipid biosynthesis are associated with Dfm1 and we report a novel function for Dfm1 in mediating sphingolipid homeostasis. Sphingolipids play diverse roles in cellular functions, which includes cell signaling, supporting cellular structure, providing energy storage, and regulating cell growth cycles. Dysregulation of sphingolipid levels has been associated with several life-threatening disorders. Overall, this study identifies derlin rhomboid pseudoproteases as key regulators of sphingolipid levels and reveals them as potential therapeutic targets for treatment of lipid disorders that are associated with the dysregulation of sphingolipid levels.

3.4. Methods

Yeast and bacteria growth media

Standard yeast *Saccharomyces cerevisiae* growth media were used as previously described (Hampton and Rine, 1994), including yeast extract-peptone-dextrose (YPD) medium and ammonia-based synthetic complete dextrose (SC) and ammonia-based synthetic minimal dextrose (SD) medium supplemented with 2% dextrose and amino acids to enable growth of auxotrophic strains at 30°C. *Escherichia coli* Top10 cells were grown in standard LB media with ampicillin at 37°C as previously described (Gardner et al., 1998). HEK293 cells were cultured in DMEM medium supplemented with 10% FBS.

Plasmids and strains

Plasmids used in this study are listed in Supplemental Table 3.4.1. Plasmids for this work were generated using standard molecular biological techniques (Sato et al., 2009) and verified by sequencing (Eton Bioscience, Inc.). Primer information is available upon request. Lcb1-RFP and Orm2-RFP plasmids were a gift from Theresa Dun (Uniformed Services University of the Health Sciences, MD). Orm2-3A-GFP and Orm2-3D-GFP plasmids were a gift from Oliver Schmidt and David Teis (Medical University of Innsbruck, Austria).

A complete list of yeast strains and their corresponding genotypes are listed in Supplemental Table 3.4.2. All strains used in this work were derived from S288C or Resgen. Yeast strains were transformed with DNA or PCR fragments using the standard LiOAc method (Ito et al., 1983). Null alleles were generated by using PCR to amplify a selection marker flanked by 50 base pairs of the 5' and 3' regions, which are immediately adjacent to the coding region of the gene to be deleted. The selectable markers used for making null alleles were genes encoding resistance to G418 or CloNat/nourseothricin. After transformation, strains with drug markers were plated onto YPD followed by replica-plating onto YPD plates containing (500 µg/mL G418 or 200 µg/mL nourseothricin). All gene deletions were confirmed by PCR.

_dfm1_Δ strain handling

Due to rapid suppression nature of *dfm1*Δ null strains, freshly transformed *dfm1*Δ null cells with the respective substrates should be used in every assay. Generation of Dfm1 mutant strains and troubleshooting guidelines are found in (Bhaduri and Neal, 2021).

Proximity dependent-biotinylation (BioID)

WT cells expressing either BirA-3xFlag or Dfm1-BirA-3xFlag cells were inoculated in minimal media supplemented with 1 µM biotin and 0.2% raffinose and grown overnight at 30^{o}C. The following day, the cells were diluted to 0.2 OD_{600} and grown to log phase (0.3-0.5

OD_{600}). Once in log-phase, 0.2% galactose was added to induce the expression of BirA-3xFlag and Dfm1-BirA-3xFlag. After 1 hour of incubation, cells were pelleted and stored at -80°C overnight. The next day, cells were thawed and resuspended in lysis buffer (50 mM Tris-HCl pH 7.5, 150 mM NaCl, 1.5 mM $MgCl_2$, 1 mM EDTA, 0.1% SDS, 1% NP-40, 0.4% sodium deoxycholate, and 1 mM DTT supplemented with proteasezinhibitors: 1 m*M* phenylmethylsulfonyl fluoride, 260 µ*M* 4-(2-aminoethyl) benzenesulfonyl fluoride hydrochloride, 100 µ*M* leupeptin hemisulfate, 76 µ*M* pepstatin A, 5 m*M* aminocaproic acid, 5 m*M* benzamidine, and 142 µ*M* *N*-tosyl-l-phenylalanine chloromethyl ketone. Cells were lysed with grinding using liquid nitrogen. Crude lysate was transferred to a 1.5 mL Eppendorf tube and centrifuged for 5 min. at 2,500 x g to remove cellular debris. Clarified lysate was subjected to affinity purification with preactivated MyOne Sreptavidin C1 Magnetic Dynabeads (Invitrogen) for 4 hours at 4°C using a nutator. The beads were subsequently separated from the flowthrough using a magnetic stand and washed five times with cold PBS to separate the non-biotinylated proteins. Protein concentration was measured using a nanodrop, and samples (biotinylated proteins bound to magnetic beads) were submitted for mass-spectrometry to analyze the biotinylated interaction partners of Dfm1.

Liquid chromatography and mass spectrometry analysis

The BioID samples were in-solution digested overnight at 37 °C in 400 ng of mass spectrometry grade trypsin (Promega) enzyme. The digestion was stopped by adding formic acid to the 0.5% final concentration. The digested peptides were desalted by using C18 StageTips and were transferred to fresh tubes and then vacuum dried. The vacuum-dried

peptides were resuspended in 5% formic acid/5% acetonitrile buffer and added to the vials for mass spectrometry analysis. Samples were analyzed with duplicate or triplicate injections by LC-MS-MS using EASY-nLC 1000 liquid chromatography connected with Q-Exactive mass spectrometer (Thermo Scientific) with the following modifications. A fused silica microcapillary column (75-μm inner diameter, 15 cm) packed with C18 reverse-phase resin (ReproSil-pur 120 C18-AQ, 1.9 μm; Dr. Maisch GmbH) using an in-line nano-flow EASY-nLC 1000 UHPLC (Thermo Scientific) was used to resolve the peptides. Peptides were eluted over a 100-min 2%–30% ACN gradient, a 5-min 30%–60% ACN gradient, and a 5-min 60%–95% ACN gradient, with a final 10-min step at 0% ACN for a total run time of 120 min at a flow rate of 250 nl/min. All gradient mobile phases contained 0.1% formic acid. MS/MS data were collected in a data-dependent fashion using a top 10 method with a full MS mass range from 400–1800 m/z, 70,000 resolutions, and an AGC target of 3e6. MS2 scans were triggered when an ion intensity threshold of 1e5 was reached with a maximum injection time of 250 ms. Peptides were fragmented using a normalized collision energy setting of 25. A dynamic exclusion time of 40 s was used, and the peptide match setting was disabled. Singly charged ions, charge states above 8 and unassigned charge states were excluded. The MS/MS spectra were searched against the UniProt *Saccharomyces cerevisiae* reference proteome database using the Maxquant software with standard settings. Statistical analysis of interactome data was carried out using Differential Enrichment analysis of Proteomics (DEP) and Maxquant package (available online https://rdrr.io/bioc/DEP/man/DEP.html and https://www.maxquant.org/. All proteome datasets were compared to Dfm1-BioID untreated control samples. Filter cut-offs were set at $\log_2 FC \geq 2$, p value of $\leq .01$, and at least two quantitative peptide features. These parameters were chosen to minimize false positives while maximizing true positives.

Spot dilution growth assay

Yeast strains were grown in YPD or minimal selection media (-Leu -Ura) supplemented with 2% dextrose to log phase (OD_{600} 0.2-0.3) at 30°C. 0.2 OD cells were pelleted and resuspended in 500 µL dH_2O. 12 µL of each sample was transferred to a 96-well plate where a five-fold serial dilution in dH_2O of each sample was performed to obtain a gradient of 0.2-0.0000128 OD cells. The 8x12 pinning apparatus was used to pin cells onto synthetic complete (-Ura) agar plates supplemented with 2% dextrose or 2% galactose. Droplets of cells were air-dried in sterile conditions, then the plates were sealed with parafilm and incubated at 30°C. Plates were removed from the incubator for imaging after 3 days and again after 7 days.

Cycloheximide-chase assay

Cycloheximide chase assays were performed as previously described (Sato et al., 2009). Cells were grown to log-phase (OD_{600} 0.2-.03) and cycloheximide was added to a final concentration of 50 µg/mL. At each time point, a constant volume of culture was removed and lysed. Lysis was initiated with addition of 100 µl SUME with protease inhibitors (PIs) and glass beads, followed by vortexing for 4 min. 100 µl of 2xUSB was added followed by incubation at 55°C for 10 min. Samples were clarified by centrifugation and analyzed by SDS-PAGE and immunoblotting.

Fluorescence microscopy

To prepare cells, overnight cultures were diluted to ~0.20 OD in minimal media. After growing ~3 hours, to log-phase (OD_{600}~.3-.6) samples were pelleted and washed with dH2O. Fluorescence microscopy was accomplished using a CSU-X1 Spinning Disk (Yokogawa) confocal microscope at the Nikon Imaging Center on the UCSD campus.

Native co-IP

Cultures from various yeast strains were grown to OD_{600} .2-.45 and 15 ODs of cells were pelleted, rinsed with H_20 and lysed with 0.5 mM glass beads in 400 µL of MF buffer supplemented with protease inhibitors. This was followed by vortexing at 1-minute intervals for 6-8 minutes at 4^{o}C. Lysates were combined and clarified by centrifugation at 2,500 g for 5 min followed by centrifugation at 14,000 g for 15 min to obtain the microsomal pellet. The microsomal pellet was resuspended in 1 mL of Tween IP buffer (500 mM NaCl, 50 mM Tris, pH 7.5, 10 mM EDTA. 1.5% Tween-20) and incubated on ice for 30 minutes. Lysates were then centrifuged for 30 min at 14,000 x g, and the supernatant was incubated overnight with 10 µL of equilibrated GFP-Trap® agarose (ChromoTek Inc., Hauppauge, NY) at 4^{o}C. The next day, the GFP-Trap® agarose beads were combined to one tube, washed once with non-detergent IP buffer, washed once more with IP wash buffer, and resuspended in 100 µL of 2xUSB. Samples were resolved on 8% SDS-PAGE and immunoblotted for Lcb1-RFP and Orm2-RFP α-RFP and Dfm1-GFP with α-GFP.

***In vivo* ubiquitination assay**

Western blotting to detect in vivo ubiquitination was performed as described previously (Garza et al., 2009). Briefly, yeast strains were grown to log phase (OD600 of 0.2 to 0.3). 15 OD equivalents of cells were pelleted by centrifugation and resuspended in lysis buffer (0.24 M sorbitol, 1 mM EDTA, 20 mM KH2PO4, pH 7.5) with PIs, after which 0.5 mm glass beads were added to the meniscus. The cells were lysed by vortexing in 1-min cycles at 4° C, with 1 min on ice in between, for 6 to 8 cycles. Lysates were clarified by centrifugation at 2,500 x g for 5 min. The clarified lysates were moved to fresh tubes, and 600 µL immunoprecipitation buffer (IPB; 15mM Na2HPO4, 150mM NaCl, 2% Triton X-100, 0.1% SDS, 0.5% deoxycholate, 10mM EDTA, pH 7.5) and 20 µL of GFP Trap (Chromotek) were added. Samples were incubated on ice for 5 min, clarified by centrifugation at 14,000 x g for 5 min, and moved to a fresh tube. Tubes were incubated at 4° C overnight with rocking. Beads were washed twice with IPB and then washed once with IP wash buffer (50 mM NaCl, 10 mM Tris, pH 7.5). Beads were aspirated to dryness, resuspended in 55 µL 2x USB, and incubated at 65° C for 10 minutes. Samples were resolved by SDS-PAGE on 10% gels, transferred to nitrocellulose, and immunoblotted with monoclonal anti-ubiquitin (Fred Hutchinson Cancer Research Institute) and anti-RFP (ThermoFisher) primary antibodies followed by goat anti-mouse (Jackson ImmunoResearch Laboratories) or goat anti-rabbit (Bio-Rad) HRP conjugated secondary antibody.

Phosphorylation status of Orm2

Indicated strains were grown to log-phase at 30°C, pelleted, and lysed with 100 µl SUME with protease inhibitors (PIs) and glass beads, followed by vortexing for 4 min. 100 µl of 2xUSB was added followed by incubation at 55°C for 10 min. Samples were clarified by centrifugation, loaded onto Phos-tag precast gel (FujiFilm), and immunoblotted for Orm2 with α-GFP.

Lipid analyses

Yeast cells (1 A_{600} units) were suspended in 100 µL of extraction solution [ethanol/water/diethyl ether/pyridine/15 M ammonia (15:15:5:1:0.018, v/v)], mixed with internal standards, and incubated at 60 °C for 15 min. As internal standards, four types of ceramides containing nine deuterium atoms (d_9) [*N*-palmitoyl(d_9)-dihydrosphingosine (d_9-C16:0 Cer-A), *N*-palmitoyl(d_9)-D-*ribo*-phytosphingosine (d_9-C16:0 Cer-B), *N*-(2'-(*R*)-hydroxypalmitoyl(d_9))-D-*erythro*-sphinganine (d_9-C16:0 Cer-B'), *N*-(2'-(*R*)-hydroxypalmitoyl(d_9))-D-*ribo*-phytosphingosine (d_9-C16:0 Cer-C) (all purchased from Avanti Polar Lipids, Alabaster, AL)] were used (5 pmol each). After centrifugation (2,300 × *g*, room temperature, 2 min), the supernatant was recovered, and the pellets were suspended in 100 µL of extraction solution and incubated at 60 °C for 15 min again. After centrifugation (2,300 × *g*, room temperature, 2 min), the supernatant was recovered. The two supernatants were pooled, mixed with 700 µL of chloroform/methanol (1:2, v/v). To hydrolyze glycerolipids, alkaline treatment was performed by adding 37.5 µL of 3 M KOH and incubating at 37 °C for

30 min. After neutralization by adding 22.5 µL of 5 M formic acid, the samples were sequentially mixed with 250 µL of chloroform and 250 µL of water and centrifuged (20,400 × *g*, room temperature, 3 min) for phase separation. The organic phase containing lipids was recovered and dried. Lipids were resuspended in 625 µL of chloroform/methanol/water (5:4:1, v/v) and subjected to liquid chromatography (LC)-coupled tandem mass spectrometry (MS/MS) using a triple quadrupole mass spectrometer Xevo TQ-S (Waters, Milford, MA, USA) via multiple reaction monitoring and positive ion modes. The settings for LC separation and electrospray ionization were as described previously (Ohno et al., 2017) and the *m/z* values and collision energies used in the MS/MS measurement are listed in Supplemental Table 3.4.3. Ceramides were quantified by calculating the ratio of the peak area of each ceramide species to that of the internal standard corresponding to each type of ceramide. D-type ceramides were quantified using C-type ceramide standard (d_9-C16:0 Cer-C).

Detergent solubility assay

ER microsomes were isolated by centrifuging and pelleting 15OD of yeast in log phase growth. Pellets were resuspended in MF buffer with protease inhibitors and 0.5mM lysis beads were added to each sample. Samples were vortexed six times in 1-minute intervals, with 1-minute on ice in between. Lysed cells were transferred to new microcentrifuge tube and samples were clarified by spinning at 1,500x for 5 minutes at 4°C. Microsomes were separated by centrifuging clarified lysate at 14,000 × *g* for 1 minute. Fractions were incubated on ice in the presence or absence of 1% DDM for 1 hour. The mixture was then centrifuged at 14,000 × *g* for 30 min at 4°C, and the detergent soluble fraction (i.e., the supernatant) was precipitated with 20% TCA on ice for 30 minutes and then

centrifuged at 14,000 × *g* for 30 min to get a pellet of the soluble protein. Proteins from both the soluble and insoluble fractions were resuspended in sample buffer and resolved by SDS-PAGE.

Quantification and statistical analysis

ImageJ (NIH) was used for all western blot quantifications. "Mean gray value" was set for band intensity measurements. In such experiments, a representative western blot was shown and band intensities were normalized to PGK1 loading control and quantified. t=0 was taken as 100% and data is represented as mean ± SEM from at least three experiments. GraphPad Prism was used for statistical analysis. Nested t-test, unpaired t-test, or one-way factorial ANOVA followed by Bonferroni's post-hoc analysis was applied to compare data. Significance was indicated as follows: n.s, not significant; * $p<0.05$, ** $p<0.01$, *** $p<0.001$, **** $p<0.0001$. The investigators were blinded during data analysis.

3.5. Acknowledgements

Chapter 3, in full, is a reprint of the material as it appears in Bhaduri, S., Aguayo, A., Ohno, Y., Proietto, M., Jung, J., Wang, I., Kandel, R., Singh, N., Ibrahim, I., Fulzele, A., Bennett, E. J., Kihara, A., & Neal, S. E. (2023). An ERAD-independent role for rhomboid pseudoprotease Dfm1 in mediating sphingolipid homeostasis. *The EMBO journal, 42*(4), e112275. https://doi.org/10.15252/embj.2022112275. The dissertation author was a primary investigator and a first author of this material. The authors would like to thank Peter Espenshade (Johns Hopkins Medicine), Oliver Schmidt (Medical University of Innsbruck), David Teis (Medical University of Innsbruck), Teresa Dunn (National Institutes of Health), Jim Wilhelm (University of California, San Diego), and Peter Novick (University of California, San Diego) for providing plasmids, yeast strains, antibodies. We thank Dr. Oswald Quehenberger from the UCSD Lipidomic Core Facility for performing lipidomic analysis. We also thank Dr. Maho Niwa, Dr. David Teis, Dr. Oliver Schmidt, and the Neal lab members for in-depth discussions and technical assistance. These studies were supported by NIH grant 1R35GM133565-01, Pew Biomedical Award 34089, and NSF CAREER grant 2047391 (to S.E.N), NIH grants 5R01GM136994-02 and DP2GM119132 (to E.J.B), HHMI Gilliam Fellowship GT15096 (to S.E.N and A.A.), and KAKENHI grant JPSSH04986 (to A.K.).

3.6. References

Bhaduri, S., & Neal, S. E. (2021). Assays for studying normal versus suppressive ERAD-associated retrotranslocation pathways in yeast. *STAR Protocols*, *2*(3), 100640. https://doi.org/10.1016/j.xpro.2021.100640

Bode, H., Bourquin, F., Suriyanarayanan, S., Wei, Y., Alecu, I., Othman, A., Von Eckardstein, A., & Hornemann, T. (2015). *HSAN1 mutations in serine palmitoyltransferase reveal a close structure-function-phenotype relationship*. https://doi.org/10.1093/hmg/ddv611

Breslow, D. K. (n.d.). *Sphingolipid Homeostasis in the Endoplasmic Reticulum and Beyond*. https://doi.org/10.1101/cshperspect.a013326

Breslow, D. K., Collins, S. R., Bodenmiller, B., Aebersold, R., Simons, K., Shevchenko, A., Ejsing, C. S., & Weissman, J. S. (2010). Orm family proteins mediate sphingolipid homeostasis. *Nature*, *463*(7284), 1048–1053. https://doi.org/10.1038/NATURE08787

Carvalho, P., Goder, V., & Rapoport, T. A. (2006). Distinct ubiquitin-ligase complexes define convergent pathways for the degradation of ER proteins. *Cell*, *126*(2), 361–373. https://doi.org/10.1016/j.cell.2006.05.043

Christiano, R., Arlt, H., Kabatnik, S., Mejhert, N., Lai, Z. W., Farese, R. V., & Walther, T. C. (2020). A Systematic Protein Turnover Map for Decoding Protein Degradation. *Cell Reports*, *33*(6), 108378. https://doi.org/10.1016/j.celrep.2020.108378

Davis, D., Kannan, M., & Wattenberg, B. (2018). Orm/ORMDL proteins: Gate guardians and master regulators. *Advances in Biological Regulation*, *70*(August), 3–18. https://doi.org/10.1016/j.jbior.2018.08.002

Davis, D. L., Gable, K., Suemitsu, J., Dunn, T. M., & Wattenberg, B. W. (2019). The ORMDL/Orm–serine palmitoyltransferase (SPT) complex is directly regulated by ceramide: Reconstitution of SPT regulation in isolated membranes. *Journal of Biological Chemistry*, *294*(13), 5146–5156. https://doi.org/10.1074/jbc.RA118.007291

Fenech, E. J., Lari, F., Charles, P. D., Fischer, R., Laé titia-Thé zé nas, M., Bagola, K., Paton, A. W., Paton, J. C., Gyrd-Hansen, M., Kessler, B. M., & Christianson, J. C. (n.d.). *Interaction mapping of endoplasmic reticulum ubiquitin ligases identifies modulators of innate immune signalling*. https://doi.org/10.7554/eLife.57306

Foresti, O., Rodriguez-Vaello, V., Funaya, C., & Carvalho, P. (2014). Quality control of inner nuclear membrane proteins by the Asi complex. *Science*, *346*(6210), 751–755. https://doi.org/10.1126/science.1255638

Foresti, O., Ruggiano, A., Hannibal-Bach, H. K., Ejsing, C. S., & Carvalho, P. (2013). Sterol homeostasis requires regulated degradation of squalene monooxygenase by the ubiquitin ligase Doa10/Teb4. *ELife*, *2*, e00953. https://doi.org/10.7554/eLife.00953

Fun, X. H., & Thibault, G. (2020). Lipid bilayer stress and proteotoxic stress-induced unfolded protein response deploy divergent transcriptional and non-transcriptional programmes. *Biochimica et Biophysica Acta - Molecular and Cell Biology of Lipids*, *1865*(1), 158449. https://doi.org/10.1016/j.bbalip.2019.04.009

Gable, K., Slife, H., Bacikova, D., Monaghan, E., & Dunn, T. M. (2000). Tsc3p is an 80-amino acid protein associated with serine palmitoyltransferase and required for optimal enzyme activity. *Journal of Biological Chemistry*, *275*(11), 7597–7603. https://doi.org/10.1074/jbc.275.11.7597

Gardner, R., Cronin, S., Leader, B., Rine, J., Hampton, R., & Leder, B. (1998). Sequence determinants for regulated degradation of yeast 3-hydroxy-3-methylglutaryl-CoA reductase, an integral endoplasmic reticulum membrane protein. *Molecular Biology of the Cell*, *9*(9), 2611–2626.

Hampton, R. Y., Gardner, R. G., & Rine, J. (1996). Role of 26S proteasome and HRD genes in the degradation of 3-hydroxy-3-methylglutaryl-CoA reductase, an integral endoplasmic reticulum membrane protein. *Molecular Biology of the Cell*, *7*(12), 2029–2044. https://doi.org/10.1091/mbc.7.12.2029

Hampton, R. Y., & Rine, J. (1994). Regulated degradation of HMG-CoA reductase, an integral membrane protein of the endoplasmic reticulum, in yeast. *The Journal of Cell Biology*, *125*(2), 299–312.

Hampton, R. Y., & Sommer, T. (2012). Finding the will and the way of ERAD substrate retrotranslocation. *Current Opinion in Cell Biology*, *24*(4), 460–466. https://doi.org/10.1016/j.ceb.2012.05.010

Han, G., Gupta, S. D., Gable, K., Bacikova, D., Sengupta, N., Somashekarappa, N., Proia, R. L., Harmon, J. M., & Dunn, T. M. (2019). The ORMs interact with transmembrane domain 1 of Lcb1 and regulate serine palmitoyltransferase oligomerization, activity and localization. *Biochimica et Biophysica Acta - Molecular and Cell Biology of Lipids*, *1864*(3), 245–259. https://doi.org/10.1016/j.bbalip.2018.11.007

Han, S., Lone, M. A., Schneiter, R., & Chang, A. (n.d.). *Orm1 and Orm2 are conserved endoplasmic reticulum membrane proteins regulating lipid homeostasis and protein quality control*. https://doi.org/10.1073/pnas.0911617107

Hanada, K. (2003). Serine palmitoyltransferase, a key enzyme of sphingolipid metabolism. *Biochimica et Biophysica Acta - Molecular and Cell Biology of Lipids*, *1632*(1–3), 16–30. https://doi.org/10.1016/S1388-1981(03)00059-3

Hannun, Y. A., & Obeid, L. M. (2018). Sphingolipids and their metabolism in physiology and disease. In *Nature Reviews Molecular Cell Biology* (Vol. 19, Issue 3, pp. 175–191). Nature Publishing Group. https://doi.org/10.1038/nrm.2017.107

Hiller, M. M., Finger, A., Schweiger, M., & Wolf, D. H. (1996). ER degradation of a misfolded luminal protein by the cytosolic ubiquitin-proteasome pathway. *Science (New York, N.Y.)*, *273*(5282), 1725–1728.

Ito, H., Fukuda, Y., Murata, K., & Kimura, A. (1983). Transformation of intact yeast cells treated with alkali cations. *Journal of Bacteriology*, *153*(1), 163–168.

Kandel, R., Jung, J., Syau, D., Kuo, T., Songster, L., Aguayo, A., Duttke, S., Benner, C., & Neal, S. (2022). Derlin Dfm1 Employs a Chaperone Function to Resolve Misfolded Membrane Protein Stress. *BioRxiv*, 2022.01.25.477788. https://doi.org/10.1101/2022.01.25.477788

Laney, J. D., & Hochstrasser, M. (2003). Ubiquitin-dependent degradation of the yeast Matα2 repressor enables a switch in developmental state. *Genes and Development*, *17*(18), 2259–2270. https://doi.org/10.1101/gad.1115703

Leto, D. E., Morgens, D. W., Zhang, L., Walczak, C. P., Elias, J. E., Bassik, M. C., & Kopito, R. R. (2019). Genome-wide CRISPR Analysis Identifies Substrate-Specific Conjugation Modules in ER-Associated Degradation. *Molecular Cell*, *73*(2), 377-389.e11. https://doi.org/10.1016/j.molcel.2018.11.015

Mehrtash, A. B., & Hochstrasser, M. (2019). Ubiquitin-dependent protein degradation at the endoplasmic reticulum and nuclear envelope. In *Seminars in Cell and Developmental Biology* (Vol. 93, pp. 111–124). Elsevier Ltd. https://doi.org/10.1016/j.semcdb.2018.09.013

Mohassel, P., Donkervoort, S., Lone, M. A., Nalls, M., Gable, K., Gupta, S. D., Foley, A. R., Hu, Y., Alex, J., Saute, M., Moreira, A. L., Kok, F., Introna, A., Logroscino, G., Grunseich, C., Nickolls, A. R., Pourshafie, N., Neuhaus, S. B., Saade, D., … Bönnemann, C. G. (n.d.). *Childhood amyotrophic lateral sclerosis caused by excess sphingolipid synthesis*. https://doi.org/10.1038/s41591-021-01346-1

Natarajan, N., Foresti, O., Wendrich, K., Stein, A., & Carvalho, P. (2020). Quality Control of Protein Complex Assembly by a Transmembrane Recognition Factor. *Molecular Cell*, *77*(1), 108-119.e9. https://doi.org/10.1016/j.molcel.2019.10.003

Neal, S., Jaeger, P. A., Duttke, S. H., Benner, C. K., Glass, C., Ideker, T., & Hampton, R. (2018). The Dfm1 Derlin Is Required for ERAD Retrotranslocation of Integral Membrane Proteins. *Molecular Cell*, *69*(2). https://doi.org/10.1016/j.molcel.2017.12.012

Neal, S., Mak, R., Bennett, E. J., & Hampton, R. (2017). A Cdc48 'retrochaperone' function is required for the solubility of retrotranslocated, integral membrane Endoplasmic Reticulum-associated Degradation (ERAD-M) substrates. *Journal of Biological Chemistry*, *292*(8). https://doi.org/10.1074/jbc.M116.770610

Nejatfard, A., Wauer, N., Bhaduri, S., Conn, A., Gourkanti, S., Singh, N., Kuo, T., Kandel, R., Amaro, R. E., & Neal, S. E. (2021). Derlin rhomboid pseudoproteases employ substrate engagement and lipid distortion to enable the retrotranslocation of ERAD membrane substrates. *Cell Reports*, *37*(3), 109840. https://doi.org/10.1016/j.celrep.2021.109840

Ohno, Y., Kamiyama, N., Nakamichi, S., & Kihara, A. (2017). PNPLA1 is a transacylase essential for the generation of the skin barrier lipid *ω-O*-acylceramide**.** *Nature Communications.* https://doi.org/10.1038/ncomms14610

Piña, F., Yagisawa, F., Obara, K., Gregerson, J. D., Kihara, A., & Niwa, M. (2018). Sphingolipids activate the endoplasmic reticulum stress surveillance pathway. *Journal of Cell Biology*, *217*(2), 495–505. https://doi.org/10.1083/jcb.201708068

Ruggiano, A., Foresti, O., & Carvalho, P. (2014). ER-associated degradation: Protein quality control and beyond. In *Journal of Cell Biology* (Vol. 204, Issue 6, pp. 869–879). Rockefeller University Press. https://doi.org/10.1083/jcb.201312042

Sato, B. K., & Hampton, R. Y. (2006). Yeast Derlin Dfm1 interacts with Cdc48 and functions in ER homeostasis. *Yeast*, 1053–1064. https://doi.org/10.1002/yea

Sato, B. K., Schulz, D., Do, P. H., & Hampton, R. Y. (2009). Misfolded membrane proteins are specifically recognized by the transmembrane domain of the Hrd1p ubiquitin ligase. *Molecular Cell*, *34*(2), 212–222. https://doi.org/10.1016/j.molcel.2009.03.010

Schmidt, C. C., Vasic, V., & Stein, A. (2020). Doa10 is a membrane protein retrotranslocase in er-associated protein degradation. *ELife*, *9*, 1–31. https://doi.org/10.7554/eLife.56945

Schmidt, O., Weyer, Y., Baumann, V., Widerin, M. A., Eising, S., Angelova, M., Schleiffer, A., Kremser, L., Lindner, H., Peter, M., Fröhlich, F., & Teis, D. (2019). Endosome and Golgi-associated degradation (EGAD) of membrane proteins regulates sphingolipid metabolism . *The EMBO Journal*, *38*(15), 1–23. https://doi.org/10.15252/embj.2018101433

Schmidt, O., Weyer, Y., Sprenger, S., Widerin, M. A., Eising, S., Baumann, V., Angelova, M., Loewith, R., Stefan, C. J., Hess, M. W., Fröhlich, F., & Teis, D. (2020). TOR complex 2 (TORC2) signaling and the ESCRT machinery cooperate in the protection of plasma membrane integrity in yeast. *Journal of Biological Chemistry*, *295*(34), 12028–12044. https://doi.org/10.1074/jbc.RA120.013222

Shimobayashi, M., Oppliger, W., Moes, S., Jenö, P., & Hall, M. N. (2013). TORC1-regulated protein kinase Npr1 phosphorylates Orm to stimulate complex sphingolipid synthesis. *Molecular Biology of the Cell*, *24*(6), 870–881. https://doi.org/10.1091/mbc.E12-10-0753

Sicari, Igbaria, & Chevet. (2019). Control of Protein Homeostasis in the Early Secretory Pathway: Current Status and Challenges. *Cells*, *8*(11), 1347. https://doi.org/10.3390/cells8111347

Sun, Z., & Brodsky, J. L. (2019). Protein quality control in the secretory pathway. In *Journal of Cell Biology* (Vol. 218, Issue 10, pp. 3171–3187). Rockefeller University Press. https://doi.org/10.1083/jcb.201906047

Tam, A. B., Roberts, L. S., Chandra, V., Rivera, I. G., Nomura, D. K., Forbes, D. J., & Niwa, M. (2018). The UPR Activator ATF6 Responds to Proteotoxic and Lipotoxic Stress by Distinct Mechanisms. *Developmental Cell*, *46*(3), 327-343.e7. https://doi.org/10.1016/j.devcel.2018.04.023

Wang, J.-Z., & Dehesh, K. (2018). ER: the Silk Road of interorganellar communication. *Current Opinion in Plant Biology*, *45*(Pt A), 171–177. https://doi.org/10.1016/j.pbi.2018.07.012

Wangeline, M. A., Vashistha, N., & Hampton, R. Y. (2017). Proteostatic Tactics in the Strategy of Sterol Regulation. *Annual Review of Cell and Developmental Biology*, *33*(1), 467–489. https://doi.org/10.1146/annurev-cellbio-111315-125036

Wu, X., Siggel, M., Ovchinnikov, S., Mi, W., Svetlov, V., Nudler, E., Liao, M., Hummer, G., & Rapoport, T. A. (2020). Structural basis of ER-associated protein degradation mediated by the Hrd1 ubiquitin ligase complex. *Science*, *368*(6489), 1–13. https://doi.org/10.1126/SCIENCE.AAZ2449

Zelcer, N., Sharpe, L. J., Loregger, A., Kristiana, I., Cook, E. C. L., Phan, L., Stevenson, J., & Brown, A. J. (2014). The E3 Ubiquitin Ligase MARCH6 Degrades Squalene Monooxygenase and Affects 3-Hydroxy-3-Methyl-Glutaryl Coenzyme A Reductase and the Cholesterol Synthesis Pathway. *Molecular and Cellular Biology*, *34*(7), 1262–1270. https://doi.org/10.1128/mcb.01140-13

Zuzow, N., Ghosh, A., Leonard, M., Liao, J., Yang, B., & Bennett, E. J. (2018). Mapping the mammalian ribosome quality control complex interactome using proximity labeling approaches. *Molecular Biology of the Cell*, *29*(10), 1258–1269. https://doi.org/10.1091/mbc.E17-12-0714

Figure 3.2.1. BioID proximity-based labeling to identify interaction partners of Dfm1

(A) Schematic of Dfm1 fused with a biotin ligase, BirA, at the C-terminus along with un-tagged Dfm1.Cartoon representation of the labeling of rhomboid pseudoprotease Dfm1 with the biotin ligase, BirA. **(B)** GALpr-Dfm1-BirA-Flag and GALpr-BirA-Flag levels were measured by western blotting with α -FLAG at 0 (uninduced) vs. 5 hours post-galactose induction (3 biological replicates; n=3). **(C)** Dfm1-BirA is still functional and able to degrade Hmg2-GFP. *dfm1*Δ+Hmg2-GFP strains containing DFM1-BIRA, empty vector, or BIRA only addbacks were grown to log phase and degradation was measured by CHX. After CHX addition, cells were lysed at the indicated times and analyzed by SDS-PAGE and immunoblotted for Hmg2-GFP with α-GFP. **(D)** Yeast strains expressing Dfm1-Bira and BirA only negative control were incubated with different amounts of biotin: 0, 0.1, and 1 mM. *dfm1*Δ+Hmg2-GFP. Microsomes were isolated from each strain and subjected to streptavidin pulldown (3 biological replicates; n=3). Flow- through and pull-down fractions were detected by western blotting for Dfm1-BirA with α-Flag and Cdc48 with α-Cdc48 antibodies. **(E)** A volcano plot showing enrichment versus significance of proteins identified in Dfm1-BirA experiments relative to control (BirA only) experiments. Components that were significantly enriched were ERAD components in blue (Hrd1, Cdc48, Pre9, and Rpt2) and sphingolipid biosynthesis in orange (Lcb2, Tsc3, and Orm1). Statistical analysis of interactome data was carried out using Differential Enrichment analysis of Proteomics (DEP). Filter cut-offs were set at log2FC>2, p value of < .01, and at least two quantitative peptide features. **(F)** Top 10 gene ontology (GO) terms and their enrichment factor for the set of genes with the highest significance and fold enrichment.

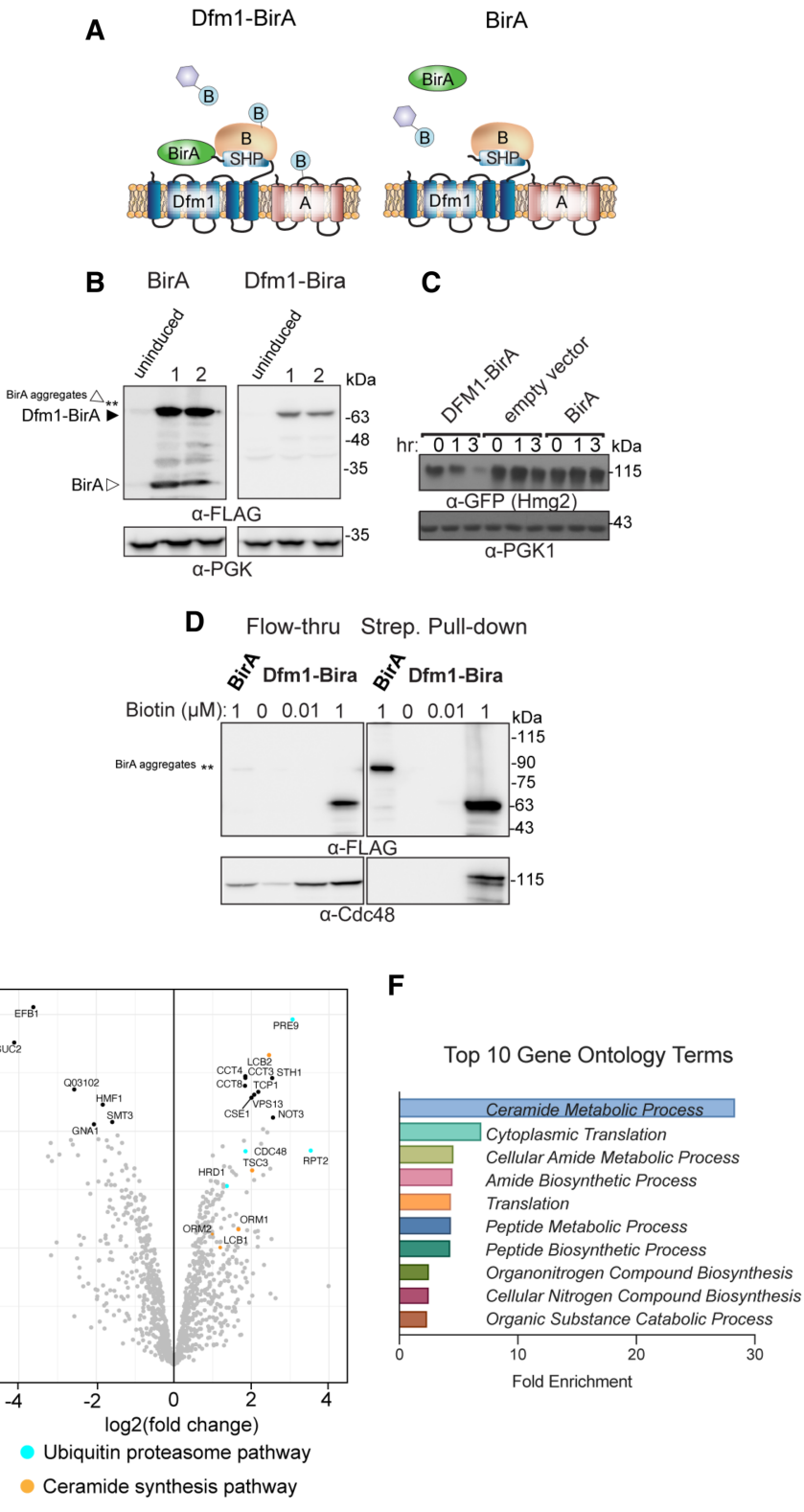

A
Dfm1-BirA
BirA
B
BirA
SHP
Dfm1
A
B
BirA
Dfm1-Bira
uninduced
1 2
kDa
BirA aggregates
Dfm1-BirA
BirA
-63
-48
-35
α-FLAG
α-PGK
C
DFM1-BirA
empty vector
BirA
hr: 0 1 3 0 1 3 0 1 3
kDa
-115
α-GFP (Hmg2)
-43
α-PGK1
D
Flow-thru
Strep. Pull-down
BirA
Dfm1-Bira
Biotin (μM): 1 0 0.01 1 1 0 0.01 1
kDa
-115
-90
-75
-63
-43
α-FLAG
α-Cdc48
E
-log10(p-value)
log2(fold change)
EFB1
RPS28B
SUC2
Q03102
HMF1
SMT3
GNA1
PRE9
LCB2
CCT4
CCT3
STH1
CCT6
TCP1
VPS13
CSE1
NOT3
CDC48
TSC3
RPT2
HRD1
ORM1
ORM2
LCB1
Ubiquitin proteasome pathway
Ceramide synthesis pathway
F
Top 10 Gene Ontology Terms
Ceramide Metabolic Process
Cytoplasmic Translation
Cellular Amide Metabolic Process
Amide Biosynthetic Process
Translation
Peptide Metabolic Process
Peptide Biosynthetic Process
Organonitrogen Compound Biosynthesis
Cellular Nitrogen Compound Biosynthesis
Organic Substance Catabolic Process
Fold Enrichment

Figure 3.2.2. Dfm1 colocalizes and binds to SPOTS complex proteins

(A) Dfm1-GFP binding to Lcb2-RFP and Orm2-RFP were analyzed by co-IP. As negative control, cells not expressing Dfm1-GFP were used (3 biological replicates; n=3). **(B)** Dfm1-GFP colocalizes with Lcb1-RFP and Orm22-RFP. Strains were grown to mid- exponential phase in minimal media GFP and RFP fluorescence was examined on an AxioImager.M2 fluorescence microscope using a 100x objective and 28HE-GFP or 20HE- rhodamine filter sets (3 biological replicates; n=3) (Zeiss). Scale bar, 5 μm.

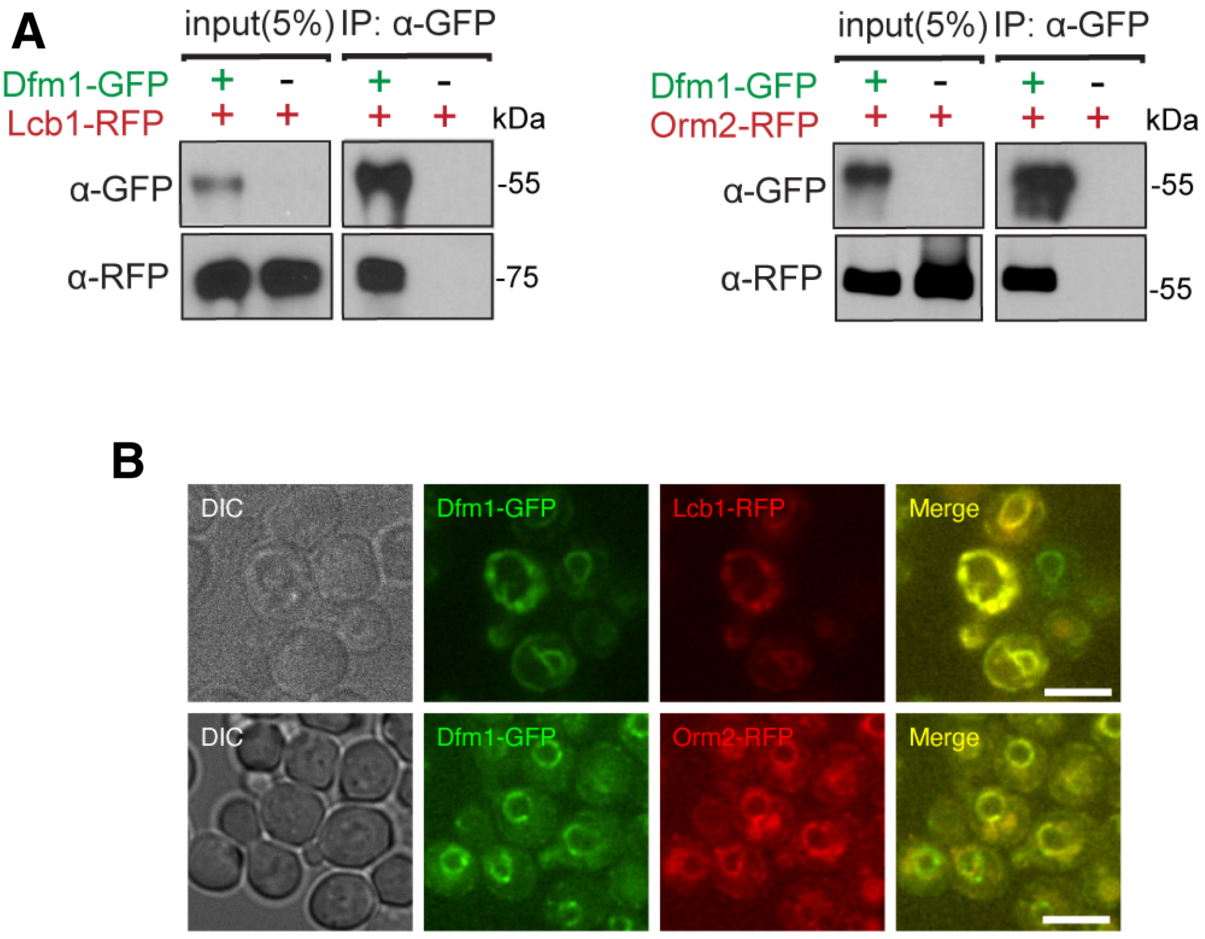


Figure 3.2.3. Dfm1 genetically interacts with Tsc3

(A) Indicated strains were spotted 5-fold dilutions on synthetic complete (SC) plates, and plates were incubated at room temperature, 30oC, and 37oC (3 biological replicates, 2 technical replicates; n=5). WT, *dfm1*Δ, *tsc3*Δ, and *dfm1*Δ*tsc3*Δ were compared for growth in the dilution assay. Arrowhead indicates growth phenotype of tsc3Δ cells; open circle indicates growth phenotype of *dfm1*Δ*tsc3*Δ cells. **(B)** *dfm1*Δ*tsc3*Δ confers resistance to myrocin. WT, *dfm1*Δ, *tsc3*Δ, and *dfm1*Δ*tsc3*Δ strains were grown to log-phase in YPD medium, and 5-fold serial dilutions of cultures were spotted on (SC) plates containing either drug vehicle alone, 1 μM of myriocin and 10 μM of PHS (3 biological replicates, 2 technical replicates; n=5). Arrowhead indicates growth phenotype of *tsc3*Δ cells; open circle indicates growth phenotype of *dfm1*Δ*tsc3*Δ cells. **(C)** WT, *dfm1*Δ, *tsc3*Δ, and *dfm1*Δ*tsc3*Δ cells were grown to log-phase at 30oC and lipids were extracted and subjected to LC-MS/MS. A- B- C- & D-Type ceramides containing C16, C18, C20, C22, C24, and C26 fatty acid (left graph) and B- C- & D-type IPCs containing C24 and C26 fatty acid (right graph) were measured. Values represent the means±S.E.M. (3 biological replicates; n=3). Pairwise Dunnett's test followed by Bonferroni's post-hoc analysis was used to determine statistically significant differences in comparison to WT cells; *P<0.05, **P<0.01). **(D)** Indicated strains were spotted 5-fold dilutions on SC plates in 3 biological replicates and 2 technical replicates (n=5), and plates were incubated at room temperature, 30oC, and 37oC (n=3). Upper panel: WT, *orm1*Δ, *tsc3*Δ, and *orm1*Δ*tsc3*Δ were compared for growth by dilution assay. Middle panel: WT, *orm2*Δ, *tsc3*Δ, and *orm2*Δ*tsc3*Δ were compared for growth by dilution assay. Bottom panel: WT, *orm1*Δ, *orm2*Δ, *tsc3*Δ, and *orm1*Δ*orm2*Δ*tsc3*Δ, were compared for growth by dilution assay. Upper panel: arrowhead indicates growth phenotype of *tsc3*Δ cells; open circle indicates growth phenotype of *orm1*Δ*tsc3*Δ cells. Lower panel: arrowhead indicates growth phenotype of *orm2*Δ cells; open circle indicates growth phenotype of *orm2*Δ*tsc3*Δ cells.

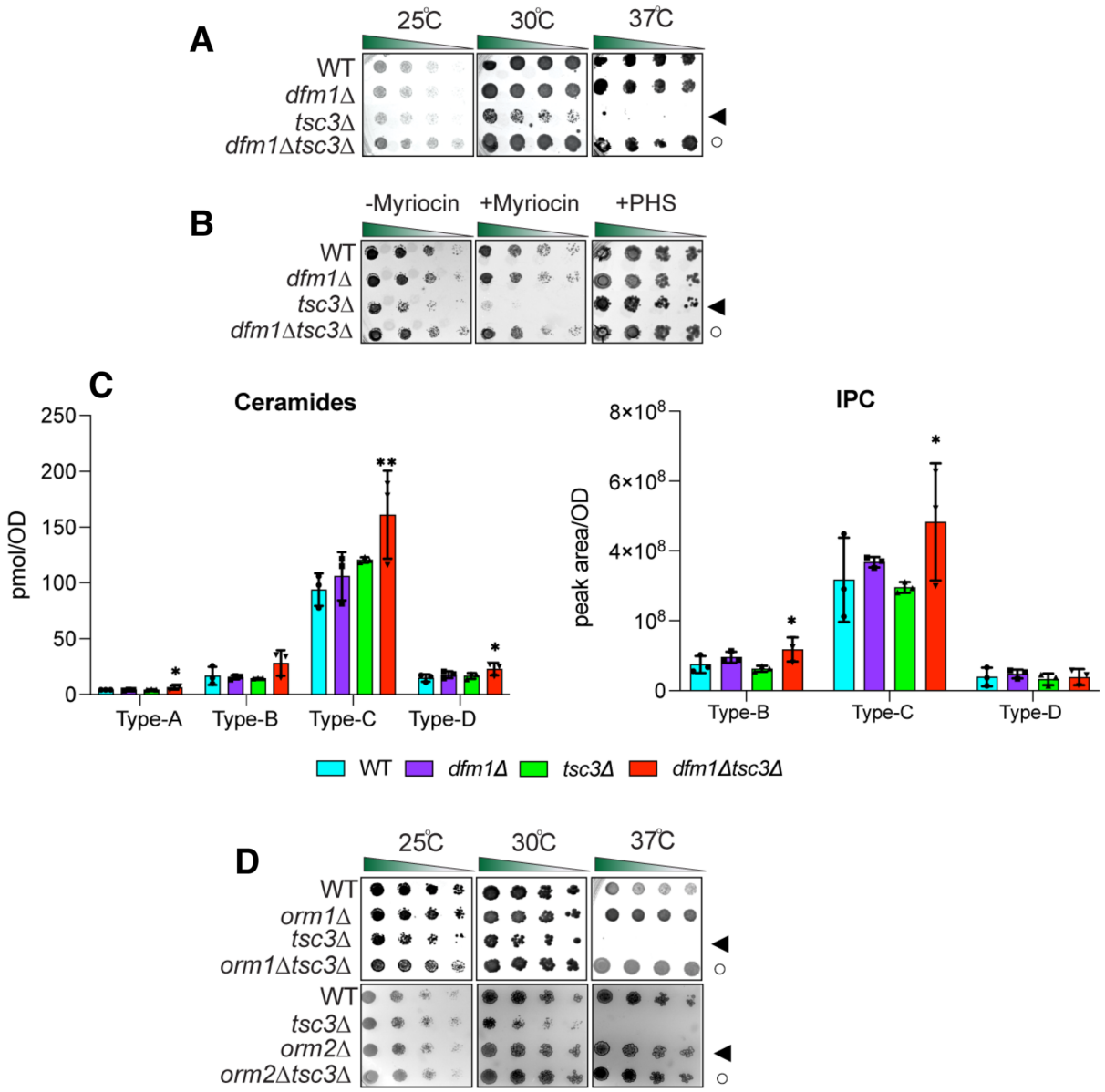

A
25℃
30℃
37℃
WT
dfm1Δ
tsc3Δ
dfm1Δtsc3Δ
B
-Myriocin
+Myriocin
+PHS
WT
dfm1Δ
tsc3Δ
dfm1Δtsc3Δ
C
Ceramides
pmol/OD
250
200
150
100
50
0
Type-A
Type-B
Type-C
Type-D
IPC
peak area/OD
8×10^8
6×10^8
4×10^8
10^8
0
Type-B
Type-C
Type-D
WT
dfm1Δ
tsc3Δ
dfm1Δtsc3Δ
D
25℃
30℃
37℃
WT
orm1Δ
tsc3Δ
orm1Δtsc3Δ
WT
tsc3Δ
orm2Δ
orm2Δtsc3Δ

Figure 3.2.4. Dfm1 genetically interacts with Orm1

(A) Indicated strains were spotted 5-fold dilutions on SC plates in 3 biological replicates and 2 technical replicates (n=5), and plates were incubated at room temperature, 30oC, and 37oC. Upper panel: WT, *dfm1*Δ, *orm1*Δ, and *dfm1*Δ*orm1*Δ were compared for growth by dilution assay. Middle panel: WT, *dfm1*Δ, *orm2*Δ, and *orm2*Δ*tsc3*Δ were compared for growth by dilution assay. Bottom panel: WT, *dfm1*Δ, *orm1*Δ, *orm2*Δ, and *orm2*Δ, and *orm1*Δ*orm2*Δ were compared for growth by dilution assay. Upper, middle, and lower panel: gray arrowhead depicts growth phenotype of *dfm1*Δ*orm1*Δ, *dfm1*Δ*orm2*Δ, and *orm1*Δ*orm2*Δ respectively. **(B)** *dfm1*Δ*orm1*Δ confers resistance to myriocin and sensitivity to PHS. WT, *dfm1*Δ, *orm1*Δ, and *dfm1*Δ*orm1*Δ strains were grown to log-phase in SC medium, and 5-fold serial dilutions of cultures were spotted on YPD plates containing either drug vehicle alone, 1 mM of myriocin and 10 μM of PHS with each condition performed in 3 biological replicates and 2 technical replicates (n=5). Plates were incubated at room temperature and photographed after 3 days. Open circle indicates growth phenotype of *dfm1*Δ*orm1*Δ cells. **(C)** WT, *dfm1*Δ, *orm1*Δ, and *orm1*Δ*dfm1*Δ cells were grown to log-phase at 30°C and lipids were extracted and subjected to LC-MS/MS. C18 PHS and DHS levels were measured as described in Methods (3 biological replicates; n=3). Values represent the means±S.E.M. Statistically significant differences compared to WT cells are indicated (Pairwise Dunnett's test followed by Bonferroni's post-hoc analysis; *P<0.05, **P<0.01). **(D)** WT, *dfm1*Δ, *orm1*Δ, *orm2*Δ, *dfm1*Δ*orm1*Δ, and *orm1*Δ*orm2*Δ cells were grown to log-phase at 30°C and lipids were extracted and subjected to LC-MS/MS. A- B- C- & D-Type ceramides containing C16, C18, C20, C22, C24, and C26 fatty acid (left graph) and B- C- & D-type IPCs containing C24 and C26 fatty acid (right graph) were measured (3 biological replicates; n=3). Values represent the means±S.E.M. Statistically significant differences compared to WT cells are indicated (Pairwise Dunnett's test followed by Bonferroni's post-hoc analysis; *P<0.05, **P<0.01).

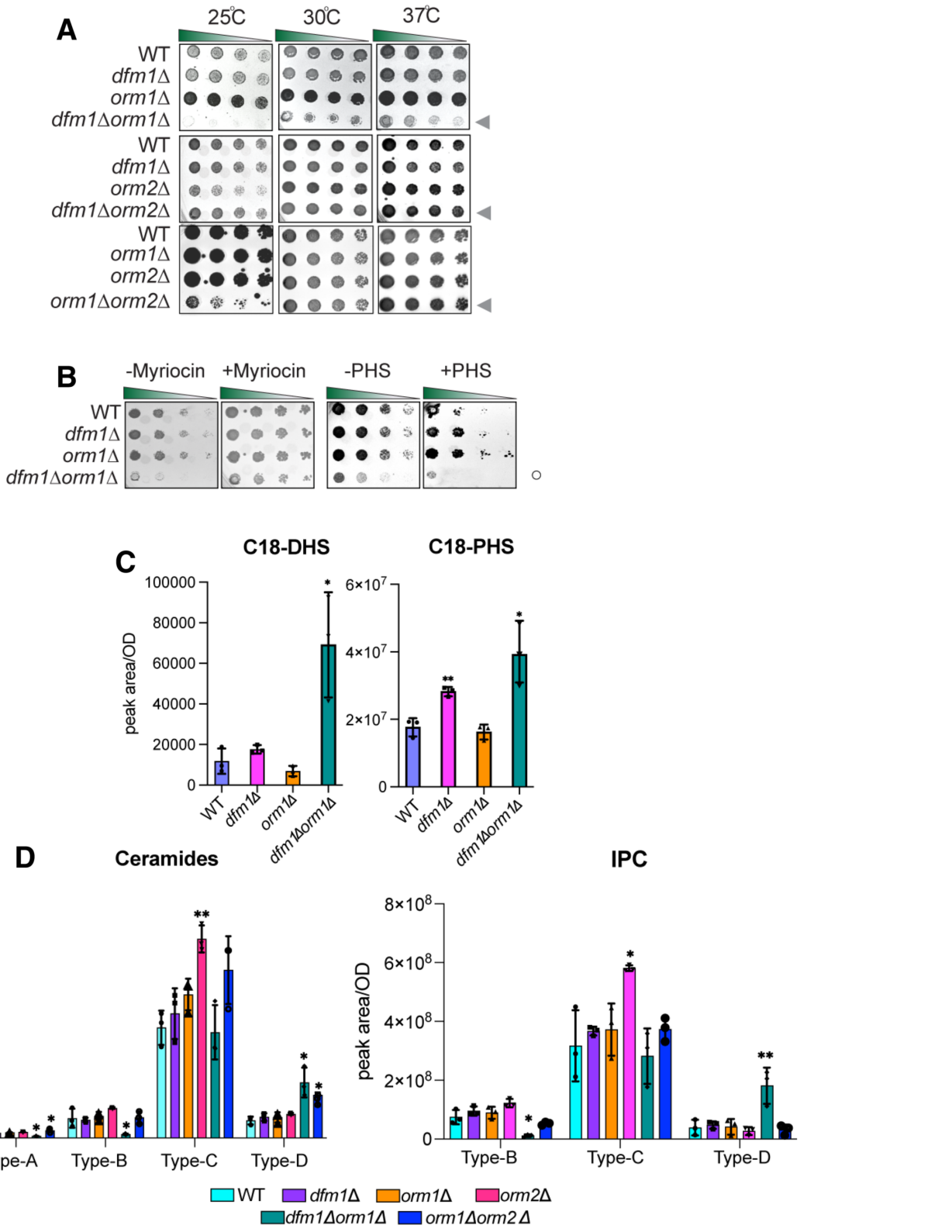

A
25℃
30℃
37℃
WT
dfm1Δ
orm1Δ
dfm1Δorm1Δ
WT
dfm1Δ
orm2Δ
dfm1Δorm2Δ
WT
orm1Δ
orm2Δ
orm1Δorm2Δ
B
-Myriocin
+Myriocin
-PHS
+PHS
WT
dfm1Δ
orm1Δ
dfm1Δorm1Δ
C
C18-DHS
C18-PHS
peak area/OD
100000
80000
60000
40000
20000
0
6×10^7
4×10^7
2×10^7
0
WT
dfm1Δ
orm1Δ
dfm1Δorm1Δ
D
Ceramides
IPC
pmol/OD
200
150
100
50
0
Type-A
Type-B
Type-C
Type-D
peak area/OD
8×10^8
6×10^8
4×10^8
2×10^8
0
Type-B
Type-C
Type-D
WT
dfm1Δ
orm1Δ
orm2Δ
dfm1Δorm1Δ
orm1Δorm2Δ

Figure 3.2.5. Dfm1 targets Orm2 for degradation

(A) Degradation of Orm2 depends on Dfm1 and not Der1. The indicated strains expressing Orm2-RFP were grown into log phase and degradation was measured by cycloheximide chase (CHX). After CHX addition, cells were lysed at the indicated times, and analyzed by SDS-PAGE and immunoblotted for Orm2-RFP with α-RFP (3 biological replicates (n=3). (B) Same as (A) except degradation of Orm2-RFP was measured in WT and der1Δ cells (3 biological replicates; n=3). (C) Depiction of Dfm1, Der1, Dfm1-5Ashp, and Der1-Shp. Dfm1 and Der1 are ER-localized membrane proteins with six transmembrane domains (Greenblatt et al., 2011). Unlike Der1, Dfm1 has an extended cytoplasmic tail containing two SHP boxes. (D) Dfm1's SHP box is not required for degradation of Orm2-RFP. In the indicated strains, degradation of Orm2-RFP was measured by CHX-chase assay. Cells were analyzed by SDS- PAGE and immunoblotted for Orm2-RFP with α-RFP (3 biological replicates; n=3). (E) Depiction of Dfm1, which highlights L1, TM2, TM6, and its SHP box domain. (F) Table indicating the location and specific function that is impaired for retrotranslocation- deficient Dfm1 mutants (Nejatfard et al., 2021). (G) Dfm1's WR motif, GxxxG motif, substrate binding and lipid thinning function are required for degradation of Orm2-RFP. In the indicated strains, degradation of Orm2-RFP was measured by CHX-chase assay. Cells were analyzed by SDS-PAGE and immunoblotted for Orm2-RFP with α-RFP (3 biological replicates; n=3). (H) Dfm1 L1 residues are required for binding to Orm2. Orm2-RFP and binding to retrotranslocation-deficient Dfm1 L1 mutants was analyzed by co-IP. The IP was analyzed for presence of Dfm1-HA. As a negative control, cells not expressing Orm2-RFP were used (3 biological replicates; n=3). Band intensities for all western blots were normalized to PGK1 loading control and quantified by ImageJ. Data information: t=0 was taken as 100% and data is represented as mean ± SEM.

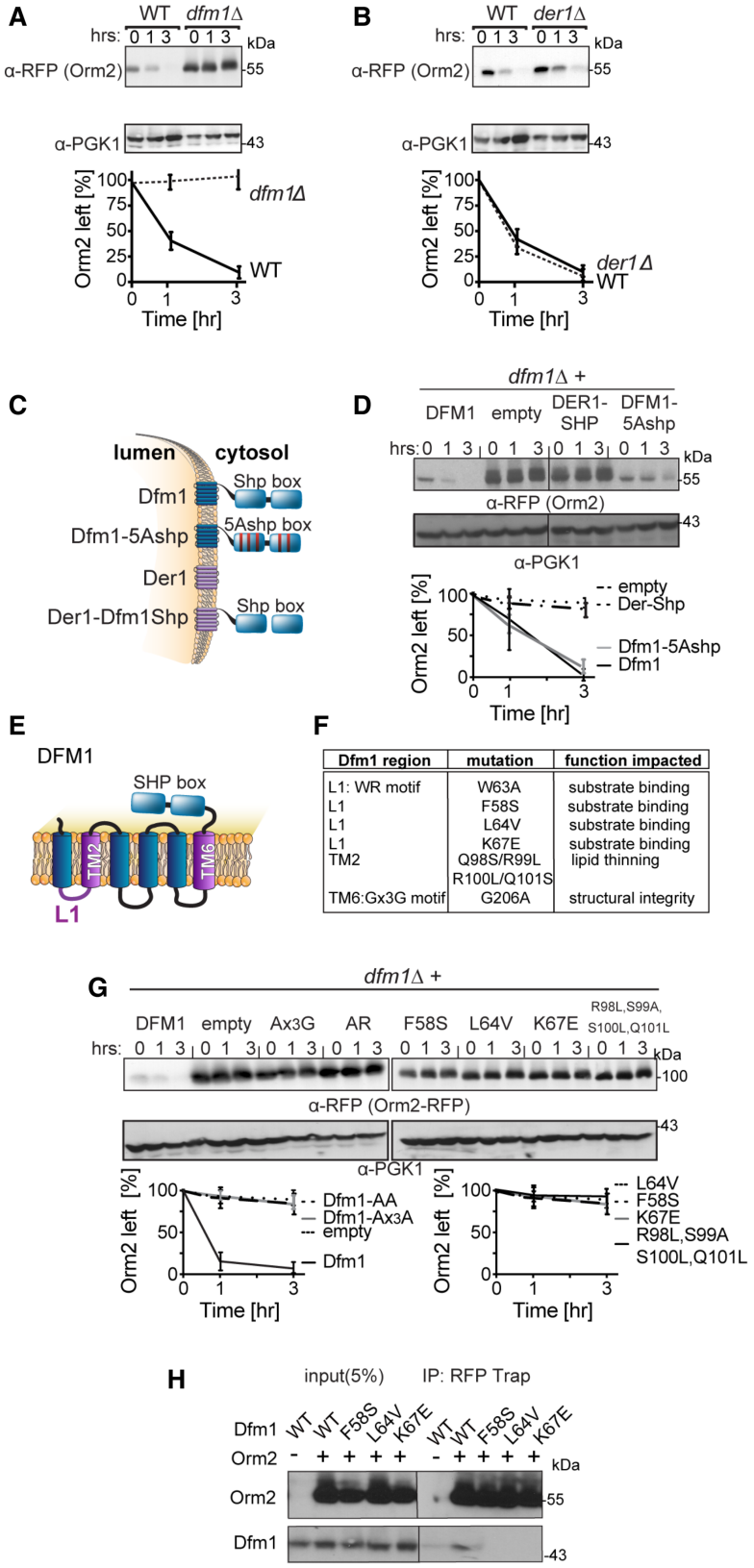

A
WT
dfm1Δ
hrs: 0 1 3 0 1 3
kDa
α-RFP (Orm2)
55
α-PGK1
43
Orm2 left [%]
100
75
50
25
0
dfm1Δ
WT
0 1 3
Time [hr]
B
WT
der1Δ
hrs: 0 1 3 0 1 3
kDa
α-RFP (Orm2)
55
α-PGK1
43
Orm2 left [%]
100
75
50
25
0
der1Δ
WT
0 1 3
Time [hr]
C
lumen
cytosol
Dfm1
Shp box
Dfm1-5Ashp
5Ashp box
Der1
Der1-Dfm1Shp
Shp box
D
dfm1Δ +
DFM1
empty
DER1-SHP
DFM1-5Ashp
hrs: 0 1 3 0 1 3 0 1 3 0 1 3
kDa
55
α-RFP (Orm2)
43
α-PGK1
Orm2 left [%]
100
50
0
empty
Der-Shp
Dfm1-5Ashp
Dfm1
0 1 3
Time [hr]
E
DFM1
SHP box
TM2
TM6
L1
F
Dfm1 region | mutation | function impacted
L1: WR motif | W63A | substrate binding
L1 | F58S | substrate binding
L1 | L64V | substrate binding
L1 | K67E | substrate binding
TM2 | Q98S/R99L R100L/Q101S | lipid thinning
TM6:Gx3G motif | G206A | structural integrity
G
dfm1Δ +
DFM1
empty
Ax3G
AR
F58S
L64V
K67E
R98L,S99A, S100L,Q101L
hrs: 0 1 3 0 1 3 0 1 3 0 1 3 0 1 3 0 1 3 0 1 3 0 1 3
kDa
100
α-RFP (Orm2-RFP)
43
α-PGK1
Orm2 left [%]
100
50
0
Dfm1-AA
Dfm1-Ax3A
empty
Dfm1
0 1 3
Time [hr]
Orm2 left [%]
100
50
0
L64V
F58S
K67E
R98L,S99A
S100L,Q101L
0 1 3
Time [hr]
H
input(5%)
IP: RFP Trap
Dfm1 WT WT F58S L64V K67E WT WT F58S L64V K67E
Orm2 - + + + + - + + + +
kDa
Orm2
55
Dfm1
43

Figure 3.2.6. Orm2 degradation requires EGAD, but not ERAD or INMAD pathway

(A) E3 ligase Tul1 is required for Orm2 degradation. In the indicated strains, degradation of Orm2-RFP was measured by CHX-chase assay. Cells were analyzed by SDS-PAGE and immunoblotted for Orm2-RFP with α-RFP (3 biological replicates; n=3). t=0 was taken as 100% and data is represented as mean ± SEM. **(B)** Cdc48 and the proteasome are required for Orm2 degradation. Same as (A), except cdc48-2 and hrd2-1 were analyzed for Orm2-RFP degradation (3 biological replicates; n=3). t=0 was taken as 100% and data is represented as mean ± SEM. **(C)** Dfm1 does not function in the post-ubiquitination step of Orm2 degradation pathway. Indicated strains expressing Orm2-RFP were grown into log phase. Cells were lysed, and microsomes were collected and immunoprecipitated with α-RFP conjugated to agarose beads. Samples were then subjected to SDS-PAGE and immunoblot by α-Ubiquitin and α-RFP (3 biological replicates; n=3). **(D)** ERAD mutants do not rescue temperature-sensitive lethality of tsc3Δ. Indicated strains were grown to log-phase in SC and serially diluted cultures were plated on SC plates and incubated at 37°C and imaged at Day 2 (3 biological replicates, 2 technical replicates; n=5).

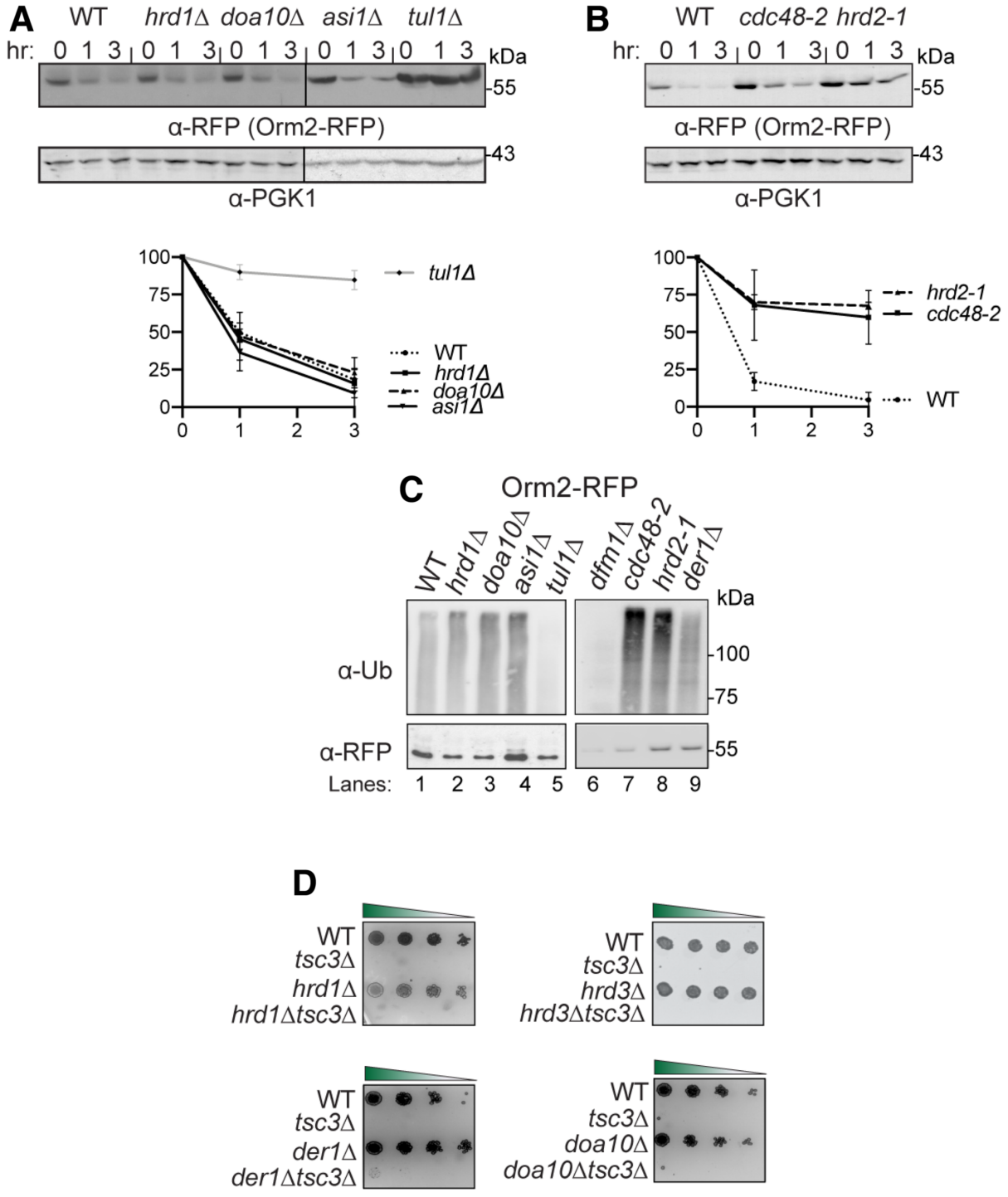

A
WT
hrd1Δ
doa10Δ
asi1Δ
tul1Δ
hr: 0 1 3 0 1 3 0 1 3 0 1 3 0 1 3
kDa
55
α-RFP (Orm2-RFP)
43
α-PGK1
100
75
50
25
0
0 1 2 3
tul1Δ
WT
hrd1Δ
doa10Δ
asi1Δ
B
WT
cdc48-2
hrd2-1
hr: 0 1 3 0 1 3 0 1 3
kDa
55
α-RFP (Orm2-RFP)
43
α-PGK1
100
75
50
25
0
0 1 2 3
hrd2-1
cdc48-2
WT
C
Orm2-RFP
WT
hrd1Δ
doa10Δ
asi1Δ
tul1Δ
dfm1Δ
cdc48-2
hrd2-1
der1Δ
kDa
α-Ub
100
75
α-RFP
55
Lanes: 1 2 3 4 5 6 7 8 9
D
WT
tsc3Δ
hrd1Δ
hrd1Δtsc3Δ
WT
tsc3Δ
hrd3Δ
hrd3Δtsc3Δ
WT
tsc3Δ
der1Δ
der1Δtsc3Δ
WT
tsc3Δ
doa10Δ
doa10Δtsc3Δ

Figure 3.2.7. dfm1Δ accumulates phosphorylated Orm2 exclusively in the ER

(A) Phosphorylated Orm2 accumulates in the absence of Dfm1. Phos-tag western blot analysis shows that there is an accumulation of phosphorylated Orm2 in *dfm1*Δ cells. The indicated strains were grown to log phase, treated with vehicle or 1.5 μM myriocin for 1 hour and subjected to SDS-PAGE or Phos-tag western blot analysis via blotting for Orm2 with α-RFP and PGK1 with α-PGK1 antibodies (2 biological replicates; n=2). **(B)** Orm2 is retained in the ER in *dfm1*Δ cells. Strains were grown to mid-exponential phase in minimal media and GFP and RFP fluorescence was examined on an AxioImager.M2 fluorescence microscope using a 100x objective and 28HE-GFP or 20HE-rhodamine filter sets (Zeiss) (2 biological replicates n=2). WT, *dfm1*Δ, and *tul1*Δ cells expressing Orm2-RFP. HDEL-GFP (ER marker, green) or VPS4-GFP (endosome marker, green) were used to test for co-localization with Orm2-RFP. Arrowheads indicate Orm2 co-localizing in post-ER compartments. Scale bar, 5 μM. **(C)** *dfm1*Δ cells block the degradation of phosphorylated mimic of Orm2 (Orm2-3D). In the indicated strains, degradation of Orm2-3A-GFP and Orm2-3D-GFP was measured by CHX- chase assay. Cells were analyzed by SDS-PAGE and immunoblotted α-GFP (3 biological replicates; n=3). t=0 was taken as 100% and data is represented as mean ± SEM. **(D)** Accumulation of phosphorylated Orm2 within the ER is sufficient for rescuing the temperature-sensitive lethality of *tsc3*Δ cells. Indicated strains were spotted 5-fold dilutions on SC plates and plates were incubated at 37°C (3 biological replicates, 2 technical replicates; n=5). **(E)** *dfm1*Δ blocks export of phosphorylated Orm2. Fluorescence imaging was performed as in (B) except WT and *dfm1*Δ cells expressing Orm2-3D-GFP was used (2 biological replicates; n=2). Sec61-mCherry (ER marker, red) or CHS5-mCherry (endosome marker, red) were used to test for co-localization with Orm2-3D-GFP. Arrowheads indicate Orm2 co-localizing in post-ER compartments. Scale bar, 5 μM. **(F)** WT and *dfm1*Δ cells expressing either Orm2-3A-GFP or Orm2-3D-GFP were grown to log- phase at 30°C and lipids were extracted and subjected to LC-MS/MS. C18 PHS and DHS levels were measured as described in Methods in 3 biological replicates (n=3). Values represent the means±S.E.M. Statistically significant differences compared to WT cells are indicated (Pairwise Dunnett's test followed by Bonferroni's post-hoc analysis; ***P<0.0001).

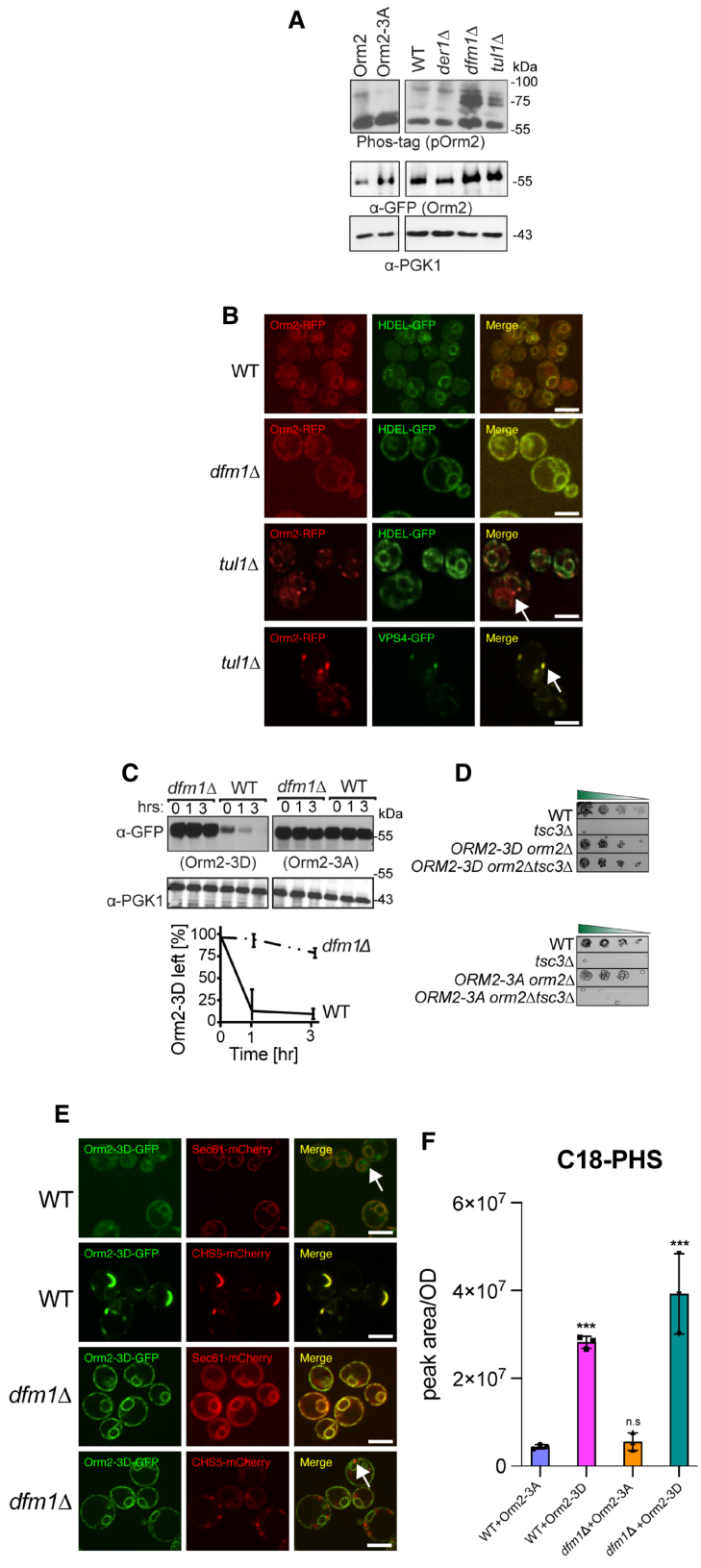
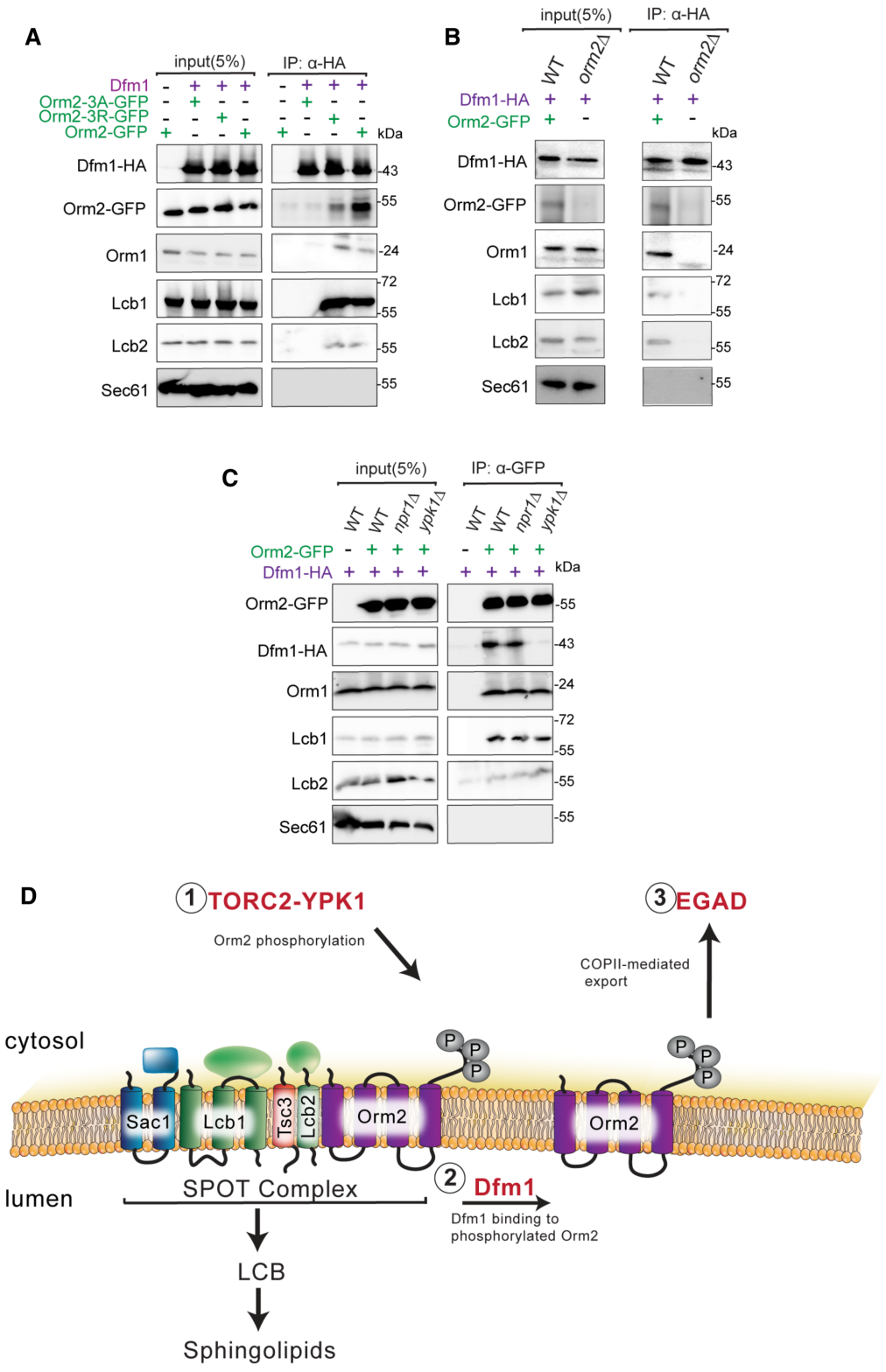

A
Orm2
Orm2-3A
WT
der1Δ
dfm1Δ
tul1Δ
kDa
-100
-75
-55
Phos-tag (pOrm2)
-55
α-GFP (Orm2)
-43
α-PGK1
B
Orm2-RFP
HDEL-GFP
Merge
WT
dfm1Δ
tul1Δ
Orm2-RFP
VPS4-GFP
Merge
tul1Δ
C
dfm1Δ
WT
dfm1Δ
WT
hrs:
0 1 3
0 1 3
0 1 3
0 1 3
kDa
α-GFP
-55
(Orm2-3D)
(Orm2-3A)
-55
α-PGK1
-43
Orm2-3D left [%]
100
75
50
25
0
dfm1Δ
WT
0
1
3
Time [hr]
D
WT
tsc3Δ
ORM2-3D orm2Δ
ORM2-3D orm2Δtsc3Δ
WT
tsc3Δ
ORM2-3A orm2Δ
ORM2-3A orm2Δtsc3Δ
E
Orm2-3D-GFP
Sec61-mCherry
Merge
WT
Orm2-3D-GFP
CHS5-mCherry
Merge
WT
Orm2-3D-GFP
Sec61-mCherry
Merge
dfm1Δ
Orm2-3D-GFP
CHS5-mCherry
Merge
dfm1Δ
F
C18-PHS
peak area/OD
6×10^7
4×10^7
2×10^7
0
***
***
n.s
WT+Orm2-3A
WT+Orm2-3D
dfm1Δ+Orm2-3A
dfm1Δ+Orm2-3D

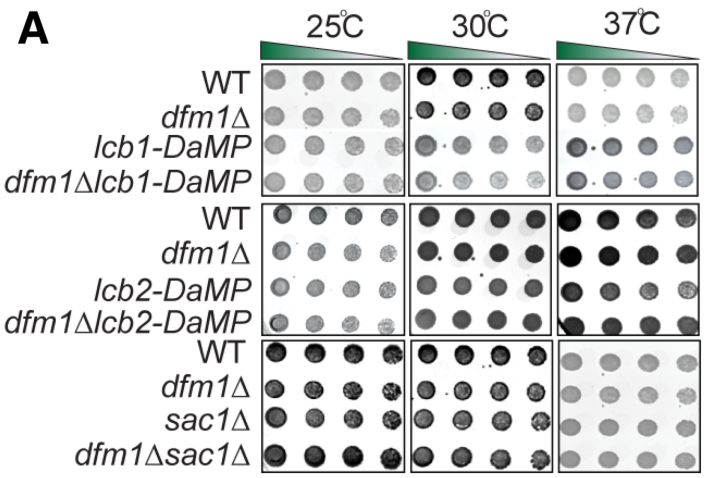
Figure 3.2.8. Dfm1 binds to phosphorylated Orm2

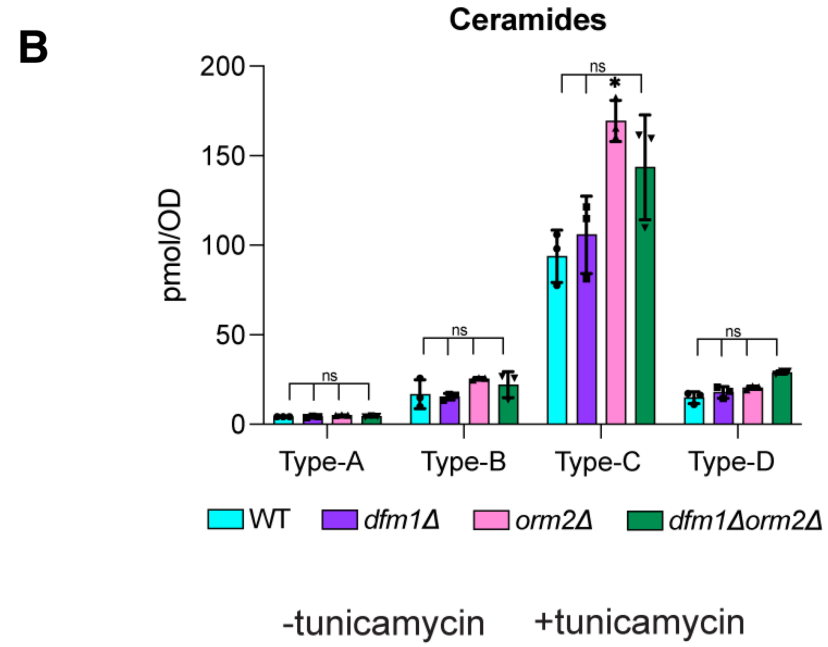
(A) Dfm1-HA binding to Orm2-GFP, Orm2-3A-GFP, Orm2-3D-GFP, Orm1, Lcb1, and Lcb2 were analyzed by co-IP. As negative control, cells not expressing Dfm1-HA were used. Also, Sec61 was also included to test for non-specific binding (3 biological replicates; n=3). **(B)** Same as (A), except co-IP was performed on WT and orm2Δ cells and Dfm1-HA binding to Orm1, Lcb1, and Lcb2 was analyzed (3 biological replicates; n=3). **(C)** Same as (A), except Orm2-GFP binding to Dfm1-HA, Orm1, Lcb1, and Lcb2 was analyzed by co-IP (3 biological replicates; n=3). **(D)** Schematic of Dfm1's role in Orm2 degradation. 1) Orm2 is inactivated via phosphorylation by TORC2-YPK1 signaling axis. 2) Dfm1 binds phosphorylated Orm2. 3) Phosphorylated Orm2 is delivered to COPII vesicles. 3) Phosphorylated Orm2 is routed to the Golgi and degraded via EGAD.

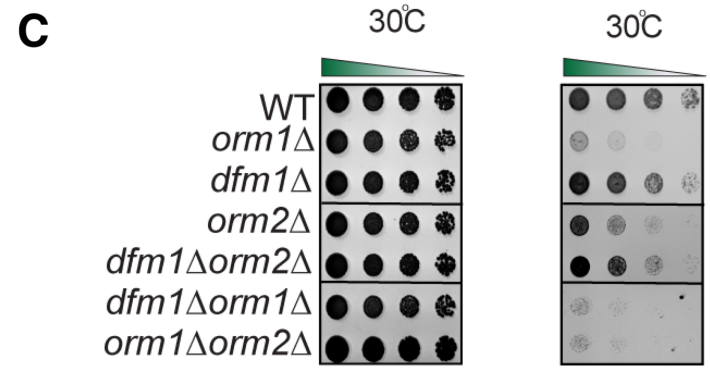

A
input(5%)
IP: α-HA
Dfm1
Orm2-3A-GFP
Orm2-3R-GFP
Orm2-GFP
kDa
Dfm1-HA
Orm2-GFP
Orm1
Lcb1
Lcb2
Sec61
-43
-55
-24
-72
-55
-55
-55
B
input(5%)
IP: α-HA
WT
orm2Δ
Dfm1-HA
Orm2-GFP
kDa
C
input(5%)
IP: α-GFP
WT
WT
npr1Δ
ypk1Δ
Orm2-GFP
Dfm1-HA
D
1 TORC2-YPK1
Orm2 phosphorylation
3 EGAD
COPII-mediated export
cytosol
Sac1
Lcb1
Tsc3
Lcb2
Orm2
P
lumen
SPOT Complex
2 Dfm1
Dfm1 binding to phosphorylated Orm2
LCB
Sphingolipids

Supplemental Figure 3.2.1. Dfm1 does not genetically interact with Lcb1, Lcb2, and Sac1

(A) Indicated strains were spotted 5-fold dilutions on SC plates in triplicates, and plates were incubated at room temperature, 30°C, and 37°C (3 biological replicates, 2 technical replicates; n=3). Upper panel: WT, *dfm1*Δ, Lcb1-DaMP, and *dfm1*ΔLcb1-DaMP were compared for growth by dilution assay. Middle panel: WT, *dfm1*Δ, Lcb2-DaMP, and *dfm1*ΔLcb2-DaMP were compared for growth by dilution assay. Bottom panel: WT, *dfm1*Δ, and *dfm1*Δ*sac1*Δ, were compared for growth by dilution assay. **(B)** WT, *dfm1*Δ, *orm2*Δ, and *orm2*Δ*dfm1*Δ cells were grown to log-phase at 30°C and lipids were extracted and subjected to LC-MS/MS. A- B- C- & D-Type ceramides containing C16, C18, C20, C22, C24, and C26 fatty acids were measured (3 biological replicates; n=3). Values represent the means±S.E.M. Statistically significant differences compared to WT cells are indicated (Pairwise Dunnett's test followed by Bonferroni's post-hoc analysis; ns=non- significant, *P<0.05). **(C)** Serial dilution growth was performed on YPD plates in the presence or absence of 1 µg/mL tunicamycin using WT, *orm1*Δ, *orm2*Δ, *dfm1*Δ, *dfm1*Δ*orm1*Δ, *orm1*Δ*orm2*Δ, and *dfm1*Δ*orm2*Δ cells (3 biological replicates, 2 technical replicates; n=3).

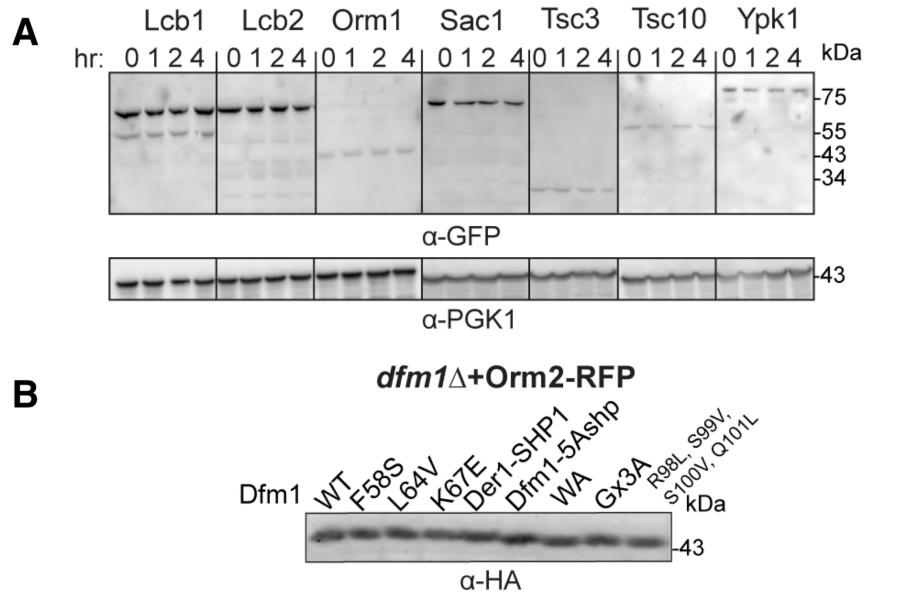

A
25°C
30°C
37°C
WT
dfm1Δ
lcb1-DaMP
dfm1Δlcb1-DaMP
WT
dfm1Δ
lcb2-DaMP
dfm1Δlcb2-DaMP
WT
dfm1Δ
sac1Δ
dfm1Δsac1Δ

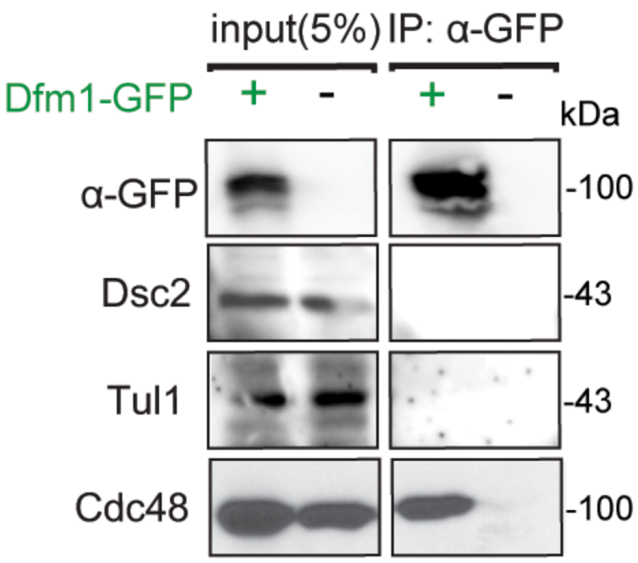

B
Ceramides
pmol/OD
200
150
100
50
0
ns
*
Type-A
Type-B
Type-C
Type-D
WT
dfm1Δ
orm2Δ
dfm1Δorm2Δ
-tunicamycin
+tunicamycin


C
30°C
30°C
WT
orm1Δ
dfm1Δ
orm2Δ
dfm1Δorm2Δ
dfm1Δorm1Δ
orm1Δorm2Δ

Supplemental Figure 3.2.2. Orm2 is degraded in WT strains

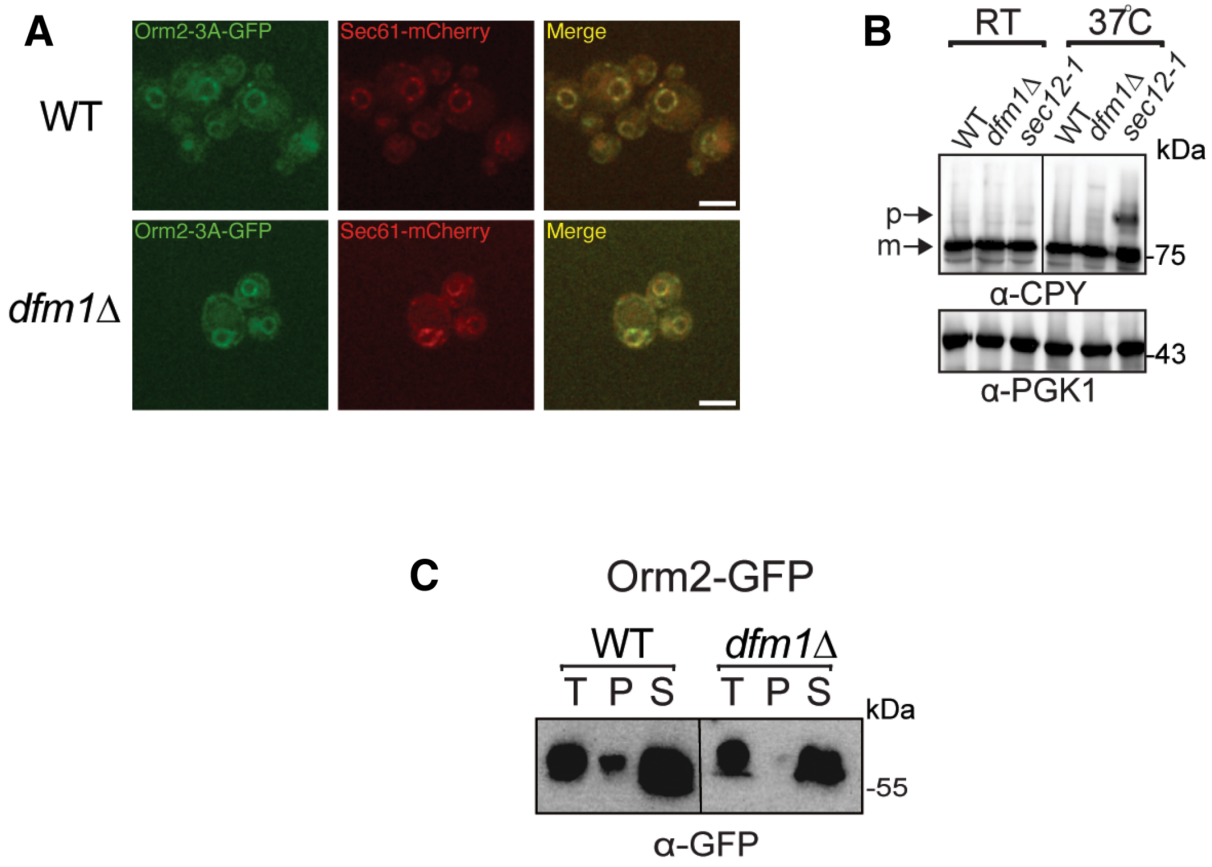
(A) In the indicated WT strains, degradation of Lcb1-GFP, Lcb2-GFP, Orm2-GFP, Orm2-GFP, Sac1-GFP, Tsc3-GFP, Tsc10-GFP, and Ypk1-GFP was measured by CHX-chase assay (3 biological replicates; n=3). Cells were analyzed by SDS-PAGE and immunoblotted with α-GFP. **(B)** Steady-state levels of Dfm1 and corresponding Dfm1 mutants. Cell were analyzed by SDS- PAGE and immunoblotted with α-HA. **(C)** Serial dilution growth assay was performed on *dfm1*Δ*orm1*Δ and strains with DFM1, DER1- SHP, DFM1-AA, DFM1-Ax3A, DFM1-5Ashpmtnt, and empty vector addback (3 biological replicates, 2 technical replicates; n=3). **(D)** Same as (C), except serial dilution growth assay was performed on *dfm1*Δ*orm1*Δ strains with L1 mutant addback: F58S, L64V, K67E and TMD2 quad mutant addback: DFM1-R98L, S99V, S100V, Q101L. Indicated strains were grown on SC-Leu plates at room temperature, 30°C and 37°C, and imaged on Day 2 and Day 7 (3 biological replicates, 2 technical replicates; n=3). **(E)** ERAD mutants do not genetically interact with *orm1*Δ. Indicated strains were spotted 5-fold dilutions on SC plates in triplicates, and plates were incubated at room temperature, 30°C, and 37°C (3 biological replicates, 2 technical replicates; n=3).


A
Lcb1
Lcb2
Orm1
Sac1
Tsc3
Tsc10
Ypk1
hr: 0 1 2 4 | 0 1 2 4 | 0 1 2 4 | 0 1 2 4 | 0 1 2 4 | 0 1 2 4 | 0 1 2 4
kDa
75
55
43
34
α-GFP
43
α-PGK1
B
dfm1Δ+Orm2-RFP
Dfm1
WT
F58S
L64V
K67E
Der1-SHP1
Dfm1-5Ashp
WA
Gx3A
R98L, S99V, S100V, Q101L
kDa
43
α-HA
C
dfm1Δorm1Δ
30℃
empty vector
DFM1
DER1-SHP1
DFM1-5Ashp
DFM1-WA
DFM1-Gx3A
D
dfm1Δorm1Δ
30℃
empty vector
DFM1
DFM1-F58S
DFM1-L64V
DFM1-K67E
DFM1-R98L, S99V, S100V, Q101L
E
25℃
30℃
37C
WT
hrd1Δ
orm1Δ
hrd1Δorm1Δ
WT
doa10Δ
orm1Δ
doa10Δorm1Δ
WT
hrd2-1
orm1Δ
hrd2-1orm1Δ
WT
cdc48-2
orm1Δ
cdc48-2 orm1Δ



Supplemental Figure 3.2.3. Dfm1 does not interact with EGAD components

Dfm1-GFP binding to EGAD members, Dsc2 and Tul1, were analyzed by co-IP. As negative control, cells not expressing Dfm1-GFP were used (2 biological replicates; n=2).



Supplemental Figure 3.2.4. Orm2-3A accumulates exclusively in the ER

(A) Fluorescence imaging was performed as in Fig. 3.2.7B except WT and *dfm1*Δ cells expressing Orm2-3A-GFP was used. Sec61-RFP (ER marker, red) was used to test for co-localization with Orm2-3A-GFP (2 biological replicates; n=2). Arrowheads indicate Orm2 co-localizing in post- ER compartments. Scale bar, 5 μM. **(B)** *dfm1*Δ cells do not abrogate COPII-mediated export of CPY. The indicated cells were either grown at room temperature or shifted to non-permissive growth at 37°C. Cells were analyzed by SDS-PAGE and immunoblotted for CPY with α-CPY and PGK1 with α-PGK1. **(C)** Western blot of aggregated versus soluble Orm2-GFP at the ER. Lysates from WT and *dfm1*Δ cells containing ORM2-GFP were blotted using anti-GFP to detect Orm2. P is ER aggregated fraction and S is ER soluble fraction.

Supplemental Table 3.4.1. Plasmids Used in this Study

Plasmid	Gene		
pSN184	YIp	ADE2/URA3	pTDH3-HMG2-GFP
pSN149	2μ	URA3	pGAL- BIRA-3xFLAG
pSN148	2μ	URA3	pGAL-DFM1-BIRA-3xFLAG
pSN246	YCp	URA3	pORM2-RFP
pSN247	YCp	LEU2	pLCB1-RFP
pSN266	YCp	URA3	pORM2-GFP
pSN267	YCp	URA3	pORM2-3D-GFP
pSN268	YCp	URA3	pORM2-3A-GFP
pSN60	YCp	LEU2	pDFM1-L64V
pSN90	YCp	LEU2	pDFM1
pSN93	YCp	LEU2	pDFM1-K67E
pSN230	YCp	LEU2	pDFM1-R98L, S99A, S100A, Q101L
pSN95	YCp	LEU2	pDFM1-F58S
pSN162	YCp	LEU2	pDFM1-5Ashp-3HA
pSN161	YCp	LEU2	pDER1-SHP-3HA
pSN164	YCp	LEU2	pDFM1-AR-3HA
pSN163	YCp	LEU2	pDFM1-Ax_3G-3HA

Supplemental Table 3.4.2. Yeast Strains Used in this Study

Strain	Genotype	Reference
SEN 1	*Mata ade2-101 met2 lys-801 ura3-52 trp1::hisG leu2 his3Δ200*	This study
BY4741	*Mata met15Δ0 his3Δ1 leu2Δ0 ura3Δ0*	This study
SEN 322	*SEN1 2μ::URA3::GAL1pr-Dfm1-BIRA-FLAG*	This study
SEN 324	*SEN1 2μ::URA3::GAL1pr- BIRA-FLAG*	This study
SEN 167	*SEN1 dfm1Δ::KanMX ade2-101::ADE2::URA3::TDH3pr-HMG2-GFP 2μ::URA3::GAL1pr-Dfm1-BIRA-3xFLAG*	This study
SEN 168	*SEN1 dfm1Δ::KanMX ade2-101::ADE2::URA3::TDH3pr- HMG2-GFP 2μ::URA3::GAL1pr-BIRA-3xFLAG*	This study
SEN 169	*SEN1 dfm1Δ::KanMX ade2-101::ADE2::URA3::TDH3pr- HMG2-GFP 2μ::URA3*	This study
SEN 280	*BY4741 DFM1::DFM1-GFP::HIS*	This study
SEN 439	*BY4741 DFM1::DFM1-GFP::HIS CEN::URA3:: prORM2-RFP*	This study
SEN 438	*BY4741 DFM1::DFM1-GFP::HIS CEN::LEU2:: prLCB1-RFP*	This study
SEN 635	*SEN1 dfm1Δ::KanMX*	This study
SEN 637	*SEN1 tsc3Δ::NatR*	This study
SEN 638	*SEN1 dfm1Δ::KanMX tsc3Δ::NatR*	This study
SEN 640	*SEN1 orm1Δ::KanMX*	This study
SEN 641	*SEN1 orm1Δ::KanMX tsc3Δ::NatR*	This study
SEN 644	*SEN1 orm2Δ::KanMX*	This study
RHY 646	*SEN1 orm2Δ::KanMX tsc3Δ::NatR*	This study
SEN 285	*SEN1 dfm1Δ::KanMX orm1Δ::NatR*	This study
SEN 291	*SEN1 dfm1Δ::KanMX orm2Δ::NatR*	This study

Supplemental Table 3.4.2 Yeast Strains Used in this Study (Continued)

Strain	Genotype	Reference
SEN 280	*BY4741 orm1Δ::KanMX*	This study
SEN 281	*BY4741 orm2Δ::KanMX*	This study
SEN 369	*BY4741 orm1Δ::KanMX orm2Δ::LEU2*	This study
SEN 282	*BY4741 Lcb2-DaMP*	This study
SEN 266	*BY4741 dfm1Δ::KanMX Lcb2-DaMP*	This study
SEN 392	*SEN1 sac1Δ:NatR*	This study
SEN 301	*SEN1 dfm1Δ::KanMX sac1Δ:NatR*	This study
SEN 599	*SEN1 CEN::URA3:: prORM2-RFP*	This study
SEN 659	*SEN1 dfm1Δ::KanMX CEN::URA3:: prORM2-RFP*	This study
SEN 615	*SEN1 der1Δ::KanMX CEN::URA3:: prORM2-RFP*	This study
SEN 623	*SEN1 dfm1Δ::KanMX CEN::URA3:: prORM2-RFP CEN::LEU2:: prDFM1-3xHA*	This study
SEN 624	*SEN1 dfm1Δ::KanMX CEN::URA3:: prORM2-RFP CEN::LEU2*	This study
SEN 625	*SEN1 dfm1Δ::KanMX CEN::URA3:: prORM2-RFP CEN::LEU2:: prDER1-SHP1*	This study
SEN 629	*SEN1 dfm1Δ::KanMX CEN::URA3:: prORM2-RFP CEN::LEU2:: prDFM1-5Ashp*	This study
SEN 626	*SEN1 dfm1Δ::KanMX CEN::URA3:: prORM2-RFP CEN::LEU2:: prDFM1-Ax3G*	This study
SEN 628	*SEN1 dfm1Δ::KanMX CEN::URA3:: prORM2-RFP CEN::LEU2:: prDFM1-AR*	This study
SEN 635	*SEN1 dfm1Δ::KanMX CEN::URA3:: prORM2-RFP CEN::LEU2:: prDFM1-F58S*	This study
SEN 632	*SEN1 dfm1Δ::KanMX CEN::URA3:: prORM2-RFP CEN::LEU2:: prDFM1-L64V*	This study
SEN 634	*SEN1 dfm1Δ::KanMX CEN::URA3:: prORM2-RFP CEN::LEU2:: prDFM1-K67E*	This study
SEN 630	*SEN1 dfm1Δ::KanMX CEN::URA3:: prORM2-RFP CEN::LEU2:: prDFM1-R98L, S99V, S100V, Q101L*	This study
SEN 598	*SEN1 hrd1Δ::KanMX CEN::URA3:: prORM2-RFP*	This study

Supplemental Table 3.4.2 Yeast Strains Used in this Study (Continued)

Strain	Genotype	Reference
SEN 604	*SEN1 doa10Δ::NatR CEN::URA3:: prORM2-RFP*	This study
SEN 607	*SEN1 asi1Δ::HphMX CEN::URA3:: prORM2-RFP*	This study
SEN 622	*SEN1 tul1Δ::KanMX CEN::URA3:: prORM2-RFP*	This study
SEN 606	*SEN1 cdc48Δ::cdc48-2::NatR CEN::URA3:: prORM2-RFP*	This study
SEN 608	*SEN1 hrd2-1 CEN::URA3:: prORM2-RFP*	This study
SEN 345	*SEN1 hrd3Δ::KanMX*	This study
SEN 346	*SEN1 tsc3Δ::KanMX hrd3Δ::NatR*	This study
SEN 437	*SEN1 tsc3Δ::KanMX hrd1Δ::NatR*	This study
SEN 3	*SEN1 hrd1Δ::KanMX*	This study
SEN 652	*SEN1 doa10Δ::HphMx*	This study
SEN 654	*SEN1 doa10Δ:: HphMx tsc3Δ::KanMX*	This study
SEN 649	*SEN1 der1Δ::NatR*	This study
SEN 650	*SEN1 der1Δ::NatR tsc3Δ::KanMX*	This study
SEN 521	*BY4741 LCB1-GFP::HIS3*	This study
SEN 522	*BY4741 LCB2-GFP::HIS3*	This study
SEN 523	*BY4741 ORM1-GFP::HIS3*	This study
SEN 524	*BY4741 ORM2-GFP::HIS3*	This study
SEN 525	*BY4741 SAC1-GFP::HIS3*	This study
SEN 526	*BY4741 TSC3-GFP::HIS3*	This study
SEN 527	*BY4741 YPK1-GFP::HIS3*	This study
SEN 528	*BY4741 TSC10-GFP::HIS3*	This study

Supplemental Table 3.4.2 Yeast Strains Used in this Study (Continued)

Strain	Genotype	Reference
SEN 662	*SEN1 dfm1Δ::KanMX orm1Δ::NatR CEN::LEU2::prDFM1-3xHA*	This study
SEN 661	*SEN1 dfm1Δ::KanMX orm1Δ::NatR CEN::LEU2*	This study
SEN 675	*SEN1 dfm1Δ::KanMX orm1Δ::NatR CEN::LEU2::prDER1-SHP*	This study
SEN 676	*SEN1 dfm1Δ::KanMX orm1Δ::NatR CEN::LEU2::prDFM1-5Ashp*	This study
SEN 677	*SEN1 dfm1Δ::KanMX orm1Δ::NatR CEN::LEU2::prDFM1-AR*	This study
SEN 678 SEN 665	*SEN1 dfm1Δ::KanMX orm1Δ::NatR CEN::LEU2::prDFM1-Ax3G* *SEN1 dfm1Δ::KanMX orm1Δ::NatR CEN::LEU2::prDFM1-L64V*	This study This study
SEN 664	*SEN1 dfm1Δ::KanMX orm1Δ::NatR CEN::LEU2::prDFM1-F58S*	This study
SEN 666	*SEN1 dfm1Δ::KanMX orm1Δ::NatR CEN::LEU2::prDFM1-K67E*	This study
SEN 667	*SEN1 dfm1Δ::KanMX orm1Δ::NatR CEN::LEU2::prDFM1-R98L, S99V, S100V, Q101L*	This study
SEN 552	*SEN1 orm1Δ::NatR*	This study
SEN 551	*SEN1 orm1Δ::NatR hrd1Δ::KanMX*	This study
SEN 543	*SEN1 hrd2-1*	This study
SEN 544	*SEN1 cdc48::cdc48-2::NatR*	This study
SEN 545	*SEN1 doa10Δ:: HphMx*	This study
SEN 546	*SEN1 hrd2-1 orm1Δ::NatR*	This study
SEN 547	*SEN1 cdc48::cdc48-2::NatR orm1Δ::KanMx*	This study

Supplemental Table 3.4.2 Yeast Strains Used in this Study (Continued)

Strain	Genotype	Reference
SEN 548	*SEN1 doa10Δ:: HphMx orm1Δ::NatR*	This study
SEN 671	*SEN1 orm2Δ::KanMX tsc3Δ::NatR CEN::URA3::prORM2-3R-GFP*	This study
SEN 672	*SEN1 orm2Δ::KanMX tsc3Δ::NatR CEN::URA3::prORM2-3A-GFP*	This study
SEN 673	*BY4741 orm2Δ::KanMX CEN::URA3::prORM2-3R-GFP*	This study
SEN 674	*BY4741 orm2Δ::KanMX CEN::URA3::prORM2-3A-GFP*	This study
SEN 679	*SEN1 CEN::TRP1::ORM2-RFP CEN::URA3::HDEL-GFP*	This study
SEN 680	*SEN1 dfm1Δ::KanMX CEN::TRP1::ORM2-RFP CEN::URA3::HDEL-GFP*	This study
SEN 681	*SEN1 tul1Δ::KanMX CEN::TRP1::ORM2-RFP CEN::URA3::HDEL-GFP*	This study
SEN 682	*SEN1 tul1Δ::KanMX CEN::TRP1::ORM2-RFP CEN::URA3:VPS4-GFP*	This study
SEN 683	*SEN1 CEN::URA3::ORM2-3R-GFP CEN::LEU2::HIS3::SEC61-mCherry*	This study
SEN 684	*SEN1 CEN::URA3::ORM2-3R-GFP CEN::TRP1::CHS5-mCherry*	This study
SEN 685	*SEN1 dfm1Δ::KanMX CEN::URA3::ORM2-3R-GFP CEN::LEU2::HIS3::SEC61-mCherry*	This study
SEN 686	*SEN1 dfm1Δ::KanMX CEN::URA3::ORM2-3R-GFP CEN::TRP1::CHS5-mCherry*	This study
SEN 687	*SEN1 CEN::URA3::ORM2-3A-GFP CEN::LEU2::HIS3::SEC61-mCherry*	This study
SEN 688	*dfm1Δ::KanMX CEN::URA3::ORM2-3A-GFP CEN::LEU2::HIS3::SEC61-mCherry*	This study

Supplemental Table 3.4.3. Key Resources Table

REAGENT or RESOURCE	SOURCE	IDENTIFIER
Antibodies		
Mouse monoclonal anti-GFP	Clontech Laboratories, Inc.	Cat#632381; RRID: AB_2313808
Mouse monoclonal anti-HA	Thermo Fisher Scientific	Cat#32-6700; RRID: AB_2533092
Rabbit polyclonal anti-myc	Genscript	Cat#A00172; RRID: AB_914457
Rabbit polyclonal anti-Cdc48	Neal et al., 2016	N/A
Mouse monoclonal anti-PGK	Thermo Fisher Scientific	Cat#459250; RRID: AB_2569747
Mouse monoclonal anti-Ubiquitin	Richard Gardner: University of Washington	N/A
Bacterial and Virus Strains		
Escherichia coli DH5 alpha Competent Cells	Thermo Fisher Scientific	Cat#18265017
Biological Samples		
Chemicals, Peptides, and Recombinant Proteins		
MG132 (benzyloxycarbonyl-Leu-Leu-aldehyde)	Sigma-Aldrich	474787; CAS: 133407-82-6
Cycloheximide	Sigma-Aldrich	C7698; CAS: 66-819
Protein A Sepharose	GE Healthcare	17-0780-01
Deposited Data		
Raw Files	This study, Mendeley Data	DOI: 10.17632/py236jc9fh.1
Experimental Models: Organisms/Strains		
Saccharomyces cerevisiae BY4741	GE Dharmacon	Cat#YSC1048
Saccharomyces cerevisiae S288C	This study	N/A
Additional yeast strains used: refer to Supplemental Table 3.4.2	This study	
Recombinant DNA		
Plasmids used: refer to Supplemental Table 3.4.1	This study	
Software and Algorithms		
Prism 7 for Mac	GraphPad Software	https://www.graphpad.com/scientific-software/prism/
Image J	NIH	https://imagej.nih.gov/ij/
FlowJo	Vashistha et al., 2016	https://www.flowjo.com/solutions/flowjo
BD Accuri C6	BD Accuri	Cat # 653122

Chapter 4: Scs7 is degraded via the ubiquitin proteasome system

4.1. Introduction

Maintaining protein homeostasis, or proteostasis, is essential for cell survival and growth. When protein disequilibrium is not corrected, cells may suffer from detrimental effects like proteotoxic stress or programmed cell death. To avoid these catastrophic events, cells have an intricate network of pathways, termed the proteostasis network (PN) (Jayaraj et al., 2020) that works to maintain protein homeostasis by refolding or degrading misfolded and aberrant proteins. In doing such, protein structure can be restored, or unusable proteins recycled and remade—thus recovering cellular protein homeostasis.

The proteostasis network is comprised of proteins, chaperones, lipids, and regulatory elements, and occurs within all compartments of the cell, including the nucleus, cytoplasm, endoplasmic reticulum (ER), the Golgi, the endolysosomal system, and the plasma membrane. Much work has been done on the proteostasis network within the ER (Parashar & Ferro-Novick, 2022), as it is the site of synthesis and transport and accounts for one third of the proteome (Wright & Plate, 2021). The ER is also known to be the site of lipid and sterol synthesis (Espenshade & Hughes, 2007; Jacquemyn et al., 2017), calcium storage (Koch, 1990), carbohydrate metabolism (Lemmer et al., 2021), and is known to intimately associate with most of the larger cellular organelles including the nucleus, mitochondria, and the Golgi via established contact sites (English et al., 2013). In a similar fashion, most eukaryotic secreted proteins are imported into the ER and folded before being transported to their final cellular destination. Taken together, the ER is an important player in the synthesis and processing of proteins and must be efficient in maintaining protein homeostasis.

Endoplasmic reticulum associated degradation (ERAD) is one of the protein quality control (PQC) mechanisms at the ER that works to eliminate proteins that fail to fold or assemble properly. ERAD functions in a multi-step process: (1) recognition of the protein targeted for degradation (Bhamidipati et al., 2005; Sato et al., 2009; Stanley et al, 2016); (2) substrate ubiquitination (Bays et al., 2001); (3) translocation of the substrate from the ER to the cytosol, termed retrotranslocation (Baldridge et al., 2016; Hampton et al., 1997; Neal et al., 2018; Sun et al., 2021; Swanson et al., 2001; Wahlman et al., 2007); and (4) degradation by the cytosolic proteasome (Farinha et al., 2005; Hampton et al., 1996; Werner et al., 1996). ERAD is a highly conserved process in all eukaryotes and has been a topic of much research over the past couple of decades.

In yeast, there are three branches of ERAD, that function to degrade proteins based on where the lesion, or misfolding, happens in the substrate; ERAD-M substrates have lesions within the membrane, ERAD-C substrates have lesions in a cytoplasmic domain, and ERAD-L substrates have lesions in the luminal domain (Zhang et al., 2019). Hrd1 acts as the E3 ubiquitin ligase for targeting ERAD-L and ERAD-M substrates for degradation, while Doa10 is the E3 ubiquitin ligase that targets in ERAD-C substrates for degradation. ERAD function is also known to be dependent on the function of certain rhomboid family proteins.

The rhomboid superfamily is a large family of proteins present in all organisms. Rhomboids have many distinct roles in development, signaling, and protein trafficking (Düsterhöft et al., 2017). They have also been found to play a significant role in lipid homeostasis and sterol regulation (Lemberg et al., 2007b; Lemberg et al., 2016), and glycosylation of newly synthesized proteins (Knopf et al., 2020). Interestingly, it has been

found that in plants, rhomboids play roles in quorum sensing, antibiotic resistance, and flower development (Clemmer et al., 2006; Knopf et al., 2012). Although rhomboids have several roles, their most notable and investigated role is that of ER PQC in ERAD, as well as in ER preemptive quality control (ERqPC) (Bhaduri et al., 2023; Kandel & Neal, 2020). They are also known to fulfill PQC roles in the nucleus (Flagg et al., 2021). Structurally, rhomboids are multi-pass (usually 6 transmembrane domains) proteins within lipid bilayers (Lemberg & Freeman, 2007a). A WR and GxxxG motif, found in loop1 (L1) and transmembrane 6 (TM6), respectively (Lemberg & Freeman, 2007a; Freeman 2014), work to stabilize the transmembrane helices (Bhaduri et al., 2023). Rhomboids are also classified into two subgroups based on their ability to proteolytically cleave substrates with a serine-histidine dyad within their active site (Kandel & Neal, 2020) or lack of ability to do so. These two subfamilies are the proteases and pseudoproteases.

This study focuses on the Dfm1 rhomboid pseudoprotease in yeast known to be essential for the retrotranslocation of ERAD substrates from the membrane to the cytosol in both the HRD and DOA pathways (Neal et al., 2018). Dfm1 accomplishes this by its ability to recognize and bind to misfolded membrane proteins, induce lipid thinning in its surrounding membrane environment, and recruit the AAA-ATPase Cdc48 to the ER (Neal et al., 2018; Nejatfard et al., 2021). In recent studies, we identified two novel roles of Dfm1 (see Chapter 2 and Chapter 3). We identified Dfm1 to have a chaperone-like activity that influences misfolded membrane protein aggregation in a Cdc48-indepenent manner (Kandel et al., 2023), and acts as a sphingolipid biosynthesis regulating protein by aiding in the degradation of Orm2, a negative regulator of the complex necessary for catalyzing the rate-limiting step of sphingolipid biosynthesis. The serine palmitoyltransferase (SPT) complex Dfm1 was found to

directly bind to phosphorylated Orm2 and facilitate its export from the ER to the Golgi, where it is ultimately degraded by endoplasmic reticulum and Golgi associated degradation (EGAD) (Bhaduri et al., 2023; Hanada, 2003).

As previously described in Chapter 1, sphingolipids are an important class of lipids localized in cellular membranes known to provide structural support, serve as energy storage, and serve as signal and regulatory molecules (Dickson, 2008; Hannun & Obeid, 2008; Hepowit et al., 2023; Quinville et al., 2021). Sphingolipids are synthesized by the serine palmitoyl transferase (SPT) complex at the ER and modified further by downstream enzymes at the Golgi (Garić, et al., 2019; Hannun & Obeid, 2018; Pralhada et al., 2013). Interestingly, Hepowit and colleagues, found that when the SPT complex function is inhibited by myriocin (Myr), sphingolipids are not generated *de novo* and cellular amino acid pools are reduced, and enter a quiescent state that aids in a prolonged cell life (Hepowit et al., 2023). Additionally, sphingolipids have been shown to be activators of the Endoplasmic Reticulum Stress Surveillance (ERSU) pathway, a pathway known to block yeast daughter cells from inheriting ER stress from their mother cell (Babour et al., 2010; Piña & Niwa, 2015; Piña et al., 2018). Combined, these studies highlight the role that sphingolipids play in maintaining the steady state processes in cells including amino acids, serving as an important effector of the proteostasis network.

Although a lot has been studied about enzymes and regulators that mediate sphingolipid metabolism, as discussed in Chapter 1, the degradation routes by which these enzymes and regulators are degraded has yet to be studied. Recently, Christiano and colleagues established a protein turnover map (TMAP) in *S. cerevisiae*, that characterized the degradation routes and turnover rates of key phospholipid and sphingolipid metabolism enzymes (Christiano et al., 2020). Among these enzymes were Tsc10, Orm2, Aur1, Sur1, Csg2, and Ipt1, enzymes involved in sphingolipid metabolism, that were shown to be short and medium-lived proteins (Christiano et al., 2020). Their studies also highlighted the fact that sphingolipid enzymes are degraded in different organelles by different degradation pathways. For example, they found Csg2 and Sur1, enzymes involved in the synthesis of complex sphingolipids (Uemura et al., 2003), are degraded by ESCRT machinery in the vacuole. Additionally, Orm2, an SPT complex regulator (Bhaduri et al., 2023; Schmidt et al., 2019; Xie et al., 2024), is degraded by the proteasome at the Golgi and endolysosomal system, and Tsc3, an enzyme that regulates the SPT complex and lipid droplets (Currie et al., 2014), is degraded by Asi1. The degradation of Tsc3 occurs at the ER and nuclear junction by the Asi branch of ERAD or by INMAD. Other degradation profiles of key sphingolipid enzymes, for example, those of Sur2, Lcb2, could not be identified due to overlapping hits in vacuolar and ERAD degradation machinery, highlighting a need to further investigate such mechanisms. It is with this study that we aimed to further understand the degradation routes of sphingolipid synthesis enzymes and explore the relationship between Dfm1 and this pathway.

4.2. Results

4.2.1. Surveying candidate sphingolipid biosynthesis enzymes and regulators targeted by ubiquitin proteasome system (UPS)

To investigate whether UPS targets other regulators or enzymes involved in sphingolipid biosynthesis for degradation, we utilized a screening approach to systematically survey for candidate substrates that are degraded by UPS. We assessed key enzymes and regulators such as Lcb1, Lcb2, Orm1, Sac1, Tsc3, Tsc10, and Ypk1 (Supp. Fig. 3.2.2). Notably, Scs7, a sphingolipid alpha-hydroxylase protein, was a top candidate substrate for many reasons. Scs7 is known to be strictly localized at the ER membrane as other ERAD machineries and previous studies have shown that Scs7 genetically interacts with Der1 (Hoppins et al., 2011; Schuldiner et al., 2015), a Dfm1 homolog within the rhomboid family, and major mediator of ERAD. Scs7 also serves as a ceramide differentiating enzyme as it catalyzes the hydrolysis reaction on Type-A ceramides resulting in Type-B' ceramides, and Type-B ceramides resulting in Type-C ceramides (Erdbrügger & Fröhlich, 2020; Guan et al., 2009). In other words, Scs7 influences the production of a variety of ceramide types. Thus, the levels of each type of ceramide could be measured after experiments as a proxy to understand the biochemical mechanisms that have occurred. Additionally, we hypothesized that Scs7 might be targeted for degradation through the UPS, as previous studies found that sphingolipid synthesis enzymes localized at the ER are degraded by the UPS through EGAD and INMAD, rather than those localized at the Golgi that are degraded by vacuolar degradation pathways (Christiano et al., 2020).

To investigate whether UPS targets Scs7 for degradation, we tagged the C-terminus of SCS7 with a fluorescent tag, mEmerald. Moreover, SCS7 expression was under the control of the TDH3/GAPDH promoter (Higuchi et al., 2024) in an S288C yeast background (Fig. 4.2.1A). We performed functional cycloheximide chase assays (CHX-chase) (Hampton et al., 1996) coupled with flow cytometry analysis (Buchanan et al., 2016) to monitor degradation of Scs7-mEmerald in different UPS mutant backgrounds (Fig. 4.2.1B). Furthermore, we used fluorescent microscopy in strains expressing Sec61-mCherry, an ER marker (Greenfield & High, 2000), to assess which compartment Scs7 accumulated in when its degradation was stabilized.

4.2.2. Scs7 degradation is stabilized in *cdc48-1*, *hrd2-1*, *tul1*Δ, and *asi1*Δ strains

Cdc48-2 and *hrd2-1* are hypomorphic allele mutants for the AAA-ATPase Cdc48 and proteasomal subunit Hrd2, respectively (Neal et al., 2017; Sato, 2008). Pep4 is a vacuolar endoprotease called proteinase A encoded by the PEP4 gene necessary for vacuole degradation (Conibear & Stevens, 2002). We found that Scs7-mEmerald degradation was stabilized in *cdc48-2* and *hrd2-1* strains to about ~90% protein remaining after 6hrs, compared to about 60% Scs7-mEmerald left in WT and *pep4*Δ cells (Fig. 4.2.2A). When we quantified the differences in stabilization of Scs7-mEmerald across timepoints, the stabilization of Scs7-mEmerald in *hrd2-1* cells was significant at time points 1hr, 2hr, and 3hr, while Scs7-mEmerald stabilization in *cdc48-2* cells was significant at 2hr, 3hr, and 6hr (Fig. 4.2.2B). These results suggest that Scs7 is degraded via proteasomal degradation pathways, rather than by the vacuole.

We next performed similar CHX-chase experiments in *dfm1*Δ and *der1*Δ mutants to understand whether derlin proteins play a role in the degradation of Scs7. By utilizing a CHX-chase assay we did not observe any differences in Scs7 degradation when compared to wild-type cells (Fig. 4.2.2C and Fig. 4.2.2D).

Next, we performed experiments of various E3 ligase mutants known to function in different UPS pathways. These mutants included a *hrd1*Δ strain as a major E3 ligase of the ERAD pathway (Baldridge & Rappaport, 2016; Hwang et al., 2017; Neal et al., 2020; Sato et al., 2009; Wu et al., 2020), *asi1*Δ as a major E3 ligase in INMAD pathway (Flagg et al., 2021; Pantazopoulou et al., 2016; Smoyer et al., 2019), *doa10*Δ as a major E3 ligase in both ERAD (Mehrtash & Hochstrasser, 2022; Ruggiano et al., 2016) and INMAD (Koch & Yu, 2019; Pantazopoulou, 2016), and *tul1*Δ□a member of the Dsc complex known to act in the EGAD pathway (Buzuk & Hellerschmied, 2023; Fonseca & Carvalho, 2019; Schmidt et al., 2019; Weyer et al., 2024). After 6hrs, there appeared to be a slight stabilization of Scs7-mEmerald in *asi1*Δ and *tul1*Δ cells (Fig. 4.2.2E), suggesting a role of both INMAD and EGAD in Scs7's degradation. Although *tul1*Δ, a member of the Dsc complex, is also involved to mediate vacuolar degradation through the VPS and AP-3 pathways (Weyer et al., 2024; Yang et al., 2018), we discounted the idea that the stabilization of Scs7-mEmerald was due to its dependance on Tul1's role in vacuolar degradation, since there was no change in degradation rate in *pep4*Δ cells in our previous CHX experiments, suggesting Scs7 degradation is vacuole-independent. When we quantified the stabilization of Scs7-mEmerald in these experiments, only *tul1*Δ cells, not *asi1*Δ cells, showed any significant stabilization at 2 hours (Fig. 4.2.2F). Since the stabilization in *asi1*Δ cells is just shy of being statistically significant, we did not want to fully discount the possibility in future experiments that INMAD could, in fact, be a degradation route for Scs7. Additionally, we could possibly presume this lack of statistical significance may be due to the redundancy of multiple pathways and could be further investigated by subsequent experiments in double knockout strains.

We wanted to further explore whether Scs7 was being degraded by vacuolar mechanisms, specifically by Dsc complex machinery. With this idea in mind, we established our methods to also include CHX-chase assays with Vld1 and Gld1 mutants, two Dsc subcomplex members that exist mutually exclusively in the Vld1-Dsc or Gld1-Dsc subcomplexes (Yang et al., 2018), respectively. Vld1 and Gld1 form the Dsc core trimer subunit with Dsc2 and Ubx3, but are never in complex with one another. Vld1 and Gld1 determine the localization of the complex and subsequent degradation pathway by which substrates will be degraded. The Gld1-Dsc subcomplex localizes at and between the Golgi and endosomes, degrading substrates through the vacuolar protein sorting (VPS) pathway and ESCRT machinery, while the Vld1-Dsc subcomplex localizes at and between the Golgi and vacuole utilizing the AP-3 pathway to degrade substrates more directly to the vacuoles, without the ESCRT machinery at late endosomes (Li et al., 2015a; Li et al., 2015b; Yang et al 2018).

When we performed CHX-chase experiments of Scs7-mEmerald in *vld1*Δ and *gld1*Δ cells, we did not observe any stabilization of the Scs7-mEmerald, as expected (Fig. 4.2.2G and Fig. 4.2.2H). Rather, Scs7 still did not appear to be degraded through the vacuolar degradation routes of the Dsc complex. These results were in line with our previous CHX-chase assay findings that suggested Scs7 is degraded by the proteasome rather than by vacuolar machinery.

4.2.3. Scs7 localizes in the ER in *cdc48-2*, *hrd2-1*, *tul1*Δ, and *asi1*Δ cells

After performing CHX chase assays, we next wanted to test which cellular compartment Scs7 was accumulating in when its degradation was stabilized. We utilized the following mutant strains in which degradation of Scs7 was stabilized: *cdc48-2*, *hrd2-1*, *pep4*Δ, *asi1*Δ, and *tul1*Δ. Based on our results that Scs7 might be degraded by INMAD via Asi1/3 complex and EGAD via Tul1, we hypothesized that in cells lacking Asi1/3 or Tul1, Scs7 would accumulate in the inner nuclear membrane and/or Golgi/endosome, respectively.

We performed confocal microscopy experiments and observed that Scs7-mEmerald co-localized with ER marker Sec-61-mCherry in WT cells (Fig. 4.2.3). This was expected, since Scs7 is known to localize at the ER membrane. *Cdc48-2*, *hrd2-1*, and *tul1*Δ cells showed distinct puncta of Scs7-mEmerald that didn't colocalize with ER marker, Sec61-mCherry, while Scs7-mEmerald appeared to accumulate in *asi1*Δ cells (Fig. 4.2.3, orange arrows). When we quantified normalized fluorescence intensity of each strain across trans-nuclear transverse lines via line scan analysis (Wegeng et al., 2024), all strains had similar fluorescence profiles across both channels except for *hrd2-1* and *asi1*Δ strains which had regions along the transverse line with distinctly bright Scs7-mEmerald fluorescence, demonstrated as dissonant signals of normalized fluorescent intensity between the mEmerald and mCherry channels (Fig. 4.2.3; blue arrows).

It is unclear what and where these distinct puncta and accumulation of Scs7-mEmerald might be. The puncta may be localizing to several regions like the Golgi and the

Trans Golgi Network (TGN), endosomes, the vacuole membrane, or aggresomes. To differentiate where these puncta might be, we could consider tagging the different yeast strains with various other fluorescently fused molecular markers like Sec7; VPS4 and CHS5; TM4-64, VPH1, Pep4, Vps10, Snf7; and p62, vimentin, hsp70/90 tubulin, respectively. It is also plausible that the puncta and accumulations that we observe are artifacts from the overexpression of the fluorescently tagged protein, in which case, we could investigate endogenous levels of proteins of interest with super resolution microscopy. However, considering, that these puncta of Scs7 are seen in *cdc48-2* and *hrd2-1* cells, as well as *tul1*Δ, when Scs7 is overwhelmingly overexpressed, we can surmise that the proteasome and possibly Dsc machinery play a role in the degradation of Scs7. Additionally, seeing as the only pathway where the Dsc complex and proteasome overlap is EGAD, we could possibly suggest that Scs7 might be degraded through this pathway. That said, this is a preliminary idea, and more experiments would be needed to support this hypothesis. Additionally, the puncta in *asi1*Δ mutants might suggest a role of INMAD in degrading Scs7 as well. Interestingly, though, the aggregations of Scs7 in *asi1*Δ yeast strains look distinctly larger than in the *cdc48-2* and *hrd2-1* cells, suggesting that the mechanism by which Scs7 accumulates in Asi1-defective cells is distinct. This is to be expected as Asi1's role in INMAD is different from Tul1, Hrd2, and Cdc48's role in EGAD and proteasomal degradation. As aggregates from dysregulated INMAD machinery can lead to increased apoptosis, altered gene expression, cell proliferation and differentiation, and responses to stress (Flagg et al., 2021), this phenomenon would be uniquely interesting to investigate. Again, further experiments would need to be performed to understand the mechanisms in each of these contexts.

4.3. Discussion

In efforts to further understand if and how pseudoprotease Dfm1 might regulate the sphingolipid biosynthetic pathway through interaction and degradation of its enzymes, we performed functional degradation assays and microscopy analyses. In performing these experiments, we (1) tried to devise a methodical system to perform subsequent experiments in exploring possible Dfm1-sphingolipid enzyme relationships, (2) identified Scs7 as a possible degradation substrate of the ubiquitin proteasome pathway, and (3) found that that the mechanism(s) by which Scs7 is degraded may be complex and require(s) further experimentation as well as more fine-tuned experimental methods. Most importantly, we have come up with more questions and ideas on how we might uncover more findings.

It is important to note that the findings in this chapter are not complete; rather, this chapter can be viewed as a presentation of preliminary experiments with outstanding experiments still yet to be performed. Due to personal circumstances, and time and resource constraints, the data is not all inclusive nor finalized – many questions remain, and the data presented in this chapter still requires clarification by follow-up experiments and optimizations before drawing concrete conclusions.

One issue we ran into was that, with only the Sec61-mCherry marker for cellular perspective, we could not discern or explain staining outside this marker. In addition, the Sec61-mCherry construct that we used, was not as bright nor specific as we would have liked, possibly because the construct was a yeast centromeric plasmid (YCp) rather than a yeast integrative plasmid (YIp) as the Scs7-mEmerald construct was. The expression pattern

of our ER straining construct was not fully optimized and could have been better. To better extrapolate what fluorescent signals we find in cells, we could perform similar experiments, but with additional and different molecular markers. These could include, Sec7 to visualize the Trans Golgi Network, Vps4 and Chs5 for endosomes, and Tm4-64, Vph1, Pep4, Wps10, and Snf7 for the vacuolar membrane. We could also identify if accumulated proteins are aggresomes by using p62, vimentin, Hsp70/79, or tubulin. In doing such, we could confidently identify fluorescent signals.

For future experiments, we could also try to perform multiple gene knockouts in strains. We could knock out multiple proteins along different portions of the same degradation pathway (i.e.: vacuole KO *snf*Δ and ESCRT KO *vps27*Δ (Wemmer, 2011)). Regarding vacuolar degradation pathways, we could also think about knocking out different components necessary for transport vesicles like clathrin and adapter proteins.

Regarding Dfm1-specific challenges, Dfm1 and Hrd1 have been known to have a compensatory relationship. In previous studies, when Dfm1 is absent, Hrd1 has been able to restore retrotranslocation function, resulting in a suppression of *dfm1*Δ phenotype (Neal et al., 2018; Neal et al, 2020). To prevent this suppression in strains from masking possible results, we would knock out both Dfm1 and Hrd1. Double knockouts could also function in other compensatory mechanisms, like when knocking out vld1 or gld1, as each Dsc complex has been shown to compensate for the other when overburdened (Weyer et al., 2024).

Taken together, our results and future experiments would give us more insights as to how a protein quality control protein like Dfm1, might also function in its ERAD role to regulate sphingolipids. This work could be important in a broader understanding of maladies stemming from protein and lipid dysregulation.

4.4. Materials and Methods

Yeast and bacteria growth media

Standard yeast *Saccharomyces cerevisiae* growth media were used as previously described (Hampton and Rine, 1994), including yeast extract-peptone-dextrose (YPD) medium and ammonia-based synthetic complete dextrose (SC) and ammonia-based synthetic minimal dextrose (SD) medium supplemented with 2% dextrose and amino acids to enable growth of auxotrophic strains at 30°C. *Escherichia coli* Top10 cells were grown in standard LB media with ampicillin at 37°C as previously described (Gardner et al., 1998).

Plasmids and strains

Plasmids used in this study are listed in Table S1. Plasmids for this work were generated using standard molecular biological techniques (Sato et al., 2009) and verified by sequencing (Plasmidsaurus Inc). Primer information is available in Table S3. Sec61p-mCherry plasmid (pHCMM4) was a gift from Hugo Cesar Medina-Munoz & Marvin Wickens (Addgene plasmid # 170359 ; http://n2t.net/addgene:170359 ; RRID:Addgene_170359).

A complete list of yeast strains and their corresponding genotypes are listed in Table S2. All strains used in this work were derived from S288C or Resgen. Yeast strains were transformed with DNA or PCR fragments using the standard LiOAc method (Ito et al., 1983). Null alleles were generated by using PCR to amplify a selection marker flanked by 50 base

pairs of the 5' and 3' regions, which are immediately adjacent to the coding region of the gene to be deleted. The selectable markers used for making null alleles were genes encoding resistance to G418 or CloNat/nourseothricin. After transformation, strains with drug markers were plated onto YPD followed by replica-plating onto YPD plates containing (500 µg/mL G418 or 200 µg/mL nourseothricin). All gene deletions were confirmed by PCR.

Cycloheximide-chase assay

Cycloheximide-chase assays were performed as previously described (Sato et al., 2009). Cells were grown to log-phase (OD_{600} 0.2) and cycloheximide was added to a final concentration of 50 µg/mL. At each time point (0, 1, 2, 3, and 6hr), 200uL of culture were taken and measured on the BD AccuriTM C6 Plus Flow Cytometer for further analysis.

Flow cytometry and analysis

Cell cultures were analyzed by flow cytometer using the BD AccuriTM C6 Plus Flow Cytometer by using the preset medium flow rate of 35uL/sec with a 16-um core size for each sample. The BD AccuriTM C6 Plus Flow Cytometer measured the individual fluorescence of 20,000 cells per reading of each sample. Samples were then gated for viability and fluorescence expression using Flowjo Software v10.10.0. Cells were gated for viability and fluorescence expression using the AutoGate function of populations on an SSC-A::SSC-A vs. FL1-A::FITC-A graph. Gates incorporated 85%-95% of cells at each 0hr time-point to

account for cells said to be viable and expressing the given construct. This resulted in samples of at least 17,000 cells. Samples were then subsequently analyzed using GraphPad Prism v10.

Fluorescence microscopy

To prepare cells, overnight cultures were diluted to approximately 0.20 OD in minimal media lacking histidine (-HIS). After growing approximately 3 hours, samples were pelleted and washed with dH2O before being resuspended in 80 uL of media to be used for imaging.

Confocal microscopy was performed on a Cytiva OMX SR microscope setup equipped with an Olympus PlanApo N 60X/1.42 oil objective. Multichannel alignment was performed by the manufacturer using TetraSpeck beads. Multicolor micrographs were aligned employing OMX-specific software packages (softWoRx).

Microscopy quantification and analysis

Multicolor images were analyzed using ImageJ to produce line scan measurements. Individual line scans were normalized to the highest fluorescent signal within the channel and plotted using GraphPad Prism v10.

4.5. Acknowledgements

For Chapter 4, the author would like to thank the Randolph Hampton (University of California, San Diego), and Jim Wilhelm (University of California, San Diego) Labs for providing plasmids and yeast strains, and the Andreas Ernst Lab (University of California, San Diego) for providing microscope and imaging support for this study. A special thanks to William R. Wegeng (Andreas Ernst; University of California, San Diego) for technical assistance, imaging discussions, and scientific feedback; to Christina R. Liem for positive reinforcement, in-depth scientific discussions, and technical assistance; and to the Neal Lab members who offered positive scientific discussions, feedback, and reinforcement. A special thanks to Dr. Rachel R. Kandel, Jasmine L. Jung, and Chloe J. Welch for supporting the writing of this study. The author would also like to thank Dr. Maho Niwa Rosen, Dr. Samara Reck-Peterson, and Dr. Randolph Hampton for scientific guidance. These studies were supported by NIH grant 1R35GM133565-01, Pew Biomedical Award 34089, and NSF CAREER grant 2047391 (to S.E.N), NIH grants 5R01GM136994-02 and DP2GM119132 (to E.J.B), HHMI Gilliam Fellowship GT15096 (to S.E.N and A.A.), and CSU CDIP Fellowship (to A.A.). The funders had no role in study design, data collection and analysis, decision to publish, or preparation of this study.

4.6. References

Babour, A., Bicknell, A. A., Tourtellotte, J., & Niwa, M. (2010). A surveillance pathway monitors the fitness of the endoplasmic reticulum to control its inheritance. *Cell*, *142*(2), 256-269.

Baldridge, R. D., & Rapoport, T. A. (2016). Autoubiquitination of the Hrd1 ligase triggers protein retrotranslocation in ERAD. *Cell*, *166*(2), 394-407.

Bays, N. W., Gardner, R. G., Seelig, L. P., Joazeiro, C. A., & Hampton, R. Y. (2001). Hrd1p/Der3p is a membrane-anchored ubiquitin ligase required for ER-associated degradation. *Nature cell biology*, *3*(1), 24-29.

Bhaduri, S., Aguayo, A., Ohno, Y., Proietto, M., Jung, J., Wang, I., ... & Neal, S. E. (2023). An ERAD-independent role for rhomboid pseudoprotease Dfm1 in mediating sphingolipid homeostasis. *The EMBO Journal*, *42*(4), e112275.

Bhaduri, S., Scott, N. A., & Neal, S. E. (2023). The role of the rhomboid superfamily in ER protein quality control: from mechanisms and functions to diseases. *Cold Spring Harbor Perspectives in Biology*, *15*(2), a041248.

Bhamidipati, A., Denic, V., Quan, E. M., & Weissman, J. S. (2005). Exploration of the topological requirements of ERAD identifies Yos9p as a lectin sensor of misfolded glycoproteins in the ER lumen. *Molecular cell*, *19*(6), 741-751.

Buchanan, B. W., Lloyd, M. E., Engle, S. M., & Rubenstein, E. M. (2016). Cycloheximide chase analysis of protein degradation in Saccharomyces cerevisiae. *JoVE (Journal of Visualized Experiments)*, (110), e53975.

Buzuk, L., & Hellerschmied, D. (2023). Ubiquitin-mediated degradation at the Golgi apparatus. *Frontiers in Molecular Biosciences*, *10*, 1197921.

Christiano, R., Arlt, H., Kabatnik, S., Mejhert, N., Lai, Z. W., Farese, R. V., & Walther, T. C. (2020). A systematic protein turnover map for decoding protein degradation. *Cell reports*, *33*(6).

Clemmer, K. M., Sturgill, G. M., Veenstra, A., & Rather, P. N. (2006). Functional characterization of Escherichia coli GlpG and additional rhomboid proteins using an aarA mutant of Providencia stuartii. *Journal of bacteriology*, *188*(9), 3415-3419.

Conibear, E., & Stevens, T. H. (2002). Studying yeast vacuoles. *Methods in enzymology*, *351*, 408-432.

Currie, E., Guo, X., Christiano, R., Chitraju, C., Kory, N., Harrison, K., ... & Farese, R. V. (2014). High confidence proteomic analysis of yeast LDs identifies additional droplet proteins and reveals connections to dolichol synthesis and sterol acetylation [S]. *Journal of lipid research*, *55*(7), 1465-1477.

Dickson, R. C. (2008). Thematic review series: sphingolipids. New insights into sphingolipid metabolism and function in budding yeast. *Journal of lipid research*, *49*(5), 909-921.

Düsterhöft, S., Künzel, U., & Freeman, M. (2017). Rhomboid proteases in human disease: Mechanisms and future prospects. *Biochimica et Biophysica Acta (BBA)-Molecular Cell Research*, *1864*(11), 2200-2209.

English, A. R., & Voeltz, G. K. (2013). Endoplasmic reticulum structure and interconnections with other organelles. *Cold Spring Harbor perspectives in biology*, *5*(4), a013227.

Erdbrügger, P., & Fröhlich, F. (2020). The role of very long chain fatty acids in yeast physiology and human diseases. *Biological chemistry*, *402*(1), 25-38.

Espenshade, P. J., & Hughes, A. L. (2007). Regulation of sterol synthesis in eukaryotes. *Annu. Rev. Genet.*, *41*(1), 401-427.

Farinha, C. M., & Amaral, M. D. (2005). Most F508del-CFTR is targeted to degradation at an early folding checkpoint and independently of calnexin. *Molecular and cellular biology*.

Flagg, M. P., Wangeline, M. A., Holland, S. R., Duttke, S. H., Benner, C., Neal, S., & Hampton, R. Y. (2021). Inner-nuclear-membrane–associated degradation employs Dfm1-independent retrotranslocation and alleviates misfolded transmembrane-protein toxicity. *Molecular biology of the cell*, *32*(7), 521-537.

Freeman, M. (2014). The rhomboid-like superfamily: molecular mechanisms and biological roles. *Annual review of cell and developmental biology*, *30*(1), 235-254.

Fonseca, D., & Carvalho, P. (2019). EGAD! There is an ERAD doppelganger in the Golgi. *The EMBO Journal*, *38*(15), e102679.

Fukuda, S., Kono, Y., Ishibashi, Y., Tabuchi, M., & Tani, M. (2023). Impaired biosynthesis of ergosterol confers resistance to complex sphingolipid biosynthesis inhibitor aureobasidin A in a PDR16-dependent manner. *Scientific reports*, *13*(1), 11179.

Garić, D., De Sanctis, J. B., Shah, J., Dumut, D. C., & Radzioch, D. (2019). Biochemistry of very-long-chain and long-chain ceramides in cystic fibrosis and other diseases: the importance of side chain. *Progress in lipid research*, *74*, 130-144.

Greenfield, J. J., & High, S. (2000). The Sec61 complex is located in both the ER and the ER-Golgi intermediate compartment. *Journal of cell science*, *112*(10), 1477-1486.

Guan, X. L., Souza, C. M., Pichler, H., Dewhurst, G., Schaad, O., Kajiwara, K., ... & Riezman, H. (2009). Functional interactions between sphingolipids and sterols in biological membranes regulating cell physiology. *Molecular biology of the cell*, *20*(7), 2083-2095.

Hampton, R. Y., & Bhakta, H. (1997). Ubiquitin-mediated regulation of 3-hydroxy-3-methylglutaryl-CoA reductase. *Proceedings of the National Academy of Sciences*, *94*(24), 12944-12948.

Hampton, R. Y., Gardner, R. G., & Rine, J. (1996). Role of 26S proteasome and HRD genes in the degradation of 3-hydroxy-3-methylglutaryl-CoA reductase, an integral endoplasmic reticulum membrane protein. *Molecular biology of the cell*, *7*(12), 2029-2044.

Hanada, K. (2003). Serine palmitoyltransferase, a key enzyme of sphingolipid metabolism. *Biochimica et Biophysica Acta (BBA)-Molecular and Cell Biology of Lipids*, *1632*(1-3), 16-30.

Hannun, Y. A., & Obeid, L. M. (2008). Principles of bioactive lipid signalling: lessons from sphingolipids. *Nature reviews Molecular cell biology*, *9*(2), 139-150.

Hannun, Y. A., & Obeid, L. M. (2018). Sphingolipids and their metabolism in physiology and disease. *Nature reviews Molecular cell biology*, *19*(3), 175-191.

Hepowit, N. L., Blalock, E., Lee, S., Bretland, K. M., MacGurn, J. A., & Dickson, R. C. (2023). Reduced sphingolipid biosynthesis modulates proteostasis networks to enhance longevity. *Aging (Albany NY)*, *15*(2), 472.

Higuchi, R., Fujita, Y., & Moriya, H. (2024). Improving the Z 3 EV promoter system to create the strongest yeast promoter. *Nature Communications*, *14*(1), 3810.

Hoppins, S., Collins, S. R., Cassidy-Stone, A., Hummel, E., DeVay, R. M., Lackner, L. L., ... & Nunnari, J. (2011). A mitochondrial-focused genetic interaction map reveals a scaffold-like complex required for inner membrane organization in mitochondria. *The Journal of cell biology*, *195*(2), 323.

Hwang, J., Walczak, C. P., Shaler, T. A., Olzmann, J. A., Zhang, L., Elias, J. E., & Kopito, R. R. (2017). Characterization of protein complexes of the endoplasmic reticulum-associated degradation E3 ubiquitin ligase Hrd1. *Journal of Biological Chemistry*, *292*(22), 9104-9116.

Jacquemyn, J., Cascalho, A., & Goodchild, R. E. (2017). The ins and outs of endoplasmic reticulum-controlled lipid biosynthesis. *EMBO reports*, *18*(11), 1905-1921.

Jayaraj, G. G., Hipp, M. S., & Hartl, F. U. (2020). Functional modules of the proteostasis network. *Cold Spring Harbor Perspectives in Biology*, *12*(1), a033951.

Kandel, R., Jung, J., Syau, D., Kuo, T., Songster, L., Horn, C., ... & Neal, S. E. (2023). Yeast derlin Dfm1 employs a chaperone-like function to resolve misfolded membrane protein stress. *PLoS biology*, *21*(1), e3001950.

Kandel, R. R., & Neal, S. E. (2020). The role of rhomboid superfamily members in protein homeostasis: Mechanistic insight and physiological implications. *Biochimica et Biophysica Acta (BBA)-Molecular Cell Research*, *1867*(10), 118793.

Knopf, J. D., Landscheidt, N., Pegg, C. L., Schulz, B. L., Kühnle, N., Chao, C. W., ... & Lemberg, M. K. (2020). Intramembrane protease RHBDL4 cleaves oligosaccharyltransferase subunits to target them for ER-associated degradation. *Journal of cell science*, *133*(6), jcs243790.

Knopf, R. R., & Adam, Z. (2012). Rhomboid proteases in plants–still in square one?. *Physiologia plantarum*, *145*(1), 41-51.

Koch, G. L. (1990). The endoplasmic reticulum and calcium storage. *Bioessays*, *12*(11), 527-531.

Koch, B., & Yu, H. G. (2019). Regulation of inner nuclear membrane associated protein degradation. *Nucleus*, *10*(1), 169-180.

Lemberg, M. K., & Adrain, C. (2016, December). Inactive rhomboid proteins: new mechanisms with implications in health and disease. In *Seminars in cell & developmental biology* (Vol. 60, pp. 29-37). Academic Press.

Lemberg, M. K., & Freeman, M. (2007). Cutting proteins within lipid bilayers: rhomboid structure and mechanism. *Molecular cell*, *28*(6), 930-940

Lemberg, M. K., & Freeman, M. (2007). Functional and evolutionary implications of enhanced genomic analysis of rhomboid intramembrane proteases. *Genome research*, *17*(11), 1634-1646.

Lemmer, I. L., Willemsen, N., Hilal, N., & Bartelt, A. (2021). A guide to understanding endoplasmic reticulum stress in metabolic disorders. *Molecular metabolism*, *47*, 101169.

Li, M., Koshi, T., & Emr, S. D. (2015). Membrane-anchored ubiquitin ligase complex is required for the turnover of lysosomal membrane proteins. *The Journal of cell biology*, *211*(3), 639.

Li, M., Rong, Y., Chuang, Y. S., Peng, D., & Emr, S. D. (2015). Ubiquitin-dependent lysosomal membrane protein sorting and degradation. *Molecular cell*, *57*(3), 467-478.

Mehrtash, A. B., & Hochstrasser, M. (2022). Elements of the ERAD ubiquitin ligase Doa10 regulating sequential poly-ubiquitylation of its targets. *Iscience*, *25*(11).

Neal, S., Syau, D., Nejatfard, A., Nadeau, S., & Hampton, R. Y. (2020). HRD complex self-remodeling enables a novel route of membrane protein retrotranslocation. *Iscience*, *23*(9).

Neal, S., Jaeger, P. A., Duttke, S. H., Benner, C., Glass, C. K., Ideker, T., & Hampton, R. Y. (2018). The Dfm1 Derlin is required for ERAD retrotranslocation of integral membrane proteins. *Molecular cell*, *69*(2), 306-320.

Neal, S., Mak, R., Bennett, E. J., & Hampton, R. (2017). A Cdc48 “retrochaperone” function is required for the solubility of retrotranslocated, integral membrane endoplasmic reticulum-associated degradation (ERAD-M) substrates. *Journal of Biological Chemistry*, *292*(8), 3112-3128.

Nejatfard, A., Wauer, N., Bhaduri, S., Conn, A., Gourkanti, S., Singh, N., ... & Neal, S. E. (2021). Derlin rhomboid pseudoproteases employ substrate engagement and lipid distortion to enable the retrotranslocation of ERAD membrane substrates. *Cell reports*, *37*(3).

Pantazopoulou, M. (2016). *Protein Quality Control at the Inner Nuclear Membrane–The Asi complex in Saccharomyces cerevisiae* (Doctoral dissertation, Department of Molecular Biosciences, The Wenner-Gren Institute, Stockholm University).

Pantazopoulou, M., Boban, M., Foisner, R., & Ljungdahl, P. O. (2016). Cdc48 and Ubx1 participate in a pathway associated with the inner nuclear membrane that governs Asi1 degradation. *Journal of cell science*, *129*(20), 3770-3780.

Parashar, S., & Ferro-Novick, S. (2022). Architecture of the endoplasmic reticulum plays a role in proteostasis. *Autophagy*, *18*(4), 937-938.

Piña, F. J., & Niwa, M. (2015). The ER Stress Surveillance (ERSU) pathway regulates daughter cell ER protein aggregate inheritance. *Elife*, *4*, e06970.

Piña, F., Yagisawa, F., Obara, K., Gregerson, J. D., Kihara, A., & Niwa, M. (2018). Sphingolipids activate the endoplasmic reticulum stress surveillance pathway. *The Journal of Cell Biology*, *217*(2), 495.

Pralhada Rao, R., Vaidyanathan, N., Rengasamy, M., Mammen Oommen, A., Somaiya, N., & Jagannath, M. R. (2013). Sphingolipid metabolic pathway: an overview of major roles played in human diseases. *Journal of lipids*, *2013*(1), 178910.

Quinville, B. M., Deschenes, N. M., Ryckman, A. E., & Walia, J. S. (2021). A comprehensive review: sphingolipid metabolism and implications of disruption in sphingolipid homeostasis. *International journal of molecular sciences*, *22*(11), 5793.

Ruggiano, A., Mora, G., Buxó, L., & Carvalho, P. (2016). Spatial control of lipid droplet proteins by the ERAD ubiquitin ligase Doa10. *The EMBO journal*, *35*(15), 1644-1655.

Sato, B. K. (2008). *ER quality control: Understanding misfolded protein recognition and retrotranslocation*. University of California, San Diego.

Sato, B. K., Schulz, D., Do, P. H., & Hampton, R. Y. (2009). Misfolded membrane proteins are specifically recognized by the transmembrane domain of the Hrd1p ubiquitin ligase. *Molecular cell*, *34*(2), 212-222.

Schmidt, O., Weyer, Y., Baumann, V., Widerin, M. A., Eising, S., Angelova, M., ... & Teis, D. (2019). Endosome and Golgi-associated degradation (EGAD) of membrane proteins regulates sphingolipid metabolism. *The EMBO Journal*, *38*(15), e101433.

Schuldiner, M., Collins, S. R., Thompson, N. J., Denic, V., Bhamidipati, A., Punna, T., ... & Krogan, N. J. (2005). Exploration of the function and organization of the yeast early secretory pathway through an epistatic miniarray profile. *Cell*, *123*(3), 507-519.

Shimobayashi, M., Oppliger, W., Moes, S., Jenö, P., & Hall, M. N. (2013). TORC1-regulated protein kinase Npr1 phosphorylates Orm to stimulate complex sphingolipid synthesis. *Molecular biology of the cell*, *24*(6), 870-881.

Smoyer, C. J., Smith, S. E., Gardner, J. M., McCroskey, S., Unruh, J. R., & Jaspersen, S. L. (2019). Distribution of proteins at the inner nuclear membrane is regulated by the Asi1 E3 ligase in Saccharomyces cerevisiae. *Genetics*, *211*(4), 1269-1282.

Stanley, M., & Virdee, S. (2016). Chemical ubiquitination for decrypting a cellular code. *Biochemical Journal*, *473*(10), 1297-1314.

Sun, Z., Guerriero, C. J., & Brodsky, J. L. (2021). Substrate ubiquitination retains misfolded membrane proteins in the endoplasmic reticulum for degradation. *Cell reports*, *36*(12).

Swanson, R., Locher, M., & Hochstrasser, M. (2001). A conserved ubiquitin ligase of the nuclear envelope/endoplasmic reticulum that functions in both ER-associated and Matα2 repressor degradation. *Genes & development*, *15*(20), 2660-2674.

Uemura, S., Kihara, A., Inokuchi, J. I., & Igarashi, Y. (2003). Csg1p and newly identified Csh1p function in mannosylinositol phosphorylceramide synthesis by interacting with Csg2p. *Journal of Biological Chemistry*, *278*(46), 45049-45055.

Wahlman, J., DeMartino, G. N., Skach, W. R., Bulleid, N. J., Brodsky, J. L., & Johnson, A. E. (2007). Real-time fluorescence detection of ERAD substrate retrotranslocation in a mammalian in vitro system. *Cell*, *129*(5), 943-955.

Wegeng, W. R., Bogus, S. M., Ruiz, M., Chavez, S. R., Noori, K. S., Niesman, I. R., & Ernst, A. M. (2024). A Hollow TFG Condensate Spatially Compartmentalizes the Early Secretory Pathway. *bioRxiv*.

Wemmer, M. A. (2011). *Regulation of ESCRT-III assembly and membrane scission activity in the budding yeast Saccharomyces cerevisiae* (Doctoral dissertation, University of Colorado at Boulder).

Werner, E. D., Brodsky, J. L., & McCracken, A. A. (1996). Proteasome-dependent endoplasmic reticulum-associated protein degradation: an unconventional route to a familiar fate. *Proceedings of the National Academy of Sciences*, *93*(24), 13797-13801.

Weyer, Y., Schwabl, S. I., Tang, X., Widerin, M. A., Niedrist, V., Tettamanti, M. G., ... & Teis, D. (2024). The Dsc ubiquitin ligase complex identifies transmembrane degrons to degrade orphaned proteins at the Golgi. *bioRxiv*, 2024-03.

Wright, M. T., & Plate, L. (2021). Revealing functional insights into ER proteostasis through proteomics and interactomics. *Experimental cell research*, *399*(1), 112417.

Wu, X., Siggel, M., Ovchinnikov, S., Mi, W., Svetlov, V., Nudler, E., ... & Rapoport, T. A. (2020). Structural basis of ER-associated protein degradation mediated by the Hrd1 ubiquitin ligase complex. *Science*, *368*(6489), eaaz2449.

Xie, T., Dong, F., Han, G., Wu, X., Liu, P., Zhang, Z., ... & Gong, X. (2024). Collaborative regulation of yeast SPT-Orm2 complex by phosphorylation and ceramide. *Cell Reports*, *43*(2).

Yang, X., Arines, F. M., Zhang, W., & Li, M. (2018). Sorting of a multi-subunit ubiquitin ligase complex in the endolysosome system. *Elife*, *7*, e33116.

Zhang, Z. R. (2019). Mechanism of Quality Control of Nascent Membrane Proteins. *Advances in Membrane Proteins: Building, Signaling and Malfunction*, 111-130.

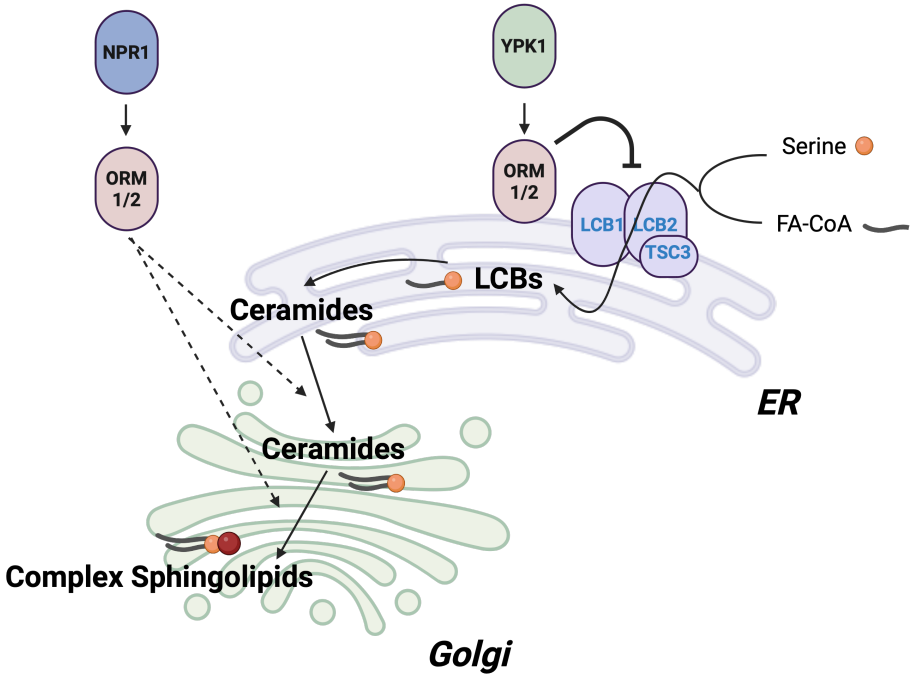


Figure 4.1.1. Maturation of sphingolipids from the ER to the Golgi

Sphingolipid biosynthesis begins with the joining or serine with fatty acid/palmitoyl coenzyme A by the SPT complex at the ER, which is regulated by a YPK-Orm1/2 axis. From there long chain bases (LCBs) are catabolized into ceramides before being transported to the Golgi for further processing. At the Golgi, ceramides are processed further into complex sphingolipids, with possible regulation of Orm1/2. (Adapted from Shimobayashi et al., 2013). Created with BioRender.com.

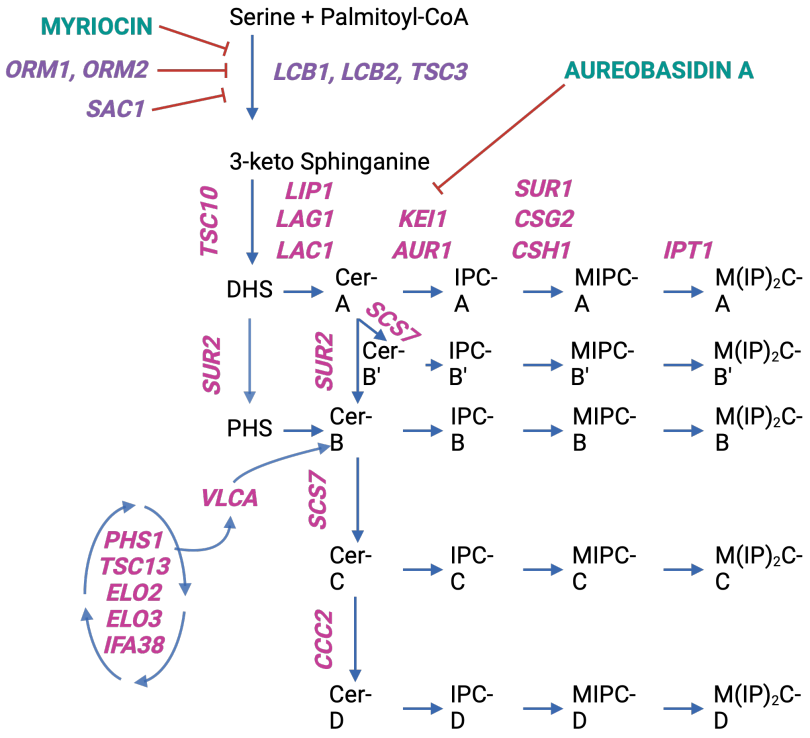


Figure 4.1.2. Investigating the sphingolipid pathway in yeast requires and enzyme-centric approach

(A) Ceramide intermediates are shown in black, reactions in blue arrows, SPOTS complex members in purple, drug inhibitors in aqua, and enzymes in magenta. Adapted from Fukuda et al., 2023. Created with BioRender.com.

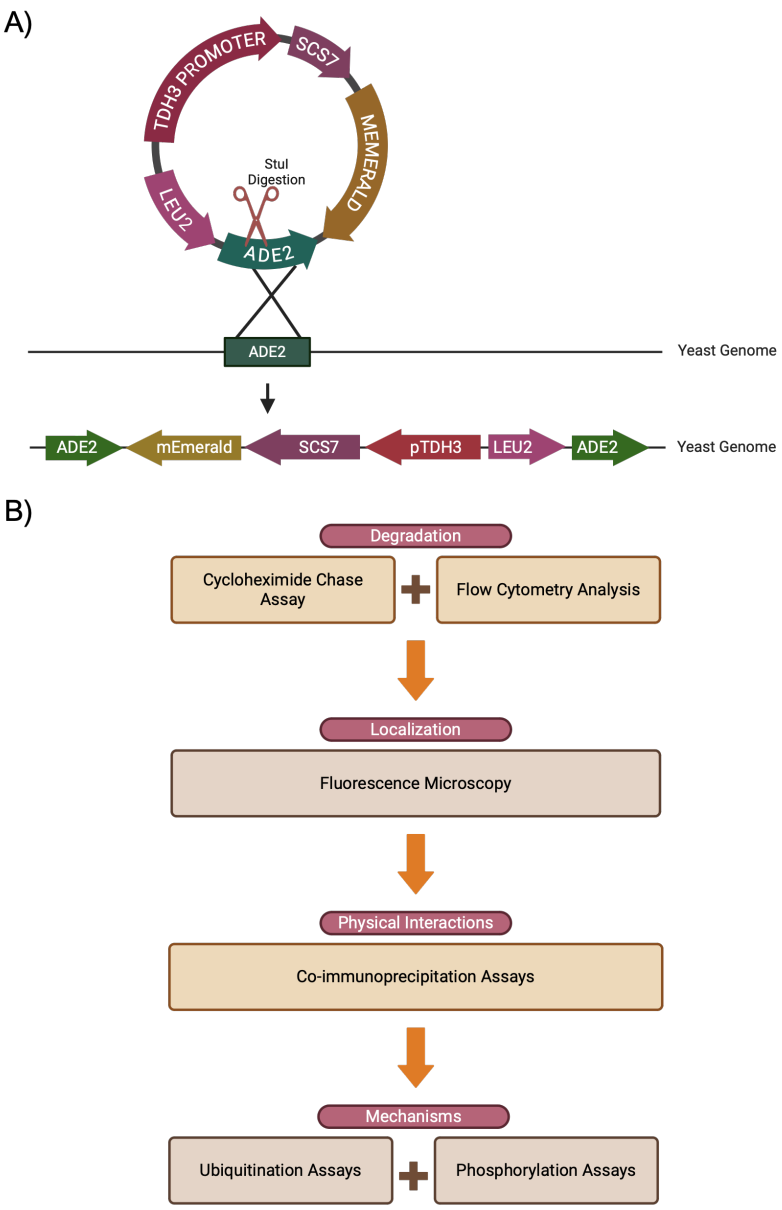


Figure 4.2.1. Approach to investigate candidate Dfm1-regulated sphingolipid biosynthesis enzymes

(A) Genome editing schematic for overexpression of Scs7-mEmerald under the TDH3/GAPDH promoter by a yeast integrating plasmid and homologous recombination. **(B)** Workflow of experiments to understand how Dfm1 might regulate sphingolipid biosynthesis enzymes includes degradation, localization, physical interaction, and mechanistic assays. Created with BioRender.com.

Figure 4.2.2. Scs7 degradation is stabilized in *cdc48-1*, *hrd2-1*, *tul1*Δ, and *asi1*Δ strains

(A) Cdc48 and Hrd2 are required for Scs7 degradation. In the indicated strains, degradation of Scs7-mEmerald was measured by CHX-chase assay. Cells were analyzed by measuring mean fluorescence intensity via flow cytometry (3 biological replicates; n=3). Measurements were taken at time 0, 1, 2, 3, and 6hrs. t=0 was taken as 100% and error bars depict SEM. **(B)** Cdc48-2 and Hrd2-1 strains stabilize degradation of Scs7. Data from (A) was quantified using 2way ANOVA with multiple comparisons using Dunnett's multiple comparison test with WT strain as a control. * denotes P ≤ 0.05, and ** denotes P ≤ 0.01. **(C)** Derlins Derlin1 and Dfm1 are not required for Scs7 degradation. Scs7-mEmerald degradation was measured by CHX-chase assay as in (A) and **(D)** quantified similarly to (B) in *der1Δ* and *dfm1Δ* cells. * denotes P ≤ 0.05, and ** denotes P ≤ 0.01. **(E)** Asi1 and Tul1 blunt Scs7 degradation. Scs7-mEmerald degradation was measured via CHX-chase like assays (A) and (C) using mutant strains of different E3 ubiquitin ligases (*hrd1Δ*, *doa10Δ*, *asi1Δ*, *tul1Δ*), then **(F)** quantified similarly to (B) and (D). * denotes P ≤ 0.05, and ** denotes P ≤ 0.01. **(G)** Competing DSC complex subunits are not necessary for Scs7 degradation. Scs7-mEmerald degradation was measured via CHX-chase like assays (A), (C), and (E) using mutant strains *gld1Δ* and *vld1Δ,* known Dsc subunits that dictate Golgi degradation substrate fate. Degradation rates were also **(H)** quantified by methods listed above. * denotes P ≤ 0.05, and ** denotes P ≤ 0.01.

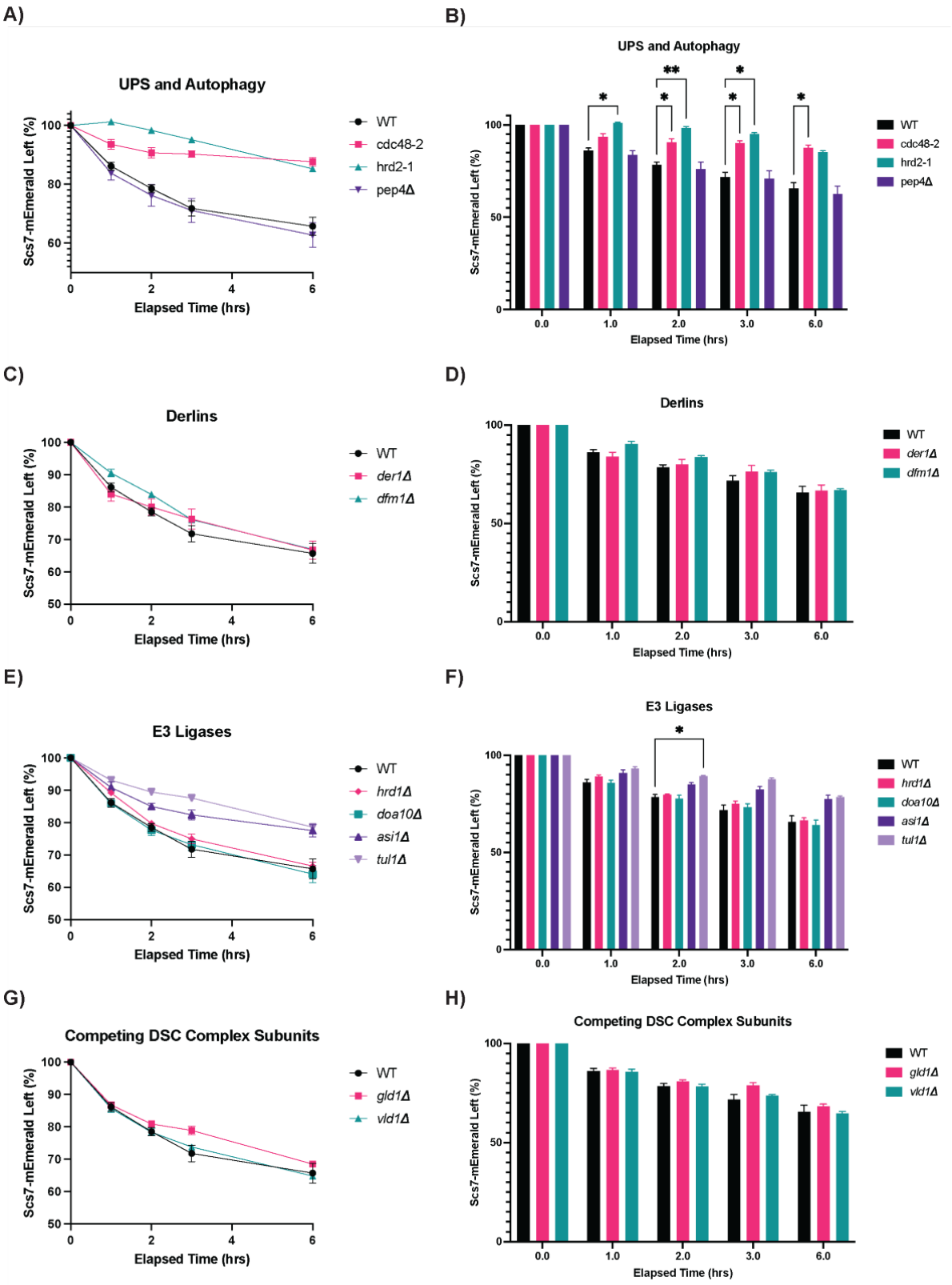
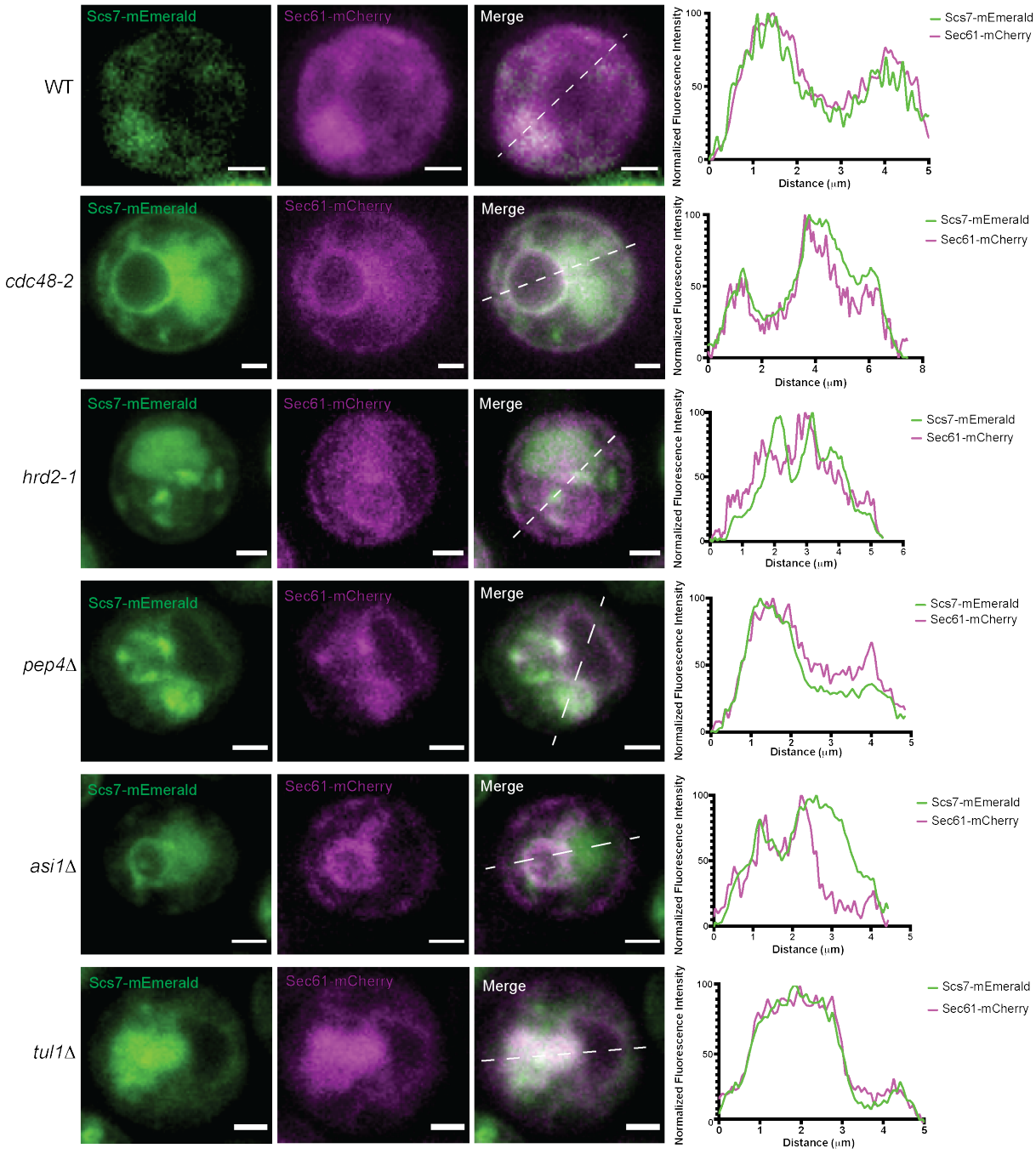

A)
UPS and Autophagy
Scs7-mEmerald Left (%)
Elapsed Time (hrs)
WT
cdc48-2
hrd2-1
pep4Δ
B)
UPS and Autophagy
Scs7-mEmerald Left (%)
Elapsed Time (hrs)
WT
cdc48-2
hrd2-1
pep4Δ
C)
Derlins
Scs7-mEmerald Left (%)
Elapsed Time (hrs)
WT
der1Δ
dfm1Δ
D)
Derlins
Scs7-mEmerald Left (%)
Elapsed Time (hrs)
WT
der1Δ
dfm1Δ
E)
E3 Ligases
Scs7-mEmerald Left (%)
Elapsed Time (hrs)
WT
hrd1Δ
doa10Δ
asi1Δ
tul1Δ
F)
E3 Ligases
Scs7-mEmerald Left (%)
Elapsed Time (hrs)
WT
hrd1Δ
doa10Δ
asi1Δ
tul1Δ
G)
Competing DSC Complex Subunits
Scs7-mEmerald Left (%)
Elapsed Time (hrs)
WT
gld1Δ
vld1Δ
H)
Competing DSC Complex Subunits
Scs7-mEmerald Left (%)
Elapsed Time (hrs)
WT
gld1Δ
vld1Δ

Figure 4.2.3. Scs7 localizes in the ER in *cdc48-2*, *hrd2-1*, *tul1*Δ, and *asi1*Δ cells

Conventional confocal widefield deconvolution microscopy images of WT *cdc48-2*, *hrd2-1*, *tul1*Δ, *pep4*Δ, and *asi1*Δ cells. Cells were grown overnight and diluted to 0.2 OD in minimal media and grown for 3 hrs. Samples were then washed, pelleted, resuspended in media, and imaged. Microscopy was performed on a Cytiva OMX SR microscope setup equipped with an Olympus PlanApo N 60X/1.42 oil objective Multichannel alignment was performed by the manufacturer using TetraSpeck beads. Fluorescence intensity was then measured using FIJI: ImagJ software, normalized to max intensity fluorescence signal, and graphed using GraphPad Prism v10. Scale bars mark = 1μm.


WT
cdc48-2
hrd2-1
pep4Δ
asi1Δ
tul1Δ
Scs7-mEmerald
Sec61-mCherry
Merge
Normalized Fluorescence Intensity
Distance (μm)

Supplemental Table 4.4.1. Plasmids Used in this Study

Plasmid	Gene
pSN258	YCp HIS3/LEU2 pCYC1-SEC61-mCherry
pSN309	YIp ADE2/LEU2 pTDH3-SCS7-mEmerald

Supplemental Table 4.4.2. Yeast Strains Used in this Study

Strain	Genotype	Reference
SEN1	*Mata ade2-101 met2 lys2-801 ura3-52 trp1::hisG leu2Δ his3Δ200*	This study
BY4741	*Mata met15Δ0 his3Δ1 leu2Δ0 ura3Δ0*	This study
SEN24	*Mata ade2-101 met2 lys2-801 ura3-52 trp1::hisG leu2Δ his3Δ200 hrd1Δ::KanMX*	This study
SEN137	*Mata ade2-101 met2 lys2-801 ura3-52 trp1::hisG leu2Δ his3Δ200 dfm1Δ::KanMX*	This study
SEN543	*Mata ade2-101 met2 lys2-801 ura3-52 trp1::hisG leu2Δ his3Δ200 hrd2::hrd2-1::NatR*	This study
SEN544	*Mata ade2-101 met2 lys2-801 ura3-52 trp1::hisG leu2Δ his3Δ200 cdc48::cdc48-2::NatR*	This study
SEN545	*Mata ade2-101 met2 lys2-801 ura3-52 trp1::hisG leu2Δ his3Δ200 doa10Δ::NatR*	This study
SEN585	*Mata ade2-101 met2 lys2-801 ura3-52 trp1::hisG leu2Δ his3Δ200 asi1Δ::HphMX*	This study
SEN586	*Mata met15Δ0 his3Δ1 leu2Δ0 ura3Δ0 tul1Δ::KanMX*	This study
SEN764	*Mata met15Δ0 his3Δ1 leu2Δ0 ura3Δ0 der1Δ::KanMX*	This study
SEN798	*Mata met15Δ0 his3Δ1 leu2Δ0 ura3Δ0 gld1Δ::KanMX*	This study
SEN799	*Mata met15Δ0 his3Δ1 leu2Δ0 ura3Δ0 vld1Δ::KanMX*	This study
SEN800	*Mata met15Δ0 his3Δ1 leu2Δ0 ura3Δ0 pep4Δ::KanMX*	This study
SEN802	*Mata ade2-101::ADE2::pTDH3-SCS7-mEmerald::LEU2 met2 lys2-801 ura3-52 trp1::hisG leu2Δ his3Δ200*	This study
SEN803	*Mata ade2-101::ADE2::pTDH3-SCS7-mEmerald::LEU2 met2 lys2-801 ura3-52 trp1::hisG leu2Δ his3Δ200 hrd1Δ::KanMX*	This study
SEN804	*Mata ade2-101:: ADE2::pTDH3-SCS7-mEmerald::LEU2 met2 lys2-801 ura3-52 trp1::hisG leu2Δ his3Δ200 dfm1Δ::KanMX*	This study
SEN805	*Mata ade2-101::ADE2::pTDH3-SCS7-mEmerald::LEU2 met2 lys2-801 ura3-52 trp1::hisG leu2Δ his3Δ200 hrd2::hrd2-1::NatR*	This study
SEN806	*Mata ade2-101::ADE2::pTDH3-SCS7-mEmerald::LEU2 met2 lys2-801 ura3-52 trp1::hisG leu2Δ his3Δ200 cdc48::cdc48-2::NatR*	This study
SEN807	*Mata ade2-101::ADE2::pTDH3-SCS7-mEmerald::LEU2 met2 lys2-801 ura3-52 trp1::hisG leu2Δ his3Δ200 doa10Δ::NatR*	This study
SEN808	*Mata ade2-101::ADE2::pTDH3-SCS7-mEmerald::LEU2 met2 lys2-801 ura3-52 trp1::hisG leu2Δ his3Δ200 asi1Δ::HphMX*	This study

Supplemental Table 4.4.2. Yeast Strains Used in this Study (Continued)

Strain	Genotype	Reference
SEN809	*Mata met15Δ0 his3Δ1 leu2Δ0 ura3Δ0 ADE2::pTDH3-SCS7-mEmerald::LEU2 tul1Δ::KanMX*	This study
SEN810	*Mata met15Δ0 his3Δ1 leu2Δ0 ura3Δ0 ADE2::pTDH3-SCS7-mEmerald::LEU2 der1Δ::KanMX*	This study
SEN811	*Mata met15Δ0 his3Δ1 leu2Δ0 ura3Δ0 ADE2::pTDH3-SCS7-mEmerald::LEU2 gld1Δ::KanMX*	This study
SEN812	*Mata met15Δ0 his3Δ1 leu2Δ0 ura3Δ0 ADE2::pTDH3-SCS7-mEmerald::LEU vld1Δ::KanMX*	This study
SEN813	*Mata met15Δ0 his3Δ1 leu2Δ0 ura3Δ0 ADE2::pTDH3-SCS7-mEmerald::LEU2 pep4Δ::KanMX*	This study
SEN816	*Mata ade2-101::ADE2::pTDH3-SCS7-mEmerald::LEU2 met2 lys2-801 ura3-52 trp1::hisG leu2Δ his3Δ200 CEN::*pCYC1-SEC61-mCherry:: *LEU2::HIS3*	This study
SEN819	*Mata ade2-101::ADE2::pTDH3-SCS7-mEmerald::LEU2 met2 lys2-801 ura3-52 trp1::hisG leu2Δ his3Δ200 hrd2::hrd2-1::NatR CEN::*pCYC1-SEC61-mCherry:: *LEU2::HIS3*	This study
SEN820	*Mata ade2-101::ADE2::pTDH3-SCS7-mEmerald::LEU2 met2 lys2-801 ura3-52 trp1::hisG leu2Δ his3Δ200 cdc48::cdc48-2::NatR CEN::*pCYC1-SEC61-mCherry:: *LEU2::HIS3*	This study
SEN822	*Mata ade2-101::ADE2::pTDH3-SCS7-mEmerald::LEU2 met2 lys2-801 ura3-52 trp1::hisG leu2Δ his3Δ200 asi1Δ::HphMX CEN::*pCYC1-SEC61-mCherry:: *LEU2::HIS3*	This study
SEN823	*Mata met15Δ0 his3Δ1 leu2Δ0 ura3Δ0 ADE2::pTDH3-SCS7-mEmerald::LEU2 tul1Δ::KanMX CEN::*pCYC1-SEC61-mCherry:: *LEU2::HIS3*	This study
SEN827	*Mata met15Δ0 his3Δ1 leu2Δ0 ura3Δ0 ADE2::pTDH3-SCS7-mEmerald::LEU2 pep4Δ::KanMX CEN::*pCYC1-SEC61-mCherry:: *LEU2::HIS3*	This study
SEN830	*Mata ade2-101 met2 lys2-801 ura3-52::URA3::1MYC-HMG2-S215A-GFP trp1::hisG leu2Δ his3Δ200*	This study
SEN554	*ade2-101 met2 lys2-801 ura3-52::URA3::HMG2-GFP trp1::hisG leu2Δ his3Δ200 pdr5Δ::KanMX*	This study

Supplemental Table 4.4.3. Key Resources Table

REAGENT or RESOURCE	SOURCE	IDENTIFIER
Bacterial and Virus Strains		
Escherichia coli DH5 alpha Competent Cells	Thermo Fisher Scientific	Cat#18265017
Biological Samples		
Chemicals, Peptides, and Recombinant Proteins		
Cycloheximide	Sigma-Aldrich	C7698; CAS: 66-819
Experimental Models: Organisms/Strains		
Saccharomyces cerevisiae BY4741	GE Dharmacon	Cat#YSC1048
Saccharomyces cerevisiae S288C	This study	N/A
Additional yeast strains used: refer to Supplemental Table 4.4.2	This study	
Recombinant DNA		
Plasmids used: Supplemental Table 4.4.1	This study	
Software and Algorithms		
Prism 10 for Mac	GraphPad Software	https://www.graphpad.com/scientific-software/prism/
Image J	NIH	https://imagej.nih.gov/ij/
FlowJo	Vashistha et al., 2016	https://www.flowjo.com/solutions/flowjo
BD Accuri™ C6 Plus	BD Accuri	Cat #660517

Chapter 5: Conclusions and Closing Remarks

5.1 Conclusions and Closing Remarks

During my doctoral studies in Dr. Neal's lab, I have been able to grow along with the dedicated researchers in the field, as well as grow individually as a scientist and educator. Dr. Neal's lab has furthered the understanding of rhomboid family proteins, and their intricate mechanistic involvement in protein homeostasis and lipid regulation and is continuing to work on finding novel roles of the multidimensional protein superfamily. The lab's research is based on Dr. Neal's fundamental work in discovering Dfm1's role in retrotranslocating integral membrane substrates in endoplasmic reticulum associated degradation (ERAD). Since then, our lab has worked to further understand the mechanisms by which this occurs, as well as understand other functions of Dfm1 in associated contexts apart from ERAD.

Chapter 2 and Chapter 3 describe Dfm1's ERAD independent roles in the proteostasis network (PN). In Chapter 2, our work describes Dfm1's chaperone-like function in preventing cellular stress by promoting solubility of membrane proteins. In Chapter 3, our work describes Dfm1's role in regulating sphingolipid homeostasis as Dfm1 is critical for trafficking Orm2 to the Golgi for degradation by endosome and Golgi-associated degradation (EGAD). In Chapter 4, we try to further understand Dfm1's role in regulating sphingolipid homeostasis by probing for other interactions between Dfm1 and key sphingolipid regulating enzymes.

The work presented in this dissertation follows my growth through my graduate research career from training to independent researcher. My work in Chapter 2 as a contributing author stemmed from my training in the lab, learning how to perform

fundamental yeast experiments under the guidance of the primary author, my mentor and friend, Dr. Kandel. Not only did these studies help establish the first of Dfm1's ERAD-independent roles, but they served as guidance to my independent research in the lab. In Chapter 3, I performed as an independent researcher while collaborating with the other primary author, Dr. Bhaduri. We worked to understand Dfm1's role in regulating sphingolipid enzymes from a preliminary screen done by Dr. Proietto that highlighted other possible interacting partners of Dfm1. We identified Dfm1 is directly involved in the trafficking of Orm2 for degradation by endosome and Golgi-associated degradation (EGAD). In Chapter 4, I worked as the primary independent researcher to continue expanding our knowledge of how Dfm1 might serve as a broader sphingolipid regulator. Although findings do not indicate that Dfm1 regulates the sphingolipid biosynthetic enzyme Scs7, they serve as a mechanism to investigate other enzymes in the sphingolipid biosynthetic pathway.

Although the work presented in this dissertation has brought new insight into Dfm1's ERAD-independent roles, much is yet to be uncovered about Dfm1 and the mechanisms by which Dfm1 acts. In the context of chaperone-like functions, one might wonder if other rhomboid proteins also serve a chaperone-like function to alleviate stress. One might ask such questions as, "Do other rhomboid proteins work in this manner?", "What about in other organisms?", "Are these findings specific to rhomboid pseudoproteases, or "Do rhomboid proteases also function in similar ways?" One might also ask about specificity of substrates: "Are these findings specific to certain substrates?", "What about in different biological systems?", or "What other machinery or molecules are necessary for the functions that we observe?"

Regarding our findings that Dfm1 aids Orm2's trafficking to the Golgi degradation, the main question that arises is "What other sphingolipid metabolic enzyme might Dfm1 also regulate?", which I began to explore in Chapter 4. Although I did not find that Dfm1 regulates Scs7, similar approaches can be utilized to help understand Dfm1's involvement in sphingolipid homeostasis more broadly. Due to time and personal constraints, Chapter 4 investigations only follow Scs7, and not as thoroughly as planned; however, many other enzymes are involved in sphingolipid metabolism and catabolism. The introduction chapter of this dissertation highlights the role of different lipids in the proteostasis network. Naturally, one might ask, "What other membrane lipids that function in the proteostasis network might Dfm1 regulate?" Additionally, the findings of Chapter 4 suggest that Scs7 might be degraded through one of the proteasomal degradation routes, however, more research must be done to understand by which specific route it is processed through (ie: EGAD, ERAD, INMAD, etc.). Considering the degradation routes of many of the enzymes involved in sphingolipid biosynthesis are unknown, one could use similar experiments to understand such.

The Neal Lab has made great strides in further understanding rhomboid proteins and has recently begun researching sphingolipids. Both families of molecules have various functions, as demonstrated by our work as well as others' work. By continuing this type of research, much can be learned about the interplay of systems and how cells ultimately maintain homeostasis despite perturbances.